

## **Thesis submission: Examination - Thomas Newman**

---

### **Student form**

#### **Restricting access**

In a very small number of cases it may be necessary following examination to restrict access to a thesis by placing it under an embargo. An embargo may be needed where, for example, the thesis contains material that is commercially sensitive or which could put at risk an individual's personal safety. An embargo must be requested using the [Embargo Request Form](#).

### **Thesis**

#### **Thesis title**

Low Carbon Lettuce: Mitigating greenhouse gas emissions from intensive agriculture on lowland peatland

#### **Do you want to update your thesis title?**

Yes

#### **If yes, please enter your updated title**

Impacts of long term drainage and agriculture on the carbon dynamics of fen peatlands in East Anglia, UK

#### **Thesis word count**

The word limit for your degree type is 50,000 words

#### **How long will your thesis be?**

50000 words

### **Thesis**

---

### **Attached files**

Thomas Richard Newman Thesis.pdf



UNIVERSITY OF  
**LEICESTER**

Impacts of long term drainage and  
agriculture on the carbon dynamics of fen  
peatlands in East Anglia, UK

Thomas Richard Newman

A thesis submitted for the degree of Doctor of  
Philosophy at the University of Leicester, School of  
Geography, Geology and the Environment

September 2021

## Abstract

Over the last 150 years, extensive reclamation of UK lowland peatlands for agriculture, particularly in the East Anglian Fens, has provided some of the most fertile land in the UK, but resulted in a peat depth loss of up to 4.8 m and a significant carbon (C) emission. A large portion of formerly deep peat is now classified as ‘wasted’ (peat depth  $\leq 0.4$  m). In the Fens, both deep and wasted peats are used for intensive arable agriculture.

Arable cropland on peatland contributes an estimated 7,600 kt CO<sub>2</sub>e yr<sup>-1</sup> to UK emissions (32% of peatland emissions from 7% of the peatland area). This estimate is derived from emissions data for deep peats. No data for wasted peats were available despite their significant land area. To improve the emission estimate, CO<sub>2</sub> fluxes at an arable wasted peatland were measured over two years using Eddy Covariance. Additionally, aeolian erosion was measured from the wasted and compared to a deep peatland.

The average emission from wasted peatland was  $676 \pm 188.5$  g C m<sup>-2</sup> yr<sup>-1</sup> over two years ( $812 \pm 195.6$  and  $540 \pm 181.4$  g C m<sup>-2</sup> yr<sup>-1</sup>). This was lower than the emission factor for deep peat, suggesting the need for a separate emission factor for wasted peat. Primary drivers of Net Ecosystem Exchange were Air Temperature and crop growth, with Soil Water Content and Vapour Pressure Deficit also identified as influencing factors.

Aeolian erosion of the deep peat site was 1525 (1170–1880) g m<sup>-2</sup> yr<sup>-1</sup>. At the wasted peat site, 1401 (1324–1477) g m<sup>-2</sup> yr<sup>-1</sup> was transported onto and 995 (842–1233) g m<sup>-2</sup> yr<sup>-1</sup> off the field. Net field C losses were 0.75 (0.57–0.92) t C yr<sup>-1</sup> from deep peat and 0.21 (0.18–0.26) t C yr<sup>-1</sup> from wasted peat. Field cover and field boundary vegetation height limited erosion losses.

## Acknowledgements

Firstly, I would like to thank my supervisors, Dr Jörg Kaduk, Professor Susan Page and Professor Chris Evans for all their help and guidance they have provided over the last 4 years of my PhD. I would also like to thank the technicians and support staff within the School of Geography, Geology and the Environment. In particular: Simon Benson who provided help with much of the fieldwork, Adam Cox who provided support for the technical systems and Charlotte Langley for making me feel welcome and answering so many questions I had about the University of Leicester. I would also like to thank Alex Cumming, for helping me on fieldwork and providing me with lots of explanations of how Eddy Covariance works and on data analysis.

Thank you to the University of Leicester, College of Science and Engineering who provided me with funding for my PhD. Without them, I would not have been able to perform my research and the training opportunities it has afforded me. Thank you to G's Fresh for allowing the flux towers to be located on their fields and providing information on cropping and field management. In particular I would like to thank Rob Parker, Martin Hammond and Emma Garfield who met with me on many occasions to explain farming practices.

Additionally, I would like to thank the school of Geography, Geology and the Environment for awarding me the 'Geography Award for Best Talk Postgraduate Research Day' which provided me with funding to attend and present at the WETSCAPES conference in September 2019. I would also like to thank the International Peat Society (IPS) for awarding me with the Allan Robertson award which provided the funds to be able to attend and present at the 16<sup>th</sup> International Peatland Congress in May 2021.

Thank you to the other R1 office PhD students who made my PhD fun and along with giving me advice, taught me lots about mining, volcanoes, mars, shrews, rivers and coring! Through the many ups and downs of a PhD, I would like to thank my mum and dad for always being available on the phone to chat about how things were going and my brothers (Mark and Josh) for helping me de-stress with a few video games. Thank you to my wife Sarah who has been an integral part of keeping me going until the end. There were many other people who helped me as part of both my extended and Church family and I am grateful for all the support you've given me throughout. Finally, I would like to thank God for creating such a beautiful world, and the joy it's brought me in being able to explore the secrets of how it works.

## COVID Statement

The COVID19 pandemic impacted this study. The primary impact was the suspension of fieldwork during spring and summer in 2020. This prevented field trips and therefore data collection from the field sites during this period for both the Eddy Covariance (EC) ( $\text{CO}_2$  flux) and aeolian erosion data.

This was mitigated to some extent by the farmers being able to download the EC data for me and provide basic site maintenance and crop information. Additional care was taken to check the EC data during its processing to ensure that any impacts on final  $\text{CO}_2$  flux values were minimal. As a result, two years of data collection was still possible from the field site.

Unfortunately, the aeolian erosion data collection was more severely impacted. Aeolian erosion data from both the deep and wasted peat sites was lost due to not being able to maintain or collect the dust from the collectors during the 5 month period that fieldwork was halted. As a result, the decision was made to reduce the planned one year of aeolian erosion data collection from the wasted peat site to 7 months. This 7 month period included all available data, with the last data collection taking place in March 2020, a few weeks before the pandemic started. The same was done at the deep peat site, leading to the loss of 5 months of additional data (although this was mitigated by already having data from the past 2 years). All available aeolian erosion data for both sites are presented here. The wasted peat site data were used to approximate a yearly flux value for the site, although it is appreciated that this may not be entirely representative due to the period of missing data.

## Contents

<b>Abstract.....</b>	<b>i</b>
<b>Acknowledgements .....</b>	<b>ii</b>
<b>COVID Statement.....</b>	<b>iii</b>
<b>List of Tables.....</b>	<b>viii</b>
<b>List of Figures .....</b>	<b>x</b>
<b>List of Abbreviations .....</b>	<b>xiv</b>
<b>1 Introduction .....</b>	<b>1</b>
1.1    Research Aim, Questions and Objectives .....	4
1.2    Thesis overview.....	5
<b>2 Literature Review .....</b>	<b>8</b>
2.1    Climate Change .....	8
2.2    Defining Peatlands .....	9
2.2.1    Globally Used Definitions.....	9
2.2.2    Definitions within the United Kingdom (UK).....	10
2.3    The Extent of Peatlands .....	11
2.3.1    The UK's Peatlands.....	12
2.4    Carbon Cycling in Peatlands .....	15
2.5    The NEE of Peatlands .....	20
2.5.1    What is the NEE?.....	20
2.5.2    Water Table and Temperature.....	21
2.5.3    Spatial Variability in NEE .....	22
2.6    The Impacts of Agriculture.....	23
<b>3 Methods.....</b>	<b>31</b>
3.1    Study Sites.....	31

3.1.1	Regional Climate .....	32
3.1.2	Engine Farm (EN-SP3).....	33
3.1.3	Rosedene Farm (EF-DA) .....	37
3.2	Eddy Covariance Measurements .....	41
3.2.1	Theory .....	41
3.2.2	Assumptions .....	43
3.2.3	Instrumentation .....	44
3.2.4	Raw Data Processing of EC data.....	49
3.2.5	Post Processing using Tovi .....	51
3.2.6	Energy Balance Closure .....	57
3.3	Additional C Imports and Exports other than EC .....	58
3.4	Chapter 3 Summary .....	59

## **4 Engine Farm: Drivers of CO<sub>2</sub> fluxes and a field-scale C budget at a wasted agricultural fen peatland ..... 61**

4.1	Environmental conditions .....	61
4.1.1	Air (Ta) and Soil (Ts) Temperature .....	61
4.1.2	Global Radiation (Rg).....	62
4.1.3	Rainfall and Water Table Depth.....	64
4.2	Drivers of CO <sub>2</sub> fluxes at a wasted agricultural fen peatland .....	65
4.2.1	Examination of the drivers of Reco.....	65
4.2.2	Examination of GPP as a driver of NEE.....	71
4.2.3	Discussion of Drivers of CO <sub>2</sub> emissions .....	80
4.3	Chapter 4 Summary .....	84

## **5 A field-scale C budget at a wasted arable agricultural lowland fen peatland ..... 85**

5.1	Energy Balance Closure (EBC) .....	86
5.1.1	Year one: 17 <sup>th</sup> May 2018 to 17 <sup>th</sup> May 2019.....	86

5.1.2	Year two: 17 <sup>th</sup> May 2019 to 17 <sup>th</sup> May 2020.....	88
5.2	Net Ecosystem Exchange (NEE).....	89
5.2.1	Summary of Daily NEE, GPP and Reco from 17 <sup>th</sup> May 2018 to 17 <sup>th</sup> May 2019 ...	90
5.2.2	Summary of Daily NEE, GPP and Reco from 17 <sup>th</sup> May 2019 to 17 <sup>th</sup> May 2020 ...	93
5.3	Field Carbon Balance.....	95
5.3.1	Import and Export of C from the field.....	95
5.3.2	Comparison between cumulative C flux data periods .....	99
5.4	Discussion.....	101
5.4.1	Energy Balance Closure (EBC) .....	101
5.4.2	EN-SP3: Differences in NECB between the years.....	102
5.4.3	Carbon emissions with peat depth and soil C % .....	108
5.4.4	Estimation of Emissions from the UK's wasted peatlands .....	112
5.5	Chapter 5 Summary .....	113

## **6 Aeolian erosion from two agricultural fen peatlands within East Anglia..... 115**

6.1	Aeolian erosion from peatlands.....	115
6.2	Methodology.....	118
6.2.1	Study Sites .....	118
6.2.2	Dust and Anemometer Data Collection .....	118
6.2.3	Raw Data Collection and Processing .....	122
6.2.4	Horizontal Mass Flux (HMF) and Horizontal Mass Transfer (HMT) calculation	123
6.3	Results .....	124
6.3.1	Engine Farm, EN-SP3 .....	124
6.3.2	Rosedene Farm, EF-DA.....	132
6.4	Discussion.....	136
6.4.1	HMF .....	136
6.4.2	HMT .....	138

6.4.3	The Fate of Eroded Material .....	143
6.5	Mitigation of Aeolian Erosion .....	145
6.6	Chapter 6 Summary .....	145
<b>7</b>	<b>Conclusions .....</b>	<b>147</b>
7.1	Introduction .....	147
7.2	Chapter 4: Drivers of CO <sub>2</sub> from a wasted peatland.....	148
7.3	Chapter 5: NECB from a wasted peatland .....	150
7.4	Chapter 6: Aeolian erosion from two agricultural fen peatlands within East Anglia	153
7.5	Recommendations for future research.....	155
7.5.1	GHG emission from the UK's wasted peatlands .....	155
7.5.2	Aeolian erosion from the UK's peatlands .....	156
7.6	Chapter 7 Summary .....	157
<b>8</b>	<b>References .....</b>	<b>158</b>

## List of Tables

<b>Table</b>	<b>Title</b>	<b>Page</b>
2.1	IPCC Tier 1 and UK Tier 2 categories where emission factors have been derived for direct CO <sub>2</sub> , CH <sub>4</sub> and N <sub>2</sub> O emissions from peatlands.	11
2.2	Characteristics of different types of peatlands found in the northern hemisphere.	12
2.3	UK peatland area by the condition categories adapted from Evans et al. (2017a). Area data for England is split into deep and wasted peat.	13
2.4	UK peatland area and greenhouse gas (CO <sub>2</sub> , N <sub>2</sub> O and CH <sub>4</sub> ) emissions as CO <sub>2</sub> equivalents for each country. England is split into deep and wasted peatland areas.	15
2.5	Studies which have examined peat wastage within the East Anglian Fens.	26
2.6	Example EFs and current representative studies for CO <sub>2</sub> emissions from drained agricultural peatland in the UK and other temperate countries.	28
3.1	A list of farm management practices that occurred during the data collection period on Engine Farm, Spooners 3 field.	36
3.2	A list of farm management practices that occurred during the data collection period on Rosedene Farm, R39 field.	40
3.3	Major EC assumptions, table created from list of assumptions provided by Burba (2013).	
3.4	A description of processing steps used by EddyPro when processing raw flux data.	44
3.5	Absolute limits applied to flux variables during post processing.	50
3.6	Table 3.6. Gap filling methodology used for each case (adapted from Reichstein et al. (2005)).	52
4.1	The R <sub>10</sub> and E <sub>0</sub> values for each model parameterisation with standard error and associated R <sup>2</sup> to indicate model fit.	56
4.2	The R <sub>10</sub> and E <sub>0</sub> values for each model parameterisation and associated R <sup>2</sup> to indicate model fit.	68
4.3	Fitted model variables for each of the cropping periods examined and for the peak assimilation rate over a 4 week period with standard error indicated within the brackets.	71
4.4	Spearman's rank correlations between the residuals for the cropping and peak α cropping period.	77
5.1	Energy Balance Closure coefficients calculated through linear regression and the Energy Balance Ratio (EBR) for all data (including it being split into day and night) and for each major field management period.	78
5.2	Energy Balance Closure coefficients calculated through linear regression for all data (including it being split into day and night) and for each major field management period.	87

5.3	Maximum GPP, $R_{eco}$ and NEE for the different management periods of EN-SP3 between 17 <sup>th</sup> May 2018 and 17 <sup>th</sup> May 2019.	89
5.4	Maximum GPP, Reco and NEE for the different management periods of EN- SP3 between 17 <sup>th</sup> May 2019 and 17 <sup>th</sup> May 2020.	92
5.5	Significant C inputs and Exports from planting and harvesting during the two measurement periods mat EN-SP3.	95
5.6	Estimated NECB of the two measurement periods on EN-SP3. C imports are due to: 1. Maize planting, 2. Phacelia & Buckwheat planting and 3. Celery plug plant planting. Exports are due to: 4. Maize harvesting and 5. Celery Harvesting.	96
5.7	NECB, peat depth and where available soil C % (0–0.1 m) for studies of CO <sub>2</sub> emissions from agricultural peatlands under arable coping within the UK and Europe.	99
5.8	Most recent EF calculated for cropland by Evans et al. (2017a) and the new EF for cropland on wasted peat calculated using direct CO <sub>2</sub> data from this study. All fluxes are shown in tCO <sub>2</sub> e ha <sup>-1</sup> yr <sup>-1</sup> . Table adapted from Evans et al. (2017a).	109
6.1	Equipment used to measure the wind and dust blow at each of the field sites	113
6.2	Field boundary descriptions for each BSNE and sonic tower.	118
6.3	Yearly, highest, lowest and overall average HMF (g d <sup>-1</sup> ) from each individual array from EN-SP3.	120
6.4	Total HMT, highest, lowest and overall average HMT (g d <sup>-1</sup> ) from each individual array from EN-SP3.	128
6.5	HMT at BSNEs 1, 2, 3 and 4 and average wind speed for sonic towers 2 and 3 over the study period. Estimated amount of sediment eroded across each half of the field boundary is presented.	130

## List of Figures

<b>Table</b>	<b>Title</b>	<b>Page</b>
1.1	Percentage area of peatland under cropland and percentage of Greenhouse Gas (GHG) emissions from cropland compared to all other land uses on peatland within the UK. The percentage (%) area of Deep and Wasted peat currently being used as cropland within England. All data taken from Evans et al. (2017a).	2
1.2	Deep and wasted peatland within England. Taken from Evans et al. (2017a)	3
2.1	The locations and status of peatland within East Anglia (Natural England, 2010).	14
2.2	Carbon cycling within a near-naturally functioning peatland and a peatland which has been drained for agriculture. Microbial communities are indicated. Images modified from Page et al. (2011).	19
2.3	Wastage of peat between 1848 and 1932 recorded at Denton Fen using an iron post driven into the peat. Taken from Fowler (1933).	25
3.1	Regional and local map of the locations of study fields at Engine Farm (EN-SP3) and Rosedene Farm (EF-DA). Base map taken from Google Earth 2021, <a href="http://earth.google.com/web/">earth.google.com/web/</a> .	31
3.2	Climate data between 1968 and 2018 for average minimum and maximum monthly daytime temperature, and annual precipitation. From the NIAB station (UK Met Office, 2019).	32
3.3	EN-SP3 study site; the northern edge of the NE field boundary in mid-summer with boundary vegetation left uncut; and the southern half of the NE field boundary. Pictures taken by author.	34
3.4	Soil profile from EN-SP3 and EF-DA study sites taken from a singular borehole within the field close to the study site instrumentation. Survey performed by R.G.O. Burton & M. Bidwell, June 2021 and diagram created and used with permission from R.G.O. Burton & M. Bidwell.	35
3.5	EF-DA study site; study site focusing on the BSNE (Big Spring Number Eight) used to gather aeolian erosion data; field R39 and trees along the SW field boundary; and NE field boundary the study site is located on. Pictures taken by author.	38
3.6	Diagram showing a simplified example of eddy flux from Burba (2013).	41
3.7	How eddies transport gas particles allowing flux from a study site to be measured (adapted from Burba (2013)).	42

3.8	Eddy covariance and biometeorlogical instrumentation set up at EN-SP3. Picture taken by author.	48
3.9	Satellite image of field Spooners 3 within Engine Farm with important site features marked. Picture taken by author.	48
3.10	Eddy covariance and biometeorlogical instrumentation set up at Rosedene Farm on field R39. Picture taken by author.	49
3.11	Satellite image of field R39 within Rosedene Farm with important features marked.	49
3.12	Wind direction (frequency of counts %) and strength over the data collection period at EN-SP3 by season. It should be noted that there is reduced data for winter and spring 2019 due to instrument malfunction.	53
3.13	Reasons for data loss and removal of half hourly EC flux data during data processing and QC at EN-SP3 during the two data collection periods.	55
3.14	Flow diagram from Reichstein et al. (2005) showing how the case for gap filling was chosen and the subsequent data filling quality.	56
4.1	Monthly mean air temperature, mean seasonal air temperature, monthly mean soil temperature, mean seasonal soil temperature, monthly totals of Rg (Global Radiation), and seasonal totals of Rg.	63
4.2	Rainfall over the 27 month period of data collection (May 18 to June 20) at Engine Farm, EN-SP3, and the 50 year average..	64
4.3	Water table depth at Engine Farm on Spooners 3 field from 1 <sup>st</sup> April 2018 to 1 <sup>st</sup> June 2020.	65
4.4	Reco for data period 1 against air temperature (Ta) along with the Lloyd & Taylor Reco model, a 1:1 plot of modelled and predicted values, and analysis of the residuals against SWC.	67
4.5	Reco for data period 2 against air temperature (Ta) along with the Lloyd & Taylor Reco model, a 1:1 plot of modelled and predicted values, and analysis of the residuals against SWC.	69
4.6	The residuals of the model for period 2 over the time the field was bare (3 <sup>rd</sup> March to 2 <sup>nd</sup> May 2020) plotted against date collected.	71
4.7	The monthly diurnal pattern of NEE, VPD, Rg, Ta and Ts for 2018, 2019 and 2020.	74
4.8	Light use efficiency of the Phacelia and Buckwheat cover crop and the Celery crop, and the 4 week peak α period for Phacelia and Buckwheat and Celery crop.	76

4.9	Light use efficiency of the Phacelia and Buckwheat cover crop and the Celery crop, and the 4 week peak $\alpha$ period for Phacelia and Buckwheat and Celery crop along with the model fit $R^2$ value and associated 1:1 plot. Residuals for each model fit plotted against Ta, Ts, VPD and SWC.	79
5.1	Energy Balance Closure using quality controlled (but not gap filled) LE ( $W\ m^{-2}$ ), H ( $W\ m^{-2}$ ), Rn ( $W\ m^{-2}$ ) and G ( $W\ m^{-2}$ ) for all available data for the period 17 <sup>th</sup> May 2018 to 17 <sup>th</sup> May 2019.	86
5.2	Energy Balance Closure using quality controlled (but not gap filled) LE ( $W\ m^{-2}$ ), H ( $W\ m^{-2}$ ), Rn ( $W\ m^{-2}$ ) and G ( $W\ m^{-2}$ ) for all data for the period 17 <sup>th</sup> May 2019 to 17 <sup>th</sup> May 2020.	88
5.3	Cumulative daily Net Ecosystem Exchange (NEE), Gross Primary Productivity (GPP) and Total Ecosystem Respiration (Reco) from Engine Farm between 17 <sup>th</sup> May 2018 and 17 <sup>th</sup> May 2019.	90
5.4	Cumulative daily Net Ecosystem Exchange (NEE), Gross Primary Productivity (GPP) and Total Ecosystem Respiration (Reco) from Engine Farm between 17 <sup>th</sup> May 2019 and 17 <sup>th</sup> May 2020.	93
5.5	Cumulative C emission from EN-SP3 between 17 <sup>th</sup> May 2018 and 17 <sup>th</sup> May 2019 where a) shows the NEE and b) shows the NECB which includes inputs and offtake from crop harvesting.	97
5.6	Cumulative C emission from EN-SP3 between 17 <sup>th</sup> May 2019 and 17 <sup>th</sup> May 2020 where a) shows the NEE and b) shows the NECB which includes inputs and offtake from crop harvesting.	98
5.7	Cumulative C flux for EN-SP3 during the two years of data collection. Management practices that took place in 2018/19 are indicated above the graph, while those in 2019/20 are below.	100
5.8	The Net Ecosystem Carbon Balance at 17 different study sites in relation to Peat Depth (a) and, where available, surface soil C% (top 0.1 m) (b).	110
6.1	A. Example BSNE array from EN-SP3. B. Example sonic tower from EN-SP3. C. BSNE array at EF-DA.	119
6.2	Map of the Spooners 3 field within Engine Farm, EN-SP3. Satellite image provided by Google Maps 2019.	119
6.3	Map of field R39 situated within Rosedene farm, EF-DA. BSNE Satellite image provided by Google Maps, 2019.	121
6.4	Data collection periods for EN-SP3 and EF-DA.	122

6.5	Rose plots of wind speed ( $\text{ms}^{-1}$ ) and direction recorded by each sonic tower for each sonic anemometer over each data collection periods. Wind speed was measured in 1 minute averaging periods.	125
6.6	Air and Soil temperature over the 9 dust collection periods.	126
6.7	Average Soil Water Content ( $\theta$ ) at EN-SP3 over each Dust Collection Period, on the upwind side of the field (measured at sonic tower 1) and downwind side of the field (measured at sonic tower 3).	127
6.8	Crop growth on the field Engine SP3 whilst BSNEs were present on the field.	128
6.9	Horizontal Mass flux ( $\text{g d}^{-1}$ ) of dust from EN-SP3.	129
6.10	Horizontal Mass Transfer ( $\text{g m}^{-2} \text{d}^{-1}$ ) of dust from EN-SP3.	131
6.11	Rose plots of wind speed ( $\text{ms}^{-1}$ ) and direction recorded for each data collection period recorded from the Csat3 Sonic Anemometer as part of the Rosedene Farm EC tower set up. Wind speed was measured in 30 minute averaging periods.	132
6.12	Air and soil temperature recorded by the Rosedene Flux Tower over the dust data collection period. Number of 30 min averaging periods where air temperature averaged $< 0^\circ\text{C}$ .	133
6.13	Soil Water Content ( $\theta$ ) average at EF-DA.	134
6.14	Vegetation height from the EF-DA field site from 22/06/17 to 01/03/2020.	135
6.15	Horizontal Mass Flux ( $\text{g d}^{-1}$ ) and Horizontal Mass Transfer ( $\text{g m}^{-2} \text{d}^{-1}$ ) of dust collected from EF-DA.	135
6.16	Average HMT of each different distinct field vegetation (or lack of) period over the data collection period for EF-DA. Bars show total HMT ( $\text{g m}^{-2} \text{yr}^{-1}$ ) recorded for years of complete data collection.	136
6.17	Contribution of each collector in the Rosedene Farm BSNE array to the total HMF ( $\text{g m}^{-2}$ ) recorded for each collection period. Contribution of each collector in the Engine Farm BSNE arrays to the total HMF ( $\text{g m}^{-2}$ ) recorded for each collection period.	137
6.18	The HMT and the number of frost periods, rainfall periods, soil water content each dust collection period.	142
6.19	Examples of dust that has been deposited on a burdock leaf and nettle leaves, both of which are commonly found within the field boundaries of EN-SP3 and EF-DA.	144

## List of Abbreviations

<b>Abbreviation</b>	<b>Definition</b>
BEIS	Department for Business, Energy & Industry Strategy
BSNE	Big Spring Number Eight
C	Carbon
CCC	Climate Change Committee
CO <sub>2</sub> -C	Carbon in Carbon Dioxide
CEH	Centre for Ecology and Hydrology
CO <sub>2</sub> e	Equivalent value of carbon dioxide
d	Day
DEFRA	Department for Environment, Food and Rural Affairs
DOC	Dissolved Organic Carbon
E	East
EBC	Energy Balance Closure
EBR	Energy Balance Ratio
EC	Eddy Covariance
EF	Emission Factor
EF-DA	Rosedene Farm
EN-SP3	Engine Farm
F	Eddy flux
FAO	Food and Agriculture Organization of the United Nations
GHG	Green House Gas
GPP	Gross Primary Production
H	Sensible heat flux
h <sup>0.5</sup>	Half an hour
ha	Hectare
HMF (q)	Horizontal Mass Flux
HMT (Q)	Horizontal Mass Transfer
IDB	Internal Drainage Board
IPCC	Intergovernmental Panel on Climate Change
IRGA	Infrared Gas Analyser
IUSS	International Union of Soil Sciences
LE	Latent heat flux
MDSGF	Marginal distribution sampling gap filling
N	North
NE	North East
NECB	Net Ecosystem Carbon Balance
NEE	Net Ecosystem Exchange
NIAB	Cambridge National Institute of Agricultural Botany
NPP	Net Primary Production
NW	North West
PAR	Photosynthetically active radiation
POC	Particulate Organic Carbon
QC	Quality control

$R^2$	Coefficient of determination
Ra	Autotrophic respiration
Reco	Ecosystem respiration
Rg	Global radiation
Rh	Heterotrophic respiration
Rn	Net radiation
$r_s$	Spearman's rank
$s$	Mixing ratio (dry mole fraction)
SE	South East
Sw	Short wave radiation
SWC	Soil Water Content
Ta	Air temperature
Ts	Soil temperature
u	Horizontal wind speed in meters per second
$u^*$	Friction velocity
$\mu\text{mol}$	Micromole (one-millionth of a mole)
UNFCCC	United Nations Framework Convention on Climate Change
UoL	University of Leicester
USGS	United States Geological Survey
V	Volt
v	Z axis velocity in meters per second
VPD	Vapour Pressure Deficit
w	Vertical wind speed
w	Vertical velocity in meters per second
y	Year
$\rho_d$	Dry air density

## 1 Introduction

The lowland fen peatlands of East Anglia in the East of England are considered to be some of the most fertile land within the UK (Natural England, 2011). Widespread intensive agriculture on the fenlands allows for the growth of a wide range of horticultural and arable crops, providing many of the UK's supermarkets with salad crops, such as lettuce and celery. However, this has come at the loss of a significant amount of carbon (C) from the peat soils over the last 150 years as the fenlands have been 'reclaimed' for agriculture (Rotherham, 2013). This reclamation involved drainage, leading to consolidation, aeration and subsequent mineralization of the peat (Hutchinson, 1980, Evans et al., 2017b). The scale of this loss has been recorded since 1848 by the Holme Post, an iron pole that was driven into the peat layer with its top level with the original peat surface. Today, the post protrudes 4.8 m above the peat surface, providing a stark reminder of peat loss and subsidence over the last three centuries (Hutchinson, 1980). Today, drainage continues in an effort to keep water tables low enough to allow intensive agriculture to persist, leading to continuing peat loss.

Globally, peatlands are increasingly recognised as a critical C store. Peatlands cover just 3% of the Earth's total land area, but are estimated to store one third of the Earth's soil terrestrial C (Yu et al., 2010, Scharlemann et al., 2014). Due to their increased utilization for farming and other human land uses, peatlands globally account for 3.5% of all anthropogenic greenhouse gas (GHG) emissions (IPCC, 2013), emitting 1.91 Gt CO<sub>2</sub>e annually, and hold enough C to increase atmospheric CO<sub>2</sub> concentrations by 75% if all that C was released (Leifeld and Menichetti, 2018).

Mitigation of C loss from drained peatlands is a crucial component of meeting the international targets of global net-zero emissions by 2050 and to limiting warming to 1.5 °C compared to pre-industrial levels, as set out in the Paris Agreement (UNFCCC, 2015). Preserving or restoring peatlands are considered much more effective GHG mitigation measures than increasing C sequestration in other ecosystems (Leifeld and Menichetti, 2018, Evans et al., 2021)

The UK government is one of the 189 countries to have joined the Paris Agreement, and has set the additional target of reducing national GHG emissions by 78% by 2035 compared to 1990 (The Carbon Budget Order, 2021). The management of peatlands has been highlighted as a crucial component in achieving this target (HM Government, 2018), with studies indicating that emissions could be significantly reduced with mitigation strategies (Evans et al., 2017a, Evans et al., 2021). Overall, the UK has ~3 million hectares of peatlands (Evans et al., 2017a), which occupy 12.2 % of its total land area (Bain et al., 2011) and with an estimated GHG emission of 23,100 kt CO<sub>2</sub>e yr<sup>-1</sup> (Evans et al., 2017a).

Of these peatland emissions, arable cropland is estimated to contribute 7,600 kt CO<sub>2</sub>e yr<sup>-1</sup>, accounting for 32% of total peatland emissions in the UK from only 7% of the UK peatland area (Figure 1.1a). This value is calculated from emissions data derived only from deep peats and not from 'wasted' peats (formerly deep peat which has ≤ 0.4 m peat and is becoming increasingly dominated by the underlying mineral layer). Wasted peats account for 3% of peatland within the UK, with most under some form of agricultural management. There have been no studies to date to measure GHG emissions from wasted peatlands in the UK, hence it has not been possible to assess the contribution that they make to national GHG emissions.

In England, most of the estimated 186,372 ha of wasted peat soils are primarily under either arable or horticultural agriculture, with two thirds of cropland on peatlands located on wasted peat (Figure 1.2). Most is located within the East Anglian Fens (Figure 1.1b). Their predominance in this region is a consequence of the long history of peatland drainage for agriculture (Hutchinson, 1980), resulting in formerly deep peat soil profiles being greatly reduced as a result of many decades of peat oxidation and erosion.

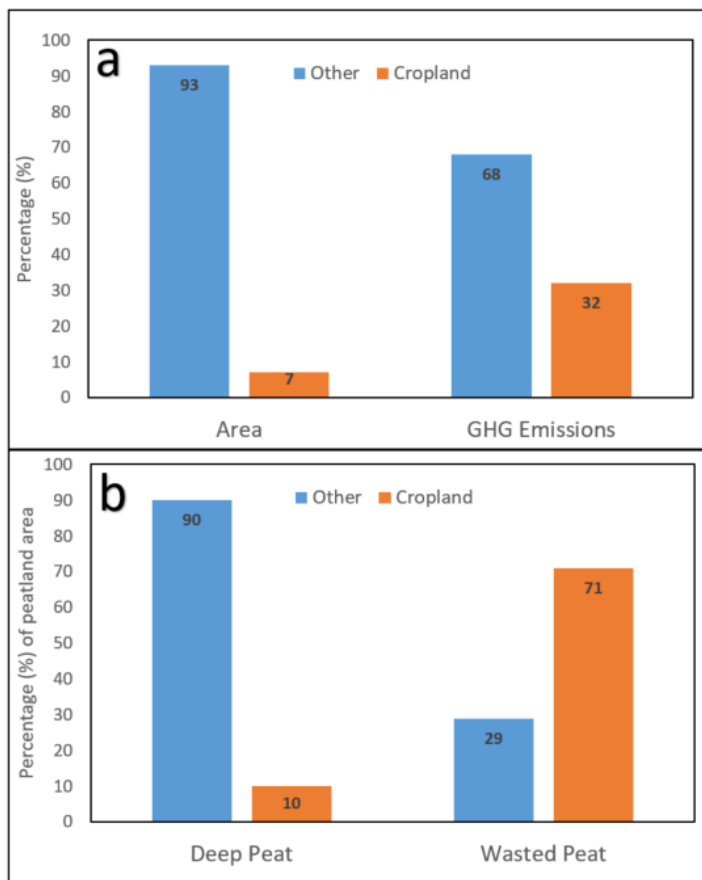


Figure 1.1(a) Percentage area of peatland under cropland (orange) and percentage of Greenhouse Gas (GHG) emissions from cropland compared to all other land uses on peatland within the UK. (b) The percentage (%) area of Deep and Wasted peat currently being used as cropland (orange) within England. All data taken from Evans et al. (2017a).

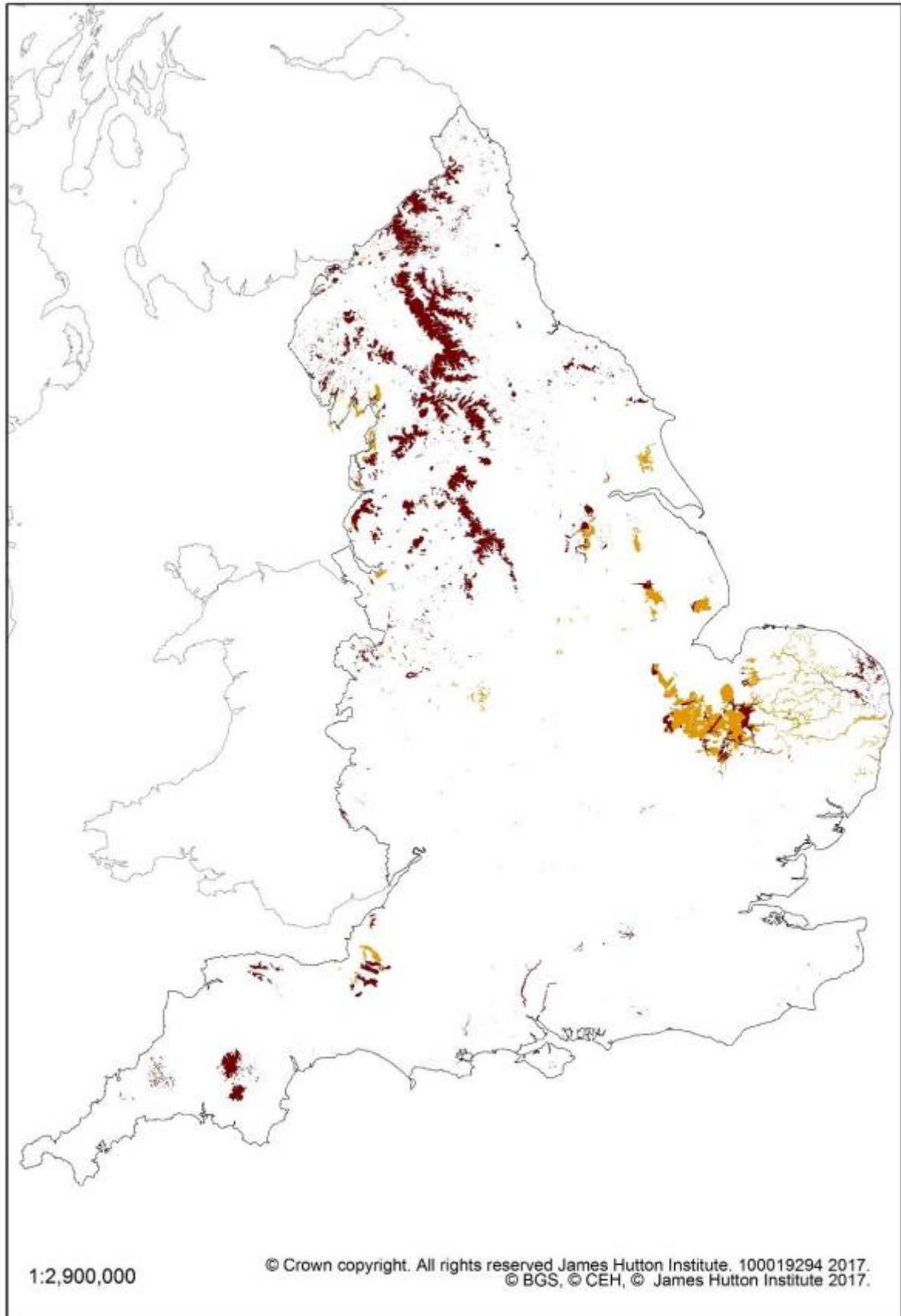


Figure 1.2. Deep (brown) and wasted (yellow) peatland within England. Taken from Evans et al. (2017a).

The large area of wasted peatland under agriculture represents a significant knowledge gap, with the most recent GHG inventory produced for the UK's peat highlighting that estimates of emissions from wasted peatlands remain uncertain (Evans et al., 2017a). This is particularly true of wasted peats under agriculture, which make up their primary land use (Figure 1.1b).

Of primary importance is understanding the CO<sub>2</sub> flux from wasted peatlands, since CO<sub>2</sub> emissions make the greatest contribution (74%) to total anthropogenic emissions (IPCC, 2013). Deep peatlands have been shown to be high emitters of CO<sub>2</sub>, with peat oxidation the primary pathway by which C is lost to the atmosphere from drained peatlands (Evans et al., 2017b). Knowledge of other pathways for C loss, such as wind driven (aeolian) soil erosion, is limited, with no studies to date of aeolian erosion and C loss from UK wasted peatlands. This is despite accounts of significant historical (Pollard and Millar, 1968) and current wind erosion episodes (Rob Parker, pers. comm.) within the East Anglian Fens.

Against this background, there is an identified need to develop accurate inventories of current C emissions from croplands on wasted peatlands within the UK. This thesis addresses this need by providing the first estimates of CO<sub>2</sub> emissions and of aeolian erosion from an intensively managed, arable, agricultural lowland wasted peatland. The research results not only contribute to improved understanding of the scale of C emissions from wasted peat soils, allowing the development of more accurate Tier 2 emission factors for the UK emissions inventory, but also provide land managers with insights into the drivers of emissions and an evidence base in support of the development of appropriate emissions mitigation practices.

## 1.1 Research Aim, Questions and Objectives

The overall aim of this thesis is to address the knowledge gap surrounding the lack of GHG emission (CO<sub>2</sub>) and aeolian erosion data from agriculturally managed lowland fen peatlands in the UK, specifically those which have undergone significant drainage and peat depletion and are now classified as wasted. This aim has been achieved through the collection of two years of CO<sub>2</sub> flux data from a wasted agricultural peatland and the collection of aeolian soil erosion data from a deep and wasted agricultural peatland (two years and seven months of data, respectively). The research questions below were addressed by the following objectives, with the relevant chapters indicated in brackets:

1. What are the key drivers of Net Ecosystem Exchange (NEE) from a wasted lowland peatland under arable agriculture? (Chapter 4)
  - To set up and maintain an Eddy Covariance (EC) flux tower over a multi-year period.

- To analyse CO<sub>2</sub> flux data in relation to meteorological and field management events to highlight key drivers of NEE.
2. What are the C emissions from a wasted lowland peatland under arable agriculture with varying crop and field management? (Chapter 5)
- To calculate the first daily and annual fluxes of NEE, Gross Primary Productivity (GPP) and Ecosystem Respiration (Reco) for a wasted lowland peatland under arable agriculture through multiple years and varying cropping and field management practices.
3. Do the C emissions from a wasted lowland peatland under arable agriculture vary compared to those from arable agriculture on deeper lowland peat? (Chapter 5)
- To calculate the first yearly Emission Factor (EF) for wasted lowland peatland under arable agriculture.
    - To compare the yearly C emission with those measured on deeper lowland peats under similar management practices.
4. What are the magnitudes of aeolian soil erosion and C flux on deep and wasted lowland peatlands under arable and horticultural agriculture? (Chapter 6)
- To set up and maintain BSNE (Big Spring Number Eight) dust collectors at a wasted and deep agricultural fen peatland.
    - To provide the first field-scale balance of aeolian erosion on a wasted lowland peatland under agriculture.
    - To compare aeolian erosion results from wasted peat with a multi-year record of aeolian erosion from a deep fen peatland under agriculture.
5. What are the environmental and field management practices that impact aeolian soil erosion? (Chapter 6)
- To compare aeolian erosion data from different field management and meteorological periods to discover key drivers of aeolian erosion.
    - To compare erosion data from multiple differing field boundaries.

## 1.2 Thesis overview

This thesis consists of seven chapters covering: A review of the current literature, the methodology used for this work, an examination of the drivers of CO<sub>2</sub> flux, the C balance of a wasted peatland, and the aeolian erosion from a wasted peatland. These are followed by a conclusion. A brief overview of each chapter is provided:

## **Chapter 2: Literature Review**

This chapter provides the background and a critical look at the current knowledge within the topics considered in the rest of the thesis. An overview is given of the importance peatlands within the wider landscape of GHG emissions and policy. This is followed by information on how peatlands are defined and their extent leading into a discussion of how C is cycled within peatlands and the drivers of GHG emissions, with a specific focus on CO<sub>2</sub>. The chapter concludes with a review of current knowledge of the impacts of agriculture on fen peatlands, with particular focus given to the UK's fen peatlands. Gaps within current understanding are highlighted as the foundation for the research described in the rest of the thesis.

## **Chapter 3: Methodology**

The location of and background information on the field sites are given including a brief history of climate for the region. Field site management and cropping practices that took place over the study period are described. The chapter then focuses on the theory of the Eddy Covariance (EC) method which was used to measure CO<sub>2</sub> and energy flux over the data collection period. This includes the instrumentation used, and the methods for data processing, quality control, gap filling and evaluating the data's quality.

## **Chapter 4: Drivers of CO<sub>2</sub> flux from a wasted agricultural East Anglian fen peatland**

This chapter examines the drivers of the emission of CO<sub>2</sub> flux over the two year data collection period from the main study site: Engine Farm – Spooners 3 (EN-SP3). The temperature sensitivity of Ecosystem Respiration (Reco) was examined by modelling night time Net Ecosystem Exchange (NEE) as a function of air temperature (Ta), with the impacts of Soil Water Content and farm management practises also examined. Gross Primary Productivity (GPP) for two crops in relation to Photosynthetically Active Radiation (PAR) was also examined along with the limiting environmental factors.

## **Chapter 5: A field-scale C budget of a wasted agricultural East Anglian Fen peatland over 2 years**

This chapter describes the magnitude of daily and yearly CO<sub>2</sub> fluxes at EN-SP3, providing an assessment of CO<sub>2</sub> fluxes throughout fallow and cropped periods. This is followed by a discussion of the variations between the magnitude of fluxes in relation to meteorology and field management and cropping practices. The wider implications of the research are explored with an examination of the relationship between peat depth and soil C %, and peatland C emissions

from similar studies across Europe. This chapter concludes with the derivation of a proposed Tier 2 emission factor for UK wasted peatland.

### **Chapter 6: Aeolian erosion from deep and wasted agricultural East Anglian Fen peatlands**

This chapter describes the magnitude of aeolian erosion from deep (Rosedene Farm, EF-DA) and wasted (EN-SP3) agricultural peatland sites, including an estimation of the amount of C transported within the eroded soil fraction. The fate of eroded material along with the drivers and controls of erosion are discussed, and suggestions made for field management practices to mitigate soil loss.

### **Chapter 7: Conclusions**

This final chapter provides a synthesis of the key findings from each of the data chapters (4, 5 and 6) along with a discussion of the limitations of the research and a discussion of areas that require further investigation.

## 2 Literature Review

### 2.1 Climate Change

Since pre-industrial times, GHG concentrations ( $\text{CO}_2$ ,  $\text{CH}_4$  &  $\text{N}_2\text{O}$ ) within the Earth's atmosphere have increased dramatically, reflecting the imbalance of GHG emissions from human activity with natural oceanic and terrestrial sinks (IPCC, 2013). Concentrations of Carbon Dioxide ( $\text{CO}_2$ ) had increased by 40% since 1750 to 391 ppm in 2011 (IPCC, 2013). Since 2011, further increases in  $\text{CO}_2$  have been observed with current atmospheric concentrations reaching 419 ppm in June 2021 (ESRL NOAA, 2021) and concentrations predicted to likely increase above 700 ppm by 2100 (IPCC, 2013, Nazarenko et al., 2015). This increase of GHG concentrations in the Earth's atmosphere from anthropogenic emissions has caused a steady rise in the Earth's surface temperature of  $0.85^\circ\text{C}$  between 1880–2012. Global temperature is estimated to rise between  $2.6^\circ\text{C}$  and  $4.8^\circ\text{C}$  by the end of this millennium relative to the 1986–2005 period under a "business as usual" emission scenario (RCP 8.5 used by the IPCC) (IPCC, 2013).

The impacts of such a temperature rise will have far reaching climatic effects. Increasing frequency of severe weather, changes in the terrestrial water cycle, temperature change and sea level rise are predicted to have significant world-wide impacts (IPCC, 2013, Donnelly et al., 2017, Serdeczny et al., 2017), some of which are already being observed (Loisel et al., 2017, Cui et al., 2018).

Globally, through the Paris agreement (UNFCCC, 2015) 191 countries, including the UK, have committed themselves to the target of limiting warming to  $2^\circ\text{C}$  compared to pre-industrial levels with the aim of limiting warming to  $1.5^\circ\text{C}$  by the end of century to reduce the environmental and socioeconomic impacts of a changing climate. Within the UK, increasingly aggressive targets to limit GHG emissions have been adopted. Currently, the UK government has committed to reduce emissions to 78% by 2035 and to be net zero by 2050, when compared to 1990 levels (2021).

Whilst the UK has made progress towards these goals, emissions reduced by 40% from 1990 to 2019, further significant mitigation is required to meet the target of a 78% reduction by 2035 (CCC, 2021). The recent Climate Change Committee (CCC) Report (2021) highlighted that progress within agriculture has failed to meet indicators set to reduce emissions and that more work is required within this area to meet emissions targets. The recent implementation of an emissions inventory for UK peatlands (Evans et al., 2017a), emphasised that agriculture on peatlands has a large potential for GHG mitigation, with cropland estimated to emit  $\sim 7,600 \text{ kt}$

$\text{CO}_2\text{e yr}^{-1}$  from 7% of the UK's peatland area. Peatlands themselves have been highlighted as priority habitats within the government's 25 year Environment Plan (HM Government, 2018) with the recent England Peat Action Plan (HM Government, 2021) funding the restoration of 35,000 ha of peatland by 2025. UK peatlands currently account for emissions of 23,100 kt  $\text{CO}_2\text{e yr}^{-1}$  (Evans et al., 2017a), thus a better understanding of their carbon (C) dynamics can support improved peatland management and make a critical contribution to the UK Government attaining emissions targets in the future. In particular, the C dynamics of the UK's wasted peatlands are currently not well quantified, despite two thirds of their area being used for intensive agriculture, which likely makes them a substantial contributor to total peatland emissions (Evans et al., 2017a).

## 2.2 Defining Peatlands

### 2.2.1 Globally Used Definitions

Peat forming wetlands (peatlands) are located within every continent on earth and consist of a diverse range of peat forming ecosystems from tropical peatland formed by peat swamp forest to temperate and boreal peatlands dominated by *Sphagnum* moss (Limpens et al., 2008, Strack, 2008). In their natural state, a peatland is characterised by an organic soil with a fluctuating, near surface water table allowing for the accumulation of partially decomposed organic matter due to low decomposition rates.

Globally, peats are often referred to as Histosols, as per the USGS (United States Geological Survey) and FAO (Food and Agriculture Organization of the United Nations) soils definitions (FAO, 1997, Soil Survey Staff, 2014). However, these terms are not exclusive, for example: within Australia they are known as "Organosols", whilst the terms 'muck' or 'muck soils' are also broadly used, particularly within Canada where they form part of the organic soil order (Agriculture and Ari-Food Canada, 1998).

Whilst these terms are generally interchangeable, definitions for what constitutes an organic soil vary with region: The USGS define a soil as a histosol (or histel where covered by permafrost) if half or more of the top 0.8 m of the soil profile is primarily organic material, consisting of between 12-18% organic matter or more by weight depending on clay content (Soil Survey Staff, 2014). This is very similar to the Australian definition (more than 0.4 m of organic materials in the top 0.8 m of soil) whilst the Canadian soil classification is slightly different, with Canada defining 'muck' soils as 0.4 m of >30% organic matter by weight in the top 0.8 m of soil (Canada Soil Survey Committee, 1978). Many soil scientists within Europe use the FAO's World Reference Base soil classification (which is attempting to unify soil classifications globally) where at least

0.4 m of the top 1 m of soil contains organic material or 0.6 m if 75% (by volume) of moss fibres (IUSS Working Group, 2015).

## 2.2.2 Definitions within the United Kingdom (UK)

Within the UK, classification of peat soils varies between countries with Scotland and Ireland having their own distinct classifications compared to England and Wales (JNCC, 2011). All definitions within the UK originate from the ‘Soil classification of England and Wales’ (Avery, 1980), which defines peat as an organic deposit of at least 0.5 m in depth which contains greater than 50% organic material within the top 0.8 m of the soil profile. Within England and Wales, a peat soil is often defined as a soil containing 20% or more organic matter to a depth of greater than 0.1 m (JNCC, 2011, Natural England, 2010). Within the UK, the typical C content of peat is around 52% (Lindsay, 2010).

Peatlands are then further subdivided into two classifications:

1. ‘Deep peats’ where the layer of peat is greater than 0.4 m thick.
2. ‘Shallow peats’ where the layer of peat is between 0.1 m and 0.4 m thick.

Additionally, the degradation state of the peatland is often also classified. While a detailed set of classification criteria has been set out for raised bogs (Lindsay and Immirzi, 1996), a simplified version is often used to describe the degradation state of all peatlands (JNCC, 2011). Broadly this sets out 5 categories:

1. Active Peat – Which defines a near or semi-natural peatland which retains or has regained its peat forming capability. It is characterised by high water tables and complete peat forming vegetation cover.
2. Degraded Peat – Where through adverse management such as changing water table, vegetation has been altered from primarily peat forming. Peat forming capabilities have been lost.
3. Bare Peat – Which defines a peatland where all vegetation has been removed and peat forming capability lost but has not undergone significant degradation through land use change.
4. Archaic Peat – Bare peat which has been drained deeply and undergone some form of cultivation or cropping. Soil oxidation leads to large amounts of CO<sub>2</sub> release.
5. Wasted Peat – A peatland which has lost its peat-forming vegetation and a significant depth of original peat soil through drainage and cultivation, leading to the peat becoming more dominated by the underlying mineral layer.

Of these five degradation classifications, wasted peat has become one of the most important categories due to the increasingly large area it covers within the UK, particularly in the UK's fenlands (Natural England, 2010, Evans et al., 2017b). While the descriptive definition of wasted peat given above is widely used, it is hard to determine exact criteria for a wasted peat. For example, within East Anglia, all fen peat has undergone some degree of peat loss and subsidence, with many cultivated 'deep peats' having lost over 1.0 m of material (for example Rosedene Farm site (EF-DA), cited in (Evans et al., 2017b)) and to a degree its original characteristics. Within the UK, it has become common for a deep peat to be classified as wasted once it has a remaining peat layer  $\leq$  0.4 m and shows a reduction in organic content from its former deep peat status as the underlying mineral layer begins to dominate. Within recent emission inventories, peatlands are often referred to by their emission factor (EF) category which describes the condition of the peatland along with its land use, with descriptors becoming increasingly specific with increasing emission factor tier (Table. 2.1).

*Table 2.1. IPCC Tier 1 and UK Tier 2 categories where emission factors have been derived for direct CO<sub>2</sub>, CH<sub>4</sub> and N<sub>2</sub>O emissions from peatlands (Evans et al., 2017a).*

IPCC Tier 1 category	UK Tier 2 category
Forest land, drained	Woodland
Cropland,	Cropland
Grassland, drained, nutrient-poor	Modified eroded bog Modified bog Extensive grassland
Grassland, deep drained, nutrient-rich	Intensive grassland
Peatland managed for extraction	Extracted Domestic Extracted industrial
Rewetted organic soils, nutrient poor	Rewetted bog Near natural bog
Rewetted organic soils, nutrient rich	Rewetted fen Near natural fen

### 2.3 The Extent of Peatlands

Peatlands are globally vital ecosystems due to the ecosystem services they provide, in particular their function as a long term C store. Peatlands store ~550 Pg C of the 1460.5 Pg C (504–3000 Pg C, n = 27 studies) of Earth's terrestrial soil C within 3% of the Earth's land area, making them C-dense ecosystems and critical components of C cycling (Gorham, 1991, Yu, 2012, Scharlemann et al., 2014).

Peatlands are found on every continent on Earth (Strack, 2008, Loisel et al., 2017). Most peatlands were initiated and formed within the Holocene period, with average accumulation rates of 19, 13 and 22 g C m<sup>-2</sup> yr<sup>-1</sup> estimated for northern, tropical and southern peatlands respectively throughout the Holocene period (Yu et al., 2010). These slow rates of C accumulation indicate formation over millennia, and whilst restored and near natural peatlands have been found to sequester C (Clymo et al., 1998, Nwaishi et al., 2016, Borren et al., 2004, Cui et al., 2017, Loisel et al., 2017), long term accumulation rates are low (19.0 to 69 g C m<sup>-2</sup> yr<sup>-1</sup>) (Borren et al., 2004). In many cases, calculated accumulation rates are over estimates and do not take into account that not all C additions to the surface peat layer will become part of the long term C store, with recently formed peat still subject to some decomposition (Young et al., 2019). This allows peat to be thought of as a finite resource, which once lost will not be replaced. Peatlands are differentiated via hydrogeochemistry into two trophic classes: Bogs (ombrotrophic peatlands) and Fens (minerotrophic peatlands) (for more information, see Table 2.2).

*Table 2.2. Characteristics of different types of peatlands found in the northern hemisphere.*

Peatland Type	Characteristics
Bog	Bogs are ombrotrophic peatlands receiving all water and nutrients meteorically leaving them nutrient poor. Bogs are acidic (3.5–4.2) unless located near ocean areas (Rydin and Jeglum, 2013). Sphagnum mosses are the keystone species in bogs (Hájek and Vicherová, 2014) and are the primary peat forming vegetation in northern peatlands.
Fen	Fens are minerotrophic peatlands water entering the peatland has passed on or through a surrounding mineral soil leading to base-rich waters. Fens are further classified via pH gradient into poor (4–5.5), intermediate and moderately rich (5–7) and extremely rich (6.8–8). The pH of a fen is influenced by the properties of the parent rockwater entering the peatland (Rydin and Jeglum, 2013) and ratio of water from meteoric origins (Worrall et al., 2011).

### 2.3.1 The UK's Peatlands

The total UK's land area currently consists of over ~3,000,000 ha of peatlands, covering 12.2% of the UK's total land area (Evans et al., 2017a) and containing at least 2302 Mt C (Billett et al., 2010). This represents the largest soil C stock in the UK. It should be noted that estimated total C is likely an underestimate due to calculation of soil C being based on old peatland area estimates. The largest proportion of peatlands are located within Scotland (68%), whilst England contains the second largest area (18%) (Table. 2.3).

The largest area of peat in England is found within blanket bogs and upland valley mires (52%) of the Pennines, Lake District, the North Yorkshire moors and the South West uplands. Approximately 5% of England's peatlands are classified as raised bogs, while the remaining 40% are classified as lowland fens (Natural England, 2010).

*Table 2.3. UK peatland area by the condition categories adapted from Evans et al. (2017a). Area data for England is split into deep and wasted peat. Currently, no data is available to do the same for other countries.*

Country	England		Scotland	Wales	NI
Peat Category	Deep peat	Wasted peat	All	All	All
Forest	51,764	13,728	332,746	9,520	31,534
Cropland	50,594	132,107	8,181	102	3,141
Drained Eroded Modified Bog	5,653	0	75,147	19	2,170
Undrained Eroded Modified Bog	43,560	8	198,116	206	3,470
Drained Heather Dominated Modified Bog	19,208	0	155,196	1,588	6,667
Undrained Heather Dominated Modified Bog	87,166	55	409,154	6,237	10,702
Drained Grass Dominated Modified Bog	24,053	0	33,130	1,588	6,667
Undrained Grass Dominated Modified Bog	32,992	1,833	87,344	29,000	15,747
Extensive grassland	1,377	518	31,794	8,993	1,932
Intensive grassland	38,416	35,265	78,641	6,577	31,248
Near Natural Bog	83,930	2,348	490,497	23,548	35,915
Near Natural Fen	0	0	0	2,674	0
Extracted Domestic (fuel peat)	4,254	137	44,923	0	87,539
Extracted Industrial (horticultural)	4,627	1	2,881	0	525
Rewetted Bog	23,784	286	0	0	5,032
Rewetted Fen	24,451	86	0	0	334
Total	<b>495,829</b>	<b>186,372</b>	<b>1,947,750</b>	<b>90,050</b>	<b>242,623</b>

Whilst 83,930 ha of near natural bog still remains in England, there is no near natural fen and only 86 ha of re-wetted fen. Within England, fen peats are primarily situated within

Cambridgeshire, Lincolnshire and Norfolk (Figure 2.1). Almost all fen peatland within the UK is used for some form of agriculture on both deep and wasted peats, with 182,701 ha (37%) of England's peat area classed as cropland (Table 2.3) Most fen peats are currently classified as grade 1 agricultural land, i.e. they are considered the most fertile and productive soils in Britain (Natural England, 2011), and this high fertility has provided the motivation for their drainage and cultivation.

Within the East Anglian region, almost all of the fens are being drained and cultivated (Figure 2.1). This has led to on-going mineralisation leading to the loss of peat at a rate of  $1\text{--}2 \text{ cm yr}^{-1}$  (Richardson and Smith, 1977, Burton and Hodgson, 1987). This loss can be observed most dramatically at the Holme Post, where 3.9 m of peat loss was recorded between 1848 and 1978 (Hutchinson, 1980). This loss of peat depth has led to many formerly deep fen peats now being classified as wasted. Indeed, the majority of the fen peatland within East Anglia is classified as wasted and makes the largest contribution to the 186,372 ha of wasted peat within England.

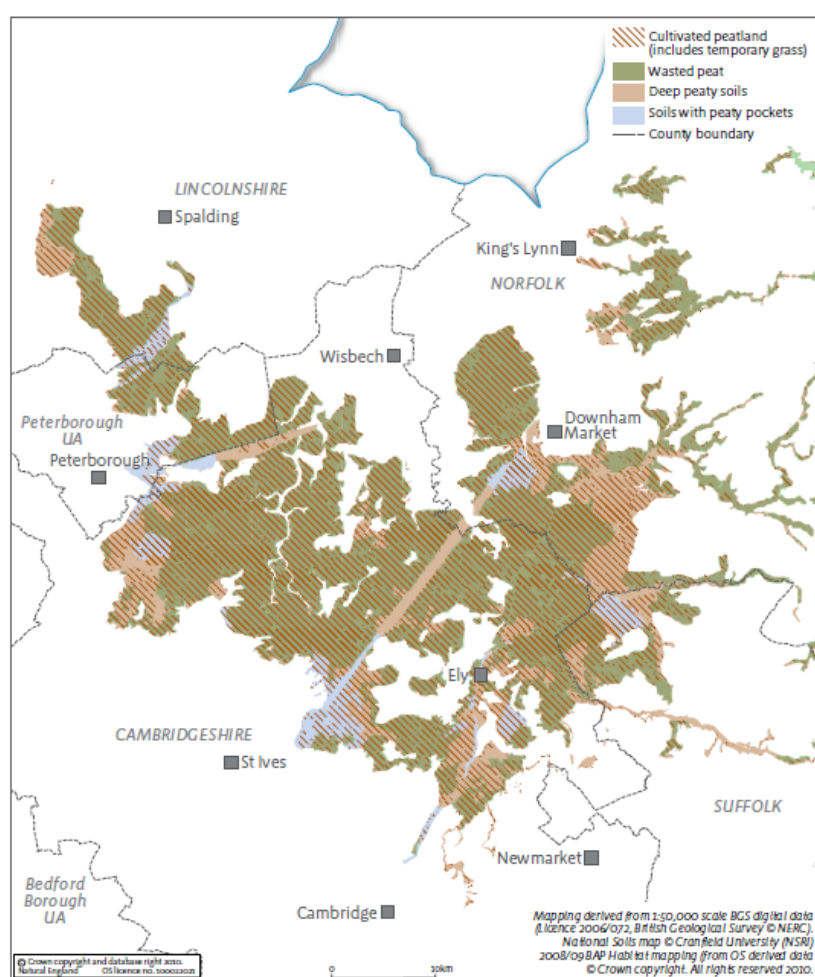


*Figure 2.1. The locations and status of peatland within East Anglia. Almost all of the former deep peat is classified as wasted and is under cultivation. Areas where the peat remains uncultivated are associated with nature reserves and restoration schemes (Natural England, 2010).*

The continued degradation and mineralisation of England's peatlands accounts for a significant amount of UK GHG emissions. In total, UK peatlands account for 23.2 Mt CO<sub>2</sub>e yr<sup>-1</sup>; of this total, English peatlands make the largest contribution of 10.9 Mt CO<sub>2</sub>e yr<sup>-1</sup> (Evans et al., 2017a), with wasted peatlands accounting for 59% of the emission despite only occupying 17% of England's total peatland area. A large part of this emission is due to arable cropland, which accounts for 7.6 Mt CO<sub>2</sub>e yr<sup>-1</sup> (31%) of the UK's total peatland emissions, and with two thirds derived from wasted peat, primarily within the East Anglian Fens. These emissions estimates highlight the significant contribution of lowland fen peats to both England's and the UK's total GHG emissions. It should be noted, however, that emissions from cropland on wasted peat are currently not well quantified, with studies to date focused on deep peats.

*Table 2.4. UK peatland area and greenhouse gas (CO<sub>2</sub>, N<sub>2</sub>O and CH<sub>4</sub>) emissions as CO<sub>2</sub> equivalents for each country. England is split into deep and wasted peatland areas, this was not possible with other countries due to lack of data on peatlands where emissions were measured. \*Wasted peat emissions are estimated from data on non-wasted peatlands and are uncertain.*

Country	Area (ha)	Emissions (Mt CO <sub>2</sub> e yr <sup>-1</sup> )
Scotland	1,947,750	9.6
England	Deep: 495,828	4.5
	Wasted: 86,372	6.4*
	Total: 582,200	10.9
Wales	90,050	0.5
Northern Ireland	242,622	2.2
United Kingdom	3,145,197	23.2

## 2.4 Carbon Cycling in Peatlands

C cycling within peatlands is complex, involving multiple pools linked by a varying array of processes. These processes lead to the transport of C both vertically and horizontally, in numerous different forms. In near-natural peatlands, the primary drivers of C cycling are the uptake of C via photosynthesis (also referred to as Gross Primary Productivity, GPP), and the release of C through autotrophic (Ra) and heterotrophic (Rh) respiration in the form of CO<sub>2</sub> and methane (CH<sub>4</sub>) (Page et al., 2011).

Autotrophic respiration is responsible for the release of ca. 40–50% of the C fixed through photosynthesis as CO<sub>2</sub> from both plant and root systems (Dawson and Smith, 2007, Smith et al., 2010). The rest is fixed as Net Primary Production (NPP), which ultimately provides the C in dead organic matter, a portion of which is available for long term storage as peat.

Heterotrophic respiration is the biological decomposition of stored organic matter (including peat), plant litter, root exudates and organisms within the soil by microbes utilising aerobic and anaerobic decomposition; Rh causes the loss of up to 90% of this C to the atmosphere as either CO<sub>2</sub> or CH<sub>4</sub> (Page et al., 2011, Rydin and Jeglum, 2013). Decomposition involves the breakdown of fresh plant litter that has been recently accumulated but also that accumulated over millennia; these differences can be important when considering the net C balance of the peatland. Collectively, these processes can be summarised as Net Ecosystem Productivity (NEP) (Dawson and Smith, 2007) where Reco is the summation of Ra and Rh (Equation 2.1):

$$NEP = GPP - Reco \quad \text{Equation 2.1}$$

The position of the water table is the key abiotic factor affecting the rate of decomposition (Hatala et al., 2012, Evans et al., 2017b, Evans et al., 2021), and thereby directly influences both the amount and type of microbial respiration (Rydin and Jeglum, 2013). The water table of a peatland directly affects the redox potential within the near-surface peat layer (the acrotelm) where most decomposition occurs. Within deeper peat layers below the water table (the catotelm), decomposition proceeds much more slowly and mostly by anaerobic processes.

It has been observed that CO<sub>2</sub> and CH<sub>4</sub> emissions show an inverse relationship (Laine and Vasander, 1996, Evans et al., 2017b, Evans et al., 2021). Within near-natural or restored peatlands where a near-surface water table prevails, anaerobic (anoxic) conditions prevail near or up to the peat surface, leading to microbial CH<sub>4</sub> production via methanogenic Archaea (Levy et al., 2012). In contrast, drained peatlands, such as those under agricultural management, exhibit primarily aerobic (oxic) conditions within the near-surface peat layer, leading to the microbial production of CO<sub>2</sub> (Limpens et al., 2008) with increasing CO<sub>2</sub> emissions observed with increasing depth of the water table (Evans et al., 2021).

Peat accumulation occurs within near-natural peatlands whose water tables are conducive to enabling primarily anaerobic conditions; this suppresses the rate of decomposition since anaerobic decomposition is a much slower process than aerobic decomposition and allows plant material to accumulate and become incorporated into the peat surface. This C then undergoes long term storage providing anoxic conditions are maintained, subject to a very slow anaerobic decay rate in the order of 0.0001 cm yr<sup>-1</sup> (Rydin and Jeglum, 2013). Methane emissions from anoxic peat layers rise up through the overlying peat layer via ebullition (Baird et al., 2004, Tokida et al., 2007), or diffusion and transport through vascular wetland plants (Brix et al., 2001), to be emitted back to the atmosphere.

Temperature is another important factor controlling the rate of Rh, due to its effect on microbial activity and thus ecosystem respiration (Lloyd and Taylor, 1994, Limpens et al., 2008, Preston et al., 2012), particularly when water is not limiting (Parmentier et al., 2009). In general, Rh is seen to increase with both increasing air and peat temperatures, with the temperature response ( $Q_{10}$ ) shown to be larger at low temperatures (Svensson, 1980, Lafleur et al., 2005).

The quality of decomposable substrate (Limpens et al., 2008, Rydin and Jeglum, 2013) is also known to impact microbial activity and in turn soil respiration for both CO<sub>2</sub> and CH<sub>4</sub> (Bergman et al., 1998) production. Substrates with higher quantities of easily degradable C show higher rates of decomposition (Rydin and Jeglum, 2013). This leads to differences in the decomposition rates of different types of peatlands whose peat has differing plant origins (Verhoeven and Toth, 1995, Scheffer et al., 2001, Preston et al., 2012). The proportion of C that is lost through decomposition impacts the overall accumulation rate of C within a near natural peatland. In this way it is possible for a *Sphagnum*-dominated nutrient poor fen, exhibiting low productivity but also low decomposition, to have a higher C accumulation rate than a sedge-dominated nutrient rich fen (Glenn et al., 2006).

Whilst gaseous exchange at the peat surface is central to a peatland's overall rate of C accumulation, an additional proportion of C is lost through fluvial and aeolian export. Fluvial C is leached from the organic matter and then lost as either Dissolved Organic Carbon (DOC), Particulate Organic Carbon (POC) or Dissolved Inorganic Carbon (DIC) (Billett et al., 2010, Dinsmore et al., 2013) into the surrounding hydrological pathways. It is then subjected to biodegradation with a significant proportion re-emitted as CO<sub>2</sub> and CH<sub>4</sub> via evasion from the water surface, whilst the rest is transported laterally (Dyson et al., 2011, Teh et al., 2011, Evans et al., 2016). DOC, POC and DIC represent a significant lateral transport mechanism for organic C at a landscape scale (Pawson et al., 2007, Dinsmore et al., 2010).

Aeolian C loss occurs through wind erosion of bare peat (Warburton, 2003) and has the potential to be an important loss pathway of C from some peatlands at ecosystem scale. Aeolian erosion is a particular feature of agriculturally managed peatlands which tend to be managed with a water table that may be at or below 1 m from the peat surface leading to the drying out of the soil surface (Evans et al., 2017b). In addition, agricultural peatlands are often left bare for months at a time between crop cycles which again increases the risk of aeolian C loss (Funk and Engel, 2015). A more detailed review of the literature surrounding aeolian C loss from peatlands can be found in Chapter 6.

Within agricultural peatland systems, there can be additional inputs and exports of C in the form of seeds or additive substrates (e.g. growing media) and exports of the harvested crop (Aubinet et al., 2009, Smith et al., 2010, Cumming, 2018, Wen et al., 2019). To account for these gains and losses, the Net Ecosystem C Budget (NECB) can be calculated, which is the overall net C lost or gained from all sources (Chapin et al., 2006). Studies on peatlands primarily consider the NEE (Net Ecosystem Exchange) (e.g. Dinsmore et al., 2009, Mander et al., 2012, Hadden and Grelle, 2017, Taft et al., 2017), with individual studies often focusing on one aspect of NECB (e.g. Huttunen et al., 2003, e.g. Warburton, 2003, Pawson et al., 2007). It is common for studies on agricultural peatlands to provide NEE alongside an estimated NECB that includes the C imported and exported via crop planting and harvesting, which is the largest C flux other than CO<sub>2</sub> exchange within these ecosystems (e.g. Elsgaard et al., 2012, Poyda et al., 2016, Cumming, 2018).

Currently, most near-natural peatlands are considered to be a small net C sink while peatlands that have been drained or undergone agricultural management are a net C source. Figure 2.2 summarises these processes and the differences between a natural and a degraded peatland.

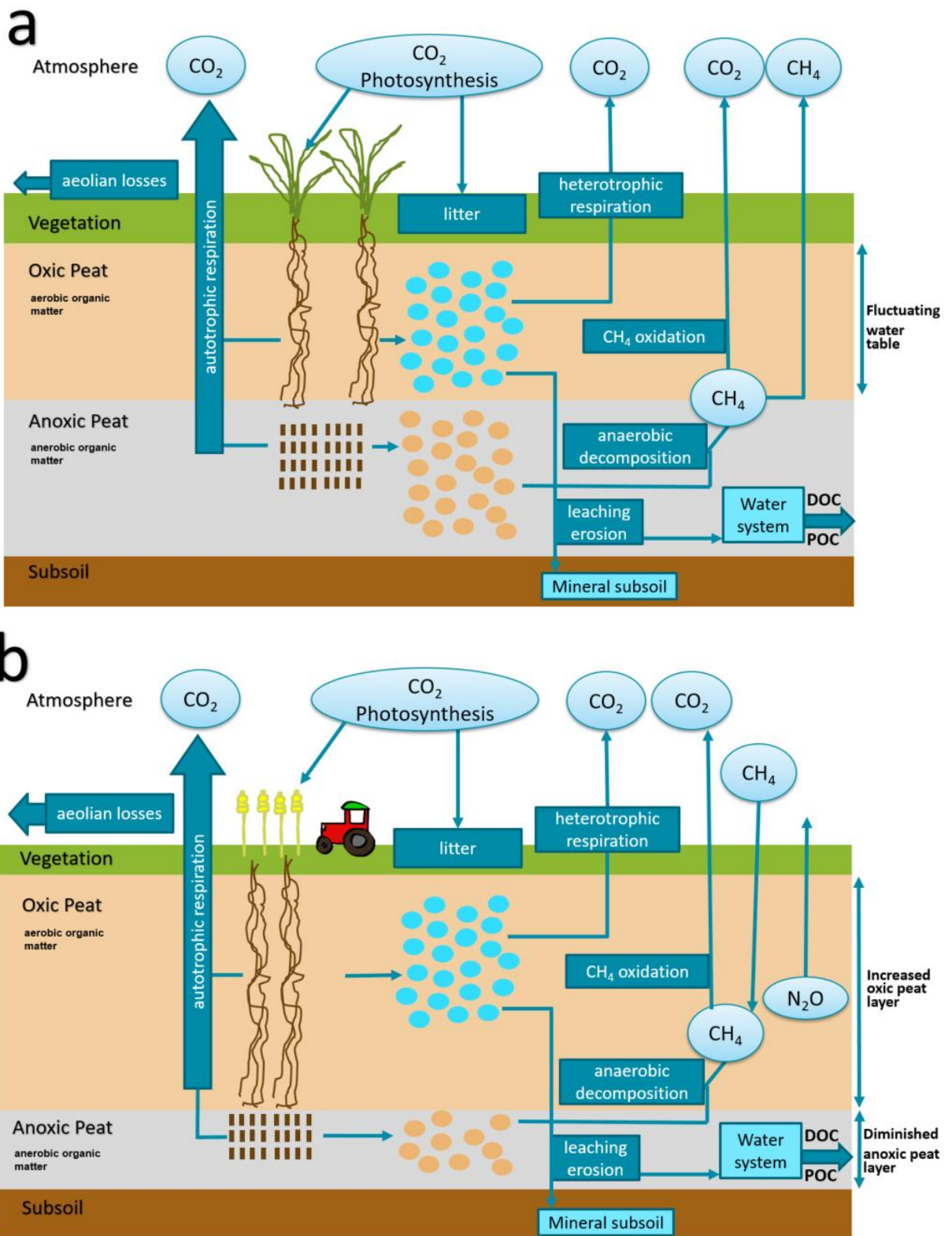


Figure 2.2. Carbon cycling within (a) a near-naturally functioning peatland and (b) a peatland which has been drained for agriculture. Within (a), seasonally fluctuating water tables lead to changes in the depth of the oxic peat layer, which may not be present at all within periods of wet weather or seasonal flooding. Within the agricultural peatland (b), the oxic layer is increased significantly through artificial drainage. In some severely depleted agricultural peatlands, water tables may drop below the peat horizon, leaving no remaining anoxic layer. Microbial communities are indicated by blue (aerobic) and brown (anaerobic) circles. Images modified from Page et al. (2011).

## 2.5 The NEE of Peatlands

### 2.5.1 What is the NEE?

Within peatlands, the biggest proportion of C flux is through gas exchange in the form of CO<sub>2</sub> between the peatland and the atmosphere (Roulet et al., 2007). The overall CO<sub>2</sub> flux of a peatland is defined as the Net Ecosystem Exchange (NEE) and is the summation of the individual CO<sub>2</sub> fluxes into and out of the peatland. Thus, the NEE is calculated using the equation:

$$NEE = Reco - GPP \quad \text{Equation 2.2}$$

Where Reco is Ecosystem Respiration and GPP is Gross Primary Productivity of the ecosystem.

Within this literature review, the sign convention used is a positive NEE to denote a flux from the peatland (source / emission of C), whilst a negative NEE denotes a net flux into the peatland (sink / accumulation of C). As NEE encompasses the two biggest fluxes into and out of a peatland (Rydin and Jeglum, 2013), its magnitude is crucial to determining the overall C balance, often forming the core of NECB (Dawson and Smith, 2007, de Wit et al., 2015).

Ecosystem respiration consists of numerous processes (detailed within Figure 2.2 above), that influence the overall gas balance of a peatland. In particular, ecosystem respiration is sensitive to moisture and temperature (Reichstein et al., 2003, Cai et al., 2010, Juszczak et al., 2013, Rezanezhad et al., 2016). This leads to a significant amount of variability in NEE between peatland ecosystems and within the same ecosystem due to both spatial and temporal climatic variability.

Peatlands are heterogeneous leading to small scale variations of Reco and GPP to occur. To capture these variations, the NEE of a peatland ecosystem is often measured using the eddy covariance technique which attempts to capture all positive and negative CO<sub>2</sub> fluxes into and out of the ecosystem (Baldocchi, 2003). Additionally, the use of the chamber method to capture gas flux is also commonly used to infer NEE or other trace gas exchanges from peatlands (more information in Chapter 3, Methods) (Elder and Lal, 2008, Taft et al., 2017). By using the eddy covariance method, the NEE of a peatland can be recorded continuously over a period of time to give the emissions status of a peatland. Typically, NEE is recorded over multiple years to account for inter-annual variability in gas flux due to climatic variability.

In general, GPP in natural peatlands is higher than Reco, leading to the steady accumulation of C as peat (Rydin and Jeglum, 2013). Yu et al. (2010) estimated that accumulation rates over the last millennia within northern peatlands were ~ 20 g C m<sup>-2</sup> yr<sup>-1</sup>, making them significant C sinks. Currently, C accumulation rates for these peatlands are lower (Malmer and Wallén, 2004) in part

due to the natural decrease of C accumulation rates over time (Rydin and Jeglum, 2013), but also due to changing climate over the past millennia which has caused fluctuations throughout the Holocene period.

### 2.5.2 Water Table and Temperature

Within a naturally functioning peatland, NEE encompasses the main drivers of both C loss and accumulation, through photosynthesis and Reco. As the balance between GPP and Reco is regulated primarily by the temperature and the hydrology of the peatland, fluctuations in these two factors can significantly affect the C source / sink status of a peatland. Studies have shown that a relative increase in the water table leads to a reduction in Reco and an overall decrease in NEE (Dinsmore et al., 2009, Susilawati et al., 2016, Chimner et al., 2017, Jeanneau et al., 2020, Evans et al., 2021). Conversely, lowering of the water table leads to aeration of previously anaerobic peat leading to increased decomposition, a decrease in substrate quality and overall an increase in Reco, leading to positive NEE values (Evans et al., 2017b, Hribljan et al., 2017).

Atmospheric warming has been shown to increase soil respiration (Bardgett et al., 2008, Craine et al., 2010) leading to a positive increase in NEE. Additionally, studies on peatlands using experimental warming have shown increases in both Reco and photosynthesis (e.g. Moore et al., 1998, Davidson and Janssens, 2006, Dorrepaal et al., 2009, Cai et al., 2010, Flanagan and Syed, 2011). Despite some studies suggesting that the increase in photosynthesis will exceed that of Reco under warmer conditions (Melillo et al., 2002, Flanagan and Syed, 2011), the general consensus is that warming will increase Reco more than photosynthesis, leading to a positive increase in NEE.

It is suggested that the regional response to warming will vary due to increased temperature sensitivity of soil organic C in cold regions (Melillo et al., 2002, Dorrepaal et al., 2009). This is due to the increased sensitivity of soil respiration at low temperatures (Kirschbaum, 1995, Biasi et al., 2005). The sensitivity of NEE to temperature and hydrology causes peatlands to show significant variations in NEE between growing seasons and inter-annually due to climatic variations (Bubier et al., 2003, Riutta et al., 2007, Teh et al., 2011). Within agricultural peatlands, this can be further exacerbated through management practices and crop cycling (Taft et al., 2017). As temperature is widely considered to be the key driver of Reco, a model for Reco derived from temperature is often used to partition or gap fill missing CO<sub>2</sub> fluxes (Lloyd and Taylor, 1994, Reichstein et al., 2005) (See Chapter 3.2.5.6).

### 2.5.3 Spatial Variability in NEE

Within northern peatlands (peatlands with arctic, sub-arctic, boreal and temperate climates), there is a clear contrast in reported NEE between peatlands from each region. Whilst the overall NEE of arctic, sub-arctic and boreal fens has been found to be between -1.89 and 1.00 t CO<sub>2</sub>-C ha<sup>-1</sup> yr<sup>-1</sup> (Morrison, 2013), reported fluxes from temperate regions (with permanent vegetation cover) are found to be much larger, ranging from -4.66 to ~2.20 t CO<sub>2</sub>-C ha<sup>-1</sup> yr<sup>-1</sup> (Morrison, 2013). This reflects the impact of the warmer temperatures coupled with longer growing seasons found within the temperate regions, which increase plant productivity (Teh et al., 2011), and the high fluxes from agriculturally managed peatlands (Evans et al., 2017b).

To date, there have been multiple studies within North America and Europe (e.g. Teh et al., 2011, Lai et al., 2012, Taft et al., 2017) which have examined the NEE of temperate peatlands. However, very few of these studies examine near natural temperate fens whilst there are multiple studies which examine the NEE of natural and near-natural temperate bogs (e.g. Lloyd, 2006, Essl et al., 2012, Nijp et al., 2017). This is largely due to the rarity of natural temperate fen peats, with almost all exhibiting the impacts of anthropogenic modification (Billett et al., 2010, Natural England, 2010, JNCC, 2011). The most comparable studies are those which have been conducted on natural boreal fens (Huttunen et al., 2003, Myers et al., 2012, Lozanovska et al., 2016, Wang et al., 2017b). To date, there is only one study from within the UK which examines a semi-natural fen under permanent vegetation cover, with (Peacock et al., 2019) finding that Wicken Sedge fen (undrained peatland under management by the National Trust) was a strong C sink of -1.24 t CO<sub>2</sub>-C ha<sup>-1</sup> yr<sup>-1</sup>.

The focus of a number of recent studies on temperate peatlands has been on peatlands under agricultural management (e.g. Berglund and Berglund, 2010, Evans et al., 2017b, Hadden and Grelle, 2017, Cumming, 2018) or those which have undergone some degree of re-wetting and restoration (e.g. Günther et al., 2015, Harpenslager et al., 2015, Karki et al., 2015). Within the UK, initial research into the C fluxes of peatlands was centred on ombrogenous peat systems (e.g. Nieven et al., 1998, Worrall et al., 2003, Billett et al., 2010, Ward et al., 2013) and extraction sites. Over the last 10 years, the increasing realisation of the importance of the UK's lowland fen peats in terms of both C storage (Natural England, 2010) and emissions (Worrall et al., 2011, Evans et al., 2017b) has led to a number of studies focusing on them. To date, relatively few studies have been conducted looking at restored or managed (Lloyd, 2006, Morrison, 2013, Evans et al., 2017b) and agricultural (Morrison et al., 2013, Evans et al., 2017b, Musarika et al., 2017, Taft et al., 2017, Cumming, 2018) lowland peatlands in the UK. Currently, the Tier 2 EF for

cropland on drained peatland is primarily derived from agriculturally managed lowland fens on deep peat (7.2 [95% CI: 4.0, 10.5] t CO<sub>2</sub>-C ha<sup>-1</sup> yr<sup>-1</sup>) (Evans et al., 2017a) (Table 2.5). Given that 32% of the total UK peat GHG emissions originate from the 7% of peatlands under arable cropland, these systems are a considerable source of emissions (Evans et al., 2017a). However, these emissions estimates are derived from a very limited number of studies at a small number of sites, and they likely do not capture the full range of variation in peat depth, management or degradation status. Overall, there is a marked difference in emissions between agriculturally managed fens and fens which have been re-wetted (Evans et al., 2017b, Evans et al., 2017a): peatlands with higher water tables emit less CO<sub>2</sub> than those which have been drained (Evans et al., 2021). However, there is currently debate within the literature as to whether these peatlands are a net GHG source or sink, due to high methane emissions (Mitsch et al., 2013, Chimner et al., 2017).

Overall, the importance of England's agricultural lowland peatlands as a source of GHG emissions is starting to become recognised at governmental level (HM Government, 2018, CCC, 2021). To further our current understanding of the impacts of agricultural practices on the C balance of England's lowland peatlands, significant knowledge gaps still need to be filled. Specifically, there are no known measurements of C fluxes from agriculturally managed wasted peats within the UK, something which has been highlighted as a key knowledge gap that could have a significant bearing on the overall GHG accounting for lowland peatlands (Evans et al., 2017b, Evans et al., 2017a). This is the primary data gap that this thesis aims to address.

## 2.6 The Impacts of Agriculture

Since the mid 1600's, large areas of the UK's peatlands have been 'improved' for agricultural use (Rotherham, 2013). Whilst initially this was via small scale 'improvements', facilitated primarily by man power, the advent of ever improving technology and an ever increasing need for greater farming productivity, have led to the drainage of extensive tracts, including almost all of the East Anglian fens (Rotherham, 2013). Today only 1% of England's deep peatlands can be considered to be actively accumulating peat (Natural England, 2010).

Drainage is a requirement for agricultural use of peatlands for three main reasons: 1. To allow the soil to be worked via farm machinery 2. To allow non-native wetland grassland, horticultural and agricultural species to be grown 3. To aerate the soil (Strack, 2008). For agricultural or grassland communities to be grown, lowering of the water table to 0.8 m below the peat surface for grassland and to 1–1.2 m for agricultural crops is required (Strack, 2008), although records from agricultural peatlands in East Anglia show that often the water table fluctuates between

0.6 and 1.0 m below the surface (Evans et al., 2017b, Evans et al., 2021). This allows a large portion of the top layer of peat to become aerated.

Once land has been drained and the peat forming vegetation removed, the peatland loses its peat forming capacity and begins to undergo irreversible changes (Hutchinson, 1980, Strack, 2008, Dawson et al., 2010). Subsidence of the peat surface begins to occur through a combination of consolidation, shrinkage and oxidation.

Consolidation occurs due to the loss of buoyancy of the upper peat horizons as the water is removed, compressing the saturated peat layers (Strack, 2008). This process occurs during the initial stages of drainage, reducing over time as the pore structure of the upper peat layers collapse under their own weight (Holman, 2009). Over time, this process increases the bulk density of the peat, however it does not cause a loss of peat material or C from the peatland.

Shrinkage of the peat is a similar process to consolidation. It is the loss of volume of the peat material as water is lost through both drainage and evaporation (Dawson et al., 2010), leading to an increase in bulk density. Similarly, no material is lost from the peat, so C content is maintained. Historic subsidence rates due to shrinkage and consolidation of  $18 \text{ cm yr}^{-1}$  have been reported within the UK (Hutchinson, 1980, Holman, 2009), although these can vary regionally due to climatic factors and the consistency of the original peat (Strack, 2008). Both consolidation and shrinkage can be exacerbated by agricultural traffic which leads to further compaction of the peat.

Oxidation of the peat occurs once the upper peat layers become aerated and aerobic conditions become prevalent. This allows heterotrophic decomposition (biological oxidation) under oxic conditions which emits accumulated C back into the atmosphere as  $\text{CO}_2$  (Couwenberg, 2011). Once the initial phase of consolidation and shrinkage of the peat has occurred, oxidation takes over as the largest factor causing peat subsidence (Hooijer et al., 2012). The rate of oxidation decreases over time as the most labile C is used up leaving the less decomposable recalcitrant C behind (Rydin and Jeglum, 2013). However, it is also possible for the rate to be accelerated via liming, mineral soil mixing and increasing the rate of wetting and drying (Holman, 2009). Eventually, oxidation will lead to the total loss of peat. The removal of the original peat forming vegetation drastically lowers the productivity (Strack, 2008) further compounding the disparity between Reco and GPP, particularly where fields are left bare over significant periods of time.

Further depletion of peat can occur via wind erosion (Warburton, 2003, Cumming, 2018) and hydrological transportation (DOC/POC) (Dinsmore et al., 2010, Evans et al., 2016) and the loss of peat trapped within the roots or leaves of crops that are removed at harvest. It is also possible

for peat to be imported into agricultural systems, with some crops grown in ‘plugs’ consisting of peat-based growing media, although the amount of imported C is less than the amount lost through other processes (Cumming, 2018).

Overall, drainage and cultivation have led to high rates of peat loss and the drastic lowering of the peat surface in the East Anglian fens over the last 400 years. At both Holme Fen and Denton Fen, the extent of subsidence has been measured using iron posts driven into the mineral substrate below the peat layer (Fowler, 1933, Hutchinson, 1980). At Holme Fen, 3.91 m of wastage was recorded between 1850 and 1978 (Hutchinson, 1980), while at Denton Fen, 3.45 m of wastage occurred between 1848 and 1932 (Figure 2.3, (Fowler, 1933)).



*Figure 2.3. Wastage of peat between 1848 and 1932 recorded at Denton Fen using an iron post driven into the peat. Taken from Fowler (1933).*

Both these numbers likely underestimate the peat lost up to the present day. Wastage rates in the fens have been recorded by nine studies, and range between 0.1 and 9.2 cm yr<sup>-1</sup> (Table 2.5) depending on the timing of the measurements and the land use. Higher rates of wastage are associated with periods of initial drainage (due largely to initial consolidation and shrinkage).

Contemporary studies indicate that higher rates occur on land used for intensive agriculture, with rates between 0.88 and 2.1 cm yr<sup>-1</sup> (Table 2.5) depending on the thickness of the peat, the type of peat and the underlying geologies (Holden, 2005, Dawson et al., 2010). Whilst these wastage rates give a good idea of present day loss rates, it is important to note that the actual loss rate for any individual area within the Fens will vary due to the heterogeneity of the peat. Additionally, there is a current lack of understanding of the impacts of agricultural processes on loss rates, particularly on the agriculturally managed wasted peats.

*Table 2.5. Studies which have examined peat wastage within the East Anglian Fens.*

Reference	Description	Wastage (cm yr <sup>-1</sup> )
Fowler (1932)	An average peat wastage value for the East Anglian Fens over two distinct periods: Wind pump use and intensive drainage for cultivation.	0.6 (wind pump) 2.5 (intensive drainage)
Fowler (1933)	Record of peat wastage at Denton fen from 1848 to 1932 from markings on an iron post.	3.87
Clark et al. (1935) and Clark and Godwin (1962)	Record of peat wastage at Shippea hill, Isle of Ely from 1934 to 1962.	1.8
Richardson and Smith (1977)	Wastage from between 1941 and 1971 across 14 sites within the fens.	1.37 ± 0.78
Hutchinson (1980)	Record of peat wastage on Holm fen at the Holm post from 1848 to 1978. Divided into 4 stages: (1) 1850–1877: initial pumping. (2) 1877–1924: New pump and change to grazing from arable. (3) 1924–1962: Diesel pumps installed. (4) 1962–1978: New pumps installed.	3.5 (Overall) 9.2 (Stage 1) 1.2 (Stage 2) 1.8 (Stage 3) 1.1 (Stage 4)
EPG (2006)	Wastage rates for deep (> 1m) and thin (>1 m) peat within lowland drained wetlands (including East Anglian Fens).	1.27 (deep) 0.19 (thin)
Holman (2009)	Based on past literature, estimated the current wastage rates of deep (>1 m) and thin (<1 m) peats under different land management scenarios.	Deep: 2.1 (Intensive arable) 0.8 (Intensive grassland) 0.4 (Semi-natural) Thin: 1.3 (Intensive arable) 0.7 (Intensive grassland) 0.1 (Semi-natural)
Dawson et al. (2010)	Peat wastage over a 22-year period of 1982/3 to 2004 calculated using a topographic study within the Methwold Fen area. Sites were grouped into 3 types: (A) Fibrous peat with underlying fen clay. (B) Fibrous peat with no underlying fen clay. (C) Humified peat without underlying fen clay. An addition soil survey was carried out on 33 points and depletion averaged (mean).	1.48 (mean) 1.50 (A) 1.89 (B) 0.88 (C)  1.10 (Soil survey)

Peat drainage, cultivation and loss have had considerable impacts in the East Anglian Fens. One of the most visible changes is the loss of natural fenland habitat and associated loss of biodiversity (Rotherham, 2013). Lower land levels have led to an increased flood risk (Dawson et al., 2010) and subsequent need for ever increasing intensity of pumped drainage (Morris et al., 2010). Land subsidence has also resulted in deformation and damage to built infrastructure (e.g. buildings and transport routes). However, the most important impact, given the need to limit climate warming, is the increase in GHG emissions.

Naturally functioning peatlands are a long term CO<sub>2</sub> sink and despite being a source of CH<sub>4</sub> they are overall considered to be net global coolers (Strack, 2008). But if water levels decrease, changes occur in the peat's physical, hydraulic and subsequently chemical properties, resulting in a change in the emissions of CO<sub>2</sub>, CH<sub>4</sub> and N<sub>2</sub>O from the peatland (Strack, 2008, Rydin and Jeglum, 2013, Evans et al., 2021). Within agricultural peatlands, CH<sub>4</sub> (methane) emissions reduce with lowering of the water table (e.g. Kasimir-Klemedtsson et al., 1997, Beyer et al., 2015, Chimner et al., 2017), even approaching sink status (Taft et al., 2017). This is likely due to the increased depth of the oxic layer favouring methanotrophs (Rydin and Jeglum, 2013), and a reduction in the size and activity in the anoxic methanogenic communities (Strack and Waddington, 2007). The exception to this is ditch emissions, which become hotspots for CH<sub>4</sub> flux (Teh et al., 2011, Evans et al., 2016). Conversely, N<sub>2</sub>O (nitrous oxide) emissions are enhanced (Kasimir-Klemedtsson et al., 1997, Evans et al., 2017a) due to increased mineralisation rates (Strack, 2008), particularly at nutrient rich sites which have undergone fertiliser application and have high soil nitrate concentrations (Wen et al., 2019).

CO<sub>2</sub> mineralisation accounts for the biggest GHG flux from drained agricultural peatlands (Teh et al., 2011, Evans et al., 2017b, Taft et al., 2017). CO<sub>2</sub> Emission Factors (EFs) for temperate agricultural peatlands are often generalized and reported at national level (IPCC, 2014), however in recent years there have been several EFs calculated for agricultural fens peatlands in Europe (e.g. Langeveld et al., 1997, Tubiello et al., 2013, Poyda et al., 2016) and the UK (e.g. Evans et al., 2017b). EFs are either derived from direct measurements (using chamber or eddy covariance methods) (e.g. Morrison et al., 2013, Taft et al., 2017, Cumming, 2018), or are estimated from peatland subsistence rates (e.g. Leifeld et al., 2011) and modelling (Kandel et al., 2018). A summary of the current state of UK knowledge on agricultural lowland peatland CO<sub>2</sub> emission and EFs is provided in Table 2.6. This table highlights the requirement for additional CO<sub>2</sub> flux measurements in order to derive appropriate EFs for temperate agricultural wasted peats nearing complete depletion. This will allow more accurate regional upscaling of emissions to be calculated (highlighted by Evans et al., 2017b).

Table 2.6. Example EFs and current representative studies for CO<sub>2</sub> emissions from drained agricultural peatland in the UK and other temperate countries.

Reference	Description	t CO <sub>2</sub> -C ha <sup>-1</sup> yr <sup>-1</sup>
<b>Regional EFs</b>		
IPCC (1996), IPCC (2006)	<b>Regional EF</b> for the temperate region for croplands with confidence given in brackets.	10 ( $\pm$ 90%)
IPCC (2013)	<b>Tier 1 EF</b> for boreal and temperate drained cropland (95% confidence in brackets)	7.9 (6.5 to 9.4)
Tubiello et al. (2016)	<b>Calculated the EFs</b> of croplands on organic soils at country level by estimating the extent of drained organic soils and associated emissions geospatially. These were then used to compute nation statistics in FAOSTAT.	Denmark: 5.0 Finland: 5.0 Germany: 5.02 UK: 5.2 USA: 12.08
<b>UK EFs</b>		
Evans et al. (2017b)	<b>UK Tier 2 EF</b> from 20 studies on drained peatland used for arable and horticultural crops using data primarily derived from deep peat soils.	7.2 (95% CI: 4.0 to 10.5)
Evans et al. (2016)	<b>Review of 15 studies.</b> Emission value for cropland Based on three sites within the UK (two within the East Anglian Fens using EC, one on Little Woolden Moss (a deep peat bog) using chambers). CO <sub>2</sub> flux estimates take account of C removed via harvest biomass.	6.94 (6.47 to 7.58)
Taft et al. (2017)	<b>Study</b> based on cropland sites within the East Anglian Fens in the UK. CO <sub>2</sub> flux from cropped soil (horticultural) across three differing SOC contents using the chamber method.	5.2 to 8.3
Cumming (2018)	<b>Study</b> based on a deep peat cropland site within the East Anglian Fens in the UK. CO <sub>2</sub> measured over 3 years using EC, takes into account imported and export C through planting and harvesting.	7.6 $\pm$ 0.9
<b>Other Example Temperate EFs</b>		
Maljanen et al. (2007)	<b>Study</b> on cropped organic soils in Finland (barley) from three different sites which used chambers and EC.	2.1 to 8.3
Elder and Lal (2008)	<b>Study</b> on a cropland site in Ohio, USA under varying intensities of tillage on a very degraded organic soil.	18.9 to 20.8
Berglund and Berglund (2010)	<b>Study</b> on CO <sub>2</sub> loss estimated via subsidence rates of organic soils under cropping (except row crops) in Sweden on agricultural shallow (<50 cm) and deep peat soils.	5.2 to 7.9
Berglund and Berglund (2010)	<b>Study</b> on CO <sub>2</sub> loss estimated via subsidence rates of organic soils under row cropping in Sweden on agricultural shallow (<50 cm) and deep peat soils.	8.8 to 13
Kandel et al. (2018)	<b>Study</b> on three drained and cropped (oat-potato, oat-spring barley, potato-spring barley) Danish bogs using static chambers and an empirical model.	12.4 to 16.3

Whilst all EFs for agriculture on peatlands indicate that they are a source of C, CO<sub>2</sub> emission rates are variable (Table 2.6). Some of this variation can be accounted for by the different methods used and assumptions made when calculating the EFs. The rest of this variation can be accounted for by: 1) Peat heterogeneity, 2) Climate, 3) Varying agricultural management practices, 4) Drainage depth, 5) Crop type, and 6) Time since initial drainage (Kasimir-Klemetsson et al., 1997, Tubiello et al., 2016, Evans et al., 2017b, Taft et al., 2017, Evans et al., 2021).

There is an ever-growing knowledge of emissions from the cultivated lowland fen peatlands of East Anglia, with several studies being conducted within the last 10 years (Morrison et al., 2013, Evans et al., 2017b, Taft et al., 2017, Cumming, 2018, Evans et al., 2017a). The current Tier 2 EF produced by Evans et al. (2017a) for cropped peatland is 7.2 t CO<sub>2</sub>-C ha<sup>-1</sup> yr<sup>-1</sup> (95% CI: 4.0 to 10.5) which is similar to the 95% confidence limits of the IPCC 2013 Tier 1 EF for drained peatlands under crops in boreal and temperate regions (6.5 to 9.4 t CO<sub>2</sub>-C ha<sup>-1</sup> yr<sup>-1</sup>) but with increased uncertainty (Table 2.6). This uncertainty is introduced due to the large area of wasted peat under cropland in England, which has no representative study. Taft et al. (2017) reported a decrease in CO<sub>2</sub> emission on peat with a lower Soil Organic Carbon (SOC) content (~20% compared to ~35% and ~70% at 1 m depth). Similarly, Evans et al. (2016) found peat depth varied between field sites, with deeper peat (>2.0 m) leading to higher CO<sub>2</sub> emissions than shallower peat (~1.0 m), however, neither of these studies examined the relationship in detail.

Between current studies of emissions from cropped peatland on deep peat, there is still a wide variation in reported emissions (Table 2.6). This is likely due to the impacts that individual management practices and inter-annual climatic variation have on emissions which are not captured by short term datasets. Evans et al. (2016) showed that timing and nature of soil disturbance and water management both had an influence on CO<sub>2</sub> loss from arable sites with Evans et al. (2021) indicating that raising or lowering the water table for a period of time could impact CO<sub>2</sub> emissions. Tillage has been found to increase CO<sub>2</sub> emissions in the period during and immediately after disturbance due to the increased aeration of the surface soil layer (Morrison et al., 2013). Interestingly, while crop selection is the biggest factor for NEE, no significant effect has been seen in overall C emission once C removal from harvesting the crop is taken into account (Evans et al., 2017b), although studies so far have examined only similar horticultural and arable crops.

While current studies have allowed Tier 1 and Tier 2 EFs to be calculated for the UK's lowland agricultural fens as a whole, several knowledge gaps have been highlighted which limit the

production of a truly accurate and full quantification of the GHG budget (Evans et al., 2017b). Of primary importance is the lack of any study focused on wasted peat under conventional agricultural management. Currently the closest representation is from studies of shallow peat sites which still retain ~80 cm peat depth (Evans et al., 2017b). The large area occupied by wasted peats in the UK, along with data from soil cores which has demonstrated they still contain a large stock of C (Evans et al., 2017b), indicates their potential for continuing large emissions even after significant peat loss. Therefore, it is expected that agricultural wasted fen peats continue to be a large source of GHG emissions, and one that is critical to our understanding of both current and future emissions from the UK's peatlands.

### 3 Methods

This chapter describes the study sites and the methods for data collection and analysis. This includes a detailed description of each study site location and site set up, the associated theory and methods used to calculate the carbon fluxes, specifically the use of Eddy Covariance (EC) to measure CO<sub>2</sub> flux, and the post processing and quality assessment methods used to quality control the raw flux data. The methods used for assessment of the aeolian flux are addressed in Chapter 6.

#### 3.1 Study Sites

All study sites are located in the East Anglia region of the East of England, UK (Figure 3.1). This region is characterised by a temperate oceanic climate (Kottek et al., 2006), leading to varying temperatures throughout the year across four distinct seasons. Due to the influence of the polar front jet stream, weather is often changeable, with the East of England seeing the greatest variations in yearly temperatures across the whole of the UK. All field sites were situated on lowland fen peatland under intensive agricultural management; the primary field site was situated on ‘wasted’ peat (Engine Farm (EN-SP3)) and the second on ‘deep’ peat (Rosedene Farm (EF-DA)) (Natural England, 2010). Both peatlands were selected for their homogenous terrain, making them ideal candidates for Eddy Covariance measurements. These study sites are located within adjacent Internal Drainage Boards (IDBs): Southery and District IDB and Burnt Fen IDB to the NE of Ely (Figure 3.1). Carbon Dioxide flux and aeolian erosion was quantified at EN-SP3, while only aeolian erosion was quantified at EF-DA.

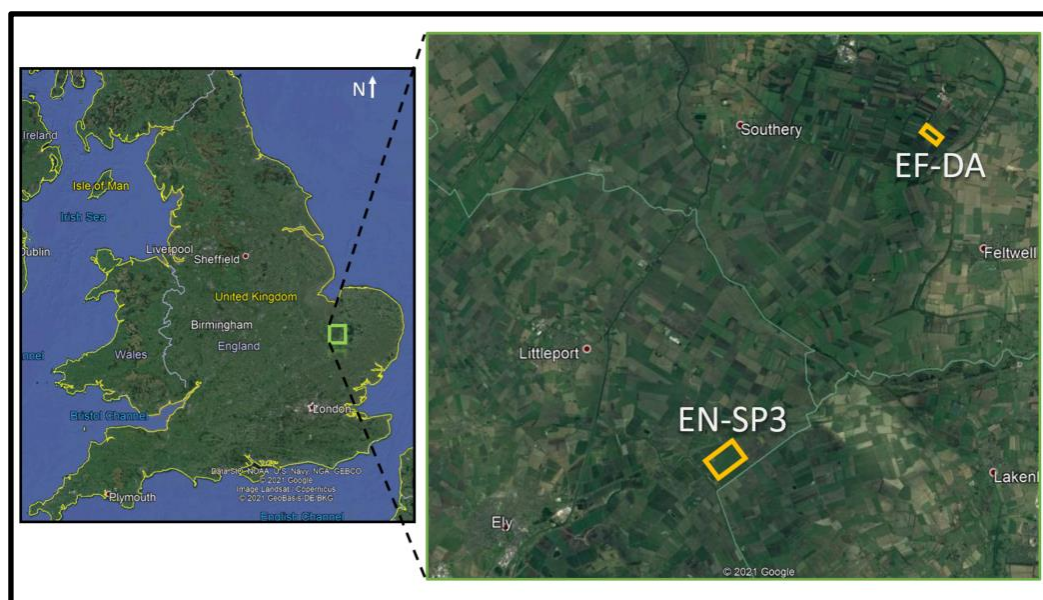
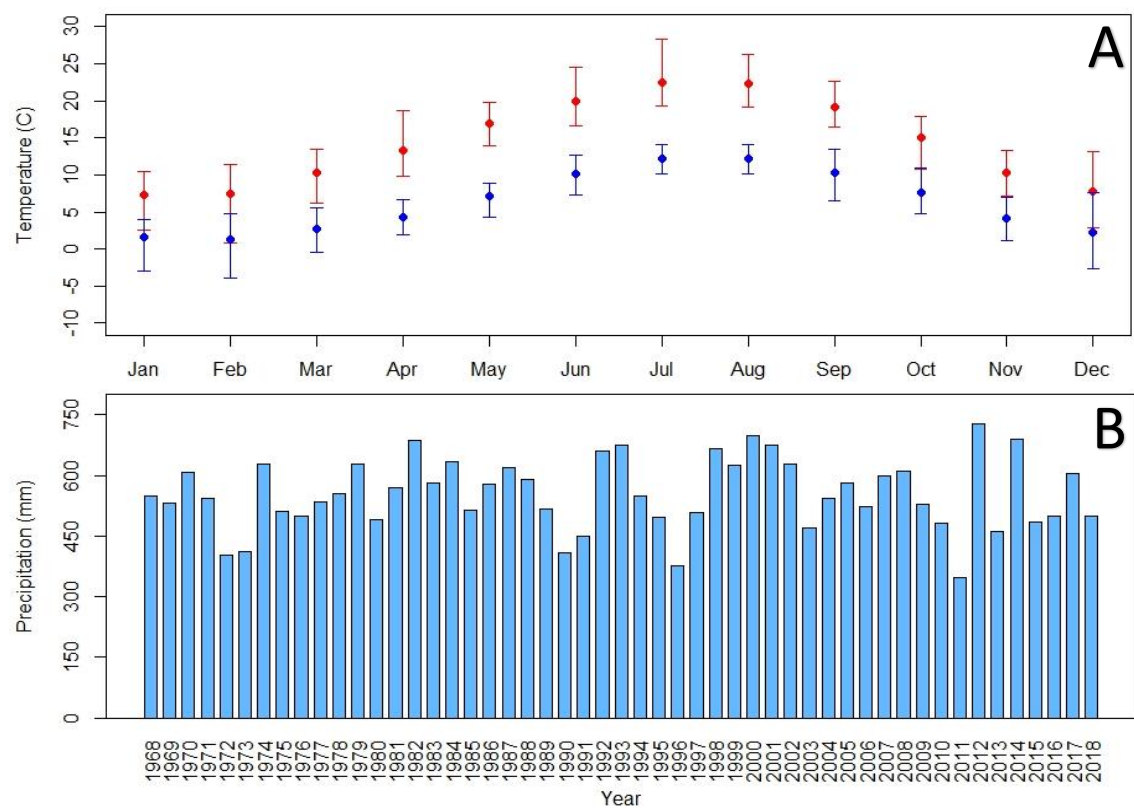


Figure 3.1. Regional and local map of the locations of study fields at Engine Farm (EN-SP3) and Rosedene Farm (EF-DA). Base map taken from Google Earth 2021, [earth.google.com/web/](http://earth.google.com/web/).

### 3.1.1 Regional Climate

Within East Anglia, the absolute mean average annual temperature over the last 50 years is 10.3 °C, with 14.4 °C and 6.3 °C being the mean maximum and minimum temperatures. Average yearly precipitation is 537.3 mm with 727.3 and 347.3 mm being the maximum and minimum precipitation in any one year. Precipitation is typically evenly distributed throughout the year. All meteorological data were obtained from the Met Office climate station at Cambridge National Institute of Agricultural Botany (NIAB) (Figure 3.2), located approximately 30 km from EN-SP3 and 45 km from the EF-DA. Between 1968 and 2012, the thermal growing season averaged 263 days a year, with 330 and 190 days being the minimum and maximum in any one year. In the last 30 years, a slight trend of increasing thermal growing season has been observed, due to the earlier onset of spring (Department of Energy and Climate Change, 2013). The prevailing wind direction is primarily South Westerly, but with periods from the North and East throughout the year.



*Figure 3.2. Climate data between 1968 and 2018 for A: Average minimum (blue) and maximum (red) monthly daytime temperature, where the error bars represent the absolute maximum and minimum temperature recorded. B: Annual precipitation. From the NIAB station (UK Met Office, 2019).*

### 3.1.2 Engine Farm (EN-SP3)

Engine Farm is an intensively managed agricultural peatland situated to the east of Ely, north east Cambridgeshire (Figure 3.2) and located within the Burnt Fen IDB catchment. Burnt Fen today consists mostly of prime agricultural land and a few settlements, surrounded on three sides by rivers (the Great Ouse, Little Ouse and Lark). Almost the entirety of Burnt Fen is below sea level, and all of it is considered to be below the flood levels of the surrounding rivers (Burnt Fen Drainage Board: Conservation, 2011).

Engine Farm is located on peatland that has undergone drainage since the mid-1600s and has been farmed intensively for most of the last century. This has led to the loss of a significant depth of peat and, as a result, it is classified as “wasted peatland” by Natural England (Natural England, 2010). In 2013, Cranfield University measured the depth of peat across two fields within Engine Farm, including the field used in this study (Hannam J.A., 2014). Peat depths in the range 0.35–0.7 m were recorded. The peat overlies a fen clay base punctuated with silt roddons. Due to its long history of drainage and peat loss, the Engine Farm peatland sits 3–4 m below the banks of the River Lark which borders its SW edge.

For the last few decades, Engine Farm has been under the management of Cambs Farms Growers Ltd, who are members of G's Growers Ltd, part of the wider G's Fresh group (G's Fresh, 2019). Over this period, the land has been under intensive farming and has experienced continued peat depletion. The farm consists of large trapezoidal fields separated by ditches which support reed (*Phragmites australis*) growth in the summer months; this growth is cut back in the late autumn. A line of trees runs through the farm and surrounds the SW side of the farm office and workshop, which sit at the centre of the farm. A variety of arable, horticultural and salad crops are grown, under typical intensive agricultural management practices (Rob Parker, pers. comm.). These include lettuce, celery, maize, wheat, potatoes, rye and other species grown as cover crops.

#### 3.1.2.1 Engine Farm Study Field Description (Spooners 3)

Spooners 3 (located 52° 25' 22"N 0° 22' 58"E) is a 988 m by 685 m (67.7 ha) field with a reported peat depth range of 0.35 to 0.45 m (Hannam J.A., 2014), with the flux tower located on NE field edge where the organic layer is between 0.35 and 0.4 m in depth (Figure 3.3.a & c). There is negligible elevation change over the whole field; this homogeneity made it a good candidate site for EC measurements. Surface soil is described as a humose/organic fen clay mix atop a compacted fen clay layer. The fen clay extends to a depth of ~1.6 m bellow which is a small layer of fibrous peat which gives way to Kimmeridge clay at depth (Figure 3.4).

Trees line the south side of the field and the southern half of the NE field edge, in front of the Farm Office, ~ 50 m SE from the location of the EC tower (Figure 3.3.c). The field is bordered on all sides by ditches, which are used to manage the water-table; these undergo regular maintenance to remove debris. The ditch running along the NW field side is known as The Engine Drain and is one of the main drains in this part of the Burnt Fen IDB (Ely Group of Internal Drainage Boards, 2019). This drain and the linked Lark Engine Pumping Station situated 200 m downstream from the start of the NW field edge where the Engine Drain meets the River Lark, are used to control the water level flowing out of Engine Farm, and the wider surrounding area. A field margin (~5 m width) surrounds the field on all sides, consisting of grasses, sedges and agricultural weeds, predominantly Nettles (*Urtica dioica*) and Cow Parsley (*Anthriscus sylvestris*) (Figure 3.3.b). The field margin vegetation is cut once a year in late autumn.

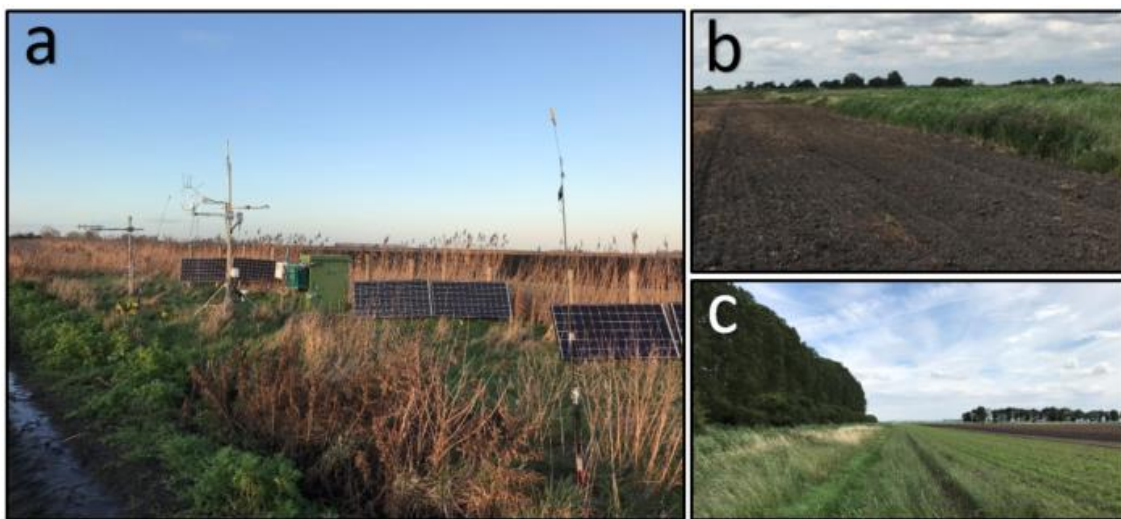


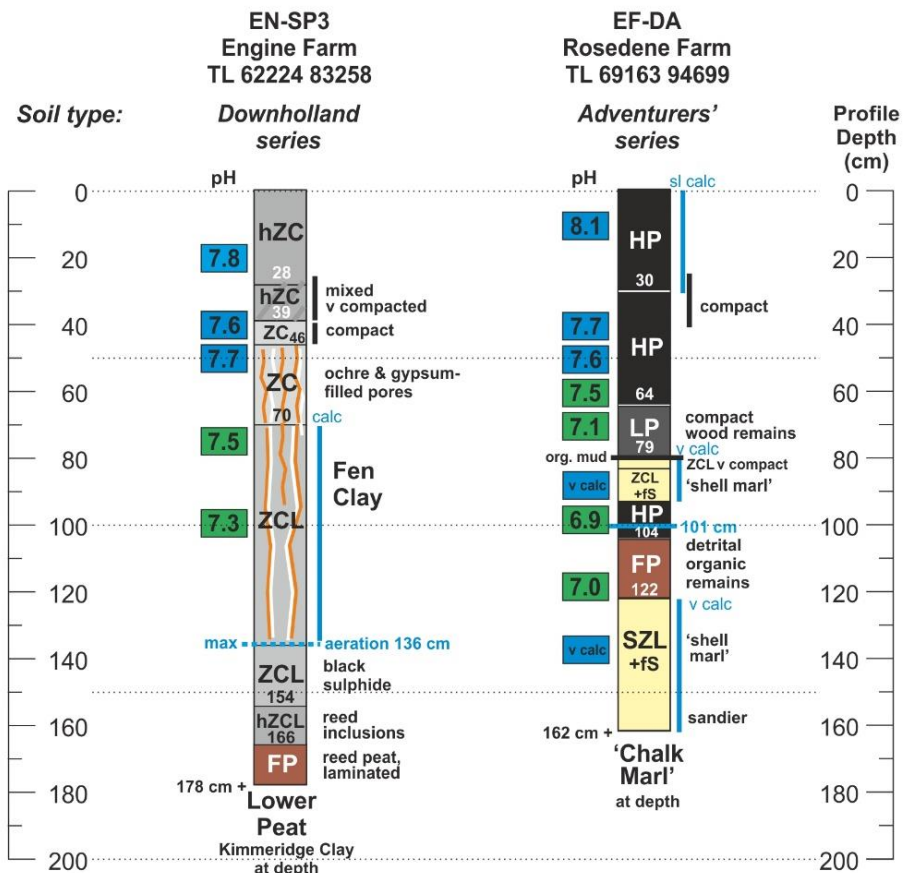
Figure 3.3. a) EN-SP3 study site; b) The northern edge of the NE field boundary in mid-summer with boundary vegetation left uncut; c) The southern half of the NE field boundary. Pictures taken by author.

# UKCEH/G's FLUX TOWER SITES

## FENLAND BOREHOLE LOGS – SOIL PROFILES

### Engine Farm, Cambridgeshire & Rosedene Farm, Norfolk

Soil Survey by R.G.O. Burton & M. Bidwell, June 2021  
for the BEIS Project 'Toward an accurate estimate of  
wasted peat GHG emissions in England'



KEY		humified peat	soil texture abbreviations	profile features
HP	humified peat		humose/organic (h)	sl.cal/calc/v.calc
LP	loamy peat		sand (S)	slightly calcareous
PL	peaty loam		loamy sand (LS)	calcareous
MP	semi-fibrous (mesic) peat		fine sand (fS)	very calcareous
FP	fibrous (fibric) peat		medium sand (mS)	water table, cm depth
ZCL	'shell marl'		coarse sand (cS)	max aeration depth cm
	ZCL, SZL		sandy loam (SL)	
ZC	Fen Clay		sandy silt loam (SZL)	iron ochre (mottles)
	ZC, ZCL		sandy clay loam (SCL)	gypsum
			clay loam (CL)	field pH (1:1 soil:water)
			clay (C)	>7.5 alkaline, calcareous
			silty clay (ZC)	6.6-7.5 neutral
			silty clay loam (ZCL)	

RGOB

Figure 3.4. Soil profile from EN-SP3 and EF-DA study sites taken from a singular borehole within the field close to the study site instrumentation. Survey performed by R.G.O. Burton & M. Bidwell, June 2021 and diagram created and used with permission from R.G.O. Burton & M. Bidwell.

During the data collection period, 3 crops were grown in the field; in 2018 maize was grown, in 2019 a phacelia and buckwheat cover crop was grown followed by a main crop of celery. A list of field and crop management can be found in Table 3.1.

*Table 3.1. A list of farm management practices that occurred during the data collection period on Engine Farm, Spooners 3 field. Crop planting and harvesting in highlighted in green. Application type is indicated by the letter, with (C) denoting an application to control weeds or pests and (F) a fertiliser application. Product name of each application is given.*

Activity	Date	Details
<b>2018</b>		
Tower Establishment	19/04	EC measurements begin
Preparation	--	Tilled with subsoiler to 0.4 m depth
Application	03/05	X-Clude (C), Azural (C)
Application	04/05	M.O.P (F)
Planting	18/05	Maize
Application	23/05	N30.3/10.8 SO3 (F)
Application	05/06	Mangamese Sulphate (F), EPSO Combitop (F), Headland Copper 43.5% (F), Headland Zinc 150 (F)
Application	20/06	Mero (C), Maister WG (C), pHorce (C), Manganese Sulphate (F)
Application	28/06	Headland Multiple (F), Headland Boron (F), Headland Zinc 150 (F), Tecmangam (F), Bittersaltz Epsotop (F)
Harvesting	02/10	Maize
Preparation	27/10	Subsoiler (0.45 m)
Preparation	12/11	Disc (0.12 m)
Preparation	21/11	Plough (0.3 m)
<b>2019</b>		
Planting	16/01	Wheat Strips (only around field edge and through middle of the field in a 12m swathe)
Planting	15/05	Cover Crop (Phacelia & Buckwheat)
Preparation	01/07	Disc (1.2 m)
Application	05/07	15-4-15 (F)
Preparation	18/07	Powerharrow (1.25 m)
Irrigation	18/07	15 mm
Preparation	23/07	Powerharrow (1.25 m)
Planting	23/07	Celery plug plants
Application	23/07	Gamit 36 CS (C)
Irrigation	23/07	15 mm overhead
Irrigation	25/07	15 mm overhead
Irrigation	30/07	15 mm overhead
Application	05/08	Stop Aqua (C), Clayton Comply (C)
Application	07/08	Amistar (C), Hallmark with Zeon Technology (C), Tecmangam (F), Bittersaltz Epsotop (F), Headland Vertex Hi N 34 (F)
Application	12/08	Defy (C)
Application	21/08	Hallmark with Zeon Technology (C), Tecmangam (F), Headland Vertex Hi N 34 (F), Switch (C), Bittersaltz Epsotop (F)
Irrigation	28/08	25 mm ground level
	30/08	Decis (C)
	04/09	Amistar (C), Plenum WG (C), Hallmark With Zeon Technology (C)
Irrigation	06/09	25 mm ground level
Irrigation	17/09	25 mm ground level
Application	18/09	Plenum WG (C), Plover (C), Decis (C)
Application	28/09	Plenum WG (C), Switch (C), Tecmangam (F), Bittersaltz Epsotop (F), Dia-Life Organic (F), Tri-Kelp (F), Headland Vertex Hi N 34 (F)
Harvesting	23/10*	Celery
<b>2020</b>		
Field Prep	12/03	Field subsoiled (0.45 m)

### 3.1.3 Rosedene Farm (EF-DA)

Rosedene Farm is an intensively managed agricultural peatland situated within Methwold Fen, East Norfolk within the Southery and District IDB. Similar to Burnt Fen, Methwold Fen consists of prime agricultural land. It is located within the catchment of the River Wissey, which borders the northern edge of the farm.

Rosedene Farm is characterised as a drained fen peatland, however, unlike Engine Farm, drainage here commenced relatively recently, just after the end of the Second World War as part of the UK's drive for agricultural self-sufficiency (Cumming, 2018). Thus, Rosedene Farm is located on deeper peat soils that are between 1 and 2m in depth (Dawson et al., 2010, Evans et al., 2017b) and can be classified as deep peats (Natural England, 2010). The land is higher in elevation than the surrounding farms which were drained prior to Rosedene Farm (Cumming, 2018). Despite the shorter history of drainage and peat loss, Rosedene sits at or just below mean sea level.

The farm consists of 1,400 ha of land, owned and managed by G S Shropshire and Sons, who are members of G's Growers Ltd, part of the wider G's Fresh group (G's Fresh, 2019). This land is divided into over 100 trapezoidal fields. These are typically divided by hedgerows and, occasionally, by tree rows that have been planted to reduce the impact of aeolian erosion of the peat surface, which is common in dry, windy conditions (Cumming, 2018, Pollard and Millar, 1968).

On 1,000 ha of the farm (including the field of interest), the fields have been laser-levelled. They are separated by a network of ditches and subsurface drains, which allows the use of a sub-irrigation system to control the field water tables. Subsurface drainage pipes run throughout the fields at 10–15 m intervals across both the length and width of the fields at a depth of 1–1.5 m. Farm managers monitor the depth of the water table across the fields, which can be altered through changing the water level of the ditches via pumping and control gauges. This is under the management of the farm and the IDB. Whilst the main source of water into the farm is the River Wissey, three reservoirs are maintained on the site and used as backup in times of drought.

During the growing season, overhead irrigation is used to supplement sub-irrigation and natural rainfall where required for specific crops. In this way, irrigation is managed specifically for the needs of each individual crop and to react to meteorological events, reducing the water requirement by up to 50% and limiting the need for fungicide applications compared with the use of purely overhead irrigation systems which keep the crop canopy wet, encouraging disease

(Martin Hammond, pers. comm.). Due to the use of sub-irrigation, overhead irrigation is used to a lesser extent at Rosedene compared to Engine Farm.

The farm primarily grows a variety of vegetable and salad crops, specializing in lettuce, celery and Chinese leaf but the full rotation also includes potatoes and bulb onions and, on rented land, beet, radish, carrots and leeks (G's Fresh, 2019).

### 3.1.3.1 Rosedene Farm (EF-DA) Study Field Description (R39)

The aeolian erosion data collected at R39 represents a continuation of the dataset for this site that was originally started by Dr. Alex Cumming as part of his PhD conducted at the University of Leicester (Cumming, 2018) and as part of the Defra-funded Lowland Peat Project and SEFLOS (Securing Long-Term Ecosystem Function in Lowland Organic Soils) Soil Security Program; see (Evans et al., 2017b) for details of the former project and (Jones et al., 2021) for the latter.

R39 is a 125 by 630 m (7.9 ha) field (located at 52° 23' 23"N 0° 29' 29"E) with the flux tower and associated BSNE (Big Spring Number Eight) situated on the NE edge (Figure 3.5.a & b). It has a reported peat depth of 1–2 m across the field (Dawson et al., 2010, Evans et al., 2017b). Surface soil consists of humified peat, extending to a depth of 0.64 m. Below which are smaller layers of loamy peat, humified peat and fibrous peat punctuated by a small layer of shell marl. Below the final peat layer is shell and chalk marl that continues at depth (Figure 3.3).



Figure 3.5. a) EF-DA study site; b) study site focusing on the BSNE (Big Spring Number Eight) used to gather aeolian erosion data; c) Field R39 and trees along the SW field boundary; d) NE field boundary the study site is located on. Pictures taken by author.

Due to the laser levelling for improved irrigation (as described above) there is negligible elevation change across the field (Figure 3.5.c). The field is surrounded by ditches on the NE, SE and NW edges with hedges punctuated by trees on the SW field edge (opposite the flux tower) (Figure 3.5.d). There is no clear field margin around the edge of the field. During the data collection period, 3 crops were grown in the field; a sugar beet crop planted in 2017 that was harvested in early 2018, a lettuce crop in 2018 and a potato crop in 2019. An overview of each crop and the management practices involved can be found in Table. 3.2.

*Table 3.2. A list of farm management practices that occurred during the data collection period on Rosedene Farm, R39 field. Crop planting and harvesting in highlighted in green. Application type is indicated by the letter, with (C) denoting an application to control weeds or pests and (F) a fertiliser application. Product name of each application is given. Missing details are denoted by ‘--’.*

Activity	Date	Details
<b>2017</b>		
Preparation	--	Tilling
Planting	08/04	Sugar Beet
Application	14/04	Betasana SC (C), Goltix 70 SC (C)
Application	21/04	Betanal Maxx Pro (C), Goltix 70 SC (C), Manganese sulphate (F)
Application	08/05	Betanal Maxx Pro (C), Goltix 70 SC (C), Nufarm Cropoli (C), Manganese sulphate (F)
Application	18/05	Falcon (C), Activator 90 (C), Manganese sulphate (F), Magnesium sulphate (F)
Application	24/05	Sniper (C), Debut (C), Nufarm Cropoli (C), Dow Sheild 400 (C), MnSO4 (F)
Application	02/06	Sniper (C), Debut (C), Nufarm Cropoli (C), Dow Sheild 400 (C), MnSO4 (F)
Application	16/06	Betasana SC (C), Ethofol 500 SC (C), Nufarm Cropoli (C), Dow Sheild 400 (C), MnSO4 (F)
Application	21/06	Manganese sulphate (F), Magnesium sulphate (F)
Application	11/07	Manganese sulphate (F), Magnesium sulphate (F)
Application	22/07	Escola (C), Epsotop (C), MnSO4 (F)
Application	29/08	Escola (C)
<b>2018</b>		
Application	10/01	Potash (F)
Harvesting	05/02	Sugar Beet
Preparation	24/04	Stomp Aqua (C), Wing-P (C), Dual Gold (C), 6-6-12 (F)
Preparation	--	Tilling
Planting	26/04	Iceberg lettuce plug plants
Irrigation	--	--
Application	10/05	Amistar (C), Manganese sulphate (F), Magnesium sulphate (F), Karamate Dry Flo Neotec (C)
Application	21/05	Manganese sulphate (F), Magnesium sulphate (F), Paraat (C), Hallmark with Zeon Technology (C), Plenum WG (C)
Application	28/05	Manganese sulphate (F), Magnesium sulphate (F), Plenum WG (C), Decis (C), Revus (C)
Application	04/06	Manganese sulphate (F), Magnesium sulphate (F), Paraat (C), Hallmark with Zeon Technology (C), Plenum WG (C)
Harvesting	21/06	Iceberg lettuce
Application	14/12	Potash (F)
<b>2019</b>		
Preparation	--	Tilling
Planting	17/05	Lanorma potatoes
Application	17/05	Nemathorin 10G (C), Monceren DS (C)
Application	03/06	Atrist (C), Shotput (C), Inigo (C), Retro (C), Nuram (C)
Application	17/06	Manganese sulphate (F), Magnesium sulphate (F), Curzate M WG (C)
Application	24/06	Manganese sulphate (F), Magnesium sulphate (F), Curzate M WG (C)
Application	26/06	Activator 90 (C), Titus (C)
Application	01/07	Manganese sulphate (F), Magnesium sulphate (F), Zorvec Enicade (C), Rhapsody (C)
Application	09/07	Manganese sulphate (F), Magnesium sulphate (F), Option, Valbon
Application	16/07	Manganese sulphate (F), Magnesium sulphate (F), Infinito
Application	23/07	Manganese sulphate (F), Magnesium sulphate (F), Zorvec Enicade (C), Rhapsody (C)
Application	30/07	Manganese sulphate (F), Magnesium sulphate (F), Sipcam C50 WG (C), Valbon (C)
Application	06/08	Manganese sulphate (F), Magnesium sulphate (F), Sipcam C50 WG (C), Revus (C)
Application	13/08	Ranman Top (C), Manganese sulphate (F), Magnesium sulphate (F)
Application	22/08	Revus (C)
Application	29/08	Ranman Top (C)
Application	06/09	Ranman Top (C)
Application	14/09	Curzate M WG (C)
Application	23/09	Relogone (C)
Application	25/09	Spotlight Plus (C), Relogone (C)
Application	27/09	Spotlight Plus (C)
Harvesting	31/10	Larnoma potatoes
<b>2020</b>		
Preparation	--	Tilling

## 3.2 Eddy Covariance Measurements

### 3.2.1 Theory

The EC method measures the flux of trace gases vertically through the boundary layer of the atmosphere. It does this by measuring the rate of atmospheric eddy transport. As the wind moves horizontally through the boundary layer, multiple eddies are formed by both thermally driven processes (convection) and via surface interactions (mechanical shear) (Stull, 2012). Each of these eddies consists of its own unique set of 3-D wind components and is created at a different size and frequency, ranging from below a second to several hours (Burba, 2013). Close to the ground there is a higher prevalence of smaller eddies which rotate at a high frequency whereas larger, slow frequency eddies are more common further from the ground.

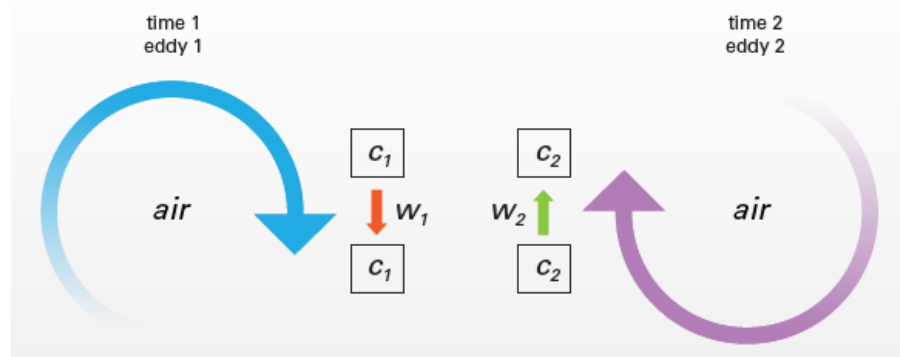
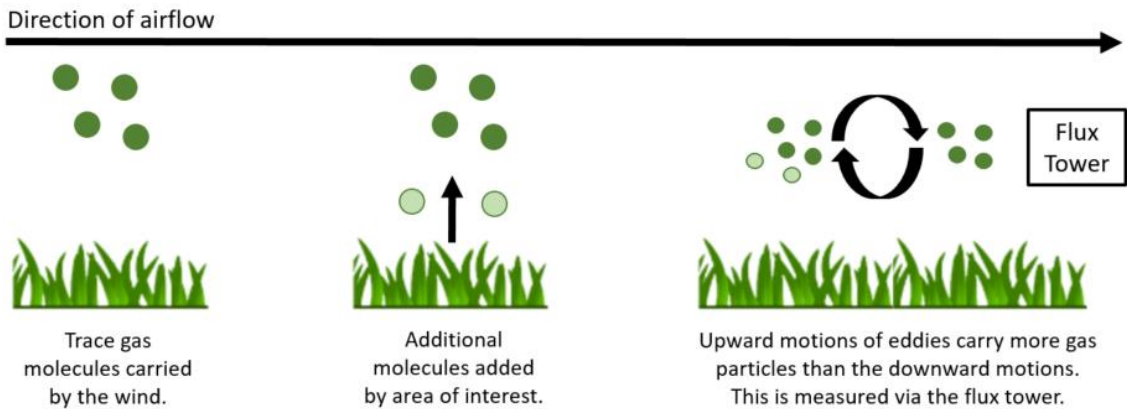


Figure 3.6. Diagram showing a simplified example of eddy flux.  $C_1$  and  $C_2$  are individual air parcels,  $W_1$  and  $W_2$  denote speeds. Taken from Burba (2013).

At any single point, each one of these eddies is moving a parcel of air either upwards or downwards (Figure 3.6). At time 1, eddy 1 moves air parcel  $C_1$  down with speed  $W_1$  whilst eddy 2 moves air parcel  $C_2$  upwards with speed  $W_2$ . Each of these air parcels ( $C_1$  &  $C_2$ ) is unique in terms of its gas concentration, temperature, density, humidity, and water vapour. At each time these properties are measured, whilst also allowing the calculation of the vertical movement of the parcel of air by measurement of the 3-d wind components. The trace gas being observed is measured in each parcel of air (i.e. CO<sub>2</sub>, CH<sub>4</sub> or N<sub>2</sub>O), making it possible to calculate the amount of gas moved (or 'fluxed') at each time. The upward and downward fluxes of the gas being examined are then compared, and the overall flux calculated. As a simplified example; if in eddy 1, 11 molecules of CO<sub>2</sub> went up and in eddy 2, 20 molecules of CO<sub>2</sub> went down, then the overall flux over that period of time would be 9 molecules of CO<sub>2</sub> downwards (Burba, 2013).



*Figure 3.7. How eddies transport gas particles allowing flux from a study site to be measured (adapted from Burba (2013)).*

This principle can be applied to a horizontal flow of air passing directly over the study area (Figure 3.7). As the eddies move over a field that is emitting CO<sub>2</sub>, additional molecules are added to the upwards motion of the eddies. This is captured by a flux tower placed downwind of the area of interest, giving a measure of the additional amount of CO<sub>2</sub> (for an absorbing field, a reduction in CO<sub>2</sub> is observed). Upward and downward fluxes are then aggregated over a discrete time period, typically 30 minutes, to give the overall source / sink of emissions from the field.

This is achieved in practice by the use of a high-speed three-dimensional sonic anemometer and Infrared Gas Analyser (IRGA) that allow simultaneous measurements of vertical wind speed and the gas being examined multiple times a second (commonly 20 Hz) at a fixed height. This gives an accurate representation of atmospheric fluxes over the study area (for further detail see (Baldocchi, 2003, Aubinet et al., 2012, Burba, 2013)).

Mathematically, a representation for eddy fluxes (F) can be derived from the equation which represents how a vertical flux (F) moves in a turbulent flow:

$$F = \overline{\rho_d w s} \quad \text{Equation 3.1}$$

where  $\rho_d$  is the dry air density,  $w$  is the vertical wind speed and  $s$  is the mixing ratio (also known as the dry mole fraction) (Burba, 2013).

Reynolds decomposition is applied, which is used to split the terms into means and deviations and allows each term to be represented as a mean over a discrete period of time and the deviation of individual measurements from the mean within each time period. This gives the equation:

$$F = \overline{(\rho_d + \rho'_d)(\bar{w} + w')(\bar{s} + s')} \quad \text{Equation 3.2}$$

where primes denote instant deviations from the mean while overbars denote the averages (Baldocchi, 2003).

This equation is then expanded before the terms representing the average deviations from the mean are removed (the average deviation from the mean is zero). From this, two important assumptions are made: 1. That air density fluctuations are negligible and 2. That for horizontal homogenous flow, vertical flow is assumed negligible, something which is observed at experimental sites on flat homogenous land (such as the arable field sites described within this thesis). This leaves us with the final equation:

$$F \approx \overline{\rho_d} * \overline{w's'} \quad \text{Equation 3.3}$$

This is the classical description of an ‘Eddy Flux’ within the EC method (Burba, 2013) where  $\rho_d$  is the dry air density,  $w$  is the vertical wind speed and  $s$  is the mixing ratio (also known as the dry mole fraction). Here the convention used is a positive eddy flux denotes transfer from the ecosystem to the atmosphere whilst a negative eddy flux denotes the reverse.

### 3.2.2 Assumptions

There are multiple theoretical assumptions that are associated with the EC method (major assumptions are listed in Table 3.3). In reality, these assumptions are rarely met in full (Aubinet et al., 2012), but can be met to a high degree through proper site selection and careful consideration of instrument placement. Some assumptions, such as those which rely on atmospheric conditions, can be impossible to meet (Burba, 2013), additionally, the instrumentation also introduces a number of key error sources (Aubinet et al., 2012). These are accounted and corrected for during processing and post-processing quality control (QC) procedures which minimize error and remove incorrect values. The processing and QC procedures undertaken within this study are described in Chapter 3.2.5.

*Table 3.3. Major EC assumptions, table created from list of assumptions provided by Burba (2013).*

Assumption	Details
Instruments can detect high frequency fluctuations	Measurement rate of the sonic anemometer and IRGA is high enough.
Measurements represent an upwind area	Relies on the assumption that there is no advection into or out of the area of interest.
Measurements are made within the boundary layer	This is the layer of constant flux, also known as the surface layer.
Fetch and footprint adequate	Fluxes originate from the area of interest.
Uniform fluxes	Fluxes are uniform within the area of interest.
Terrain is horizontal and uniform	$W'$ averages to zero, fluctuation in air density, flow convergence and divergence are negligible.
Instruments have no impact on airflow	Flux tower has no impact on the mean air flow / turbulence.

### 3.2.3 Instrumentation

Given are details of the EC and biometeorological instrumentation installed at EN-SP3 as part of this work to measure CO<sub>2</sub> and potential meteorological drivers. Details of the instrumentation used from the existing EC tower at EF-DA to compliment the aeolian erosion data collected as part of this work are also given (see (Cumming, 2018) for a complete description). For details of specific instrumentation used in the collection of aeolian erosion data, see Chapter 6.2.2.

#### 3.2.3.1 Eddy Covariance systems

The EC system used at EN-SP3 consisted of a CSAT3, 3-D sonic anemometer (Campbell Scientific Ltd., Logan, UT, USA) and a LI-COR Biosciences Li-7500A open-path H<sub>2</sub>O/CO<sub>2</sub> IRGA (LI-COR inc., Lincoln, Nebraska, USA) with barometric pressure measured at the base of the tower at the Li-7550 instrument control box. The LI-7500A and the CSAT3 were mounted on specialized mounts to reduce separation distance. The LI-7500A was positioned at a 15° angle to prevent precipitation accumulating in the optical path and to aid cleaning.

EC instruments were installed on galvanised steel tripods at an initial height of 2.03 m. Instruments were raised to keep them above twice mean vegetation height. For maize crops, which grow in excess of 2 m, an STX75-3-NC telescopic mast (Clark Masts Systems LTD., Binstead Isle of Wight, UK) was used which allowed the instruments to be raised to 5.75 m.

All EC data was logged at 20 Hz via the Li-7550 control box and stored on a portable flash drive. Routine maintenance and data collection was performed monthly, with additional trips scheduled when appropriate for instrument failure.

Between the CSAT3 and the LI-7500A there was a vertical separation of 0.015 m, 0.16 m south and 0.02 m east from the CSAT3. After instrument failure in January 2019, the LI-7500A and LI-7550 control box was removed for repair and calibration. The instrument was then returned to the site in May 2019, at which time the separation eastward was altered from 0.02 m to 0.01 m (all other measurements were kept the same).

A similar EC system was used at EF-DA, consisting of a CSAT3, 3-D sonic anemometer that was logged at 20 Hz to a 2GB CF card installed within a CR3000 (Campbell Scientific Ltd., Logan, UT, USA). This provided wind speed and direction for the EF-DA site.

### 3.2.3.2 *Biometeorological systems*

#### 3.2.3.2.1 Solar Radiation

##### *EN-SP3*

Incoming and outgoing long and short wave solar radiation was measured via a CRN1 radiometer (Kipp & Zonen, Delft, the Netherlands) from which, net radiation ( $R_n$ ) and albedo were calculated. The CRN1 was installed 1.8 m above the peat surface, 5 m NW from the EC instruments. Photosynthetically active radiation (PAR) was measured using a SKP 215 Quantum sensor (Skye Instruments, Llandrindod Wells, UK). The par sensor was installed on the flux tower at 2.5 m height on a 0.5 m long mount to the south of the EC instruments to prevent shading.

##### *EF-DA*

Net radiation was measured via an NRLite2 (Kipp & Zonen, Delft, The Netherlands) which measured incoming and outgoing solar radiation. The NRLite 2 was installed 1.5 m above the peat surface, 8 m north-west from the EC instruments. PAR was measured using a SKP 01 Quantum sensor (Skye Instruments, Llandrindod Wells, UK) installed on the flux tower at 2.5 m height on a 0.5 m long mount to the south of the EC instruments to prevent shading.

#### 3.2.3.2.2 Soil Temperature, Heat Flux and Water Content

At both sites, soil heat flux, soil temperature and soil water content were measured using two arrays of soil instruments. Each array consisted of a time domain reflectometer CS616 (Campbell Scientific Ltd., Shepshed, UK) which measured soil volumetric water content (SWC), a TCAV averaging soil thermocouple (each TCAV consisting of 4 thermistors) which measured soil temperature ( $T_s$ ), and two HFP01-SC (Hukseflux, Delft, The Netherlands) soil heat flux plates which measured approximate heat flux across the soil atmosphere interface.

#### *EN-SP3*

Soil instrumentation was installed after the initial site set up on 18<sup>th</sup> April 2018. The first array was installed on 6<sup>th</sup> June 2018, 2 m NW of the EC instruments whilst the second was installed on 8<sup>th</sup> June 2019, 1 m to the NE of the EC instruments.

Within both arrays, the two HFP01-SCs were installed at a depth of 0.08 m and 0.8 m apart. At the centre of these, a water content reflectometer (CS616) was installed horizontally at a depth of 0.05 m. Finally, four thermocouples of the TCAV were installed in sets of two between the CS616 and the HFPSCs at a depth of 0.02 m and 0.06 m, 0.6 m apart.

#### *EF-DA*

Two arrays were installed 2 m apart, 0.5 m in front of the EC system. The two HFP01-SCs were installed at a depth of 0.08 m and 1 m apart. At the centre of these, a CS616 was installed horizontally at a depth of 0.025 m. Finally, the four thermocouples of the TCAV were installed in sets of two between the CS616 and the HFPSCs at a depth of 0.02 m and 0.06 m, 0.6 m apart.

##### 3.2.3.2.3 Air Temperature, Relative Humidity and Rainfall

At both sites, air temperature (Ta) and relative humidity were measured via a HMP45 (Vaisala, Helsinki, Finland) fitted within a radiation shield at a height of 1.5 m. At EN-SP3 this was positioned below and to the south of the EC instruments. At both sites, precipitation over each 30 minute data period was recorded using an ARG100 tipping bucket rain gauge (EML, North Shield, UK) positioned 4 m to the North of the EC tower.

##### 3.2.3.2.4 Water Table Depth

At both sites, field water table depth was measured in situ via a set of automatic barrow divers (Schlumberger Water Services Ltd., Delft, The Netherlands) which measure water table depth via pressure measurements. These were suspended within a perforated PVC pipe.

#### *EN-SP3*

These were installed in November 2018, 4.5 m NNE of the EC instruments and at a depth of 1.2 m below the peat surface. Previous to this, water table depth measurements were obtained from the Burnt Fen IDB, who record daily ditch water levels at the Lark Bank pumping station on the ‘Engine Drain’ (the ditch which runs along the NW field border of the Spooners 3 field).

#### *EF-DA*

These were installed in July 2012, 8 m NW of the EC instruments and at an approximate depth of 1.2 m below the peat surface.

### 3.2.3.2.5 Data Logging

All biometeorlogical data, other than from the barrow divers which had their own internal memory and the ARG100s which recorded rainfall total over a discreet 30 minute period, was scanned at 20 Hz and stored as half hourly averages. Biometeorlogical data was collected monthly from the internal memory of a CR1000 data logger (Campbell Scientific Ltd., Logan, UT, USA) at EN-SP3 and a from a 2GB CF card installed in a CR3000 data logger (Campbell Scientific Ltd., Logan, UT, USA) from EF-DA. Both data loggers were set to GMT for the duration of data collection.

### 3.2.3.3 Power systems

Both sites used similar power systems consisting of 4 x 6 V 330 Ah block gel leisure batteries (Sonnenshine) housed within a fibreglass electrical cabinet. These were recharged by 6 monocrystalline PV panels (Canadian Solar, Ontario, Canada) via Outback FLEXmax charge regulators (Outback Power Inc., Washington, USA). At EN-SP3, an additional charge regulator was used (BlueSky Energy Solar Boost 3024i, BlueSky Energy GmbH, Vocklamarkt, Austria) due to the panels being arranged in two separate arrays.

### 3.2.3.4 Weed control

At both sites, weeding was performed year-round, especially in the summer months. This was primarily to remove any obstructions to sunlight reaching the solar panels and to stop weeds interfering with the equipment. At both sites, weeding was carried out manually. At EF-DA, permission was given by the farmer to use 'Roundup', a glyphosate-based herbicide, which was applied throughout the summer months when the weeds growth was most rapid.

### 3.2.3.5 Site Diagrams

#### 3.2.3.5.1 Engine Farm



Figure 3.8 Eddy covariance and biometeorological instrumentation set up at EN-SP3. Picture taken by author.

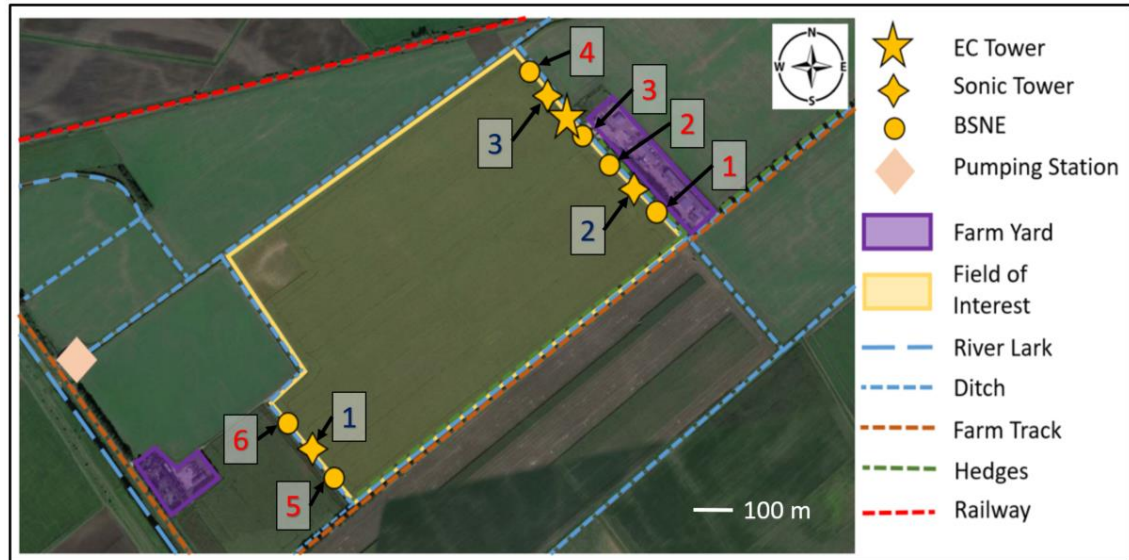


Figure 3.9. Satellite image of field Spooners 3 within Engine Farm with important site features marked. For descriptions of the instrumentation used within the aeolian erosion study Big Spring Number Eight (BSNE) dust collectors and sonic anemometer arrays (Sonic Tower) see Chapter 6.2.2. Picture taken by author.

### 3.2.3.5.2 Rosedene Farm



Figure 3.10 Eddy covariance and biometeorological instrumentation set up at Rosedene Farm on field R39. Picture taken by author.

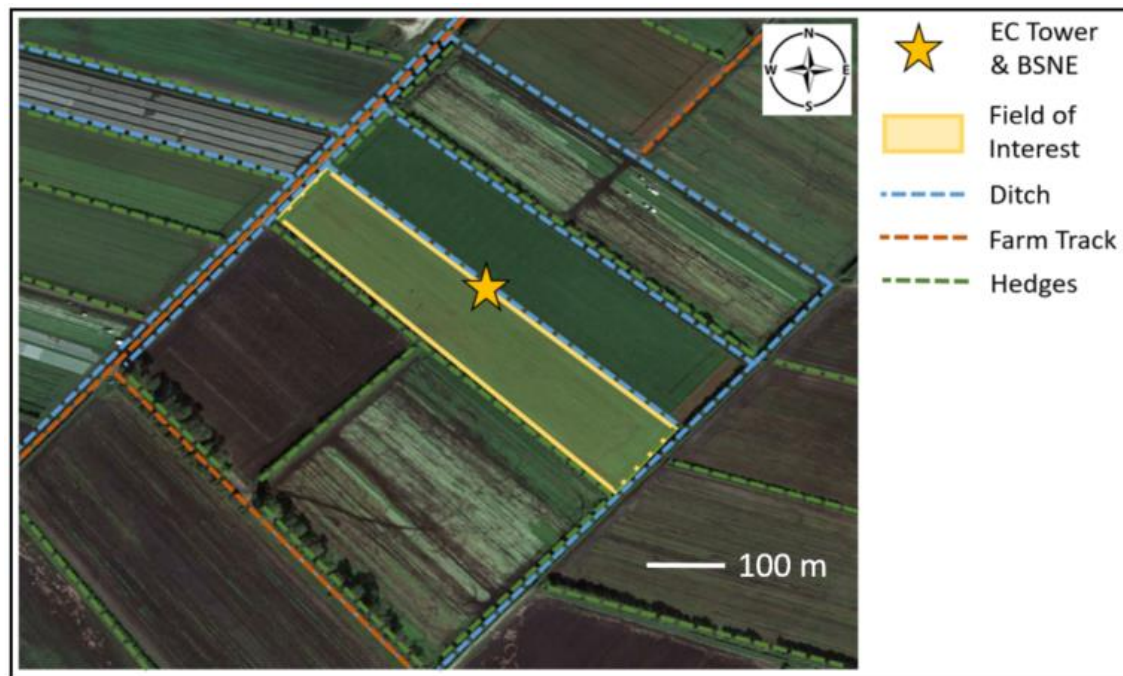


Figure 3.11 Satellite image of field R39 within Rosedene Farm with important features marked.

### 3.2.4 Raw Data Processing of EC data

Processing of the raw 20 Hz data into 30-minute flux averaging periods was done using Eddy Pro LI-COR version 6.2.2. A 30-minute averaging time was used to allow capture of both high and low frequency fluxes. Similar equations can be used to find sensible and latent heat flux and H<sub>2</sub>O flux (Burba, 2013).

Dynamic site metadata (such as vegetation height) was collected during each site visit and provided to EddyPro using a Dynamic metadata file. Biometeorological data, which is used by EddyPro to correct flux data, was averaged over 30-minute time intervals. EddyPro goes through a number of steps to process the raw 20 Hz data into fluxes; these are outlined in Table 3.4.

*Table 3.4. A description of processing steps used by EddyPro when processing raw flux data.*

Processing Step	Description
Axis rotations for tilt correction	Used to correct for misalignment of the sonic anemometer and the local wind streamlines which can cause inaccuracies within fluxes. The Double Rotation method (Wilczak et al., 2001) was used which rotates raw wind components to nullify average cross-stream and vertical wind components.
Time lags compensation	Due to the physical distance between the gas analyser and sonic anemometer, there is a delay between the instruments sampling each individual air parcel. This lag was detected and compensated for using the circular correlation technique (Aubinet et al., 2012) by comparing the lags between the scalar and vertical wind component and selecting the lag that produces the highest correlation.
Compensation of density fluctuations	Air density is used to transform the gas density measurements provided by the IRGA into a mixing ratio which is required to compute gas fluxes of CO <sub>2</sub> and H <sub>2</sub> O. To compute an accurate air density, compensations must be made for the air temperature and humidity. This is undertaken using the methods outlined in (Webb et al., 1980), allowing the production of accurate CO <sub>2</sub> and latent heat fluxes.
Statistical Tests Spike count / removal	Statistical tests for despiking, amplitude resolution, drop-outs, absolute limits, and skewness & kurtosis were used to test the quality of the raw data (Vickers and Mahrt, 1997).
Random uncertainty estimation	Using the Finkelstein and Sims (2001) method, random uncertainty due to sampling errors was estimated.
Spectral analysis and Corrections	Spectral analysis and correction is required to correct flux estimates for low and high frequency losses which occur due to instrument limitations and set up, and data processing choices. Low frequency spectral correction is done using the analytic correction for high pass filtering effects (Moncrieff et al., 2004) caused by processing on a finite time limit and through the application of de-trending. Low pass filtering losses caused by instrument limitations were corrected using the analytical method of (Moncrieff et al., 1997).
Quality flagging	Quality checks using the steady state and turbulent tests (Foken and Wichura, 1996) on each half hourly flux period and assigned a flag using the 0-1-2 system defined by (Foken et al., 2004). Fluxes were given a flag depending on flux quality (0, 1 and 2 for high, intermediate and poor quality fluxes respectively). All poor quality data was subsequently removed.
CO <sub>2</sub> storage	Storage of CO <sub>2</sub> bellow the plant canopy is calculated using the methods outlined in Aubinet et al. (2001), however, due to the low measurement height and lack of a constant plant canopy, was found to be negligible across both sites.

### 3.2.5 Post Processing using Tovi

Tovi is a software package produced by LICOR which provides a suite of tools for post processing flux data. Tovi uses the output files of flux and biomet data produced by EddyPro, along with a metadata file. Data is presented graphically within Tovi to allow for the quality control of both biometeorological and flux data, prior to further assessment of the flux data using statistical tests, flux footprints and partitioning. Quality Controlled flux data were then gap filled and partitioned. Once post processing had been completed, data was exported to R (R Core Team, 2013) which was used for further statistical analysis and to produce graphical outputs.

#### 3.2.5.1 *Biometeorological Data*

Having accurate and continuous Biometeorological data is necessary for checking eddy covariance data assumptions, for gap filling, and to understand the drivers of ecosystem flux. To all biometeorological data, absolute limits were applied and obvious data spikes were removed before a final visual inspection of the data. This captured any erroneous or implausible biometeorological data caused by instrumentation errors or influence from other outside factors, and allowed removal of values that could influence flux gap-filling and, by extension, annual flux budgets (Foken et al., 2004, Burba, 2013).

Biometeorological data was gap filled using the biomet merge and gap fill tool within Tovi which allows the merging of multiple data sets to produce one continuous record. Data sets for both sites were examined for data gaps. Gaps in temperature, humidity, incoming and outgoing radiation, and PAR were filled with corresponding data from either: 1. The nearby meteorological station at Lakenheath (52.396519, 0.547990), which is situated 8.8 miles from EF-DA and 7.5 miles from EN-SP3 or 2. via data from the co-located flux tower.

At EN-SP3, additional data gaps were present due to the staggered installation of the soil instrumentation and PAR sensor at the beginning of the data collection period. An intermittent problem was also discovered with the CS616 soil sensors leading to intermittent loss of the soil water content data throughout data collection.

#### 3.2.5.2 *Quality Control*

For each data set, absolute limits (Table 3.5) were applied to each flux variable and date exclusions set for data periods that were known to be of low quality (such as periods of instrument malfunction). After which, all half hourly periods marked with ‘poor’ quality flags assigned by EddyPro (Table 3.5) were removed before a final visual inspection was performed to remove erroneous values that had evaded flagging.

*Table 3.5. Absolute limits applied to flux variables during post processing.*

Variable	Absolute limits
CO <sub>2</sub> flux	-50 to 50 umol <sup>-1</sup> h <sup>0.5</sup>
Sensible heat flux	-200 to 600 Wm <sup>-2</sup> h <sup>0.5</sup>
Latent heat flux	-200 to 400 Wm <sup>-2</sup> h <sup>0.5</sup>

### 3.2.5.3 Footprinting

Models that describe flux footprints are used ubiquitously within eddy covariance and are a critical part of interpreting fluxes of passive scalars such as CO<sub>2</sub> and H<sub>2</sub>O to ensure that the fluxes captured originate from the area of interest (Kormann and Meixner, 2001, Kljun et al., 2015). This is particularly crucial within an agricultural landscape, where the area of interest is typically a discreet field bounded by ditches and/or hedges, with flux towers often positioned on field margins.

The footprint analysis tool within Tovi is an implementation of the two-dimensional model developed by Kljun et al. (2015). Using the tool, each half hourly flux period was examined. Flux periods which included < 75% of fluxes originating from the field (between 140 and 320°) were removed from the data set. Despite this, it was recognised that to a small degree, some contributing fluxes would have originated from the field margins, ditches or fields surrounding the flux tower, depending on atmospheric conditions.

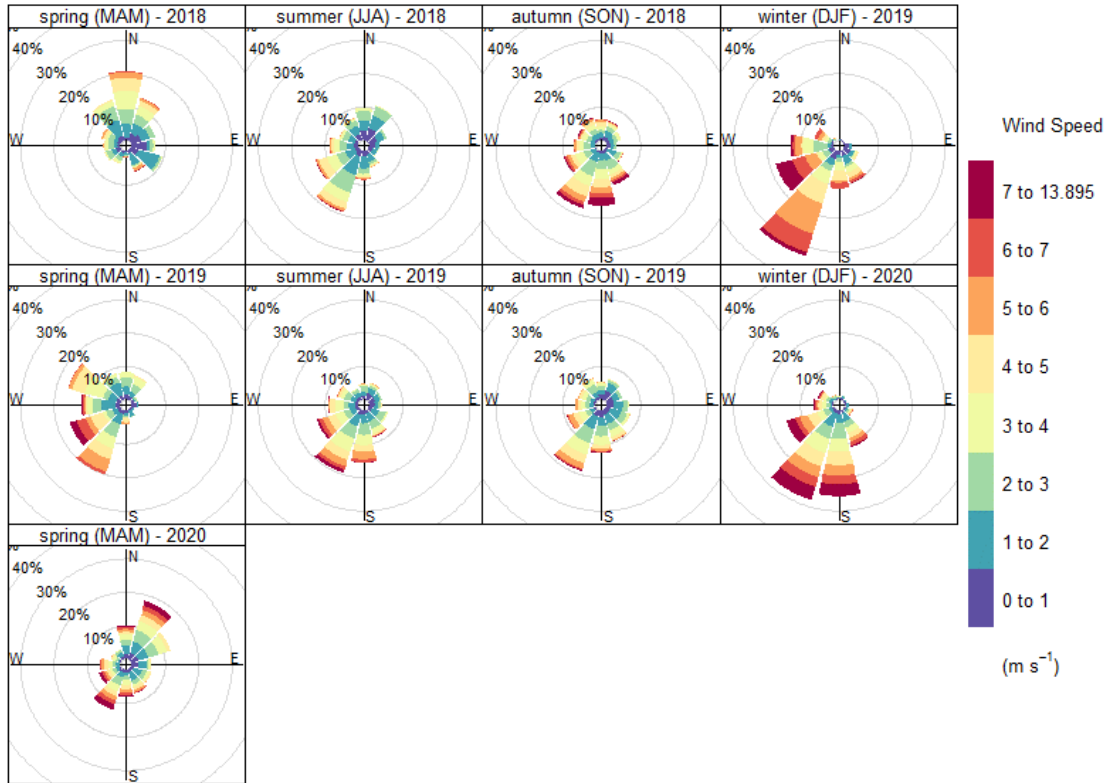


Figure 3.12. Wind direction (frequency of counts %) and strength over the data collection period at EN-SP3 by season. It should be noted that there is reduced data for winter and spring 2019 due to instrument malfunction.

Wind direction was predominantly from the SW throughout the data collection period other than in spring 2018 where the wind originated from the N and spring 2020 where the wind originated from the NE (Figure 3.12). This led to a significant loss of data during these periods. For further details, see Chapter 3.2.5.5.

#### 3.2.5.4 Friction Velocity ( $u^*$ )

The friction velocity ( $u^*$ ) is used to check for stable atmospheric conditions where turbulence is not fully developed. During periods of low turbulence, often observed during nocturnal periods, respiration measurements become negatively biased leading to an underestimation of NEE (van Gorsel et al., 2007).

The friction velocity ( $u^*$ ) is calculated within EddyPro using the equation:

$$u^* = \left( \overline{u'w'}^2 + \overline{v'w'}^2 \right)^{1/4} \quad \text{Equation 3.4}$$

where the x, y and z axis wind velocity components are represented by u, w and v respectively whilst ' represents the instantaneous difference from the mean and represents the mean value.

$u^*$  is used as a means of identifying measurements taken at periods of insufficient turbulence, allowing for their flagging and subsequent removal, indicated by the relationship between fluxes and  $u^*$ . Where fluxes are found to be dependent on  $u^*$  (i.e. they are below the  $u^*$  threshold) they are removed. This threshold is calculated using the  $u^*$  threshold detection tool within Tovi using the moving point test (MPT) described by Papale et al. (2006). Removed values are then later gap filled to create a consistent flux time series (see below).

### 3.2.5.5 Data Gaps

A significant amount of flux data was lost from EN-SP3 due to system malfunction. In the December of 2018, data was lost due to the failure of the LI-7500A chopper motor meaning the LI-7500A had to be sent to LICOR for repair and recalibration. This led to a 6-month data gap from 18<sup>th</sup> December 2018 to 16<sup>th</sup> May 2019. Therefore, data was examined in two separate periods: the first period (P1) was from 4<sup>th</sup> May 2018 to 10<sup>th</sup> December 2018 before the IRGA was repaired, the second data period (P2) was from 17<sup>th</sup> May 2019 to 17<sup>th</sup> May 2020 after the IRGA was reinstalled.

Both the data periods saw the same percentage of remaining good data after processing and QC, with 41% of the data remaining after erroneous data had been removed (Figure 3.13). Whilst removal of flagged data was similar (22% in P1 and 23% in P2), more data was removed due to not originating from the study area (27%) in P1 then in P2 (18%). This was primarily due to a period of N and NE wind directions in autumn 2018, which were a large proportion of the dataset due to its shorter length. Conversely, more data was removed in P2 for being below the  $u^*$  threshold (18%) than in P1 (9%) (Figure 3.13). This was likely due to the field being of varying field cover and condition for a large part of P2 (discussed further in Chapter 4).

Overall, data loss was similar to other studies, with a 25–65% loss observed at other studies on European and American sites (Falge et al., 2001, Papale et al., 2006). Data loss was similar to EC studies within the East Anglian Fens on agricultural peats; Cumming (2018) found an average of 45% of data was retained over 3 year period, but observed only 41.3% and 40.5% in two of those years.

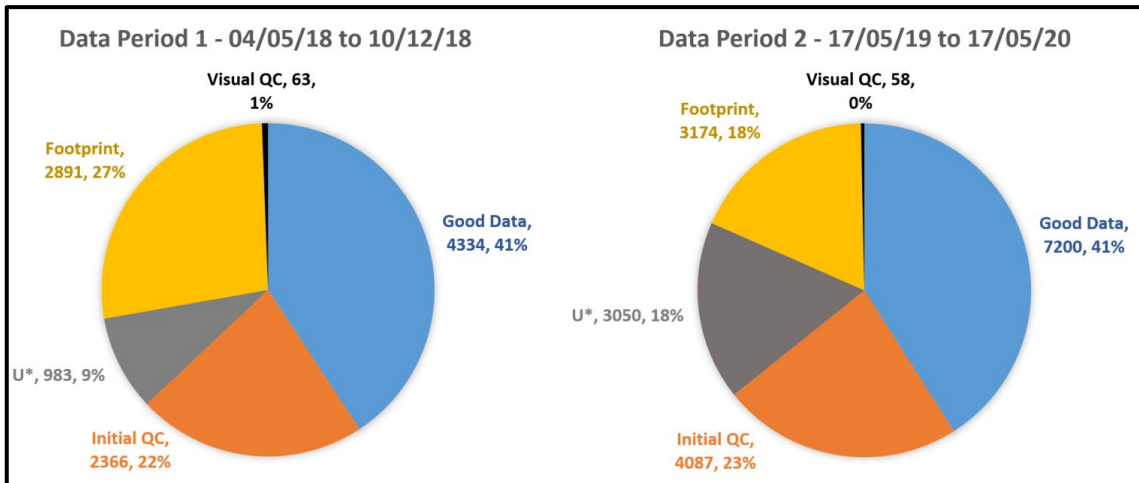


Figure 3.13. Reasons for data loss and removal of half hourly EC flux data during data processing and QC at EN-SP3 during the two data collection periods. Reason, number and % of half hourly data periods removed for each QC measure are given. Initial QC denoted data removed from applying absolute limits and removing flagged data,  $u^*$  is the data removed for being below the  $u^*$  threshold, footprint is data removed from not originating within the study area.

### 3.2.5.6 Gap filling

Gaps within flux data are expected due to the strict requirements for data to be considered of sufficient quality (as discussed previously). Over multi-year time spans, instrument malfunction is a common occurrence, despite regular maintenance. These gaps must be filled in order to produce continuous records of NEE necessary for calculating annual budgets.

To fill data gaps, the MDS Gap Fill (MDSGF) tool was used within Tovi. The MDSGF tool uses the ‘Marginal Distribution Sampling’ technique, as described by Reichstein et al. (2005) which correlates CO<sub>2</sub> fluxes with their drivers (specifically incoming solar radiation, VPD and temperature). Gaps are then categorised and filled depending on the available meteorological data for the period being filled in three different cases (Table 3.6). Filled data is then assigned a letter (A, B or C) depending on the case to indicate the quality of the gap filled data. A flow chart showing how the case, and thus the gap filling algorithm, were chosen is shown in Figure 3.14. Standard error of the datapoints used for gap filling was used to provide an error for the gap filled flux values.

Table 3.6. Gap filling methodology used for each case (adapted from Reichstein et al. (2005)).

Case	Description of Gap Filling Methodology
1	<p><i>Chosen if:</i> Only data of direct interest are missing (i.e. the CO<sub>2</sub> flux value) and all meteorological data is available.</p> <p><i>Fill method:</i> Missing value replaced by average value under similar meteorological conditions (R<sub>g</sub>, T<sub>a</sub> and VPD) within a ±7 day window and similar conditions are within 50 W m<sup>-2</sup>, 2.5°C and 5.0 hPa. If similar conditions can't be found within a ±7 day window then the window is increased to ±14 days.</p>
2	<p><i>Chosen if:</i> Data of direct interest and either air temperature or VPD is missing, but radiation data is available.</p> <p><i>Fill method:</i> Same approach to Case 1, however only R<sub>g</sub> is used to define similar meteorological conditions and the window is not increased further than ±7 days.</p>
3	<p><i>Chosen if:</i> Case 2 data that also has radiation data missing.</p> <p><i>Fill method:</i> The missing value is replaced by the average value at the same time of day (±1 hour) using the mean diurnal course. Window size starts at ±0.5 days (linear interpolation from adjacent hours). The procedure is repeated with increasing window size until the value can be filled.</p>

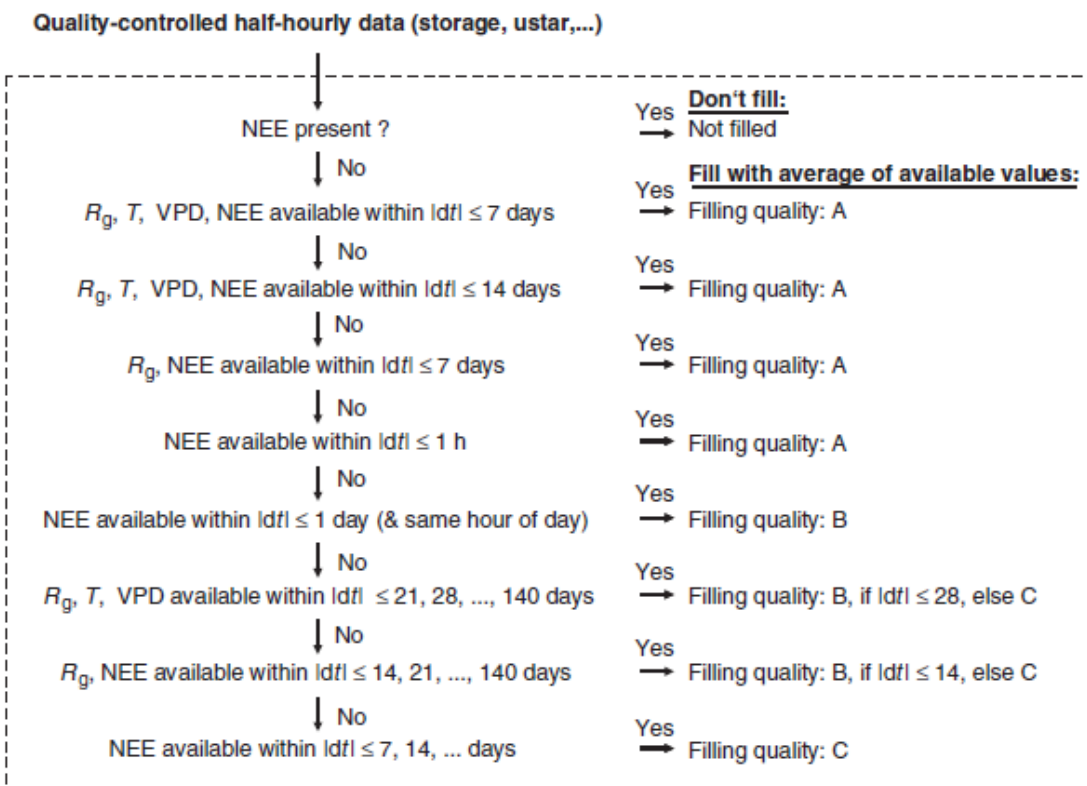


Figure 3.14. Flow diagram from Reichstein et al. (2005) showing how the case for gap filling was chosen and the subsequent data filling quality (A, B, C for High, Medium and Low), where NEE is net ecosystem CO<sub>2</sub> exchange, R<sub>g</sub> is global radiation, T is air temperature, VPD is the vapour pressure deficit and |dt| is the absolute difference in time.

### 3.2.5.7 Flux partitioning

The partitioning of fluxes which make up NEE into GPP and Reco allows the determination of the contributions made by respiratory and assimilatory processes to NEE (Equation 3.5, as seen in Equation 2.2).

$$NEE = Reco - GPP \quad \text{Equation 3.5}$$

Within research on peat greenhouse gas emissions and carbon loss, understanding the relative contributions of GPP and Reco is critical, due to Reco primarily representing a loss of carbon from decomposition of the peat. In this way, Reco can provide a measure of how fast the peat is being degraded by microbial decomposition in the ecosystem being measured, particularly when the field is bare and  $Reco = Rh$ .

The flux partitioning tool provided within Tovi was used to partition the fluxes into Reco and GPP. The tool estimates Reco using night-time NEE and Ta or Ts using the methods described by Reichstein et al. (2005). Night-time NEE is used as an estimate for Reco due to the assumption that no photosynthesis takes place at night so  $GPP = 0$ , thus  $NEE = Reco$ . The relationship is then extrapolated to calculate daytime Reco estimates.

After removing all flux values that are of poor quality, remaining flux values are partitioned into day and night-time using a global radiation threshold of  $20 \text{ Wm}^{-2}$  (on the assumption that values  $<20 \text{ Wm}^{-2}$  are night-time values) which is checked against local sunset and sunrise times. Temperature sensitivity ( $E_0$ ) for Reco is then estimated over 15 day windows. After the calculation of  $R_{ref}$  (respiration independent of temperature), Reco is then calculated for each point in time using the equation:

$$Reco(t) = R_{ref}(t)e^{E_0(1/(T_{ref}-T_0)-(1/T_i(t)-T_0))} \quad \text{Equation 3.6}$$

where time-dependent parameters and variables are indicated by (t),  $T_0$  is a constant reference temperature of  $-46.02^\circ\text{C}$  (derived in Lloyd and Taylor (1994)) and  $T_i$  is either the air or soil temperature.

Reco is subtracted from the corresponding NEE for the related half hour period to find the GPP. Within this study, Ta was used rather than Ts due to showing a stronger relationship with night-time NEE (for further examination of this relationship, see Chapter 4.2).

### 3.2.6 Energy Balance Closure

Energy balance closure (EBC) is a way of examining the quality of raw EC data that derives from the first law of thermodynamics, i.e. that the energy leaving a system must be the same as the energy put into the system. Within the context of EC, this means that the energy fluxes (latent

heat (LE) + sensible heat (H)) must be equal to or less than the available energy. This is often referred to as the energy balance closure problem as energy fluxes are often less than the available energy (Aubinet et al., 1999, Leuning et al., 2012, McGloin et al., 2018). The energy balance closure of a system is represented using the equation:

$$LE + H = R_n - G - J \quad \text{Equation 3.7}$$

where LE is the latent heat flux, H is the sensible heat flux, R<sub>n</sub> is net radiation, G is soil heat flux and J is the energy stored within vegetation through photosynthesis. At EN-SP3, it was not possible to measure the energy stored within the vegetation due to the inability to locate instrumentation within the field because of crop management practices.

Within modern EC systems, complete energy closure is seldom achievable. Typically, there is an underestimation of the energy fluxes (LE + H) at EC sites of between 5% and 30% (Wilson et al., 2002, McGloin et al., 2018). In the past, this was thought to be due to an overestimation of R<sub>n</sub>. However, technological advancements within instrumentation and improved corrective methods nowadays make it unlikely that this explains the whole of the EBC problem (Foken, 2008). Numerous alternatives have been suggested including: underestimation of the storage terms (Leuning et al., 2012), lack of homogenous land / vegetation cover (Stoy et al., 2013), the influence of meteorological variables (Franssen et al., 2010), phase differences between wind velocity and water vapour signals (Gao et al., 2017, McGloin et al., 2018), and the omission of low frequency turbulence due to the 30 minute averaging period (Mauder et al., 2010).

Two methods were used to assess the closure fraction. The first was by plotting the half hourly sums of energy fluxes against available energy and using ordinary least squares linear regression to derive slope and intercept values. A slope of 1 and an intercept of 0 represents ideal closure. In addition, the Energy Balance Ratio (EBR) was calculated using the equation:

$$EBR = \frac{\sum(LE + H)}{\sum(R_n - G)} \quad \text{Equation 3.8}$$

where the sum of energy flux (LE + H) is divided by the sum of available energy (R<sub>n</sub> - G). A ratio of 1 represents ideal closure. EBR provides a good evaluation of overall EBC over longer time scales by averaging over random errors in half-hourly measurements, however, it can miss biases in the data such as the tendency to overestimate positive fluxes during the day and underestimate negative fluxes at night (Mahrt, 1998).

### 3.3 Additional C Imports and Exports other than EC

Throughout the measurement period, additional C was imported onto the field through the planting of crops, with a small amount imported via seeds for the maize crop and a more

significant amount through plug plants grown within peat. C was primarily exported through biomass removal from the field (harvesting).

For each crop, information on the number of seeds or plug plants sown on the field was obtained from the farm manager (Rob Parker, pers. comm.). For the celery crop (planted using plug plants in peat plugs), five samples of the plug plant and plug were taken. C content was then calculated by obtaining the dry weight of the biomass (samples dried to constant weight at 60 °C). Loss on Ignition was then performed (at 550 °C for 2 hours) to find the organic C content of the peat plug (5.79 g C per plug plant).

For the C content of the crop biomass removed from the field via harvesting, five samples of each plant were taken from the field at the time of harvesting and transported in airtight bags back to the University of Leicester. They were then dried at 60 °C until they reached constant weight to provide dry weight biomass values. Using values from literature, biomass values were then converted to C content (Maize: 44% C in biomass (Latshaw and Miller, 1924), Celery: 34% C in biomass (Reitz et al., 1997, Cumming, 2018)). Using the amount of biomass harvested from the fields (Rob Parker, pers. comm.) the approximate C export was calculated.

The import and/or export of C via aeolian transportation is not captured using the EC technique and the relevant methodology is discussed separately in Chapter 6.

### 3.4 Chapter 3 Summary

This chapter provides information on the regional climate of the study area, information on the location and characteristics of the study sites, the rationale for their selection, and a summary of the farm management procedures at each site. The principal data collection method, Eddy Covariance (EC), is described along with a discussion of the data analysis methodology. Assessment of aeolian erosion is addressed separately in Chapter 6).

Study sites are located within the East Anglian region of England, EN-SP3 located on a wasted peatland and EF-DA on a deep peatland, both of which are under intensive agricultural management. This study is the first to assess the C flux (C sources and C removals) of a wasted peatland under agricultural management. Carbon dioxide flux for EN-SP3 were obtained using a micrometeorological approach, namely EC. Aeolian erosion was measured at both EN-SP3 and EF-DA (full description of methods is in Chapter 6).

EddyPro software was used to analyse the raw EC flux data and process it into the 30 minute flux periods required to calculate annual NEE budgets. The Tovi software package was then used to quality control the flux data including: foot printing,  $u^*$  filtering and filling of data gaps in both

the biometeorological and flux data sets. The EBC at the sites was assessed as a measure of how accurate the EC measurements were over the data collection period. Finally, the methods used to assess additional C imports onto and exports from the study fields was explained.

## 4 Engine Farm: Drivers of CO<sub>2</sub> fluxes and a field-scale C budget at a wasted agricultural fen peatland

This chapter addresses research question 1, defined in Section 1.1:

1. What are the key drivers of NEE (Net Ecosystem Exchange) from a wasted lowland peatland under arable agriculture?

An examination of the drivers of CO<sub>2</sub> fluxes from a study site located on a wasted agricultural peatland is presented, namely Engine Farm – Spooners 3 field site (EN-SP3) (Chapter 3.1.2). Two data periods were addressed: period one is 4<sup>th</sup> May 2018 to 10<sup>th</sup> December 2018, and period two is 17<sup>th</sup> May 2019 to 17<sup>th</sup> May 2020. The environmental conditions during the two periods are detailed before an examination of those found to be the most significant drivers of CO<sub>2</sub> fluxes.

The drivers of Reco were assessed using all available quality-controlled night time NEE values from across the data collection periods. Air Temperature (Ta) was analysed as the primary driver of Reco using an empirical Arrhenius model (Lloyd and Taylor, 1994). The residuals of the model fit were then analysed against Soil Water Content (SWC) to check for the impact of SWC on Reco and to see if SWC could explain any of the additional variation in Reco. Farm management practices are discussed as an additional driver of Reco during bare periods. Gross Primary Productivity (GPP) is investigated as the primary contributor to NEE during cropping periods by examining the light response of the crops using a modified Michaelis-Menten (rectangular hyperbole) type equation (Falge et al., 2001) which relates Photosynthetically Active Radiation (PAR) to NEE. The residuals of the model fit were then analysed against Ta, Soil Temperature (Ts), Vapour Pressure Deficit (VPD) and SWC. The importance of these environmental drivers for NEE are then discussed, highlighting those which drive the different NEE components and how these vary across crop cycles. Within this study, positive values denote C loss from the field and negative values denote C gain. Environmental conditions

### 4.1.1 Air (Ta) and Soil (Ts) Temperature

For each year, Ta and Ts followed a typical seasonal pattern. Throughout the summer months, consistently higher values for Ta and Ts were obtained in 2018 compared to 2019, with correspondingly higher Rg (Figure 4.1). This was despite 2019 having higher maximum Ta for June, July and August. These high average temperatures during 2018 coincided with a maize crop that was on the field from 18<sup>th</sup> May to 2<sup>nd</sup> October 2018. The high temperatures were

coupled with low rainfall (Figure 4.2) leading to stunting of the crop. The unusually early frost on 29<sup>th</sup> September 2018 led to an early harvest leaving the crop yield smaller than usual.

Both 2019 and 2020 experienced winter and spring air temperatures that were higher than the 50 year average. Ta in winter 2018/19 went below zero for 475 half hourly periods, with the lowest temperature observed in January 2019 (-5.3°C). This contrasted with winter 2019/20, with half hourly Ta dropping below 0°C on just 154 occasions. Autumn temperatures varied little between 2018 and 2019 and were similar to the 50 year average. Overall, seasonal Ta varied little between the years, with <1°C difference observed across all seasonal averages. There was more variation within monthly averages, with an average variation of 1.2 °C in Ta between the months, and with January 19/20 showing the biggest difference of 2.6°C.

Monthly Ta and Ts were highly correlated (Pearson's correlation:  $r = 0.98$ ,  $p < 0.001$ ,  $n = 22$ ) with observed Ts following a similar annual pattern as Ta. Overall, there was less variation between minimum and maximum Ts than Ta. No freezing soil temperatures were observed at any point, with the lowest recorded temperature of 2.2°C in December 2019. The highest Ts of 21.5°C was measured in July 2018. Between the years, average monthly soil temperatures in 2018 were higher than in 2019, with the biggest difference of 2.5°C occurring between the summer months, in particular in June and July, when the 2018 Ts was 2.8°C and 2.6°C higher respectively (Figure 4.1.B2). Less variation was observed between winter and spring data for 2019 and 2020, with a difference of less than 0.3°C.

#### 4.1.2 Global Radiation (Rg)

Monthly totals of Rg followed a typical yearly cycle, with the lowest values obtained in winter (189, 170 kW m<sup>-2</sup>) and the lowest month overall being December for both 2018 and 2019. Highest values were recorded in summer 2018 and 2019 (994, 897 kW m<sup>-2</sup>), however monthly peak Rg appeared to differ between the years, with the highest monthly Rg (and highest recorded overall) in May 2020 (388 kW m<sup>-2</sup>) compared to July (369, 320 kW m<sup>-2</sup>) for 2018 and 2019.

In contrast to Ta and Ts, spring Rg values were higher than autumn values by ~400 kW m<sup>-2</sup>, showing that both Ta and Ts lag behind Rg. Additionally, Rg followed a similar monthly pattern to Ta between the years, with months that had a higher average Ta also having a higher average Rg. Overall, the years had similar patterns other than during the summer. The Rg in June and July 2018 were 69 and 50 kW m<sup>-2</sup> higher than 2019, respectively.

Crop planting for both the maize crop and the phacelia and buckwheat cover crop occurred in May which coincided with the period of peak radiation. The celery crop in 2019 was planted just

after the period of peak radiation, but still within the summer and early autumn months that see high Rg levels. This difference in planting times is a trade-off between the temperatures that are required for a plant's optimum growth and the period of optimum Rg, with some crops requiring warmer temperatures than others to grow effectively.

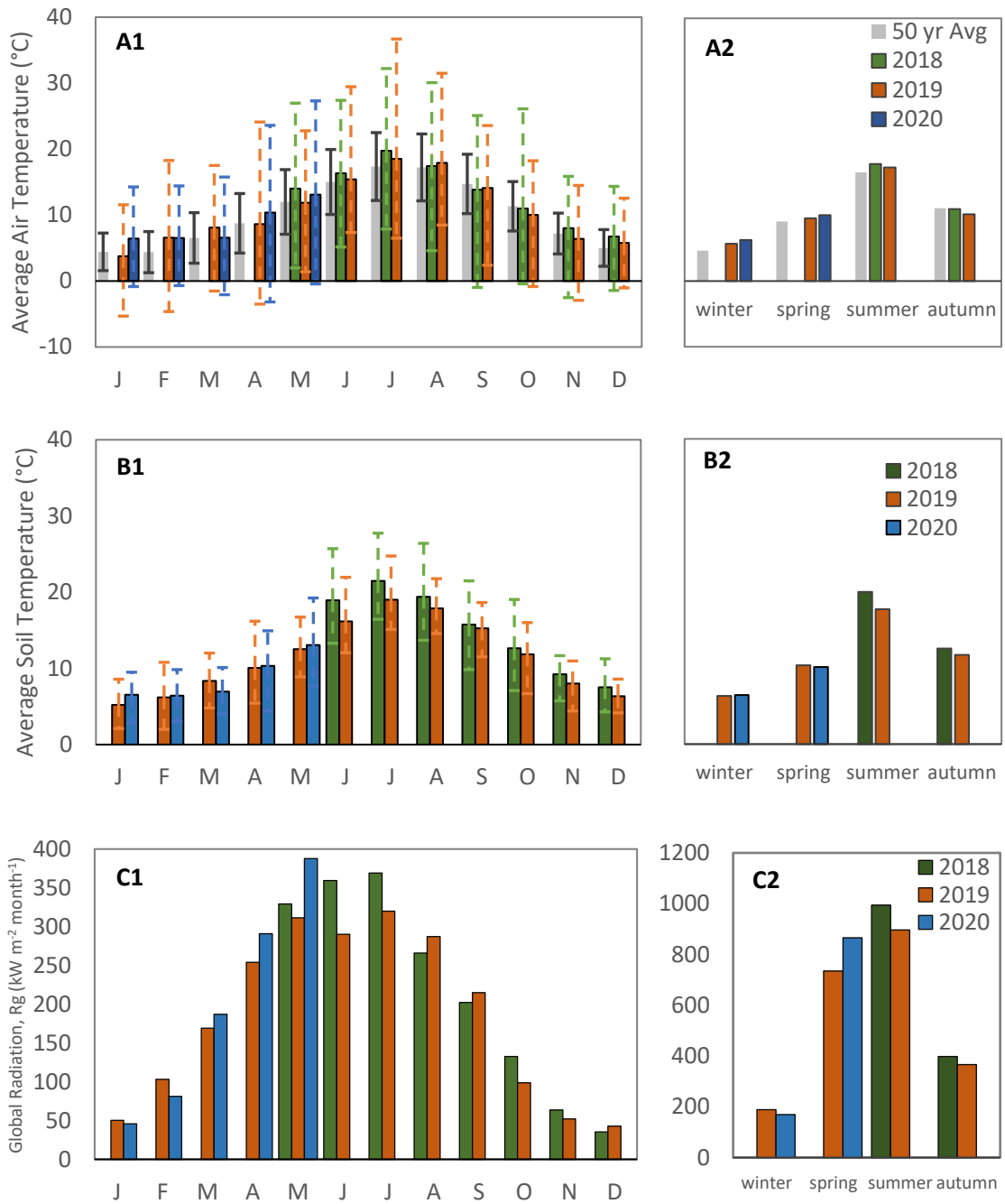
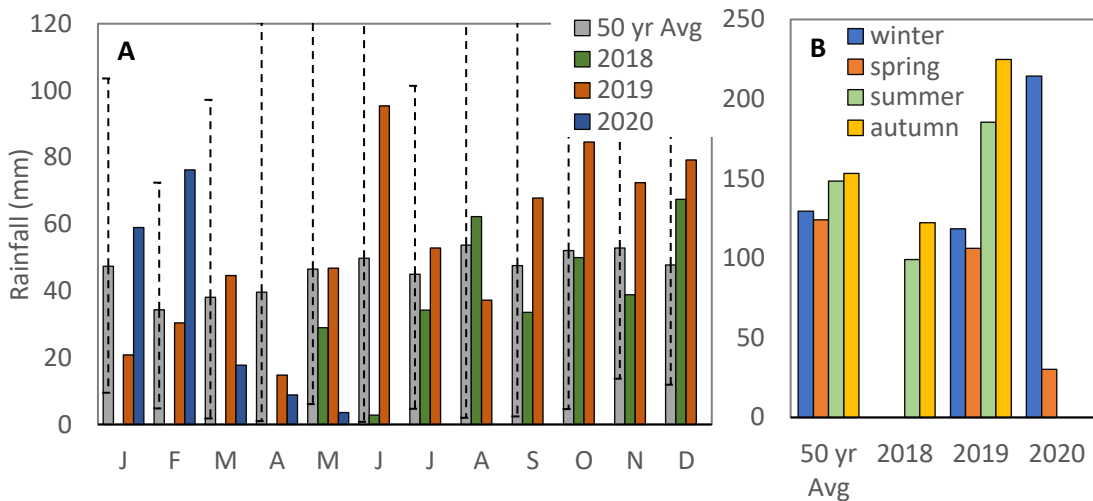


Figure 4.1. A1: Monthly mean air temperature. Error bars denote the minimum and maximum, for the 50 year average recorded at the local weather station situated at CAMBS NIAB. A2: Mean seasonal air temperature. B1: Monthly mean soil temperature. B2: Mean seasonal soil temperature. C1: Monthly totals of Rg (Global Radiation). C2: Seasonal totals of Rg.

#### 4.1.3 Rainfall and Water Table Depth

Rainfall across the 24 month period (May 2018 to June 2020) always fell within the minimum and maximum recorded values at the local CAMBS NIAB weather station (UK Met Office, 2019), other than in 2020 when rainfall in February (76.2mm) was greater than the maximum value of the 50 year average (72.4mm) (Figure 4.2).



*Figure 4.2. A. Rainfall over the 27 month period of data collection (May 18 to June 20) at Engine Farm, EN-SP3. Bars represent the total rainfall recorded at the site for each month. Grey bar denotes the 50 year average (1968 to 2018) recorded from the local weather station situated at CAMBS NIAB, error bars indicate the max and min rainfall recorded in each moth over the 50 year period. B. Yearly rainfall presented in seasons.*

Rainfall in 2018 was consistently lower than the 50 year average. In particular, the spring period had a very low rainfall total of 29 mm (95mm less than the 50 year average). This led to a stunting of the maize crop in 2018 which was planted under drought conditions. This contrasted with 2019, which had summer and autumn months that were consistently wetter than the 50 year average (Figure 4.2). This led into a wetter than average winter of 2019/20 with a total rainfall of 214 mm, 94 mm greater than the 50 year average (130 mm). This particularly impacted the harvesting of the celery crop, which took longer than usual due to machinery struggling with the waterlogged field. This led into the wet winter of 2019/20, which prevented farm machinery from tilling the field in November/December 2019. The field was left unmanaged throughout the winter, with pooling of water present on the field surface preventing normal winter ploughing operations. The field was eventually ploughed on 10<sup>th</sup> March 2020. Spring 2020 was unusually dry with rainfall of less than 20 mm observed for March, April and May of 2020.

#### Water table depth

Water table depth across the Spooners 3 field is controlled primarily by the Lark Engine Pump house which is situated on the Lark Engine Drain, bordering the NW field edge. The Burnt Fen

IDB use this to regulate the water table in the surrounding fen. They operate on a summer (~1 m below field surface) and winter setting (~2–2.5 m), with the water table raised in summer when more water is used for irrigation (March–November 2018) (Figure 4.3). During the low rainfall of 2018, the summer water table never reached 1 m and was often closer to 1.5 m below the field surface. The low rainfall in winter 18/19 led to the water table being more than 2 m below the field surface well into the spring of 2019 when the water table was 1.25 m below the surface until the start of April 2019. The wet summer of 2019 (Figure 4.2) led to a much higher water table than summer 2018, with the water table consistently within 1 m of the field surface and sometimes within 0.7 m. When the water table was dropped to its winter setting at the start of October 2019, the level dropped for a short period, before the high autumn 2019 rainfall and historic rainfall in winter 2019/20 brought the water table consistently within 1 m, and often within 0.75 m of the field surface. Winter 2019/20 exhibits sharp peaks and troughs for individual rainfall events when the water table rose quickly followed by more gradual declines as the ditches were lowered by the Lark Engine Drain pump house. The depth of the water table was always below the peat level (Figure 4.3).

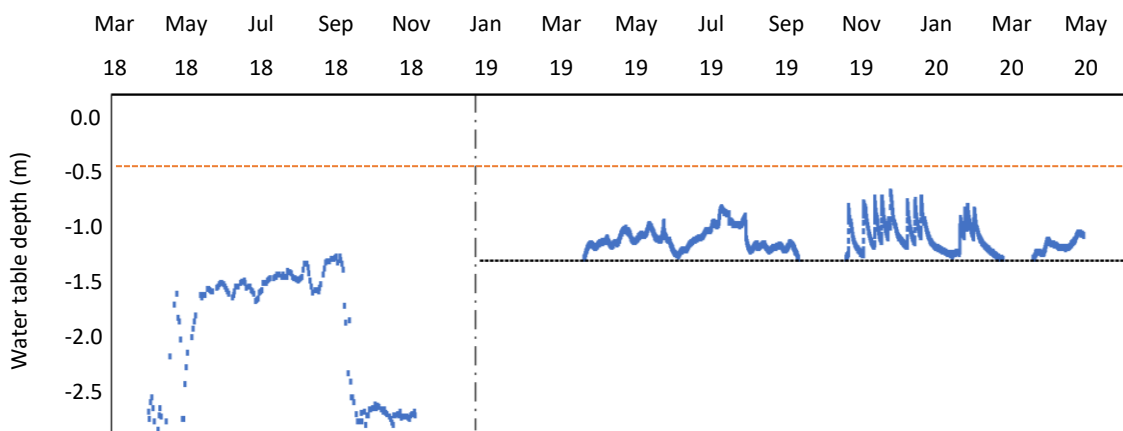


*Figure 4.3. Water table depth at Engine Farm on Spooners 3 field from 1<sup>st</sup> April 2018 to 1<sup>st</sup> June 2020. Up until November-18, water levels are from the Lark Engine Pump House which records water level daily within the Lark Engine Drain which borders the Spooners 3 field. After Nov-18, a borehole and divers (see Chapter.3) at the EC tower location was used to monitor water level (indicated by dotted and dashed line). Divers were situated at 1.25 m, measurements below that were not recorded. The horizontal orange line represents the approximate peat depth across the EC footprint area.*

## 4.2 Drivers of CO<sub>2</sub> fluxes at a wasted agricultural fen peatland

### 4.2.1 Examination of the drivers of Reco

Ecosystem respiration (Reco) is often related to temperature (either Ts or Ta) which is regarded as the main driver of Reco (e.g. Nieven et al., 1998, Cai et al., 2010, Tiemeyer et al., 2016, Matysek et al., 2019). Several different methods have been used to evaluate this, from simple models such as the Q<sub>10</sub> relationship to more complex ones such as those involving neural

networks (Richardson et al., 2006). Here, to examine the drivers of Reco, the widely used exponential model by Lloyd and Taylor (1994) was used to relate Ta to Reco. This is a model which has been widely used within the EC community for both gap filling and separation of fluxes (Reichstein et al., 2005) and for further examination of the drivers behind Reco (Parmentier et al., 2009). The equation used by Lloyd and Taylor (1994) was:

$$Reco = R_{10} e^{E_0(1/(T_{ref}-T_0) - 1/(T-T_0))} \quad \text{Equation 4.1}$$

where  $T_0$  is a constant set at  $-42.02^{\circ}\text{C}$  (Lloyd and Taylor, 1994),  $T_{ref}$  is set at  $10^{\circ}\text{C}$ . The activation energy parameter,  $E_0$  and  $R_{10}$  temperature sensitivity at  $10^{\circ}\text{C}$  are left as free parameters. Ta was chosen to parameterise the model over Ts due to better model parameterisation. This is likely due to the soil instruments being within the field boundary leading to unrealistic readings compared to what is experienced in the field. Additionally, the soil instruments may be too deep at 5 cm to capture the temperature fluctuations most affecting Reco.

The suitability of the model was assessed through the calculation of an R-Squared ( $R^2$ ) value for the model fit, giving an indication of how well variation within Reco was explained by the model. Additionally, the residuals of the model fit were analysed against SWC to assess how much of the unexplained variation could be accounted for by changes in SWC using Spearman's Rank ( $r_s$ ). Spearman's Rank was chosen to assess the strength and direction of the relationship due to the relationship between the residuals and SWC not necessarily being linear, making other tests (such as Pearson's correlation) unsuitable.

#### 4.2.1.1 Data period 1: 4<sup>th</sup> May to 10<sup>th</sup> December 2018

This first data period covers the dates in which the maize crop was collected. Within this range, there were 1,597 half hourly night time periods which had 6 usable half hourly periods or more. The rest were excluded from the dataset, in line with Reichstein et al. (2005) to remove data that might generate bias or increased variability in the data set.

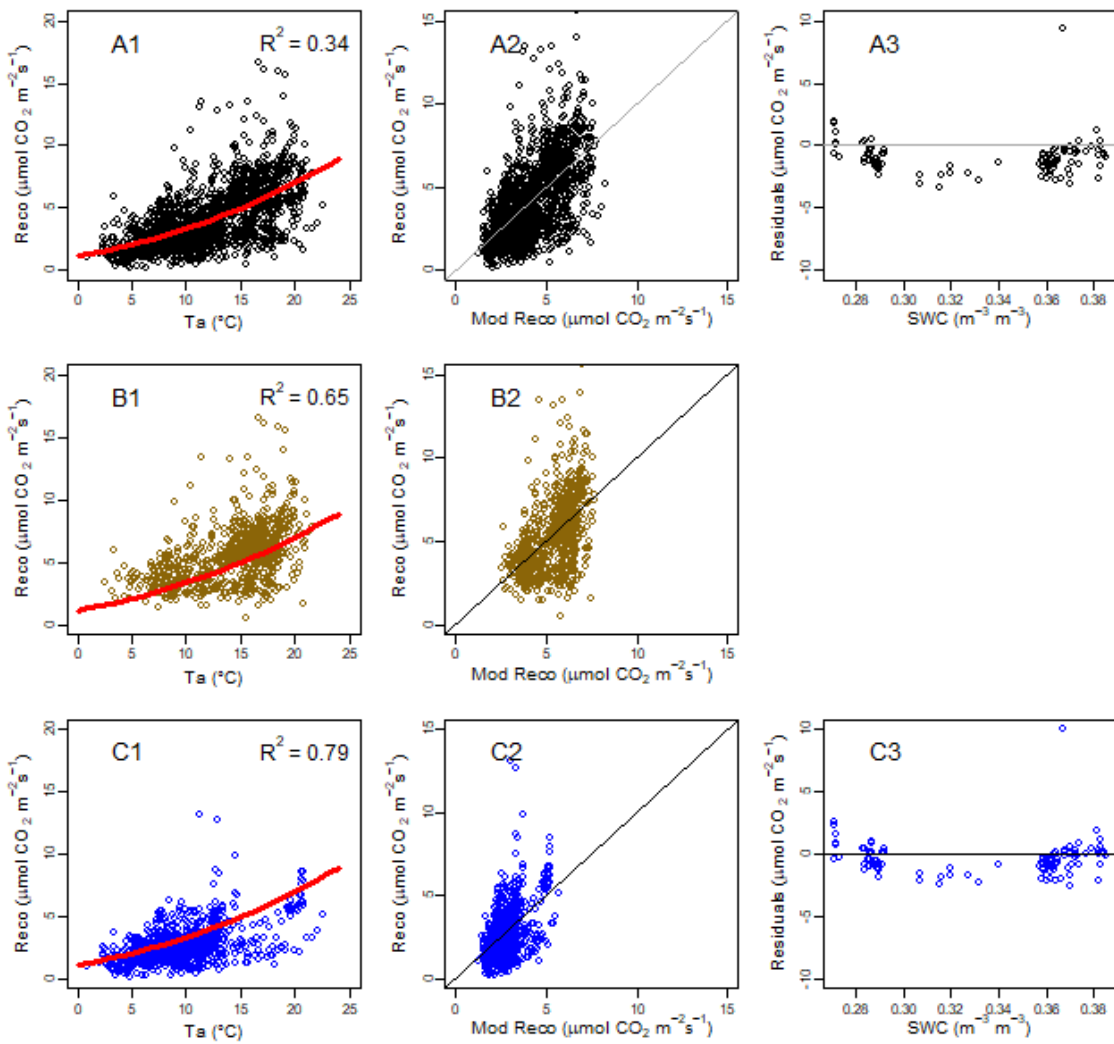


Figure 4.4. Reco for data period 1 (night time NEE for nights where there was at least 6 NEE half hourly periods) against air temperature (Ta) along with the Lloyd & Taylor Reco model (red line,  $R^2$ ), a 1:1 plot of modelled and predicted values (2), and analysis of the residuals against SWC (3). A (black) is all available data, B (yellow) is the maize cropping period, and C (blue) is the period when the field was bare.

Using Ta, the model was found to explain Reco well for the maize crop (Figure 4.4.B1, B2) and bare periods (Figure 4.4.C1, C2) with an  $R^2$  of 0.65 and 0.79 respectively (Table 4.1). The  $R^2$  values are much higher than those obtained when the model was parameterised over the entire dataset ( $R^2 = 0.34$ ). This was likely due to the model not being as accurately parameterised over a period which included multiple seasons, field conditions and farm management practices (Reichstein et al., 2005). The 1:1 plots show that overall the model is balanced (Figure 4.4.A2, B2, C2). There appears to be increasing variation at higher NEE and modelled NEE values, most clearly seen during the maize cropping period that the model struggles to explain (Figure 4.4.B1, B2).

Due to the instruments being installed in the autumn of 2018, there was no SWC data available over the maize cropping period. When the residuals were analysed against SWC, no significant

correlation was observed for data over the bare period ( $r_s = -0.04$ ,  $n = 103$ ,  $p = 0.67$ ), suggesting that SWC poorly explained any remaining variation within the dataset (Figure 4.4.A3 and C3).

The temperature independent rate of Reco,  $R_{10}$ , has been observed to vary seasonally due to seasonal changes in soil conditions (e.g. Davidson et al., 1998, Falge et al., 2002, Reichstein et al., 2005) with the potential for three-fold variance throughout a year. Variation was observed between the maize and bare periods, with the maize  $R_{10}$  1.5 times greater than the bare period (Table 4.1), likely capturing some of the seasonal variation as well as the very different soil and cropping conditions recorded in each period. This is similar to Reichstein et al. (2005) who observed an increase in  $R_{10}$  under high growth conditions. The temperature sensitivity parameter  $E_0$  showed small variations between the maize ( $E_0 = 194.12$ ) and bare ( $E_0 = 217.56$ ) cropping periods (Table 4.1), both much less than  $E_0$  for the entire data period ( $E_0 = 274.36$ ).

*Table 4.1. The  $R_{10}$  and  $E_0$  values for each model parameterisation with standard error and associated  $R^2$  to indicate model fit. Significance of the terms is indicated by \*  $p < 0.01$  and \*\* for  $p < 0.001$ .*

	Period	$R_{10}$ ( $\mu\text{mol}^{-1} \text{m}^{-2} \text{s}^{-1}$ )	$E_0$ (K)	$R^2$
All	2018-05-04 to 2018-12-10	3.32 (0.06)**	274.36 (10.22)**	0.34
Maize	2018-05-18 to 2018-10-02	4.27 (0.12)**	194.12 (14.74)**	0.65
Bare	2018-10-03 to 2018-12-10	2.78 (0.058)**	217.56 (14.61)**	0.79

#### 4.2.1.2 Data period 2: 17<sup>th</sup> May 2019 to 17<sup>th</sup> May 2020

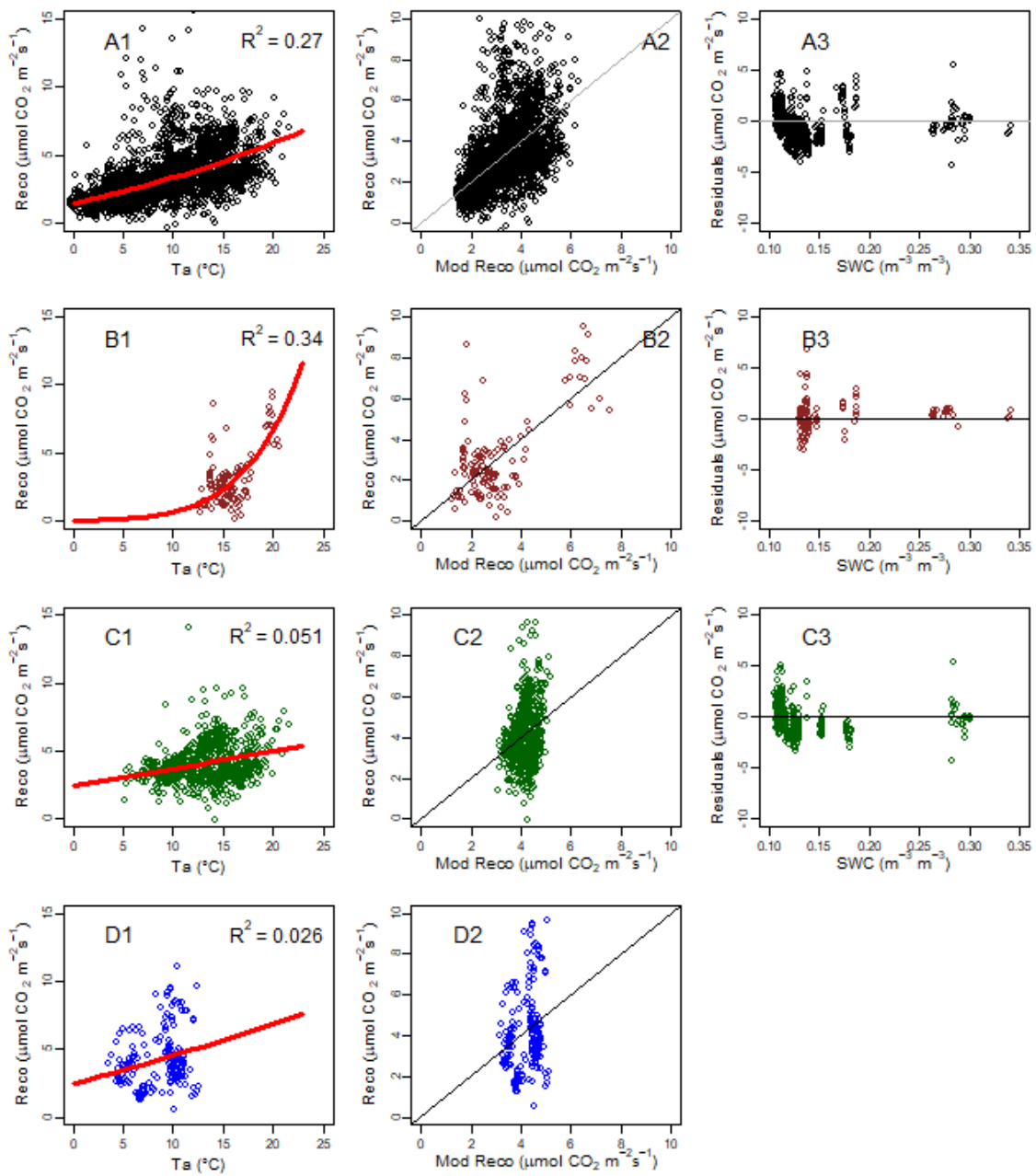


*Figure 4.5. Reco for data period 2 (night time NEE for nights where there was at least 6 NEE half hourly periods) against air temperature (Ta) along with the Lloyd & Taylor Reco model (red line, R2), a 1:1 plot of modelled and predicted values (2), and analysis of the residuals against SWC (3). A (black) is for all available data, B (brown) is the phacelia and buckwheat cropping period May-Jul '19, C (green) is the celery cropping period Jul-Oct '19, and D (blue) is the period the field was bare Mar-May '20.*

During data period 2, the Reco between 24<sup>th</sup> October 2019 and 9<sup>th</sup> March 2020 was not analysed individually. This is because the field cover was particularly heterogeneous during this time, with a 48 m wide strip of the phacelia and buckwheat cover crop remaining in front of the EC tower whilst the rest of the field was mostly bare following harvesting of the celery crop. It was therefore not representative of either a cropped or bare field.

In contrast to the first data period, the second data period varied in how well the model fitted the data (Figure 4.5) and overall showed a worse fit ( $R^2 = 0.27$ ) (Table 4.2). Individual cropping periods varied with how well Reco was represented by the model, with the model poorly representing the celery crop ( $R^2 = 0.051$ ) and the bare period ( $R^2 = 0.026$ ). The model more accurately represents the period with a phacelia and buckwheat crop ( $R^2 = 0.34$ ) but still less than any of the individual periods from data period one (Maize:  $R^2 = 0.65$ , Bare:  $R^2 = 0.79$ ). The 1:1 plots show that for the celery and bare periods the model struggled to calculate accurate estimates of Reco, with most of the data falling within a small range of modelled Reco values that cover a wider range of measured values (Figure 4.5.C2, D2). The model was more consistent for the phacelia and buckwheat cropping period, showing less variation across a wider range of NEE values (Figure 4.5.B2).

When the residuals were analysed against SWC, a moderate negative correlation was found for the whole data period ( $r_s = -0.37$ ,  $n = 633$ ,  $p < 0.001$ ), driven by the period the celery crop was on the field ( $r_s = -0.37$ ,  $n = 472$ ,  $p < 0.001$ ). From examination of the data, this relationship seems to be primarily driven by low SWC values ( $0.1\text{--}0.15 \text{ m}^3 \text{ m}^{-3}$ ) with lower SWC correlating with a greater underestimation of Reco and higher SWC a small overestimation, which is then consistent with  $\text{SWC} > 0.15 \text{ m}^3 \text{ m}^{-3}$ . This is likely due to increased Reco as the soil dries out.

There was variation within  $R_{10}$ , with the largest variation seen between the phacelia and buckwheat crop (1.69) compared to the bare period (4.52), which had a 2.7 times greater value. This variation is similar to that seen by Reichstein et al. (2005), who observed a three-fold greater  $R_{10}$  at different points of the year. The greater variation in this dataset compared to data period 1, is to be expected since it covers a full year as opposed to part of a year, with individual crops and periods covering different seasonal conditions.  $E_0$  shows a big variation between the phacelia and buckwheat cropping period (532.78) compared to the celery (107.02) and bare (155.79) periods.

Table 4.2. The  $R_{10}$  and  $E_0$  values for each model parameterisation and associated  $R^2$  to indicate model fit.

	Period	$R_{10}$ ( $\mu\text{mol}^{-1} \text{m}^{-2} \text{s}^{-1}$ )	$E_0$ (K)	$R^2$
All	2019-05-26 to 2020-05-02	3.31 (0.032)**	211.40 (6.52)**	0.27
Phacelia and Buckwheat	2019-05-26 to 2019-07-01	1.69 (0.19)**	532.78 (67.15)**	0.34
Celery	2019-07-23 to 2019-10-23	3.71 (0.091)**	107.02 (17.42)**	0.051
Bare	2020-03-10 to 2020-05-02	4.52 (0.17)**	155.79 (47.2)*	0.026

As the model gave a poor fit for the celery and bare periods, an additional factor: ‘when the data was recorded’ was analysed against the residuals. This was done to assess the impact that soil disturbance through tillage had on Reco. For the bare period, a strong negative relationship was indicated ( $r_s = -0.72$ ,  $n = 183$ ,  $p < 0.001$ ), with a large under-estimation of emissions given immediately after ploughing took place on 10<sup>th</sup> March 2020 that steadily reduced over time (Figure 4.6). This indicates that the disturbance of the field played an important role in C emission, with soil disturbance increasing emissions immediately after it took place.

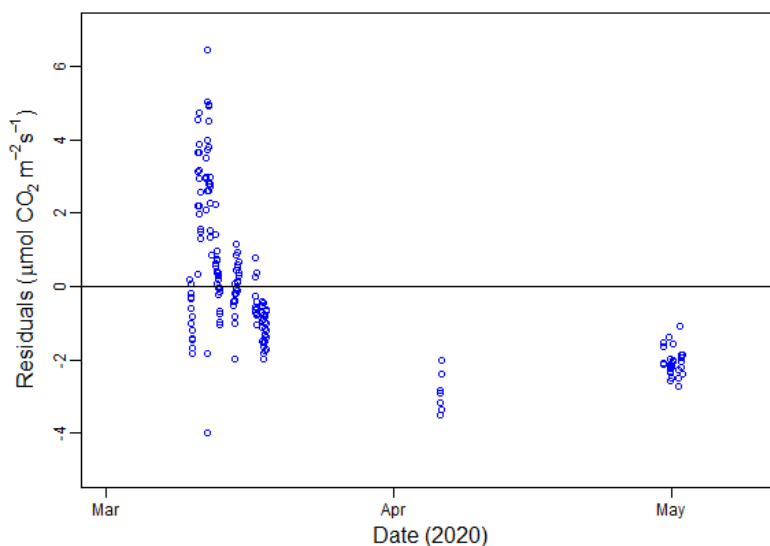


Figure 4.6. The residuals of the model for period 2 over the time the field was bare (3<sup>rd</sup> March to 2<sup>nd</sup> May 2020) plotted against date collected.

#### 4.2.2 Examination of GPP as a driver of NEE

When a crop is on the field, the primary contributor of daytime NEE is expected to be crop growth – expressed as GPP. The primary driver of GPP is normally the light response of the crop, especially within the setting of intensive agriculture where other potential limiting factors to

crop growth (such as nutrient and water availability) are mitigated through fertilisation and irrigation.

To examine different crop light responses through varying seasonal and cropping periods, Michaelis-Menten (rectangular hyperbole) models are often used (Falge et al., 2001, Lohila et al., 2004, Wang et al., 2017a, Burman et al., 2020).

Here a modified Michaelis-Menten equation (Falge et al., 2001) was used:

$$NEE = \frac{-\alpha * PPFD}{\left(1 - \left(\frac{PPFD}{2000}\right) + \left(\frac{\alpha * PPFD}{GPP_{2000}}\right)\right)} + Reco \quad \text{Equation 4.2}$$

where  $PPFD$  is photosynthetically active radiation ( $\mu\text{mol photons m}^{-2} \text{s}^{-1}$ ),  $\alpha$  is the ecosystem quantum yield,  $GPP_{2000}$  ( $\mu\text{mol m}^{-2} \text{s}^{-1}$ ) is the photosynthetic rate at  $PPFD$  2000 ( $\mu\text{mol m}^{-2} \text{s}^{-1}$ ) and  $Reco$  is ecosystem respiration ( $\mu\text{mol m}^{-2} \text{s}^{-1}$ ) (the intercept) where  $Reco$ ,  $\alpha$  and  $GPP_{2000}$  are fitted values parameterised using non-gap filled, quality controlled half hourly NEE and PAR data.

The equation was parameterised in R (R Core Team, 2013) using the `nls()` function from the `statsv3.6.2` base R package for the 2018 maize cropping period and the 2019 phacelia and buckwheat and celery cropping periods. Additionally, the four-week peak growing period was examined (the four week period over which  $\alpha$  was highest). Both day and night time values were used to parameterise the equation to avoid erroneous values for fitted variables which were observed when only daytime values were used.

The suitability of the model was assessed through the calculation of an R-Squared ( $R^2$ ) value for the model fit, which gave an indication of how well variation within NEE was explained by the model. Additionally, the residuals of the model fit were analysed against environmental factors ( $T_a$ ,  $T_s$ , VPD and SWC) using Spearman's Rank ( $r_s$ ) to assess how much of the unexplained variation could be accounted for.

#### 4.2.2.1 Diurnal pattern of Environmental and $CO_2$ Flux variables

Throughout the data collection period, some variation was seen within the diurnal patterns of the environmental variables which are known to drive  $Reco$  and  $GPP$  (Figure 4.7). For all drivers of NEE, they followed a typical daily and monthly diurnal pattern, with a progression of all drivers showing their lowest values and average daily variation in January and December and their highest values and daily variation in June, July and August. The exception to this was  $R_g$ , which reached peak values and variation in May, June and July and started to decrease in August.

Inter-annual variation was observed, and occurred most significantly within the summer months, with higher peak Rg in June and July 2018 than in 2019. This corresponded with higher daytime temperatures for Ta and higher VPD, with all Ts half hourly mean values higher than during the equivalent 2019 period. Higher Ta and Ts values were recorded in 2018 compared to 2019 in the summer and autumn months and also corresponded with a higher daytime VPD. During winter of 2019/20, January 2020 saw a diurnal pattern that was between 2–3°C higher than January 2019, with the preceding February indicating a much higher variation in Ta in 2019 than 2020. Ta had a greater diurnal variation in the spring months than the autumn months. Night time Ta was similar between the years within the summer and autumn months but showed inter-annual variation in the winter and spring months.

Ts overall had a much smaller daily temperature variation than Ta, with minimum and maximum diurnal values varying less than 5°C (other than June and July 2018). A higher Ts was observed in 2018 compared to 2019, whereas 2019 and 2020 were similar apart from January 2020 which was warmer than 2019 and March 2020.

Trends in monthly diurnal NEE were dominated by crop presence, with C drawdown observed when crops were present on the field. In 2018, peak NEE was observed in July and August which corresponded to the peak growth rate of the maize crop – slightly after peak Rg (June, July) but corresponding to peak Ta and Ts (July). This was the period when Ta had the smallest variation between day and night, reducing the risk of low night time temperatures damaging the crop.

There was little difference between night time NEE values in the autumn and winter months of 2018/19, despite 2019 having a cropped strip in front of the flux tower producing a daily C drawdown that persisted until March when the field was ploughed. This was partially due to the high temperatures observed in winter 2019/20, allowing for crop growth around the diurnal maximum for Ta and Rg. Peak maize crop growth in July and August 2018 corresponded with higher night time NEE values than during July 2019 (bare field) and August 2019 (initial growth of a celery crop), likely due to the addition of root respiration from the maize crop.

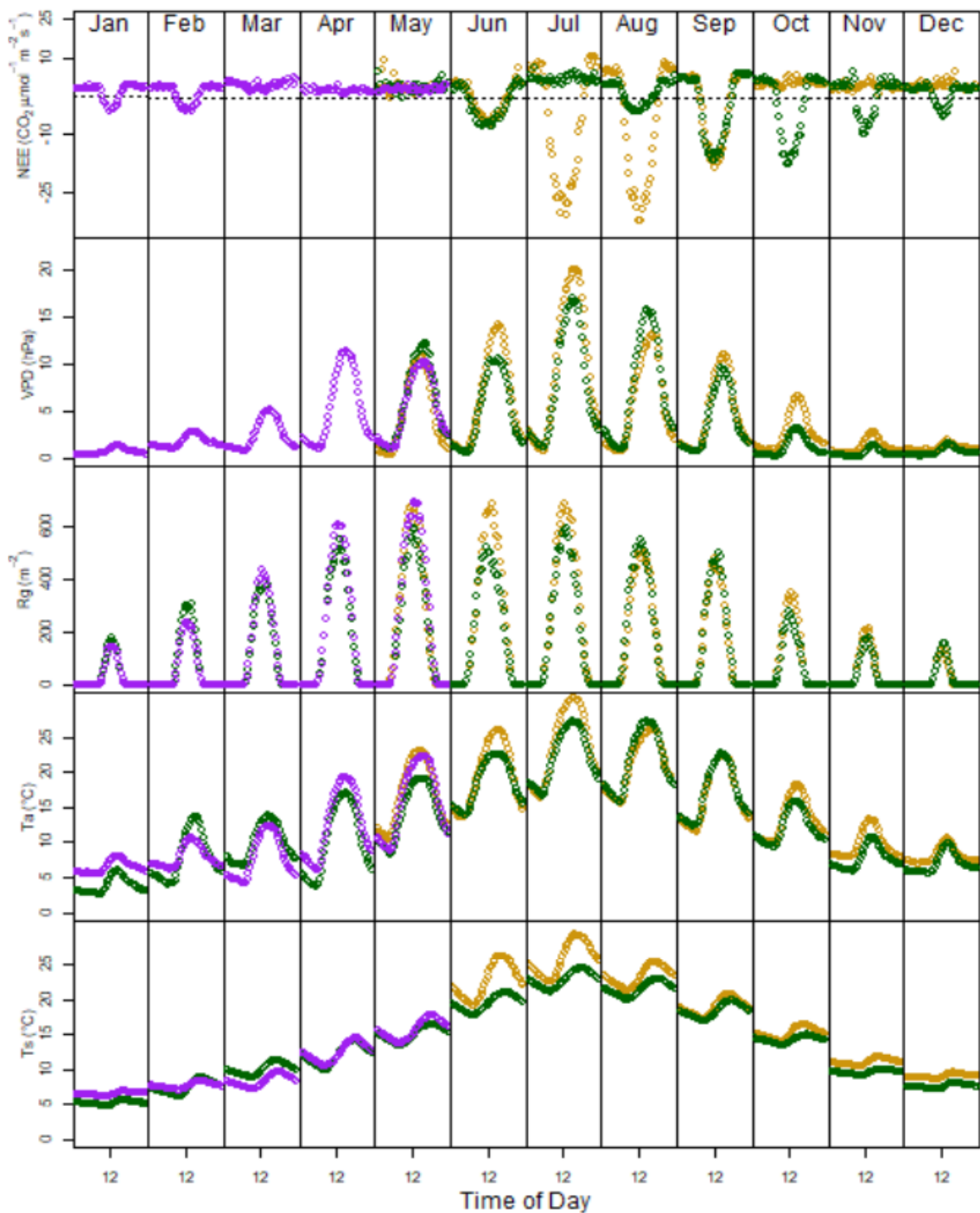


Figure 4.7. The monthly diurnal pattern of NEE, VPD, Rg, Ta and Ts for 2018 (yellow), 2019 (green) and 2020 (purple). Each point represents the mean half-hourly value over the month. For environmental variables Rg, Ta and Ts, data collected included May 2018 to May 2020, for variables NEE and VPD which were recorded as part of the flux tower, data was collected from May to December 2018 at which point the instrumentation required repair and was subsequently replaced in May 2019, running continuously until May 2020.

#### 4.2.2.2 Light Use Efficiency of crops grown in 2019

Light use efficiency (LUE) was analysed for various cropping periods in 2019 (Figure 4.8). LUE was not examined for the 2018 maize cropping period due to the lack of a PAR sensor at the site during that year.

Whilst the primary crop grown in 2019 across the field was celery, this was complicated by the phacelia and buckwheat cover crop planted prior to the celery and retained in a 48 m wide strip along the field edge in front of the flux tower. Additionally, the slow establishment of crops on the field once planted also caused issues with modelling (Cumming, 2018), as growth and LUE steadily increase over time before reaching their peak GPP.

This complex field situation led to issues with modelling LUE, and a wide variability in how well models explained cropping periods: for the celery crop the model explained 38% of the variability, but for the period when the phacelia and buckwheat cover crop covered the entire field this was just 15% (Table 1.2). The model was tested and found not to explain the data during the period with the 48 m cover crop strip present in front of the flux tower as it only covered a small portion of the field and flux tower footprint.

The celery crop showed an  $\alpha$  of  $0.08 \pm 0.1 \text{ } \mu\text{mol } \mu\text{mol}^{-1}$ , much higher than the phacelia and buckwheat cover crop ( $0.02 \pm 0.008 \text{ } \mu\text{mol } \mu\text{mol}^{-1}$ ) and an accompanying higher  $\text{GPP}_{2000}$  of  $11.1 \pm 0.4 \text{ } \mu\text{mol } \text{m}^{-2} \text{ s}^{-1}$  compared to  $6.37 \pm 0.6 \text{ } \mu\text{mol } \text{m}^{-2} \text{ s}^{-1}$  indicating that the celery crop was able to assimilate much more than the cover crop for maximum PAR. The celery crop reached peak assimilation faster and for a much longer period of time (Figure 4.8.C) than the cover crop (Figure 4.8.B) which only just started to reach peak assimilation before it was disked. This was likely due to the celery being grown closer to the optimum growth period (Figure 4.7) and the minimisation of limiting growth factors through fertilisation and irrigation. The celery crop showed a higher  $\text{Reco}$  of  $4.3 \pm 0.2 \text{ } \mu\text{mol } \text{m}^{-2} \text{ s}^{-1}$  compared to  $3.2 \pm 0.4 \text{ } \mu\text{mol } \text{m}^{-2} \text{ s}^{-1}$ .

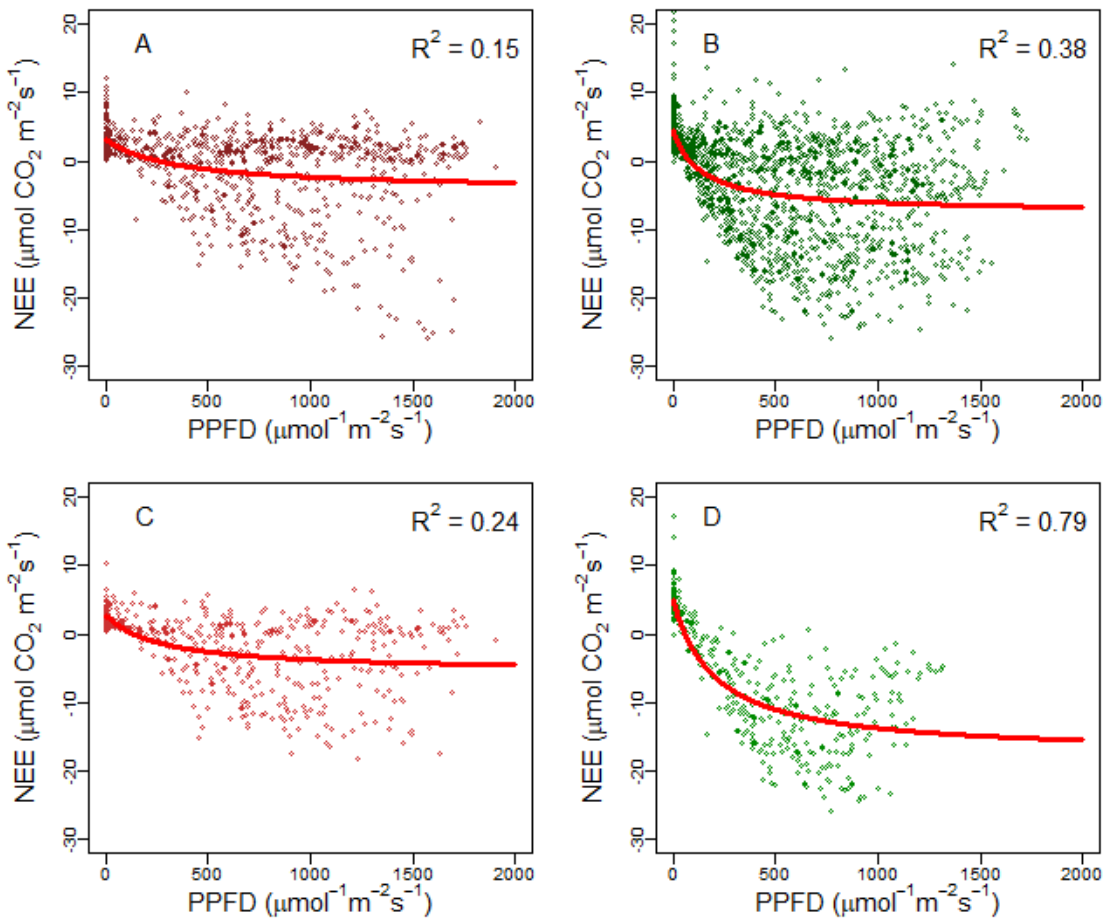


Figure 4.8. Light use efficiency of the Phacelia and Buckwheat cover crop (A) and the Celery crop (B), and the 4 week peak  $\alpha$  period for Phacelia and Buckwheat (C) and Celery crop (D).

Light response was further examined at the four week period which provided peak  $\alpha$  (Table 1.2) to see if it would better explain NEE than for the entire cropping period. A four week period was used to allow good model parameterisation whilst still capturing the peak growth period of the crops.

Overall, the model fit the four week peak  $\alpha$  period better than over the whole period for both cropping periods (Table 1.2). The model explained a high degree of variability in NEE for peak celery growth ( $R^2 = 0.79$ ) indicating that during peak assimilation, NEE was modelled well by LUE. This was not observed for the cover crop, which improved ( $R^2 = 0.24$ ) but still poorly explained the data. The celery crop showed peak  $\alpha$  of  $0.11 \pm 0.1 \mu\text{mol}^{-1}\mu\text{mol}^{-1}$ , much higher than the peak for the phacelia and buckwheat cover crop ( $0.03 \pm 0.01 \mu\text{mol}^{-1}\mu\text{mol}^{-1}$ ) and with an accompanying higher  $\text{GPP}_{2000}$  of  $20.54 \pm 0.6, 7.32 \pm 0.6 \mu\text{mol m}^{-2} \text{s}^{-1}$  respectively, indicating that at its peak, celery was able to better utilize PAR than the cover crop and than the entire celery cropping period ( $\text{GPP}_{2000} 11.1 \pm 0.4 \mu\text{mol m}^{-2} \text{s}^{-1}$ ).

The peak period for the cover crop showed similar  $\alpha$ , GPP<sub>2000</sub> and Reco compared to the overall cropping period (Table 4.3), indicating little change in LUE across its time on the field (though it should be noted that the cover crop was on the field for a much short period of time).

*Table 4.3. Fitted model variables for each of the cropping periods examined and for the peak assimilation rate over a 4 week period with standard error indicated within the brackets. \* indicates a model term found significant ( $p < 0.01$ ),  $r^2$  indicates the model fit to the data.*

Cropping period	Date	n	a ( $\mu\text{mol } \mu\text{mol}^{-1}$ )	Gpp <sub>2000</sub> ( $\mu\text{mol}^{-1} \text{m}^{-2} \text{s}^{-1}$ )	Reco ( $\mu\text{mol}^{-1} \text{m}^{-2} \text{s}^{-1}$ )	R <sup>2</sup>
Phacelia & Buckwheat cover crop	2019-05-18 to 2019-07-01	834	0.02 (0.008)*	6.37 (0.6)*	3.2 (0.4)*	0.15
Peak Phacelia & Buckwheat cover crop	2019-06-01 to 2019-06-28	481	0.03 (0.01)*	7.32 (0.6)*	2.8 (0.5)*	0.24
Celery	2019-07-23 to 2019-10-23	2045	0.08 (0.01)*	11.1(0.4)*	4.3 (0.2)*	0.38
Peak Celery	2019-04-19 to 2019-10-11	555	0.11 (0.01)*	20.54 (0.6)*	5.0 (0.3)*	0.79

#### 4.2.2.3 Residual analysis for the light use efficiency model

Whilst the models explained some of the variation seen within NEE, particularly within the peak growth period of the celery crop, there was still unexplained variation in NEE (Figure 4.9). SWC showed moderate negative correlation for the phacelia and buckwheat ( $r_s = -0.53$ ,  $n = 723$ ,  $p < 0.001$ ) and a strong negative correlation to peak phacelia and buckwheat ( $r_s = -0.61$ ,  $n = 370$ ,  $p < 0.001$ ). This indicated that at low SWC (particularly below  $0.15 \text{ m}^3 \text{ m}^{-3}$ ), water stress impacted the plant growth reducing the GPP. This was also observed for the peak celery growing period ( $r_s = -0.43$ ,  $n = 231$ ,  $p < 0.001$ ) (Table 4.4). In contrast, the celery period overall indicated a weak positive correlation ( $r_s = 0.28$ ,  $n = 1519$ ,  $p < 0.001$ ), though it is important to note that the celery full crop includes a seedling stage where the ground is bare whilst the celery establishes. During this stage, the GPP would be lower than predicted, leading to an under-estimation of CO<sub>2</sub> uptake.

VPD showed a moderate positive correlation for the phacelia and buckwheat crop ( $r_s = 0.31$ ,  $n = 834$ ,  $p < 0.001$ ), phacelia and buckwheat peak growth period ( $r_s = 0.31$ ,  $n = 481$ ,  $p < 0.001$ ) and the celery crop ( $r_s = 0.31$ ,  $n = 2045$ ,  $p < 0.001$ ). This is as expected, with high VPD causing a reduction in GPP as photosynthesis becomes limited by stomatal closure as the crop closes its stomata to prevent water loss. This matches with the similar correlations seen between the residuals and Ta, as VPD rises with temperature (Table 1.3). This matched with Ts for the celery cropping period which showed moderate correlations during both the peak growth period ( $r_s = 0.35$ ,  $n = 555$ ,  $p < 0.001$ ) and over the whole crop ( $r_s = 0.47$ ,  $n = 2045$ ,  $p < 0.001$ ). These relationships were not observed to be as strong during the peak celery growing period compared to the whole celery cropping period (Table 4.4). This was likely due to a smaller range of temperatures observed during the celery peak growing period (Ts peak: 10°C to 17°C; Ta peak: 5°C to 23°C) compared to the whole growing period (Ts all: 10°C to 24°C; Ta all: 5°C to 32°C) which prevented the crop from being significantly limited by VPD (Figure 4.9).

The positive correlation with Ta was not as strong during the phacelia and buckwheat crop (Table 4.4). During this period, temperatures less consistently reached above 25°C, resulting in fewer occasions when the crop growth would be limited. In contrast, Ts for the phacelia and buckwheat cropping period showed weak negative correlations, suggesting a slight overestimation of CO<sub>2</sub> uptake at Ts above 18°C.

*Table 4.4. Spearman's rank correlations between the residuals for the cropping and peak a cropping period. All correlations were found to be significant below  $p < 0.001$ . Weak correlation ( $<0.3$ , white), moderate correlation ( $0.3 >$  and  $<0.6$ , light blue positive, light yellow negative) and strong correlation ( $>0.6$ , dark blue positive, dark yellow negative) are indicated.*

	Ta	Ts	VPD	SWC
<b>Phacelia and Buckwheat</b>	0.23 (n = 834)	-0.28 (n = 834)	0.31 (n = 834)	-0.53 (n = 723)
<b>Peak Phacelia and Buckwheat</b>	0.18 (n = 481)	-0.16 (n = 481)	0.31 (n = 481)	-0.61 (n = 370)
<b>Celery</b>	0.41 (n = 2045)	0.47 (n = 2045)	0.31 (n = 2045)	0.28 (n = 1519)
<b>Peak Celery</b>	0.27 (n = 555)	0.35 (n = 555)	0.21 (n = 555)	-0.43 (n = 213)

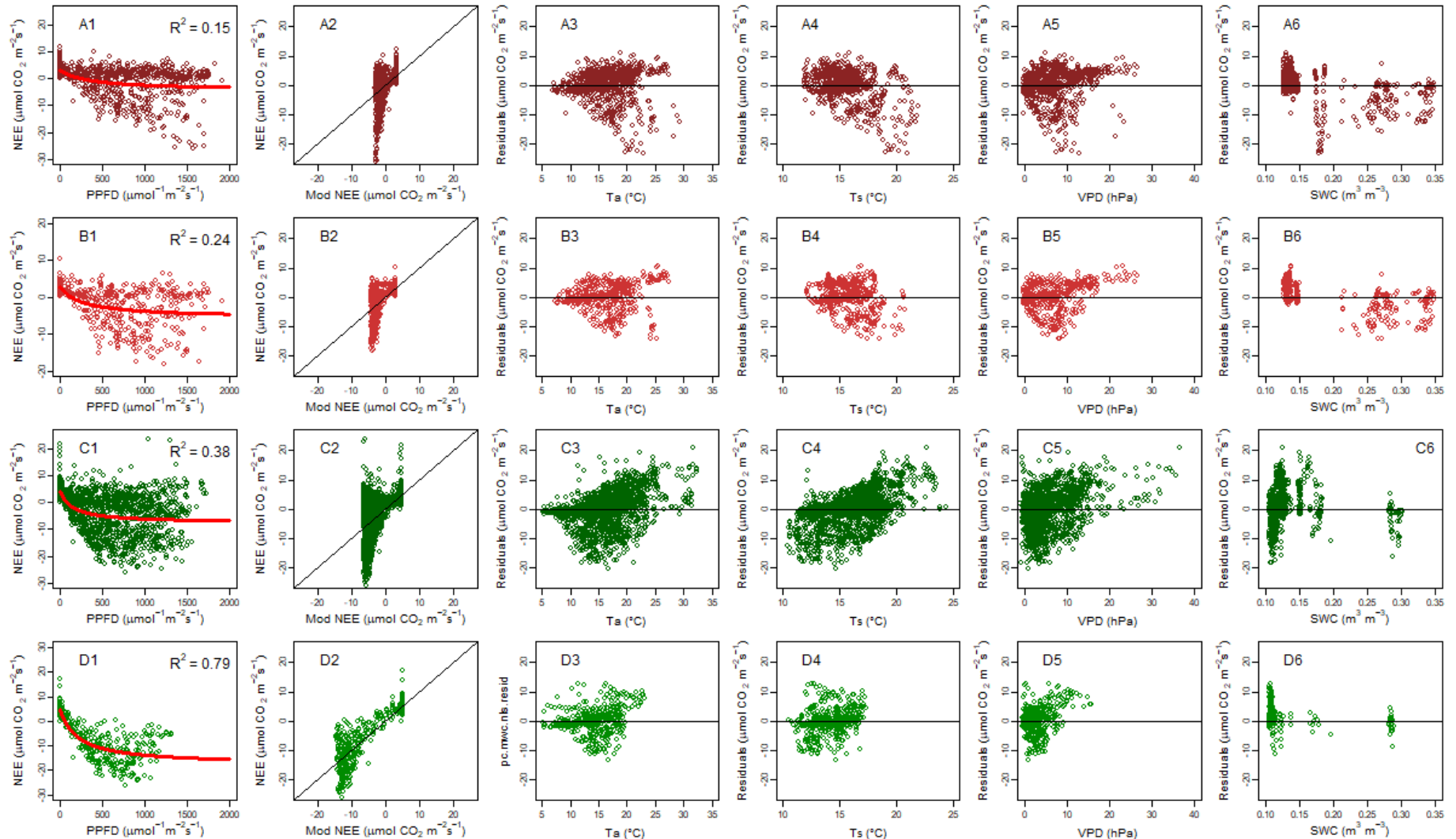


Figure 4.9. Light use efficiency of the Phacelia and Buckwheat cover crop (A1) and the Celery crop (B1), and the 4 week peak  $\alpha$  period for Phacelia and Buckwheat (C1) and Celery crop (D1) along with the model fit  $R^2$  value and associated 1:1 plot (2). Residuals for each model fit plotted against Ta (3), Ts (4), VPD (5) and SWC (6).

#### 4.2.3 Discussion of Drivers of CO<sub>2</sub> emissions

##### 4.2.3.1 Ecosystem Respiration (*Reco*)

###### 4.2.3.1.1 Temperature

Overall, Reco was shown overall to be primarily driven by Ta, consistent with the wider literature where Ts or Ta is often found to be one of the primary drivers (e.g. Richardson et al., 2006, Elsgaard et al., 2012, Morrison et al., 2013, Taft et al., 2017). For the celery crop and bare period in 2019/20, Ta was not clearly established as a primary driver. This is likely a result of the complex situation on the field in 2019/20. The phacelia and buckwheat strip was left unploughed throughout the time the celery crop was on the field, and for a large portion of the bare period after the field was harvested until the whole field was ploughed on 10<sup>th</sup> March 2020. This meant that a significant portion of the EC tower footprint was reflecting the phacelia and buckwheat strip as opposed to the celery field pre/post-harvest. This heterogeneity across the field impacted the expected relationship, as opposed to the strong relationships observed when the field had a homogeneous cover. This was particularly true over the bare period where the heterogeneity of conditions were increased by pockets of celery waste left to decay on the soil surface. During the celery crop, multiple applications were made to the field and it was consistently managed for weeds, especially during early crop growth (Rob Parker, Pers. Comm.). Soil disturbance is known to cause an increase in CO<sub>2</sub> emission when the field is ploughed (Morrison et al., 2013), so constant disturbance of the soil likely increased Reco during this period and confounded the relationship with Ta. Additionally, for the bare period in 2020, data was only collected over a small range of temperatures (4–13°C) compared to the bare period in 2018 (1–23°C) which showed a much stronger relationship to Ta.

The higher R<sub>10</sub> recorded during the maize cropping period compared to the following bare period (Maize 2018: 4.27 ± 0.12; Bare 2018: 2.78 ± 0.058 μmol<sup>-1</sup> CO<sub>2</sub> m<sup>-2</sup> s<sup>-1</sup>) indicates that the presence of the crop provided an additional contribution to Reco of ~65%. This has been observed by Jiang et al. (2010), who measured the contribution of maize root respiration to Reco on a mineral soil in Chongqing, China. Jiang et al. (2010) found that root respiration contributed between 47 and 64% of total soil respiration, similar to the amount seen within this study. These values are similar to those from studies on peatlands with non-maize crops (Kasimir-Klemedtsson et al., 1997, Taft et al., 2017). Across three sites with varying SOM (low: ~20%, med: ~35%, high: 70%), Taft et al. (2017) found cumulative annual CO<sub>2</sub> fluxes for cropped soil were higher compared to bare soils (low: 48%, med: 44%, high: 8%) and suggested that root respiration could be responsible for 4–42% of Reco.

While the celery crop in 2019 had a similar  $R_{10}$  ( $3.71 \pm 0.091 \mu\text{mol}^{-1} \text{CO}_2 \text{m}^{-2} \text{s}^{-1}$ ) to the maize crop suggesting a similar contribution to Reco, the same was not true for the phacelia and buckwheat crop ( $1.69 \pm 0.19 \mu\text{mol}^{-1} \text{CO}_2 \text{m}^{-2} \text{s}^{-1}$ ), although this could have been due to a lack of data points at temperatures below  $12^\circ\text{C}$  (Figure 4.5.B1). The bare period following the celery crop had the highest  $R_{10}$  ( $4.51 \pm 0.17 \mu\text{mol}^{-1} \text{CO}_2 \text{m}^{-2} \text{s}^{-1}$ ), in contrast to what was seen in the bare period following the maize crop which is what would be expected with no additional Reco from the presence of a crop. The high Reco after the celery harvest is likely due to the ploughing of the field during the bare period having a large impact on Reco through aeration and decomposition of available labile C, including crop residues (discussed further in section 4.2.3.1.3).

For all periods,  $E_0$  fell within a similar range (107 to 218 K) for the phacelia and buckwheat cover crop which had a much higher  $E_0$  (532.78 K). Thus, the phacelia and buckwheat crop exhibited a much greater increase in Reco with temperature (Figure 4.5.B1). This could have been due to temperatures rarely rising above  $18^\circ\text{C}$ , which is required for optimum phacelia (Tribouillois et al., 2016) and buckwheat growth (Płażek et al., 2019). When temperatures did reach this threshold, growth increased leading to subsequent higher Reco. This lack of growth explains the lack of a significant contribution to Reco during the phacelia and buckwheat crop, in contrast to what was observed for the maize and celery crops.

#### 4.2.3.1.2 Soil Water Content

Water table depth (WTD) is known to be a key factor in C emissions from the UK peatlands (Evans et al., 2021), with  $\text{CO}_2$  emissions being lower from peatlands with a higher water table. Multiple studies have indicated the importance of WTD on  $\text{CO}_2$  emissions in peat soils (Lloyd, 2006, Poyda et al., 2016, Tiemeyer et al., 2016, Taft et al., 2017, Musarika et al., 2017, Cumming, 2018) and it has also been suggested to be important on non-peat soils (Wang et al., 2017a).

In this study, SWC was examined, as WTD was always below the peat depth of 0.4 m (Figure 4.3). SWC has been used by similar studies (Lafleur et al., 2005, Parmentier et al., 2009) and has been suggested as a better indicator in these types of ecosystems where top irrigation and rain can keep peat the soil moist, with its high water retention capabilities, despite a lower water table.

Lafleur et al. (2005) measured  $\text{CO}_2$  emissions from peat cores collected from 0–0.45 m depth taken from a low-shrub ombrotrophic bog in Ontario, Canada. They found that the drying of the surface samples reduced  $\text{CO}_2$  emission, and that the peat was most sensitive in the uppermost portions of the peat profile (0–0.05 m). Despite this, they ultimately concluded that surface moisture varied too little to show any significant change in C emission. This is similar to the results found here, with SWC varying little over the course of the study period leading to small

associated changed in CO<sub>2</sub> emission. In some ways this is similar to Parmentier et al. (2009), who found that due to enduring wet soil conditions, respiration changes were primarily controlled by temperature. However, when analysed against the Reco model residuals, SWC was not found to have any significant correlations, suggesting that SWC within this setting had little impact on Reco. This consistency of conditions was generally observed at EN-SP3, particularly in 2018 during the maize crop.

However, despite the small variation observed in SWC, a moderate negative correlation was observed to the residuals of the Reco model during the celery crop. This was during a very dry, warm period and indicated that SWC was limiting Reco below 0.15 m<sup>3</sup> m<sup>-3</sup>. This could be due to low SWC limiting the production of CO<sub>2</sub> by either soil microbes or the celery crop. Similar results were also found by Cumming (2018) at SWC <0.55 m<sup>3</sup> m<sup>-3</sup> on a similar study situated on a deep agricultural peatland.

#### 4.2.3.1.3 Field management

Soil disturbance through field management practices were observed to have an impact on Reco. This effect was most clear in the bare period in 2020 after the field was ploughed on 10<sup>th</sup> March. This was the first time the field had been ploughed since before planting the celery crop and resulted in mixing of the soil with crop residues and breaking up of the soil surface to a depth of ~0.4 m (the entire organic layer). The impact of ploughing was demonstrated by analysing the residuals against time after ploughing (Figure 4.6), with a strong negative correlation ( $r_s = -0.72$ ,  $n = 183$ ,  $p < 0.001$ ) indicating that Reco was underestimated significantly by the temperature model. Reasons for this are likely to be the aeration of the organic layer and the fast decomposition of substrates containing labile C. This response was also observed by Morrison et al. (2013) who found the highest daily net C losses after ploughing and field preparation and suggested that it was due to increased aeration of the soil. The fast decomposition of labile C after ploughing in of crop residues has also been noted for crops on mineral soils (Köbke et al., 2018), and has been suggested by other studies on agricultural peatland (Taft et al., 2017). This effect still needs further quantification for lowland peatlands and would be a fruitful avenue for further study.

#### 4.2.3.2 GPP as a driver of NEE

Overall, the LUE model provided mixed results, and was much better at explaining NEE for the celery crop ( $R^2 = 0.38$ ) than for the phacelia and buckwheat cover crop ( $R^2 = 0.15$ ), especially when peak cropping periods were observed ( $R^2 = 0.79$  and  $R^2 = 0.24$ , respectively). During the peak cropping period for the phacelia and buckwheat crop, daytime values for NEE were still

often above 0, even during periods with PPFD values greater than  $1500 \mu\text{mol m}^{-2} \text{s}^{-1}$ . This was in stark contrast to the peak celery crop which showed consistent net C drawdown when PPFD  $>250 \mu\text{mol m}^{-2} \text{s}^{-1}$  and was associated with better utilisation of PAR by the celery crop ( $\alpha = 0.08 \pm 0.01 \mu\text{mol mol}^{-1}$ ) than the phacelia and buckwheat ( $\alpha = 0.02 \pm 0.008 \mu\text{mol mol}^{-1}$ ). This was primarily due to the phacelia and buckwheat being grown outside of its optimum temperature range for growth of  $18^\circ\text{C}$ – $23^\circ\text{C}$  (Tribouillois et al., 2016, Płażek et al., 2019), in what would typically be considered a more favourable time of the year with longer day lengths and increased  $R_g$  (Figure 4.7). This may have reflected in the residuals analysis, with the model underestimating  $\text{CO}_2$  uptake at higher  $T_s$  ( $>18^\circ\text{C}$ ).

A similar correlation was not seen with  $T_a$ , which instead showed weak positive correlations when analysed against the residuals of the model fit. This was akin to the celery and peak celery cropping period, which showed moderate positive correlations for  $T_a$  and  $T_s$ . This matched with the moderate correlations seen when VPD was analysed against the residuals and is expected with high temperatures driving high VPD and indicates that high temperatures and high VPD were limiting factors for crop growth and thus for GPP, something which has also been described in other studies (Nieveen et al., 1998, Grossiord et al., 2020). Nieveen et al. (1998) observed that high VPD  $>15 \text{ hPa}$ , which is similar to this study, coincided with high temperatures, and that high VPD had a limiting effect on GPP, reducing assimilation rate by an average of 50% from a disturbed former raised bog within the northern Netherlands. This agrees with a recent review by Grossiord et al. (2020) who found that in response to rising VPD, plants exhibit a reduction in stomatal conductance and increased transpiration, reducing C assimilation between 9.4–36.6% depending on the plant species. Differences between plant responses to high VPD could also explain why the peak phacelia and buckwheat crop showed a slightly stronger positive correlation between high VPD and a reduction in NEE compared to the peak growth period of the celery crop. However, it is also likely that this is due to peak celery growth being later in the calendar year, coinciding with lower temperatures and therefore a lower VPD in September and October compared to the summer months of 2019. This meant that VPD was less of a limiting factor to GPP during this period (Figure 4.9).

SWC showed the strongest correlation to the residuals of any additional factor examined (Table 4.4) with a moderate negative correlation to the residuals of the model during the phacelia and buckwheat crop, and with a stronger correlation during the peak cropping periods. This result indicated that SWC became limiting at low SWC (below  $0.15 \text{ m}^3 \text{ m}^{-3}$ ), with water stress impacting plant growth (Osakabe et al., 2014). This effect was not observed as strongly during the celery cropping period due to the irrigation that took place throughout the growth of the celery crop

and the higher than average rainfall for summer 2019 and autumn 2019 (for details, see Chapter 3.1.2.1). During the phacelia and buckwheat crop, no irrigation was performed which allowed water stress of the plant to become more of a factor, especially as the phacelia and buckwheat was grown during the middle of the summer when temperatures were highest.

### 4.3 Chapter 4 Summary

In this chapter, the of the drivers of NEE at EN-SP3 over two data periods (4<sup>th</sup> May 2018–10<sup>th</sup> December 2018 and 17<sup>th</sup> May 2019–17<sup>th</sup> May 2020) are presented. The drivers of Reco (night time NEE) were examined using an empirical Arrhenius model using Ta, which was examined as the primary driver. The residuals of the model were then investigated to see if SWC was an additional driving variable. Farm management practices (such as cropping and ploughing) were also examined as additional driving variables. Whilst Ta was shown to be the primary driving factor, this relationship was not so clear during the second data period due to heterogeneity of crop cover across the field. Reco from the following bare period also showed a poor relationship with Ta due to the impact of ploughing and subsequent aeration of the field, leading to high Reco. Crop presence on the field generally led to higher Reco.

The contribution of GPP to NEE was investigated by examining the light response of the crops using a Michaelis-Menten type model. The residuals of the model were then investigated to see if Ta, Ts, VPD and SWC were additional driving variables. VPD was determined to be a limiting factor to GPP during periods of high VPD. This coincided with high Ta which was also found to be a limiting factor, with high Ta leading to high VPD. Whilst for the celery crop high Ts was also shown to be a limiting factor, the same was not seen for the phacelia and buckwheat crop, likely due to the low range of Ts values recorded during its presence on the field. SWC was found to limit the GPP at low values due to crop water stress, particularly during peak growth periods. This was not observed during the celery peak growth period as a result of crop irrigation and a higher than average rainfall.

## 5 A field-scale C budget at a wasted arable agricultural lowland fen peatland

This chapter address research questions 2 and 3 set out in Section 1.1:

2. What are the C emissions from a wasted lowland peatland under arable agriculture with varying crop and field management?
3. Do the C emissions from a wasted lowland peatland under arable agriculture vary compared to those from arable agriculture on deeper lowland peat?

The chapter presents the first two full years (year one: 17<sup>th</sup> May 2018 to 17<sup>th</sup> May 2019 and year two: 17<sup>th</sup> May 2019 to 17<sup>th</sup> May 2020) of CO<sub>2</sub> flux measurements and carbon budgets from a study site located on wasted agricultural peatland, namely Engine Farm – Spooners 3 field site (EN-SP3) (Chapter 3.1.2). Data was considered in terms of the two year-long periods separately due to the varying field conditions and contrasting challenges they presented. Data presented in Chapter 4 between 4<sup>th</sup> and the 16<sup>th</sup> May 2018 was not considered within this chapter. This was to allow two year-long data periods equal in length to be examined. The implications of this are discussed in Chapter 7.5.

The Energy Balance Closures (EBC) of the flux measurements were examined to assess the reliability of the flux measurements over the two data collection periods. This was done through calculation of the linear regression coefficients between the energy fluxes (LE + H) and the available energy (Rn - G), and the calculation of the Energy Balance Ratio (EBR) which is the sum of energy fluxes divided by the available energy over each time period (both of these methods are described in Chapter 3.2.6) using all available quality-controlled data.

The daily Net Ecosystem Exchange (NEE) is presented over a two year period including quality controlled and gap filled flux data. The NEE is partitioned into Gross Primary Productivity (GPP) and Ecosystem Respiration (Reco) and presented as daily values alongside NEE. A calculation of the annual Net Ecosystem C Balance (NECB) is then produced for each year of data, using CO<sub>2</sub> fluxes and the C imported and exported through planting and harvesting the crops.

Differences in NEE and NECB between the two years are compared within the context of the wider literature to draw out insights into why emissions from the field differed over the two year period. Additionally, the NECB is compared with the wider literature on C loss from arable agricultural peatlands throughout the UK and Europe accompanied by an examination of the relationships between annual NECB in relation to peat depth and soil C content. Finally, an

estimated emission factor (EF) for cropped wasted peat within the UK is estimated and used to calculate and updated emissions total.

Within this study, positive values denote C loss from the field and negative values denote C gain. All C flux values are given in g C m<sup>-2</sup> (NECB) or g CO<sub>2</sub>-C m<sup>-2</sup> (NEE). Energy Balance Closure (EBC)

Over the two years of data collection, 3 different crops were grown on the field. The maize crop in 2018 had a very different profile, being much taller in height compared to the following phacelia and buckwheat and celery crops in 2019. This required the tower to be raised to a height of 5.75 m during the maize cropping period to accurately capture the fluxes from EN-SP3 during this time. In contrast, the tower height was lowered after the maize crop and remained at 2.37 m during the rest of 2019 and 2020. The malfunction of the IRGA used to measure CO<sub>2</sub> on 10<sup>th</sup> December 2018 left less original flux data for the first year of data collection compared the second year. Finally, flux data in 2018 was during a drier year than in 2019 and 2020 (Chapter 4.1). This is highlighted best by May, which in 2018 experienced nearly zero rainfall compared to over 80 mm in 2019. This led to differences observed within the EBC over the two year period:

#### 5.1.1 Year one: 17<sup>th</sup> May 2018 to 17<sup>th</sup> May 2019

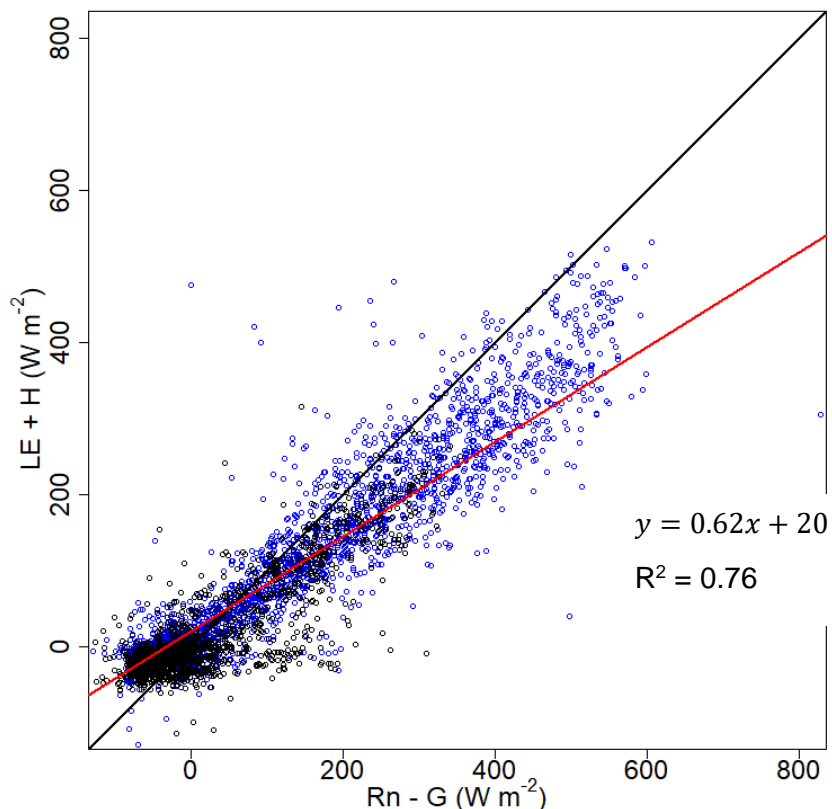


Figure 5.1. Energy Balance Closure using quality controlled (but not gap filled) LE (W m<sup>-2</sup>), H (W m<sup>-2</sup>), Rn (W m<sup>-2</sup>) and G (W m<sup>-2</sup>) for all available data for the period 17<sup>th</sup> May 2018 to 17<sup>th</sup> May 2019. Cropped (blue) and bare (black) periods. The black line denotes the 1:1 line and the Red line indicates a linear regression model between the variables.

For the first year of data collection, the overall EBC was 62%, indicated by a slope value of 0.62 (Figure 5.1, Table 5.1). Energy fluxes (LE, H) tended to be underestimated (or available energy (Rn-G) overestimated) at high energy fluxes, while the opposite was observed at low energy fluxes. This affected night time data the most, with these data consisting primarily of low energy fluxes ( $< 100 \text{ W m}^{-2}$ ), showing the worst closure with a slope of 0.0067 and an intercept of -11.59  $\text{W m}^{-2}$  with an EBR of 0.44. This was lower than the EBR for daytime data (0.86) and the dataset as a whole (0.80) (Table 5.1). Overall, available energy was a good explanatory variable of the energy fluxes ( $R^2 = 76\%$ ), but not when exclusively looking at night time data ( $R^2 = 0.025$ ).

Cropped and bare periods exhibited similar closure, with the cropping period having a slope of 0.61 compared to 0.59 for the bare period. The intercept for the cropping period was much higher ( $31.26 \text{ W m}^{-2}$ ) than for the bare period ( $5.09 \text{ W m}^{-2}$ ), indicating that the cropping period had a greater underestimation of available energy or overestimation of the energy fluxes at higher fluxes. This was likely due to the increased amount of high energy fluxes during the cropping period. EBR for the cropping period was higher (0.88) than for the bare period (0.77).

*Table 5.1. Energy Balance Closure coefficients calculated through linear regression and the Energy Balance Ratio (EBR) for all data (including it being split into day and night) and for each major field management period.*

Period	n	Slope	Intercept ( $\text{W m}^{-2}$ )	$R^2$	EBR
<b>All data</b> (17/05/18 – 17/05/19)	4493	0.62	20.29	0.76	0.86
<b>All day data</b> (17/05/18 – 17/12/18)	2362	0.56	45.85	0.65	0.80
<b>All night data</b> (17/05/18 – 17/12/18)	2130	0.0067	-11.59	0.025	0.44
<b>Maize crop</b> (17/05/18 – 02/10/18)	2875	0.61	31.26	0.75	0.88
<b>Bare</b> (02/05/18 – 17/12/18)	1616	0.59	5.09	0.73	0.77

### 5.1.2 Year two: 17<sup>th</sup> May 2019 to 17<sup>th</sup> May 2020

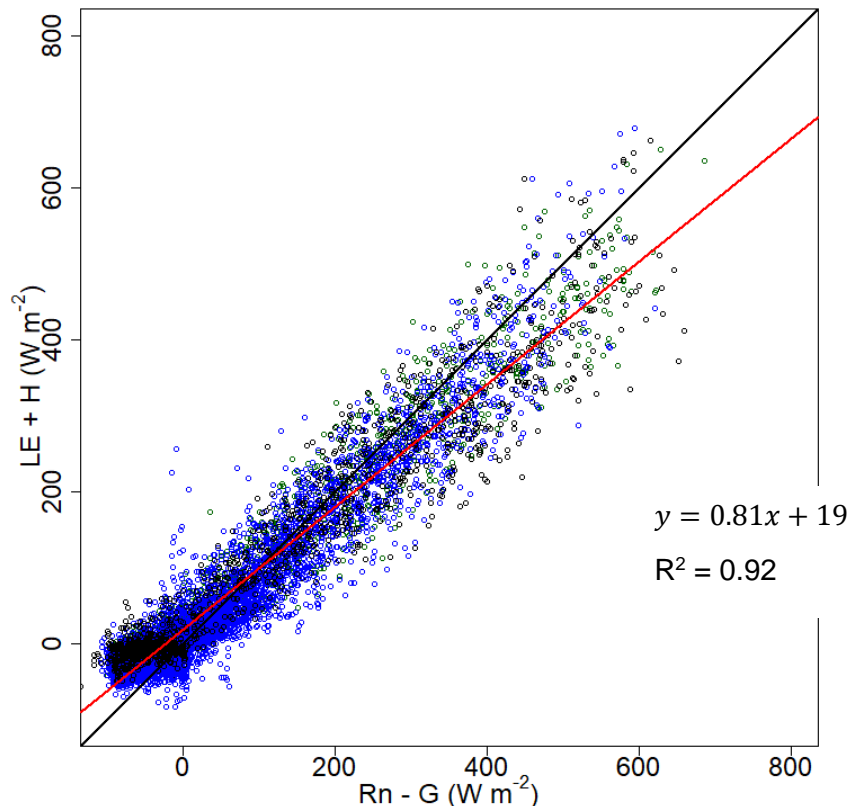


Figure 5.2. Energy Balance Closure using quality controlled (but not gap filled) LE ( $W\ m^{-2}$ ), H ( $W\ m^{-2}$ ),  $R_n$  ( $W\ m^{-2}$ ) and G ( $W\ m^{-2}$ ) for all data for the period 17<sup>th</sup> May 2019 to 17<sup>th</sup> May 2020. Cropped (blue) and bare (black) periods. The black line denotes the 1:1 line and the red line indicates a linear regression model between the variables.

Over the second year of data collection, the ECB was 81%, indicated by a slope value of 0.81 (Figure 5.2, Table 5.2) showing a much better closure than the first year (62%). Again, energy fluxes tended to be underestimated (or available energy overestimated) at high energy fluxes, while the opposite was observed at low energy fluxes (Figure 5.2). Again, this affected night time data the most (slope: 0.28, intercept:  $-3.08\ W\ m^{-2}$ ), but showed a better closure than the 2018/19 period, and contained a greater range of magnitude of energy fluxes and available energy (likely due to being a full year dataset). Over the entire period, available energy was a good explanatory variable of the energy fluxes ( $R^2 = 92\%$ ) (Table 5.2). An EBR of 1.15 indicated more energy flux than available energy over the whole period, which appears to be driven by high energy fluxes at low available energy ( $< 100\ W\ m^{-2}$ ) (Figure 5.2). This was also seen for individual cropping (1.04, 1.12) and bare periods (0.98, 1.13).

Cropped and uncropped periods generally exhibited similar closure (cropping period slope of 0.81 for both, bare periods slope of 0.81 and 0.75) (Table 5.2). The time period when there was a 48m cover crop strip present in front of the tower whilst the rest of the field was bare showed the worst closure (slope: 0.65) and a negative EBR of -1.60, indicating an overestimation of energy flux, particularly at low available energy ( $< 50\ W\ m^{-2}$ ). Despite this, the intercept value of

$8 \text{ W m}^{-2}$  was closer to the ideal value of  $0 \text{ W m}^{-2}$  than all other individual periods ( $25\text{--}33 \text{ W m}^{-2}$ ) and for the dataset as a whole ( $19.53 \text{ W m}^{-2}$ ) with only night time data having a closer intercept ( $-3.08 \text{ W m}^{-2}$ ).

Table 5.2. Energy Balance Closure coefficients calculated through linear regression for all data (including it being split into day and night) and for each major field management period.

Period	n	Slope	Intercept (W m <sup>-2</sup> )	R <sup>2</sup>	Energy Balance Ratio
All data (17/05/19 - 17/05/20)	9241	0.81	19.53	0.92	1.15
All data day (17/05/19 - 17/05/20)	4521	0.83	15.2	0.90	0.92
All night data (17/05/19 - 17/05/20)	4719	0.28	-3.08	0.20	0.35
Cover crop (17/05/19 - 01/07/19)	1111	0.81	32.86	0.94	1.04
Bare period 1 (01/07/19 - 23/07/19)	563	0.81	25.9	0.95	0.98
Celery crop (23/07/19 - 23/10/19)	2479	0.81	26.18	0.93	1.12
Cover crop strip (23/10/19 - 10/03/20)	3978	0.65	8.07	0.77	-1.60
Bare period 2 (10/03/20 - 17/05/20)	1104	0.75	31.29	0.91	1.13

## 5.2 Net Ecosystem Exchange (NEE)

The NEE was calculated daily from the sum of gap filled half hourly flux values on a daily time scale for both years of data. Fluxes were gap filled using the methodology described in Reichstein et al. (2005) (further details are provided in Chapter 3.2.5.6), after which half hourly flux values were partitioned into GPP and Reco (further details are provided in Chapter 3.2.5.7). Gap filling of the period between 11<sup>th</sup> December 2018 and 17<sup>th</sup> May 2019 was done using the relationship derived in Chapter 4.2.1 between the Reco and Ta during the bare period (3<sup>rd</sup> October 2018 to 10<sup>th</sup> December 2018). This period was chosen due to the similar field conditions to the gap filled period, and because the model appeared to explain Reco well ( $R^2 = 0.79$ ). Daily sums of GPP and Reco were then calculated and used to provide insights into their contribution to NEE through the different cropping and bare periods.

### 5.2.1 Summary of Daily NEE, GPP and Reco from 17<sup>th</sup> May 2018 to 17<sup>th</sup> May 2019

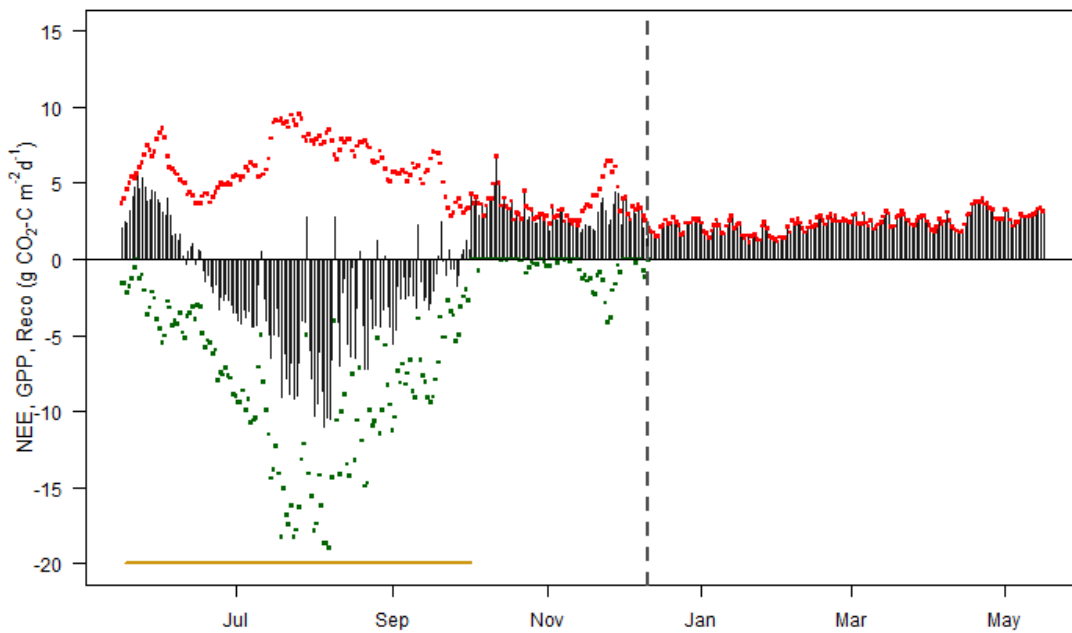


*Figure 5.3. Cumulative daily Net Ecosystem Exchange (NEE – Black Bars), Gross Primary Productivity (GPP – Green points) and Total Ecosystem Respiration (Reco – Red points) from Engine Farm between 17<sup>th</sup> May 2018 and 17<sup>th</sup> May 2019. During this period, a maize crop was present on the field (Planted: 18<sup>th</sup> May (germination occurs approximately two weeks afterwards), Harvested: 2<sup>nd</sup> October) indicated by the yellow line. Due to equipment malfunction, all fluxes after 11<sup>th</sup> December 2018 were filled using the relationship derived in Chapter 4.2.1 between Reco and Ta during the bare period in 2018.*

Overall, a crop was present on the field for 138 days, with the field left bare for 227 days. Both before and after planting there was a net daily emission from the field before the maize germinated. The highest daily NEE value of 6.72 g CO<sub>2</sub>-C m<sup>2</sup> d<sup>-1</sup> was recorded on the 12<sup>th</sup> October 2018 during the bare period, after the maize was harvested. The bare period after the maize crop had an average C emission of NEE of 2.60 g CO<sub>2</sub>-C m<sup>2</sup> d<sup>-1</sup> (Table 5.3).

Once germinated, the maize crop steadily grew, and reached peak growth in early August with a peak average daily GPP of -17.42 g CO<sub>2</sub>-C m<sup>2</sup> d<sup>-1</sup> between 1<sup>st</sup> and 8<sup>th</sup> of August 2018 which also included the highest daily GPP value (-18.99 g CO<sub>2</sub>-C m<sup>2</sup> d<sup>-1</sup>). This coincided with the highest net drawdown of C into the field, with peak NEE of -9.5 g CO<sub>2</sub>-C m<sup>2</sup> d<sup>-1</sup> recorded between 1<sup>st</sup> and 8<sup>th</sup> August 2018. After this, the crop steadily slowed in growth and over time C uptake dropped until it was harvested on 2<sup>nd</sup> October 2018. Overall, the maize cropping period saw an average daily C uptake of -2.12 g CO<sub>2</sub>-C m<sup>-2</sup> (from planting to harvesting).

During the cropping period, the highest Daily Reco was 9.52 g CO<sub>2</sub>-C m<sup>2</sup> d<sup>-1</sup>, the highest overall for the field, and had the highest average Reco of 6.21 g CO<sub>2</sub>-C m<sup>2</sup> d<sup>-1</sup>, more than double the following bare period (2.76 g CO<sub>2</sub>-C m<sup>2</sup> d<sup>-1</sup>). The peak Reco of 9.10 g CO<sub>2</sub>-C m<sup>2</sup> d<sup>-1</sup>, recorded between 21<sup>st</sup> and 27<sup>th</sup> July 2018 during the cropping period, was higher compared to the peak

Reco recorded during the bare period ( $5.83 \text{ g CO}_2\text{-C m}^2 \text{ d}^{-1}$ , recorded during the period 23<sup>rd</sup> to 29<sup>th</sup> November 2018). The bare period did see some weed growth on the field, with highest daily GPP of  $-4.19 \text{ g CO}_2\text{-C m}^2 \text{ d}^{-1}$  and a peak average of  $-2.4 \text{ g CO}_2\text{-C m}^2 \text{ d}^{-1}$  between 22 and 28<sup>th</sup> November 2018. This short period of weed growth coincided with the peak Reco seen during the bare period across the field due to the additional root respiration of the plants. At the end of November, the weeds were sprayed off in preparation for the winter period, when fields are typically ploughed and left bare until late spring when the following year's crop is planted. There was no further weed growth meaning GPP was negligible during the rest of bare period. During the bare period, Reco was as expected from a bare field left over winter, with the lowest Reco observed in late January (20<sup>th</sup> January 2018,  $1.09 \text{ g CO}_2\text{-C m}^2 \text{ d}^{-1}$ ) before slowly rising as temperatures increased through spring (Figure 5.3).

Gap filled data for the bare period compared well with the original data. Whilst the gap filled data showed a lower average Reco and NEE ( $2.37 \text{ g CO}_2\text{-C m}^2 \text{ d}^{-1}$ ) compared to the original data (average NEE: 3.04, Reco:  $3.57 \text{ g CO}_2\text{-C m}^2 \text{ d}^{-1}$ ), this was expected due to the lower temperatures experienced during the winter months reducing Reco. Minimum daily Reco of ( $1.09 \text{ g CO}_2\text{-C m}^2 \text{ d}^{-1}$ ) was recorded on 20<sup>th</sup> January 2019 in the first year. This is similar to the daily minimum Reco in the second year ( $1.26 \text{ g CO}_2\text{-C m}^2 \text{ d}^{-1}$ ) as recorded on 21<sup>st</sup> January 2020. Both were during the period of the year where temperatures are their coldest.

*Table 5.3. Maximum GPP,  $R_{eco}$  and NEE for the different management periods of EN-SP3 between 17<sup>th</sup> May 2018 and 17<sup>th</sup> May 2019. Peak periods are the 7 days where the average of NEE, GPP or Reco were found to be the highest. Values are provided for the entire bare period which included gap filled values. Additionally, gap filled and original values are provided to allow for a comparison of the gap filled and original data.*

	<b>Maize Crop (g CO<sub>2</sub>-C m<sup>-2</sup>) (17/05/18– 02/10/18)</b>	<b>Entire Bare Period (g CO<sub>2</sub>-C m<sup>-2</sup>) (03/10/18– 17/05/19)</b>	<b>Bare period (original) (g CO<sub>2</sub>-C m<sup>-2</sup>) (03/10/18– 11/12/18)</b>	<b>Gap Filled (gap filled) (g CO<sub>2</sub>-C m<sup>-2</sup>) (12/12/2018– 17/05/19)</b>
<b>NEE daily min</b>	-11.04 05/08/18	1.09 20/01/19	1.33 10/12/18	1.09 20/01/19
<b>NEE daily max</b>	5.60 23/05/18	6.72 12/10/18	6.72 12/10/18	3.94 22/04/19
<b>NEE average</b>	-2.12	2.60	3.04	2.37
<b>NEE peak average</b>	4.71 21/05/18– 27/05/18 -9.50 01/08/18– 07/08/18	4.57 9/10/18–15/10/18	4.57 9/10/18–15/10/18	3.72 18/04/19–24/04/19
<b>GPP daily min</b>	0 (multiple)	-4.19	0 (multiple)	n/a
<b>GPP daily max</b>	-18.99 07/08/18	0	-4.16 25/11/18	n/a
<b>GPP average</b>	-8.33	-0.52	-0.52	n/a
<b>GPP peak average</b>	-17.42 01/08/18– 07/08/18	-2.4 22/11/18–28/11/18	-2.4 22/11/18–28/11/18	n/a
<b>Reco daily min</b>	2.84 24/09/18	1.09 20/01/19	1.42 11/12/18	1.09 20/01/19
<b>Reco daily max</b>	9.52 26/07/18	6.72 12/10/18	6.72 12/10/18	3.94 22/04/19
<b>Reco average</b>	6.21	2.76	3.57	2.37
<b>Reco peak average</b>	9.10 21/07/18– 27/07/18	5.83 23/11/18–29/11/18	5.83 23/11/18–29/11/18	3.72 18/04/19–24/04/19

### 5.2.2 Summary of Daily NEE, GPP and Reco from 17<sup>th</sup> May 2019 to 17<sup>th</sup> May 2020

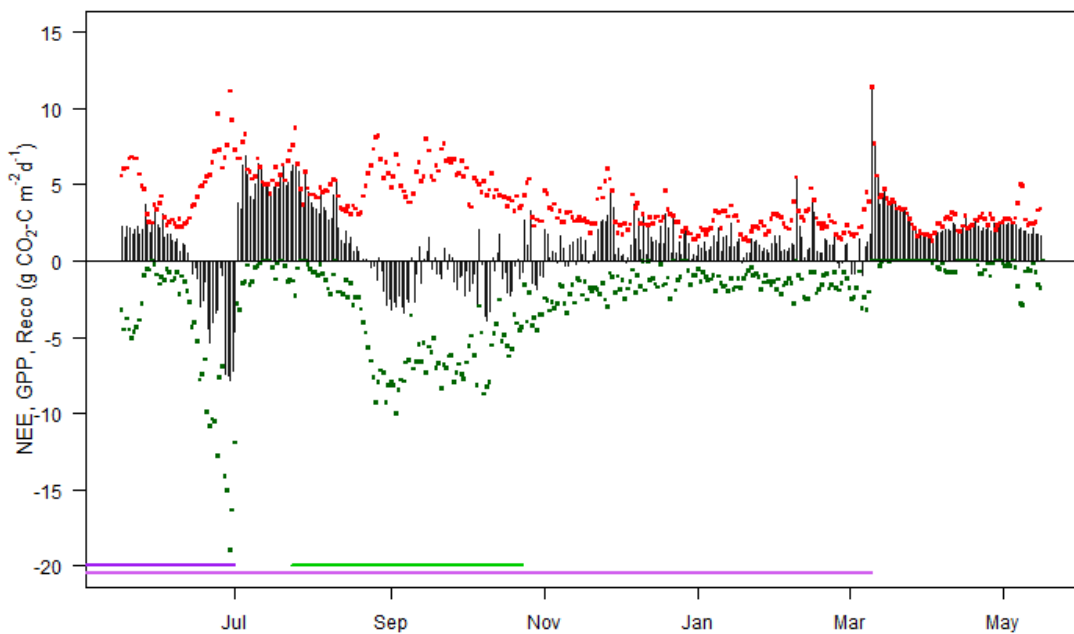


*Figure 5.4. Cumulative daily Net Ecosystem Exchange (NEE – Black Bars), Gross Primary Productivity (GPP – Green points) and Total Ecosystem Respiration (Reco – Red points) from Engine Farm between 17<sup>th</sup> May 2019 and 17<sup>th</sup> May 2020. During this period, a phacelia and buckwheat cover crop was present on the field (Planted: 15<sup>th</sup> May 2019 (germination occurs approximately one to two weeks after), Disked: 1<sup>st</sup> July 2020, indicated by the purple line), before being disked into the field prior to a celery crop (Planted: 23<sup>rd</sup> July, Harvested: 23<sup>rd</sup> October, indicated by the green line) other than a 48 m wide strip of phacelia and buckwheat (indicated by the pink line) that was left untouched until 10<sup>th</sup> March 2020. On 10<sup>th</sup> March 2020 the entire field was ploughed and left bare until the end of the data collection period.*

Overall, crop was present on the entire field for 139 days over two distinct periods (phacelia and buckwheat for 46 days and celery with a 48 m strip of phacelia and buckwheat for 93 days). After the celery was harvested, the field was left bare other than for celery waste and a strip of phacelia and buckwheat which was present on the field for 140 days before the field was ploughed to a depth of 0.45 m, leaving the field completely bare for 69 days.

During the period with the phacelia and buckwheat cover crop, a maximum daily drawdown of -7.8 g CO<sub>2</sub>-C m<sup>2</sup> d<sup>-1</sup> was seen on 29<sup>th</sup> June 2019, which coincided with its peak growth rate indicated by the highest daily NEE/GPP peak average (NEE: -4.92 g CO<sub>2</sub>-C m<sup>2</sup> d<sup>-1</sup>, GPP: -13.14 g CO<sub>2</sub>-C m<sup>2</sup> d<sup>-1</sup> from 23<sup>rd</sup> to 30<sup>th</sup> June 2019). This was higher than the rates of C accumulation on the field observed during the celery crop (peak average NEE: -2.86 g CO<sub>2</sub>-C m<sup>2</sup> d<sup>-1</sup> 1<sup>st</sup> to 7<sup>th</sup> September and peak GPP: -8.56 g CO<sub>2</sub>-C m<sup>2</sup> d<sup>-1</sup> 30<sup>th</sup> August to 5<sup>th</sup> September 2019). Overall, the celery crop showed an average daily C emission 0.28 g CO<sub>2</sub>-C m<sup>2</sup> d<sup>-1</sup>, compared to the average net draw down for the phacelia and buckwheat cover crop of -0.19 g CO<sub>2</sub>-C m<sup>2</sup> d<sup>-1</sup>. This shows that, despite the celery crop being the main crop, the phacelia and buckwheat had a greater daily C accumulation for the time this cover crop was on the field compared to the celery crop. The phacelia and buckwheat peak CO<sub>2</sub> uptake was seen just before it was disked into the field

during preparation for the celery crop, showing a big change in daily NEE from uptake of CO<sub>2</sub> to loss of CO<sub>2</sub> at the beginning of July before the celery crop was planted (Figure 5.4).

From 23<sup>rd</sup> October 2019 to 9<sup>th</sup> March 2020 (Partial Crop Period) the field was partially covered by a 48 m strip of phacelia and buckwheat cover crop and celery waste. While a small amount of growth was observed from the remaining phacelia and buckwheat crop (average GPP: -0.37 g CO<sub>2</sub>-C m<sup>2</sup> d<sup>-1</sup>), this was less than Reco shown from the primarily bare field during this period (2.77 g CO<sub>2</sub>-C m<sup>2</sup> d<sup>-1</sup>). This left the field a small but consistent net C source during this period (average NEE of 1.08 g CO<sub>2</sub>-C m<sup>2</sup> d<sup>-1</sup>). Reco for this period was less than for either the first (6.04 g CO<sub>2</sub>-C m<sup>2</sup> d<sup>-1</sup>) or second (3.01 g CO<sub>2</sub>-C m<sup>2</sup> d<sup>-1</sup>) bare ground periods, despite the increased celery waste on the soil surface, pointing to other management practices or field conditions (such as increased aeration) being more important drivers of C emission.

The highest NEE values were observed on 10<sup>th</sup> March 2021 during/post ploughing of the entire field (NEE: 11.36 g CO<sub>2</sub>-C m<sup>2</sup> d<sup>-1</sup>). However, this was a short-lived spike in emission (NEE peak 5.89 g CO<sub>2</sub>-C m<sup>2</sup> d<sup>-1</sup> from 10<sup>th</sup> to 16<sup>th</sup> March 2020) with the average NEE over the whole of the second bare period being 2.67 g CO<sub>2</sub>-C m<sup>2</sup> d<sup>-1</sup>, less than for the first bare period (4.73 g CO<sub>2</sub>-C m<sup>2</sup> d<sup>-1</sup>).

Table 5.4. Maximum GPP, Reco and NEE for the different management periods of EN-SP3 between 17<sup>th</sup> May 2019 and 17<sup>th</sup> May 2020. Peak periods are the 7 days where the average of NEE, GPP or Reco were found to be the highest.

	<b>Phacelia and Buckwheat (g CO<sub>2</sub>-C m<sup>-2</sup>) (17/05/19– 01/07/19)</b>	<b>Bare Period One (g CO<sub>2</sub>-C m<sup>-2</sup>) (02/07/19– 22/07/19)</b>	<b>Celery (g CO<sub>2</sub>-C m<sup>-2</sup>) (23/07/19– 23/10/19)</b>	<b>Partial Crop Period (g CO<sub>2</sub>-C m<sup>-2</sup>) (24/10/19– 09/03/20)</b>	<b>Bare period Two (g CO<sub>2</sub>-C m<sup>-2</sup>) (10/03/20– 17/05/20)</b>
<b>NEE daily min</b>	-7.8 29/06/19	-4.66 1/7/19	-3.96 9/10/19	-1.90 29/10/19	0.04 17/05/20
<b>NEE daily max</b>	3.66 26/05/19	6.92 05/07/19	6.38 25/07/19	5.46 9/2/20	11.36 10/03/20
<b>NEE average</b>	-0.19	4.73	0.28	1.08	2.61
<b>NEE peak average (for cropping periods, peak drawdown is included)</b>	2.64 26/05/19– 01/05/19  -4.92 23/06/19– 30/06/19	5.50 4/07/19– 10/07/19	5.45 23/07/19– 29/07/19  -2.86 01/09/19– 07/09/19	2.99 22/11/19– 28/01/19  -0.41 27/10/19– 02/11/19	5.89 10/03/20– 16/03/20
<b>GPP daily min</b>	0 29/05/19	0 (multiple)	0 (multiple)	0 (multiple)	0 (multiple)
<b>GPP daily max</b>	-18.95 29/06/19	-11.93 01/07/19	-10.00 03/09/19	-4.58 29/10/19	-2.96 09/05/20
<b>GPP average</b>	-5.06	-1.31	-4.85	-1.69	-0.37
<b>GPP peak average</b>	-13.14 23/06/19– 30/06/19	-3.26 01/07/19– 06/07/19	-8.56 30/8/19– 05/09/19	-3.68 25/10/19– 31/10/19	-1.41 06/05/20– 12/05/20
<b>Reco daily min</b>	2.24 08/06/19	4.38 15/07/19	3.01 16/08/19	1.26 21/01/20	1.32 03/04/20
<b>Reco daily max</b>	11.12 29/06/19	8.31 05/07/19	8.69 25/07/19	6.04 26/11/19	11.36 10/03/20
<b>Reco average</b>	4.86	6.04	5.13	2.77	3.01
<b>Reco peak average</b>	8.22 23/06/19– 30/06/19	6.94 01/07/19– 06/07/19	6.88 04/09/19– 10/09/19	4.86 22/11/19– 28/11/19	5.96 10/03/20– 16/03/20

## 5.3 Field Carbon Balance

### 5.3.1 Import and Export of C from the field

In addition to gaseous exchange, there are multiple pathways for C to enter or leave the ecosystem, including the import and export of C via crop planting and harvesting and aeolian erosion (see Chapter 6) and deposition. Here, a C balance is created based on C imports and exports through crop planting and harvesting for each distinct period. Due to time constraints, C loss via ditches was not measured. The field is treated as a distinct ‘box’, where only C imports

and exports from the field are considered and not the ultimate fate of the C. For example, C stored within crops is counted as a loss from the field once the crop is harvested and removed from the field ecosystem. Due to time constraints, a full crop life cycle analysis was not performed, but it is suggested that future studies should analyse the life and ultimate fate of C within agricultural peatlands to assess the true value of the C ‘cost’ from the field. The most significant imports and exports are associated with the planting and harvesting of crops and have been listed within Table 5.5. From this, a Net Ecosystem Carbon Balance (NECB) can be calculated for the field which includes not only the CO<sub>2</sub> flux data (NEE), but also the C imported and exported onto the field. NECB here was calculated using the C imported and exported through cropping. This is typical of similar studies (e.g. Elsgaard et al., 2012, Poyda et al., 2016) due to the C import and export being dominated by cropping.

*Table 5.5. Significant C inputs and Exports from planting and harvesting during the two measurement periods mat EN-SP3.*

Date	Description	Import (g C m <sup>-2</sup> )	Export (g C m <sup>-2</sup> )
18/05/2018	Maize Planting	1	
02/10/2018	Maize Harvesting		506
15/05/2019	Phacelia and Buckwheat Planting	1	
23/07/2019	Celery Plugs	52	
23/10/2019	Celery Harvest		143

5.3.1.1 Year 1 – 17<sup>th</sup> May 2018 to 17<sup>th</sup> May 2019

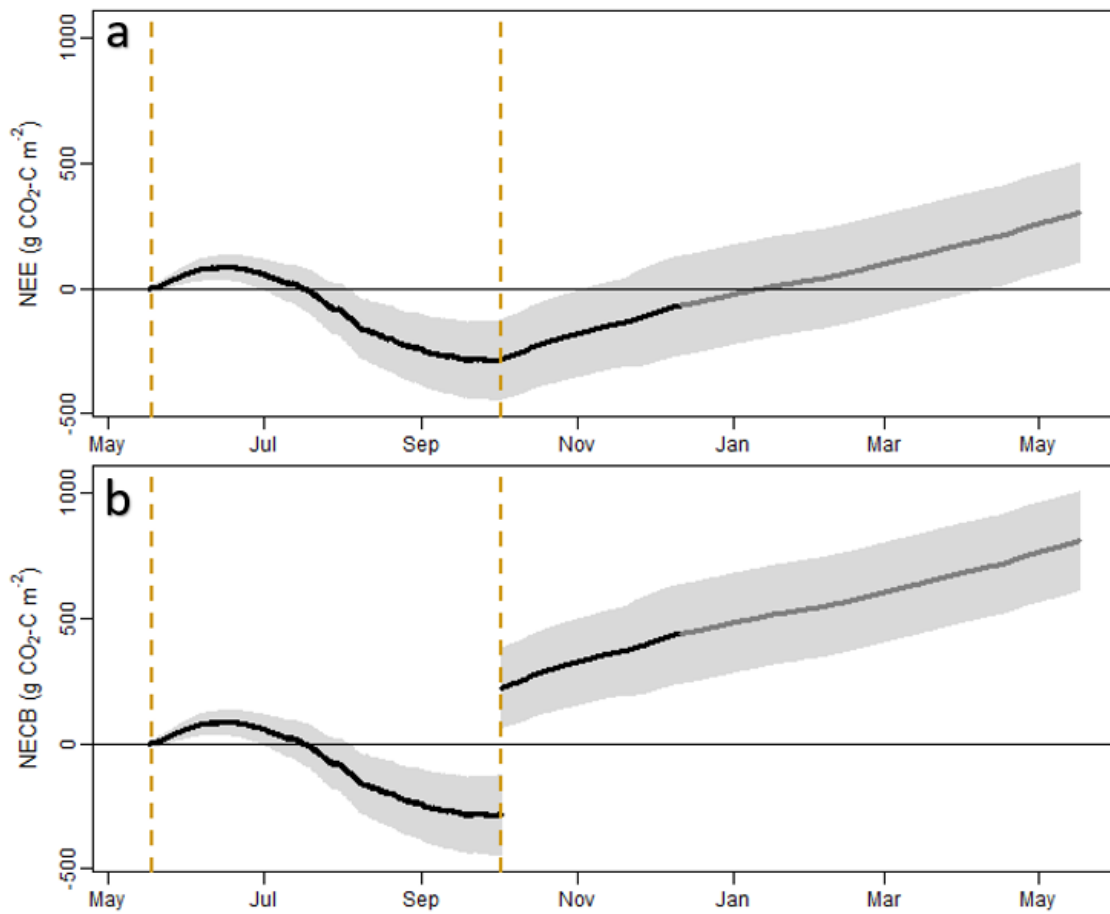


Figure 5.5. Cumulative C emission from EN-SP3 between 17<sup>th</sup> May 2018 and 17<sup>th</sup> May 2019 where a) shows the NEE and b) shows the NECB which includes inputs and offtake from crop harvesting (See Table 5.6 for further information). Cumulative flux error is indicated by the light grey shading. The black line is original data whilst the dark grey line is gap filled data filled by the relationship described in Chapter 4.2.1).

Between 17<sup>th</sup> May 2018 and 17<sup>th</sup> May 2019, EN-SP3 showed a NECB of  $812.1 \pm 195.6 \text{ g C m}^{-2}$ , including a cumulative NEE of  $305.7 \pm 195.6 \text{ g C m}^{-2}$  (Table 5.6) due to the large amount of C drawdown by the maize crop during its growth period (Figure 5.5.a, b). Before and initially after planting, C emission dominated the ecosystem until June when the growth of the maize crop consistently resulted in a C drawdown which was higher than C emissions. This lasted until late September when an early frost stopped crop growth and the maize was subsequently harvested on 2<sup>nd</sup> October. Once harvested, the field remained bare and was a consistent net C source.

5.3.1.2 Year 2 – 17<sup>th</sup> May 2019 to 17<sup>th</sup> May 2020

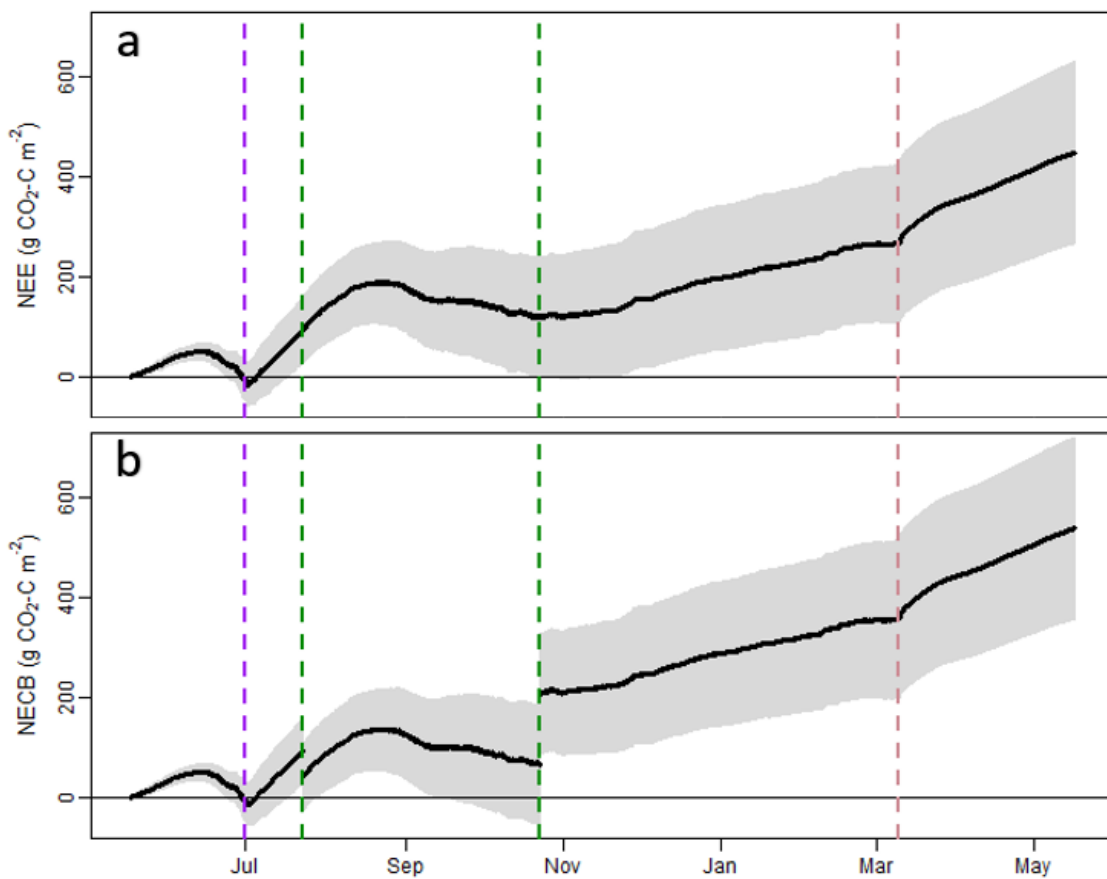


Figure 5.6. Cumulative C emission from EN-SP3 between 17<sup>th</sup> May 2019 and 17<sup>th</sup> May 2020 where a) shows the NEE and b) shows the NECB which includes inputs and offtake from crop harvesting (See Table 5.6 for further information). Cumulative flux error is indicated by the grey shading. Dashed lines indicate: Green – the planting and harvest date of the celery crop; Purple – the disking of the phacelia and buckwheat crop into the field; Pink – the ploughing of the field after the celery was harvested.

Between 17<sup>th</sup> May 2019 and 17<sup>th</sup> May 2020, EN-SP3 showed a NECB of  $539.6 \pm 181.4 \text{ g C m}^{-2} \text{ yr}^{-1}$ , including a cumulative NEE of  $449.5 \pm 181.4 \text{ g CO}_2\text{-C m}^{-2} \text{ yr}^{-1}$  (Table 5.6). There are several distinct periods of field management over this period that influenced the C emission from the field. The first was the phacelia and buckwheat crop which was planted just before CO<sub>2</sub> measurements began (15<sup>th</sup> May 2019) and which resulted in a sharp increase in uptake once established in late July. It was then disked into the soil surface prior to the planting of the celery crop, leaving the field bare other than a 48 m strip of remnant cover crop in front of the flux tower. At this time, the majority of the field had several applications of fertiliser and was surface irrigated in preparation for celery plug plant planting. This was followed by a consistent C emission through July, which started to reverse once the celery plug plants were established and started to reach their peak growth period. This period of C accumulation continued until the celery crop was harvested on 23<sup>rd</sup> October. Once the celery crop was harvested, the field returned to being a small source of C, albeit a smaller source than any of the totally bare periods.

This was due to the presence of the 48 m phacelia and buckwheat strip which sequestered a small amount of C throughout the winter months. The field was ploughed in its entirety on 10<sup>th</sup> March, later than normal due to wet winter months preventing farm machinery entering the field (normally fields are ploughed in preparation for winter). In the week immediately after ploughing, a high rate of emission was seen which gradually reduced to a constant rate which persisted for the rest of the measurement period.

*Table 5.6. Estimated NECB of the two measurement periods on EN-SP3. C imports are due to: 1. Maize planting, 2. Phacelia & Buckwheat planting and 3. Celery plug plant planting. Exports are due to: 4. Maize harvesting and 5. Celery Harvesting.*

Period	Imports (g C m <sup>-2</sup> )	Exports (g C m <sup>-2</sup> )	Cumulative NEE (g CO <sub>2</sub> -C m <sup>-2</sup> yr <sup>-1</sup> )	Cumulative NECB (g C m <sup>-2</sup> yr <sup>-1</sup> )
17 <sup>th</sup> May 2018 to 17 <sup>th</sup> May 2019	<1 <sup>1</sup>	506 <sup>4</sup>	305.7 ± 195.6	812.1 ± 195.6
17 <sup>th</sup> May 2019 to 17 <sup>th</sup> May 2020	<1 <sup>2</sup> 52 <sup>3</sup>	143 <sup>5</sup>	449.5 ± 181.4	539.6 ± 181.4

### 5.3.2 Comparison between cumulative C flux data periods

NECB between the two data collection periods differed; in 2018/19, the field showed an NECB of  $812.1 \pm 195.6$  g C m<sup>-2</sup> yr<sup>-1</sup> compared to  $539.6 \pm 181.4$  g C m<sup>-2</sup> yr<sup>-1</sup> in 2019/20, a difference of 272.5 g C m<sup>-2</sup> yr<sup>-1</sup> (Table 5.6). These results indicate that C was emitted from the field at a higher rate overall in 2018/19 when C lost via crop removal was factored in. This was despite the maize having a higher C uptake than the celery, leading to a lower cumulative NEE of  $305.7 \pm 195.6$  g C m<sup>-2</sup> yr<sup>-1</sup> for the maize crop compared to  $449.5 \pm 181.4$  g C m<sup>-2</sup> yr<sup>-1</sup> for the celery crop. Celery planting added a small yet significant amount of C into the field (Table 5.6) with 52 g C m<sup>-2</sup> added to the field via the plant plugs, compared to the minor addition of C to the field by the planting of maize crop and the phacelia and buckwheat cover crop (1 g C m<sup>-2</sup>).

When the maize crop was present on the field, there was a large amount of C sequestration into the maize crop, shown by the high daily GPP values seen during this time. Maize is the most productive crop grown on EN-SP3, sequestering high amounts of C during its growth, and the largest cumulative daily C sink seen during the data collection periods. Despite this large C sequestration, most of it was removed from the field when the maize was harvested for use in an anaerobic digestion plant. During 2019/20, the phacelia and buckwheat showed a strong uptake of C, with the field reaching net C uptake in the period immediately before it was disked into the field for use as ‘green manure’ for the celery crop. During and immediately after disking, the highest rate of emission was observed before the planting of the celery crop. The celery crop

had a net uptake of C into the field during its peak growth period. However, this was not as strong a C drawdown as observed during the growth of the maize crop, with the field remaining a net C emission source during this period (Figure 5.7).

Post-harvest, the field situations were dissimilar; once harvested, the maize crop left minimal residue in the form of stubble, with the field surface mostly bare. This also coincided with a period of very dry and hot weather. Any remnant stubble was ploughed into the field in October and November 2018, leaving the field bare and aerated, although little change in C emission rate is noticeable during the period after harvesting. The same was not seen in the second year of data collection. After harvesting of the celery crop, pockets of celery waste were left on the field (5 cm deep in places) and the 48 m wide strip of phacelia and buckwheat cover crop remained in front of the tower. Wet conditions in the winter and early spring of 2019/20 then prevented the field being ploughed until March 2020, which prevented high aeration of the soil and left the strip of phacelia and buckwheat to grow. This reduced net C emissions during this time compared to the completely bare field post maize harvesting. Once ploughed on 10<sup>th</sup> March 2020, an initial spike immediately post ploughing was observed followed by a higher rate of C emission similar to 2019.

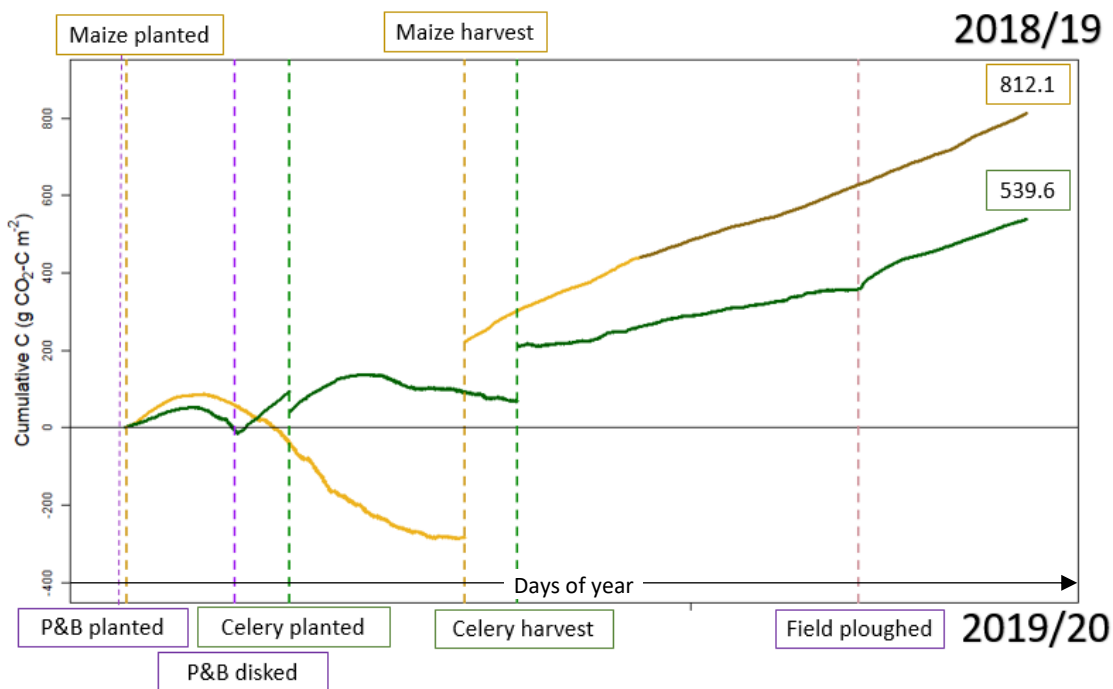


Figure 5.7. Cumulative C flux for EN-SP3 during the two years of data collection. The first year (17<sup>th</sup> May 2018 to 17<sup>th</sup> May 2019) is indicated by the yellow line during which a maize crop was grown. The dark yellow portion of the line indicates data gap filled by the relationship described in Chapter 4.2.1. The second year (17<sup>th</sup> May 2019 to 17<sup>th</sup> May 2020) is indicated by the green line, during which a phacelia and buckwheat cover crop was grown prior to a celery crop. Key management practices are highlighted by the dashed lines and corresponding coloured labels. Management practices that took place in 2018/19 are indicated above the graph, while those in 2019/20 are below.

## 5.4 Discussion

### 5.4.1 Energy Balance Closure (EBC)

The EBC at EN-SP3 was 62% in 2018 and 81% in 2019/20. This is within the range of ECBs observed at other sites which range from 55% to 99% (Stoy et al., 2013, Franssen et al., 2010, Foken, 2008, Yu et al., 2006, Yuling, 2005, Wilson et al., 2002). The typical mean EBC across the FLUXNET research sites (Stoy et al., 2013, Wilson et al., 2002) has been reported as of ~80%, close to what was observed at EN-SP3 2019/20. Whilst EBC was lower in 2018, and well below the mean across FLUXNET sites, it was not below the lowest observed value of 55% (Wilson et al., 2002). Compared to other studies conducted on similarly managed agricultural peatlands within East Anglia, the EBC in 2019/20 was slightly lower than Cumming (2018) (87–89 %) and similar to Morrison et al. (2013) (89%–81%). Across the two years, a general trend of underestimation of energy fluxes or an overestimation of available energy at high energy levels was observed, which is typical of EC sites (e.g. Yuling, 2005, Stoy et al., 2013, Morrison et al., 2013, Cumming, 2018).

The 19% variation in EBC between the years was large but could be attributable to several reasons. The incoming energy flux measurements were likely impacted by the soil instruments not being installed in their entirety straight away. In the first year of data collection, only one set of soil instruments measuring soil heat flux were installed (installed on 6<sup>th</sup> June 2018), with the second set installed a year later on 8<sup>th</sup> June 2019 (Chapter 3.2.3). This may have exacerbated an underestimation of soil heat flux which has been observed to occur in many instances (Hsieh et al., 2009) and the known problems of measuring soil heat fluxes within peat soils (Laurila et al., 2012, Harding and Lloyd, 2008). Differences between measured and actual soil heat flux would have impacted both years of data as the soil instrumentation was located within the field margin rather than under the crop. This was due to ongoing farm practices in the field (such as ploughing and disking) making it impossible to have the soil instruments located away from the field edge. This will likely have resulted in differences in soil texture and moisture between the irrigated and ploughed field compared to the field margin. Additionally, in 2018 the height of the flux tower was raised from 2.03 m to 5.75 m to allow for a maize crop which caused a bigger disconnect between the instruments measuring energy flux and available energy.

Night time values of EBC (<1% and 28%) were lower than daytime values (56% and 83%), which is typical of other studies (McGloin et al., 2018, Stoy et al., 2013, Wilson et al., 2002). This is found to be due to low friction velocity ( $u^*$ ) leading to an increase in the relative amount of energy leaving the site via advection rather than via turbulent fluxes (Wilson et al., 2002,

Franssen et al., 2010). For example, McGloin et al. (2018) observed a sharp decrease in EBC during stable conditions compared to unstable conditions. They reported particularly low EBC at a cropland site compared to three forested sites and a sedge-grass marsh within the Czech Republic due to lower frequency of less stable conditions. Energy Balance Ratio (EBR) showed better night time closure (0.44 and 0.35) than EBC through linear regression, which is expected due to more energy being available in the daytime (Stoy et al., 2013).

There were no clear differences in closure between cropped and bare periods despite bare periods typically being at times of the year when day length and consequently available energy was less. The period between 23<sup>rd</sup> October 2019 and 10<sup>th</sup> March 2020 was the worst period of EBC during the second year (65%) and had a negative EBR (-1.60). This was likely caused by the lack of homogeneity in field cover during this time, with only part of the field covered by a partially senesced cover crop and the rest of it bare, conditions which have been observed to relate to low EBC (Stoy et al., 2013, PANIN, 2001). This was likely exacerbated by the inconsistent celery waste that was present on the field during this period.

In addition to field conditions and error of measurements, minor components that are hard to quantify are missing from the EBC equation (Burba, 2013), such as the energy stored and used in photosynthesis, or heat stored within the canopy or dead plant material overlaying the field (such as the residues remaining after harvest of the celery crop).

While corrections to the fluxes to correct energy imbalance are available (Charuchittipan et al., 2014, Mauder et al., 2013) they are generally not used. Overall, it is agreed that in most cases there will be an acceptably small degree of underestimation in energy fluxes that leads to a lack of closure. This indicates a small underestimation of positive NEE. Overall, EBC at EN-SP3 indicated a small underestimation of energy fluxes and therefore an underestimation of positive NEE, which fell within the range of previously observed values at other European EC flux sites.

#### 5.4.2 EN-SP3: Differences in NECB between the years

The two years of data collection at Engine Farm showed differing cumulative emissions of  $812.1 \pm 195.6 \text{ g C m}^{-2} \text{ yr}^{-1}$  in 2018/19 to  $539.6 \pm 181.4 \text{ g C m}^{-2} \text{ yr}^{-1}$  in 2019/20 (Table 5.6). EN-SP3 fell within (year 1) or below (year 2) the error bounds of the IPCC Tier 1 emission factor for temperate drained cropland of  $790 \pm 150 \text{ g C-CO}_2 \text{ m}^{-2} \text{ yr}^{-1}$  (IPCC, 2014). Between the years, NECB varied by  $272.5 \text{ g C m}^{-2} \text{ yr}^{-1}$ . This variation is larger than observed by Cumming (2018) across 3 years, but less than the variation seen in studies arable agriculture on peat within Europe over multiple years (Poyda et al., 2016, Beyer et al., 2015).

#### 5.4.2.1 Cropping

The two years saw very contrasting cropping, with 2018/19 characterised by a maize crop that was on the field for 138 days (18<sup>th</sup> May–2<sup>nd</sup> October 2018). Conversely, in 2019/20, although a crop was present over the whole field for 139 days, it was split between 46 days for the phacelia and buckwheat (25<sup>th</sup> May–1<sup>st</sup> July) and 93 for the celery (23<sup>rd</sup> July–23<sup>rd</sup> October).

The combination of maize being a high growth crop and being planted at a time of the year with longer day length and better growing conditions led to a higher seven day peak average NEE for the maize (-9.50 g C m<sup>-2</sup> d<sup>-1</sup>) than the celery (-2.86 g C m<sup>-2</sup> d<sup>-1</sup>) or for phacelia and buckwheat (-4.92 g C m<sup>-2</sup> d<sup>-1</sup>). This was despite the maize being stunted due to abnormally low rainfall during May and June 2018 (Rob Parker, pers. comm.).

Whilst the maize did have the highest seven-day peak average GPP (-17.42 g C m<sup>-2</sup> d<sup>-1</sup>), the highest Reco was also seen during the maize crop (9.10 g C m<sup>-2</sup> d<sup>-1</sup>). There are several possible reasons for this.

Photosynthesis is known to be closely linked to root respiration, with higher photosynthesis leading to increases in root respiration within hours of photosynthesis taking place (Kuzyakov and Gavrichkova, 2010). This also matches findings by Wen et al. (2019), who found that Reco was higher in peat mesocosms sown with a cover crop than bare peat mesocosms, describing a pattern of decreased NEE despite an increase in Reco within the crop covered mesocosms.

In addition, it is possible that the difference in photosynthetic pathway used by maize (C4) compared to phacelia and buckwheat (C3) led to an increase in soil respiration. Chen et al. (2016) observed that between the two dominant plant species of Tian'e Zhou wetland, China, the C4 species with a lower total biomass produced higher soil respiration than a C3 species, despite the latter's higher productivity.

Additionally, roots of maize crops are much deeper and more expansive than the other crops grown during the study periods, typically growing up to 2 m deep and 1 m wide (Feldman, 1994). In comparison, celery's roots typically only penetrate ~0.3 m deep. While phacelia's roots are dense they are primarily located within the upper 0.3 m of soil (De Baets et al., 2011). Buckwheat roots are mostly concentrated in the upper 0.4 m of soil, despite the plant having a taproot that can penetrate down to 1 m (Murakami et al., 2002). This suggests that the more expansive maize root system led to a greater penetration, aeration and exploitation of the soil, allowing for increased CO<sub>2</sub> emission during the growing period.

Whilst multi-year studies on the same sites do show some variation in emissions with crop type (Cumming, 2018, Poyda et al., 2016, Beyer et al., 2015), overall it has been suggested that variation in emissions due to crop type is low and inconsistent (Norberg et al., 2016). However, in contrast to these previous studies, including Norberg et al. (2016) who grew crops with similar growth profiles (wheat, barley, grasses, carrot, potato and rape), the difference in growth between celery and maize in this current study is significant. Overall, results indicate differences between the crops and how they impacted the C cycling from EN-SP3, however, an in-depth examination of these differences was outside the scope of this study. A detailed analysis of the key effects of the crops on the soil and how this impacts crop C cycle needs to be addressed in future studies.

#### 5.4.2.2 *Cover cropping*

Within mineral soils, recent real world (Jian et al., 2020, Guardia et al., 2019) and modelled (Launay et al., 2021) studies have indicated that cover crops can add considerable amounts of C to surface soil. Globally, cover cropping has been shown to increase near-surface SOC by an average of 15.5% (Jian et al., 2020). However, as noted in Jian et al. (2020), C increases are concentrated within the top 0.3 m of the soil and are more labile than long term stored C with peatlands (Taft et al., 2018).

The impact of cover cropping on C emissions from agricultural peatlands is not currently well studied, with the only known UK-based study (Wen et al., 2019) specifically examining cover crops. In recent years, G's Fresh have moved towards cover cropping before planting main crops. Most cover crops (including phacelia and buckwheat) have shallow root systems, mostly concentrated in the upper 0.4 m, thus reducing the need for tillage before sowing a main crop (such as celery or maize). Cover crops provide several benefits such as the aggregation and aeration of the topsoil. Cover crops also help with nutrient cycling, absorbing excess nitrogen which is then re-released when the crop is disked into the field before the main crop (Wen et al., 2019). Due to this, cover crops are often referred to as 'green manure'. Once the cover crop is disked, main crops can be drilled or planted directly into the field, reducing the need to tillage before the crop. On peat soils in eastern England, growing cover crops also helps reduce the 'fen blow' phenomenon by reducing the amount of aeolian erosion of top soil (See Chapter 6).

Cover cropping was implemented on the field in the 2019/20 year, with the phacelia and buckwheat present on the field for 46 days over the entire field and in a strip in front of the flux tower for 140 days. The phacelia and buckwheat cover crop grown in 2019 showed the highest drawdown of C in terms of average GPP ( $-5.06 \text{ g C m}^{-2} \text{ d}^{-1}$ ) and average NEE ( $-0.19 \text{ g C m}^{-2} \text{ d}^{-1}$ )

than at any other point during the 2019/20 data period. The cover crop was present on the field within a 48 m strip throughout the rest of the year, and despite only being a small portion of the flux towers footprint, was seen to reduce the NEE from the field compared to bare periods (Table 5.3). This was in part helped by a warm winter in 2018/19 that allowed small amounts of crop growth to persist throughout the winter months. Wen et al. (2019) saw a similar pattern of decreased NEE during cover cropping with vetch and rye. An increase in Reco during the cover crop was also observed and found to be primarily autotrophic, and not heterotrophic respiration, due to increased productivity. It was also noted that there was a potential increase in microbial activity in the soil due to higher rhizodeposition, with increases higher in vetch due to its higher productivity.

In the days immediately after the phacelia and buckwheat was disked, the field showed elevated Reco and a high net C emission, the highest seen over the data collection period (peak average seven day peak NEE:  $5.50 \text{ g C m}^{-2} \text{ d}^{-1}$ ) other than for the period following ploughing on 10<sup>th</sup> March 2020. This indicates a possible priming effect of the soil by the cover crop, although the increased tillage and management of the soil is likely the primary cause of the C emissions increase. Taft et al. (2018) investigated the priming effect of incorporating lettuce residues into an agricultural peatland, and found that whilst emissions increased, native SOM was not primed and only the additional, more labile C within the crop residue was mineralised. However, as pointed out by Wen et al. (2019), different cover crops accumulate different amounts of N and C in the rhizosphere which could lead to different species having a different priming impact. Additionally, cover crop mixtures have been shown to result in greater increases in SOC (Jian et al., 2020) which may lead to increased emissions. A close examination of different cover crops and their impacts on C cycling within cropped peatlands was outside the scope of this study. This knowledge gap should be addressed by further work to accurately understand the C and nutrient cycling from cover cropping peatlands and to inform best practice for land managers.

While an increase in C emission was seen in the period after celery harvest, the daily C emission during this period ( $1.08 \text{ g C m}^{-2} \text{ d}^{-1}$ ) was lower than that following disked of the cover crop ( $4.73 \text{ g C m}^{-2} \text{ d}^{-1}$ ). This was in contrast to Taft et al. (2018), who observed increased soil GWP when lettuce residue was left on top of the field ( $105 \pm 4 \text{ kg CO}_2\text{-e ha}^{-1} \text{ d}^{-1}$ ) compared to when it was incorporated ( $84 \pm 4 \text{ kg CO}_2\text{-e ha}^{-1} \text{ d}^{-1}$ ). However, in this study, the difference in findings could have been due to the remaining strip of cover crop masking emissions during the post-harvest period. After the remaining cover crop strip was ploughed into the field, the following seven days showed the highest average C emission (NEE:  $5.89 \text{ g C m}^{-2} \text{ d}^{-1}$  from 10/03/2020 to 16/03/2020), after which emission remained relatively low through the rest of the year, with

the whole period having an average NEE of  $2.61 \text{ g C m}^{-2} \text{ d}^{-1}$  (10<sup>th</sup> March to 17<sup>th</sup> May 2021). This was similar to the predicted NEE of  $2.71 \text{ g C m}^{-2} \text{ d}^{-1}$  (10<sup>th</sup> March to 17<sup>th</sup> May 2019) for the same time period during the previous year when the field was also bare. This suggests that any priming effect from the cover crop was limited.

Overall, the final cumulative emissions totals for 2019/20 ( $539.6 \pm 181.4 \text{ g C m}^{-2} \text{ yr}^{-1}$ ) were lower than for 2018/19 ( $812.1 \pm 195.6 \text{ g C m}^{-2} \text{ yr}^{-1}$ ). While other contributing factors in part explain differences between the years (the drier weather conditions in 2018/19, the impact of the maize crop on the soil), it does not completely rule out the impact that the cover crop may have had on reducing the C emissions from the field. Additional studies should be performed in the future to further examine the impact of cover cropping in real world scenarios on peat soils to confirm any reduction in C emissions that they provide. In particular, they should establish whether emissions of historic C stored within the peat are either preserved or primed by the addition of more labile C into the soil surface through the incorporation of the cover crops.

#### *5.4.2.3 Impact of soil management practices*

The impact that working the soil had on emissions was clearly shown within this study, with the highest emission rate ( $11.63 \text{ g C m}^{-2} \text{ d}^{-1}$  10<sup>th</sup> March 2020) observed during ploughing, and high emission rates persisting in the days following field management. This impact is well known and has been observed in other studies on agricultural peatlands (Morrison et al., 2013, Cumming, 2018). The main driver of higher emissions is aeration of the surface organic soil layer. Increased soil temperatures from removing plant cover and fresh plant material being mixed into the surface soil have also been shown to increase heterotrophic respiration (Elder and Lal, 2008, Franzluebbers et al., 1995, Buyanovsky et al., 1986). This explains the high emissions seen on the field (NEE:  $6.92 \text{ g C m}^{-2} \text{ d}^{-1}$ ) during preparation for the celery crop, involving disking the phacelia and buckwheat which both aerated and added fresh plant material to the top portion of the soil.

#### *5.4.2.4 Weather impacts*

Temperature is known to be a main driver of Reco, due to the positive relationship between temperature and soil respiration (Lloyd and Taylor, 1994). As is common with studies on peatlands, temperature was found to be a main driver throughout this study (Chapter 4) and was used to gap fill emissions at the site, most notably for the bare period after the maize crop had been harvested (12<sup>th</sup> December 2019 to 17<sup>th</sup> May 2019), using a model similar to that described by Lloyd and Taylor (1994).

The two years covered by this study had differing weather conditions, most notably the hot and dry late spring and early summer in 2018 and the wet autumn in 2020 leading into a warm winter. This impacted the crops, with the maize in 2018 being stunted (Robert Parker, pers. comm.) and the warm winter allowing the phacelia and buckwheat strip to continue growing.

The highest Reco observed (other than immediately after ploughing) was during the maize crop (Reco Max: 9.52 26<sup>th</sup> July 2018) and was likely aided by the warm temperatures. This result is similar to that of Ding et al. (2007) who also observed that increased temperature led to increased soil respiration in a maize crop. It has been shown that wet and dry conditions impact the proportion of autotrophic and heterotrophic respiration differently, primarily through reduced heterotrophic respiration in wet conditions even when a crop is present (Olefeldt et al., 2017, Wen et al., 2019). The wet conditions along with warm winter temperatures during December 2018 and January in 2019, prevented the field from being a strong C source by supporting continual growth of the cover crop along with reduced heterotrophic respiration of the wet soil.

#### *5.4.2.5 Overall Recommendations for land managers*

From the two years of data collected from the study site, some observations and tentative recommendations can be made for farm practices on wasted peat with the aim to lower C emissions from the field and preserve the remaining peat layer:

1. Cropping appeared to make a difference between the two year-long periods, particularly when comparing main crops. The maize crop had a drastically different growth profile to the celery crop, being much more productive than the celery. Whilst this increased GPP, it also led to very high Reco. This was hypothesised to be a result of the higher productivity of the maize and the different growth profile of the roots. More research is needed on the different impacts on soil C cycling from different plants to fully ascertain any differing impacts between the crops.
2. The additional phacelia and buckwheat cover crop grown on the field before the celery crop may have had a positive impact on reducing C emissions, with lower emissions observed overall in the year that it was grown. However, it should be noted that the disking of the crop into the field led to a period of high emissions. Further studies between the same systems with consistent use of cover cropping across an entire field should be used to examine the magnitude of any effect. In addition, the nature of the C emissions from the fields with cover crops should be analysed, particularly focusing on

whether the more labile C added to the field by the cover crop reduces the loss of C already stored within the peatland.

3. Similar to the results from other studies, working of the soil surface produced spikes in C emissions during and in the immediate days following tillage due to the aeration and subsequent oxidation of SOM. Working the soil (particularly the subsoil) is likely to increase its mineralisation and should be avoided where possible.

#### 5.4.3 Carbon emissions with peat depth and soil C %

The two years of data from EN-SP3 allow for a robust comparison to be made with other sites across the UK and Europe regarding peat loss and its impacts on C emissions from agricultural peatlands under arable cropping. Overall, 17 studies were identified of CO<sub>2</sub> emissions from arable cropping on peatland (7 from the UK's Fenland Region, 6 from Denmark, 3 from Germany and 1 from Finland) on varying peat depths, most of which report soil C % content within topsoil (Table. 5.8). Using both data from EN-SP3 and the additional 17 studies, the relationship between peat depth and C emission was examined to identify if a reduction in peat depth led to a reduction in C emission. Similarly, surface soil C % was examined to see if a reduction in C content in the surface soil led to a reduction in C emission. The average emission value observed over the two years from EN-SP3 was used within the analyses. This is provided in Table 5.7 and is indicated by the red data point (Figure 5.8).

*Table 5.7. NECB, peat depth and where available soil C % (0–0.1 m) for studies of CO<sub>2</sub> emissions from agricultural peatlands under arable cropping within the UK and Europe. The colour denotes whether the study is from the UK (green) or the EU (blue). \* denotes a study not included in analysis due to being unrealistic. An average of the emissions found across the two years at EN-SP3 is provided which was used within subsequent analyses.*

Study	Site Description	NECB (g C m <sup>-2</sup> yr <sup>-1</sup> )	Peat Depth (m)	Surface soil C % (0 - 0.1 m)
This study	Engine Farm Year 1	812 ± 195.6	0.4	15.1
This study	Engine Farm Year 2	540 ± 181.4	0.4	15.1
This study	Engine Farm Average	676 ± 188.5	0.4	15.1
Evans et al. 2021	Rosedene Farm – East Anglia, UK	758	2.0	43.6
Evans et al. 2021	Redmere Farm (Site 1) – East Anglia, UK	678	0.75	30.8
Evans et al. 2021	Redmere Farm (Site 2) – East Anglia, UK	767	0.7	-
Evans et al. 2016	Manchester Mosses, UK	647	1	36.2
Taft et al. 2017	East Anglia, UK	518.4	0.4	19.1
Taft et al. 2017	East Anglia, UK	834.3	0.7	33.7
Taft et al. 2017	East Anglia, UK	764.1	0.9	38.8
Maljanen et al. 2007	Germany	210	0.2	-
Elsgaard et al. 2012	Denmark	1530	2.2	20
Elsgaard et al. 2012	Denmark	720	0.72	33
Elsgaard et al. 2012	Denmark	700	0.77	47
Kandel et al. 2018	Denmark	500	0.55	34
Kandel et al. 2018	Denmark	620	0.55	32
Kandel et al. 2018	Denmark	580	0.55	33
Poyda et al. 2016	Germany	1495	2.8	13.3
Lohila et al. 2004	Finland	336	0.55	22
Beyer et al. 2015*	Germany	139	2.0	29.1

A logarithmic relationship was observed to best relate NECB to peat depth, however the relationship varied between the different subsets of data (Figure 5.8). On their own, UK studies were not found to show a significant relationship, whilst the European studies (excluding UK studies) did show a significant relationship ( $p < 0.0001$ ,  $R^2 = 0.91$ ). When all the data (UK and Europe) was examined, a significant relationship was also found ( $p < 0.0001$ ,  $R^2 = 0.70$ ) although

it was found to be weaker than the European studies alone. No relationship was found between NECB and soil C %.

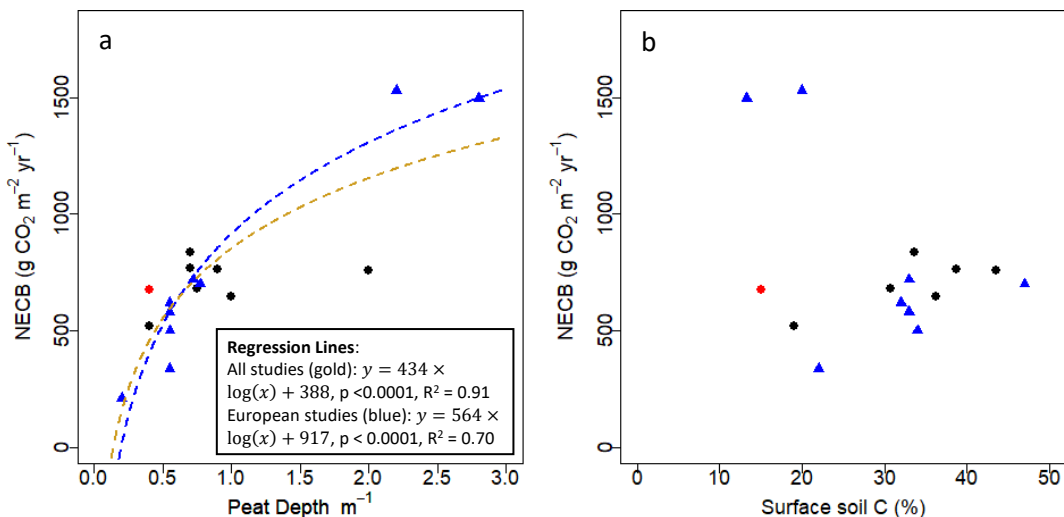


*Figure 5.8. The Net Ecosystem Carbon Balance at 17 different study sites in relation to Peat Depth (a) and, where available, surface soil C% (top 0.1 m) (b). The red point represent data from this study, the black points data from the UK and the blue triangles data from European study sites. Regression analysis was performed. NECB vs. peat depth was best related by a logarithmic relationship whilst NECB vs. C% was best related by a linear relationship. Regression lines indicate significant relationships between variables: Europe (blue line) and the complete data set (gold line).*

#### 5.4.3.1 Carbon emissions and peat depth

Overall, the significant relationship observed between C emissions and peat depth indicates that less C emissions should be observed from agricultural peatlands as the peat layer is depleted (Figure 5.8), with emissions decreasing rapidly once peat depth drops below 1 m.

Overall, within the UK, emissions from all peatland sites were similar with no significant trend observed between C emissions and peat depth when examined alone. In part this is likely due to the limited variation in studies across different peat depths, with all the UK studies focused on sites with shallow peats between 0.4 and 1.0 m deep (other than Rosedene Farm at 2.0 m deep) compared to the European studies which cover a larger range (peat depths from 0.2 to 2.8 m) (Table 5.7). This difference, coupled with the relatively few studies, make establishing a relationship difficult as variation in site specific factors between the studies can impact the overall trend.

The analysis indicates, however, that there are still large emissions from shallow peatlands within the 0.4–0.6 m depth range, with EN-SP3 (676 g C m<sup>-2</sup> yr<sup>-1</sup>, 0.4 m) showing similar emissions to those from deeper peats (Redmere Farm (Site 2), 678 g C m<sup>-2</sup> yr<sup>-1</sup>, 0.75 m; Manchester Mosses, 647 g C m<sup>-2</sup> yr<sup>-1</sup>, 1.0 m) (Table 5.7). Comparison to emissions from deeper peatlands are largely driven by the high C emission value for the first year of data collection (812 g C m<sup>-2</sup> yr<sup>-1</sup>) (see

Chapter 5.3.1). On its own, this would be one of the highest emission values seen in the UK over a single year and sits well above the regression line denoted for all data, whilst the second year of data of emissions data ( $540 \text{ g C m}^{-2} \text{ yr}^{-1}$ ) is much closer to what would be expected. Significant variation between years has also been observed in other studies (Beyer et al., 2015, Poyda et al., 2016), highlighting the importance of continuous datasets over multiple years at sites that allow for accurate averages of C emissions to be calculated despite inter-annual variations.

These comparisons suggest that, while the overall trend may be a lowering of emissions as peat depth reduces, this effect may be masked by differing management practices which also have a significant impact on C emissions. Emissions from deep peat at Rosedene Farm (Evans et al., 2021) are comparatively low compared to European studies on similar peat depths, with Elsgaard et al. (2012) finding  $1550 \text{ g C m}^{-2} \text{ yr}^{-1}$  from 2.2 m deep peat layer and Poyda et al. (2016) finding  $1495 \text{ g C m}^{-2} \text{ yr}^{-1}$  from a 2.8 m deep layer, both over twice the emission from Rosedene Farm ( $758 \text{ g C m}^{-2} \text{ yr}^{-1}$ , 2 m deep). One possible reason for this variation could be water table depth. It has been well established that higher water tables within peatlands lead to lower C emissions (Evans et al., 2017b, Taft et al., 2018, Evans et al., 2021) with arable agricultural sites often observed to have the lowest water table depths of any type of peatland land use in order to maintain trafficability for farm machinery. The water table at Rosedene Farm is managed at a higher level than many farms on deep peat, ranging between -0.38 and -1.0 m (Cumming, 2018). Levels are raised during the cropping period and lowered during fallow periods, but the water table remains within 0.6 m of the peat surface for long periods of time. A high water level (an average of -0.28 m) was also suggested by Beyer et al. (2015) as the primary reason for observing very low C emissions of  $139 \text{ g C m}^{-2} \text{ yr}^{-1}$  at an agricultural peatland with a 2.0 m depth of peat (Table 5.7). However this effect is not seen by all studies. Elsgaard et al. (2012) found emissions of  $1530 \text{ g C m}^{-2} \text{ yr}^{-1}$  at an arable site with 2.2 m depth of peat and an average -0.48 m water table, but did not provide a suggestion other than the peat depth for why emissions were higher than other sites. Poyda et al. (2016) also found high emissions of  $1495 \text{ g C m}^{-2} \text{ yr}^{-1}$  at an arable site over 2 years with 2.8 m depth of peat and an average -0.48 m water table, although lower emissions were observed in the first year with water logging of the field after harvest ( $1220 \text{ g C m}^{-2} \text{ yr}^{-1}$ ) compared to the second year ( $1770 \text{ g C m}^{-2} \text{ yr}^{-1}$ ). Both Elsgaard et al. (2012) and Poyda et al. (2016) used manual chambers rather than EC which may have impacted the emissions seen from the site, with the chamber not capturing the complete emission picture.

While water table depth is important for deep peatlands, it is less likely to have such an important impact on shallower peats. For example, EN-SP3 surface peat horizon (0.4 m) is completely above the water table line, which never got higher than a depth of -0.7 m. This kept

the peat horizon constantly aerated, so changes in water table depth are not likely to impact C emission. However, this is something that requires further research and examination across multiple peat depths to confirm.

#### 5.4.3.2 *Carbon emissions and soil C content*

Whilst both a linear and a logarithmic fit were tested to relate NECB to SO %, no significant relationship was found for either UK, European, or combined datasets (Figure 5.8.B). Additionally, data from Elsgaard et al. (2012) and Poyda et al. (2016) indicate much higher emissions ( $1530$  and  $1495 \text{ g C m}^{-2} \text{ yr}^{-1}$ ) despite low SOC% ( $20\%$  and  $13.3\%$ ) indicating that other factors (such as the aforementioned peat depth) were likely the main cause of C emission from these peatlands. Eickenscheidt et al. (2015) found similar results in study of drained fen peatland in Germany, finding that SOC had no effect on NEE and suggesting that rather than SOC content, the main driver of C emissions was land use. In a somewhat contrasting study, Taft et al. (2017) found that CO<sub>2</sub> emissions increased on bare soil between three different sites, with varying SOC ( $19.1\%$ ,  $33.7\%$  and  $38.8\%$ ). However, the same was not seen from the equivalent cropped portions of the sites, instead a significant difference was only observed between the site with lowest SOC ( $518.4 \text{ g C m}^{-2} \text{ yr}^{-1}$ ) and the two sites with higher soil carbon ( $834.3 \text{ g C m}^{-2} \text{ yr}^{-1}$  and  $764.1 \text{ g C m}^{-2} \text{ yr}^{-1}$ ). Taft et al. (2017) noted that microbial respiration for soil with the highest SOC ( $38.8\%$ ) was proportionally higher than for the other sites. This could indicate that higher SOC% leads to increased loss from peat due to higher rates of mineralisation, even when the overall emissions are similar. Future studies that partition autotrophic and heterotrophic respiration will be helpful in determining whether C loss from peat soils with higher SOC is due to increased mineralisation of the historic C stored in the peat rather than root respiration or from more labile C being added to the soils via crop residues.

#### 5.4.4 Estimation of Emissions from the UK's wasted peatlands

Currently, Tier 1 and Tier 2 emissions factors (EFs) for the UK's wasted peatlands have been derived from studies of cropland on drained, deep peats (IPCC, 2014, Evans et al., 2017a). While these EFs provide a good insight into the likely magnitude of emissions, they need to be confirmed, as emissions may decline with decreasing depth of peat and reducing soil carbon content. The large proportion of lowland peat soils in England that are classified as wasted (i.e. two thirds of the cropland on drained peat), means that scaling of current EFs by area could result in high uncertainty. This is a particularly significant issue for agricultural peatlands in the UK, since they account for more GHG emissions than any other land use per unit area (Evans et al., 2017a). The average CO<sub>2</sub> emission value generated within this study can be used to provide

an improved estimate of the total annual CO<sub>2</sub> emissions from cropland on wasted peat in England (Table 5.8).

*Table 5.8. Most recent EF calculated for cropland by Evans et al. (2017a) and the new EF for cropland on wasted peat calculated using direct CO<sub>2</sub> data from this study. All fluxes are shown in tCO<sub>2</sub>e ha<sup>-1</sup> yr<sup>-1</sup>. Table adapted from Evans et al. (2017a).*

Peat condition category	Drainage status	Direct CO <sub>2</sub>	CO <sub>2</sub> from DOC	CO <sub>2</sub> from POC	Direct CH <sub>4</sub>	CH <sub>4</sub> from ditches	Direct N <sub>2</sub> O	Indirect N <sub>2</sub> O	TOTAL
Data Source:		Evans et al. (2017a)	IPCC (2014)	Evans et al. (2016)	Evans et al. (2017a)	IPCC (2014)	Evans et al. (2017a)	IPCC (2006)	
Tier		Tier 2	Tier 1	Tier 2	Tier 2	Tier 1	Tier 2	Tier 1	
Cropland	Drained	26.57	1.14	0.30	0.02	1.46	8.97	0.54	<b>38.98</b>
<b>Cropland on wasted peat derived from this study</b> (updated values in orange)									
Cropland on wasted peat	Drained	24.8	1.14	0.30	0.02	1.46	8.97	0.54	<b>37.23</b>

Using the new derived EF for cropland on wasted peat, a new estimate of direct CO<sub>2</sub> emissions from this land use/land condition in England was calculated as 3,276 kt CO<sub>2</sub> yr<sup>-1</sup>. This represents a decrease in the direct CO<sub>2</sub> emissions reported by (Evans et al., 2017a) of 234 kt CO<sub>2</sub> yr<sup>-1</sup>, from the previous estimate of 3,510 kt CO<sub>2</sub> yr<sup>-1</sup>. Whilst this is a modest decrease in estimated emissions, given its large area, cropland on wasted peat still emits twice the total direct CO<sub>2</sub> as cropland on deep peat (1,344 kt CO<sub>2</sub> yr<sup>-1</sup>), and represents 43% of England's and 21% of the UK's annual CO<sub>2</sub> emission from peatlands. Further investigation is required to fully understand how emissions might vary spatially and temporally, e.g. over a wider range of land management regimes, soil carbon contents and peat depths and to develop advice on how land managers may be able to mitigate emissions from these ecosystems.

## 5.5 Chapter 5 Summary

Within this chapter, daily fluxes recorded over a 2 year period of NEE, GPP and Reco were presented from EN-SP3. The first year of study, which observed a maize crop, found emissions of  $812 \pm 195.6$  g C m<sup>-2</sup> yr<sup>-1</sup>. The second year of study observed the same field with a cover crop grown before the main celery crop with overall lower C emission ( $540 \pm 181.4$  g C m<sup>-2</sup> yr<sup>-1</sup>). Overall, the average emissions from EN-SP3 were found to be  $676 \pm 188.5$  g C m<sup>-2</sup> yr<sup>-1</sup>.

Differences in emissions during cropping periods were observed, with higher GPP (-17.42 g CO<sub>2</sub>-C m<sup>2</sup> d<sup>-1</sup>) but also higher Reco (9.52 g CO<sub>2</sub>-C m<sup>2</sup> d<sup>-1</sup>) observed for a maize crop during its period of peak growth compared to a phacelia and buckwheat cover crop (GPP: -13.14 g CO<sub>2</sub>-C m<sup>2</sup> d<sup>-1</sup>; Reco: 8.22 g CO<sub>2</sub>-C m<sup>2</sup> d<sup>-1</sup>) and a celery crop (GPP: -8.56 g CO<sub>2</sub>-C m<sup>2</sup> d<sup>-1</sup>; Reco: 5.13 g CO<sub>2</sub>-C m<sup>2</sup> d<sup>-1</sup>). Soil management practices were found to cause spikes in C emission from the field, with the biggest daily emission observed during ploughing (NEE: 11.36 g CO<sub>2</sub>-C m<sup>2</sup> d<sup>-1</sup>). The weather was very different between the two study years, with abnormally hot and dry weather in 2018 leading to increased C emission from the field compared to the comparatively cooler and wetter weather in 2019/20 which showed lower C emissions.

When emissions from EN-SP3 were compared to other studies across the UK and Europe, peat depth was found to be a significant factor in determining the scale of C emission. This followed a logarithmic relationship, with greater C emission observed at sites with deeper remaining peat depths. The same was not seen for surface soil C content, with no relationship observed between surface soil C % and C emissions. Using the average value of emission from EN-SP3, an improved estimate of direct CO<sub>2</sub> emissions from cropland on wasted peat within England was made. This was calculated as 3,276 kt CO<sub>2</sub> yr<sup>-1</sup>, representing a small decrease compared to the previous estimate of 3,510 kt CO<sub>2</sub> yr<sup>-1</sup>.

## 6 Aeolian erosion from two agricultural fen peatlands within East Anglia

This chapter addresses research questions 4 and 5:

4. What are the magnitudes of aeolian soil erosion and C flux on deep and wasted lowland peatlands under arable and horticultural agriculture?
5. What are the environmental and field management practices that impact aeolian soil erosion?

The lowland peatlands of East Anglia (the Fens) are dominated by large scale arable agriculture. Arable agriculture typically leaves the fields bare throughout the winter and spring months while they are being prepared for crops. This leads to the ‘fen blow’ phenomenon, where the field surface is eroded and clouds of dust blow off the fields, onto nearby roads and into nearby properties. These events, as well as less intense, on-going aeolian erosion throughout the year, generate a substantial amount of windblown material, and result in the loss of an agriculturally valuable resource and the C that it contains. In addition to aiding the steady depletion of valuable, fertile topsoil, fen blows also spoil crops so they are unfit for consumption, can prevent farmers from planting, and in some cases, where young plants are damaged, can require fields to be re-planted.

In order to ascertain the magnitude and examine the impacts of different cropping and management practices on aeolian soil erosion from agricultural peatlands, the Horizontal Mass Flux (HMF) and Horizontal Mass Transfer (HMT) are quantified from two field sites (described previously, Chapter 3 1), one situated on deep peat (Rosedene Farm) and one on wasted peat (Engine Farm) using Big Spring Number Eight (BSNE) dust collectors. Additional environmental data: wind speed, soil water content, soil and air temperature, rainfall and crop data were provided from instrumentation at the co-located EC towers and by the farm managers. At Engine Farm, soil volumetric water content (SWC) and wind speeds at 0.5, 1.0 and 2.0 m were recorded on specific field boundaries using additional Sonic Anemometer arrays.

HMF is used to infer HMT of material and associated C loss from the fields, representing the first such estimate for a wasted peatland and only the second estimate for a deep peatland. Drivers of aeolian erosion are examined and discussed through comparisons between the field sites and years. Measures for mitigating soil and associated C losses are suggested.

### 6.1 Aeolian erosion from peatlands

The long term reclamation of the East Anglian Fens for agriculture has been well documented (Hutchinson, 1980, Evans et al., 2017b), with the associated drainage leading to many long term

impacts (Rotherham, 2013, Page et al., 2020). Today, the Fens consist of highly desirable, fertile agricultural land which supports intensive arable farming. The shift to arable farming within the Fens has left much of the peat layer bare, with drainage allowing the surface peat soil to dry and become susceptible to aeolian erosion. The typical large field size to aid farming with modern machinery and few hedgerows provides little resistance to the wind as it moves across the fens. Additionally, due to the timing of field preparation in the winter and springtime which is typical for most crops, fields are left bare during spring, the season which often sees the highest wind speeds. As a consequence Fen blows (events of high aeolian erosion typically lasting a few days) have become a common occurrence, and local farmers often recount stories of memorable fen blow events (pers. comm. Rob Parker, Martin Hammond) with particularly bad events making the regional news (BBC News, 2013). Historically, severe, seasonal dust storm events around Ely have been mentioned since 1929 (Arber, 1946), coinciding with an increasing shift from pasture to arable farming on large fields.

Aeolian erosion from agricultural fields is recognised as a significant pathway for soil loss (e.g. Sandström et al., 1991, Campbell et al., 2002, Kohake et al., 2010, Borrelli et al., 2014). While some studies have been conducted on the impacts of aeolian erosion on UK farmland (e.g. Radley and Simms, 1967, Fullen, 1985, Chappell and Warren, 2003, Owens et al., 2006), only one was located on an agricultural peatland (Cumming, 2018). This is despite the ~153,000 ha of cropland on peatland within England, 27% of England's total peatland area (Evans et al., 2017a), and the regular occurrence of 'Fen blows' within the East Anglian region where almost all fen peatland is under agriculture. Despite the lack of research on aeolian erosion of agricultural peatlands, there have been a limited number of studies from upland peatlands within the UK (Pollard and Millar, 1968, Warburton, 2003, Foulds and Warburton, 2007) with two studies providing a quantitative assessment of erosional loss rates.

Warburton (2003) examined the erosion of upland blanket peat located within Northern England that formed under cool, cloudy and wet climatic conditions. Peat depth was typically 1–3 m deep. Erosion was measured using passive horizontal flux gauges with a fixed orientation (Hall et al., 1994) and Big Spring Number Eight (BSNE) dust collectors (Fryrear, 1986). Warburton (2003) calculated erosion rates of 0.46 to 0.48 t ha<sup>-1</sup> yr<sup>-1</sup> for two years from 1999 to 2000, which corresponded to 0.5 mm surface lowering (or 3 mm when a low bulk density of surface peat was assumed), primarily through the process of rain splash leading to relatively short transport distances over individual events. Warburton (2003) observed that periods characterised by high winds and heavy rainfall or frost led to the greatest movement of aeolian material, specifically within the months of December and April 2000.

Foulds and Warburton (2007) presented direct measurements and observations of aeolian erosion from a bare upland blanket peat over 3 month period in the Moss Flats, North Pennines, UK, using an array of 16 mass samplers, as described in (Warburton, 2003). Peat flux data were recorded at two week intervals over the 3 month period. They measured peat fluxes of  $0.8\text{--}3.0 \times 10^{-7} \text{ kg m}^{-2} \text{ s}^{-1}$ , finding that flux rates measured during dry periods were  $1.12\text{--}1.13 \times 10^{-8} \text{ kg m}^{-2} \text{ s}^{-1}$ , an order of magnitude lower compared to peat flux associated with rainfall events ( $4.55\text{--}6.45 \times 10^{-9} \text{ kg m}^{-2} \text{ s}^{-1}$ ).

The only study of wind-borne peat loss from an agricultural peatland to date was performed by Cumming (2018), who investigated lowland fen peatland under horticulture at Rosedene farm, Norfolk (see Chapter 3.1.3 for a more detailed site description). Losses from two adjacent fields were measured using two BSNE arrays between March 2013 and August 2015. Cumming (2018) found Horizontal Mass Transfer (HMT) rates of  $2.3\text{--}12.8 \text{ t ha}^{-1} \text{ yr}^{-1}$  in 2014/15, with the highest erosion rates between 31<sup>st</sup> March and 23<sup>rd</sup> April 2015 with a Horizontal Mass Flux (HMF) of  $10.26 \text{ g m}^{-2} \text{ d}^{-1}$ . Overall, high wind speed and bare peat correlated with the highest rates of aeolian transport. March, April and May were the months with the highest fluxes, whilst almost no erosion occurred during periods when the fields had a cover of vegetation (either crops or weeds). In contrast to Warburton (2003), wet autumn and winter months showed reduced erosion rates. This contrast is similar to what was suggested by Arber (1946), where fen blow events were thought to be caused by prolonged dry periods in spring followed by high winds.

Overall, these studies indicate that aeolian erosion is a significant component of both soil material and C loss from the UK's peatlands. As highlighted by Owens et al. (2006), basic data are still needed on the extent and magnitude of soil erosion from agricultural practices in the UK, particularly as it has been suggested as the dominant soil redistribution method from arable land (Chappell and Warren, 2003). Coupled with the more specific lack of knowledge on aeolian erosion from peatlands, this highlights a significant gap in our current knowledge.

This study aims to improve our understanding of the scale of aeolian erosion from lowland peatlands in the UK through a comparison of erosion rates from two horticultural fields in the Fens of East Anglia, one of which is located on wasted peat (a former deep peat with  $\leq 0.4 \text{ m}$  of remaining peat depth) and the other on a deep peat (peat depth  $> 0.4 \text{ m}$ ).

## 6.2 Methodology

### 6.2.1 Study Sites

Aeolian erosion was measured at the wasted peat site at Engine Farm on the field Spooners 3 (EN-SP3) and deep peat site Rosedene Farm on the field R39 (EF-DA) which are described in Chapter 3.1. A full description of regional weather is provided in Chapter 3.1.1. For a history of field management for EN-SP3 please see Chapter 3.1.2. For a full description and history of field management for EF-DA please see Chapter 3.1.3.

### 6.2.2 Dust and Anemometer Data Collection

*Table 6.1. Equipment used to measure the wind and dust blow at each of the field sites*

	<b>EN-SP3</b>	<b>EF-DA</b>
<b>Dust Samplers</b>	Six arrays of BSNEs (Figure 6.1 A). Each array consisting of 6 individual collectors at heights of 0.15, 0.2, 0.3, 0.5, 1 and 2 m. Two samplers (5 & 6) were located on the upwind (SW) field boundary while four (1, 2, 3, 4) were located on the downwind (NE) field boundary at (Figure 6.2.)	One BSNE array consisting of 5 collectors at heights of 0.15, 0.2, 0.3, 0.65 and 1 m (Figure 6.2 C).
<b>Anemometer</b>	Three ‘sonic towers’ (Figure 6.1 B) consisting of an array of 3 WindSonic Ultrasonic Wind Sensors (Gill Instruments Ltd, Lymington, UK) situated at heights of 0.5, 1 and 2 m above ground level. One array was placed on the upwind (SW) field boundary while two were situated downwind (NE) field boundary (Figure 6.2.). Data from the anemometers was logged using a CR1000 data logger. Power was provided through a 12 V, 30 W solar panel and Yuasa NP7 12 V, 7 Ah rechargeable battery (Campbell Scientific Ltd., Logan, UT, USA).	Wind speed data was collected via co-located EC tower via a C-SAT 3 sonic anemometer (as described in Chapter 3.2.).
<b>Additional Instruments</b>	Soil Water Content (SWC) and rainfall data was collected at the co-located EC tower (as described in chapter 3.1.2). Additional CS616s were installed at the upwind array and one downwind array to measure SWC on both sides of the field.	Soil Water Content (SWC) and rainfall data was collected at the co-located EC tower (as described in chapter 3.1.3).

At both field sites, passive dust samplers ‘Big Spring Number Eight (BSNE)’ (Custom Products, Big Spring, TX, USA) (Fryrear, 1986) were used to collect eroded wind-blown material. As

described in Table 6.1, six BSNE's with eight collectors were used at EN-SP3 (Figure 6.1A), while one BSNE with 5 collectors was used at EF-DA (Figure 6.1C). Wind speed was measured at the sites along with biometerological data which was recorded at the co-located EC towers and at EN-SP3, by three additional Sonic Towers (Table 6.1).

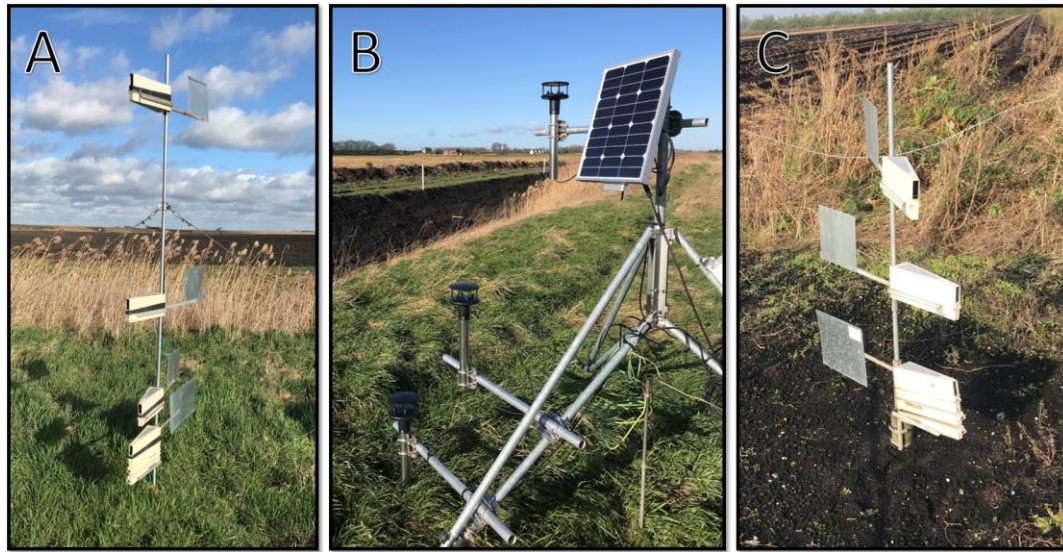


Figure 6.1. A. Example BSNE array from EN-SP3. B. Example sonic tower from EN-SP3. C. BSNE array at EF-DA.

BSNE 5 and 6 were located on the upwind field boundary to measure the soil transported onto the field, the rest were located on the downwind boundary to measure soil loss from the field. The vegetation type and height of the downwind field boundary changed along the NE field edge (see Table 6.2 for a full description). To capture any difference the field boundary caused in erosion, BSNEs were placed at 200 m points along the field edge. Sonic towers were situated between BSNE 1 & 2 and 3 & 4 to assess whether the impacts of the changing field boundary impacted the wind speeds (Figure 6.2).

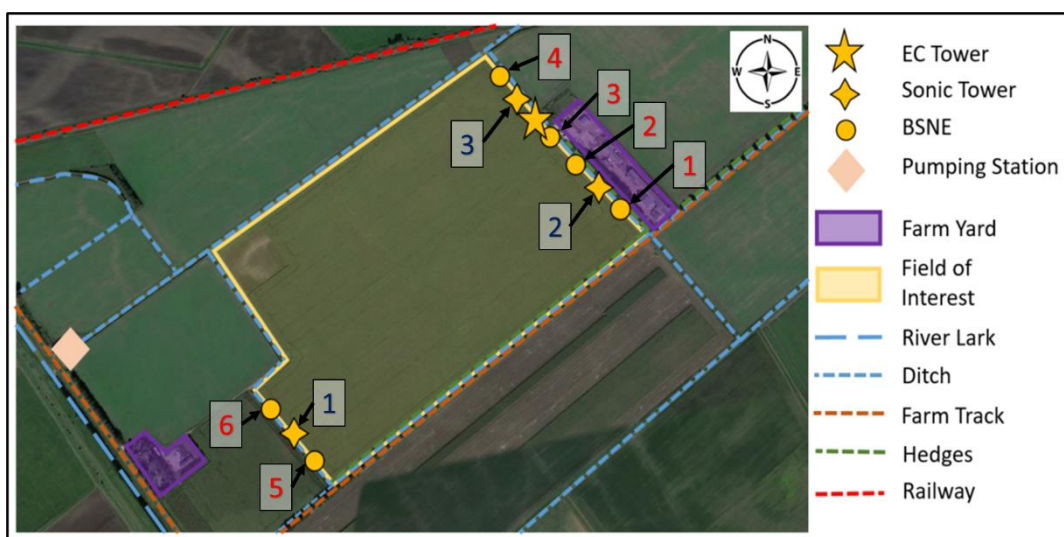


Figure 6.2. Map of the Spooners 3 field within Engine Farm, EN-SP3. BSNE dust collector IDs are indicated by the red numbers, Sonic Tower IDs are indicated by the blue numbers. BSNE's were situated at ~200 m intervals along the field boundaries with a sonic array between BSNE 1 and 2, 3 and 4 and 5 and 6 giving 3 sets of 2 BSNE's and 1 sonic tower. BSNE Satellite image provided by Google Maps 2019.

Table 6.2. Field boundary descriptions for each BSNE and sonic tower.

BSNE and sonic tower number	Field Boundary Description
<b>EN-SP3</b>	
BSNE 1 & 2 and sonic tower 2	NE field edge, typically downwind. Field boundary ~5 m wide in front of a ~5 m wide ditch. Boundary vegetation consists primarily of ~1.8 m sedge. On the other side of the ditch are mature poplar trees 20–25 m in height behind which is the main farm yard.
BSNE 3	NE field edge, typically downwind. Field boundary ~5 m wide in front of a ~5 m wide ditch. Boundary vegetation consists of primarily grass which grew to ~0.5 m in the summer and with sporadic agricultural weeds (nettles, thistle etc.) which grew to heights between 0.8 m and 1.5 m in the summer months. On the other side of the ditch is the main farm yard with machinery often parked alongside the ditch edge.
BSNE 4 and sonic tower 3	NE field edge, typically downwind. Field boundary ~5 m wide in front of a ~5 m wide ditch. Boundary vegetation consists of primarily grass which grew to ~0.5 m in the summer and with sporadic agricultural weeds (nettles, thistle etc) which grew to heights between 0.8 m and 1.5 m in the summer months. On the other side of the ditch is a field under similar management to Spooners 3.
BSNE 5	SW field edge, typically upwind. Field boundary ~5 m wide in front of a ~5 m wide ditch. Boundary vegetation consists of primarily of ~1.8 m sedge and grass. On the other side of the ditch was a field under similar management to Spooners 3. The ditch underwent work to clear it of debris and sediment which was piled on the far side of the ditch to a height of ~1.5 m during data collection.
BSNE 6 and sonic tower 1	SW fields edge, typically upwind. Field boundary ~5 m wide in front of a ~5 m wide ditch. Boundary vegetation consists of primarily grass which grew to ~0.5 m in the summer and with sporadic agricultural weeds (nettles, thistle etc) which grew to heights between 0.8 m and 1.5 m in the summer months. The ditch underwent work to clear it of debris and sediment which was piled on the far side of the ditch to a height of ~1.5 m during data collection.
<b>EF-DA</b>	
BSNE	NE field edge, typically downwind. Located on the NE field boundary, 10 m NW of the EC tower. Field boundary (3 m wide) only present around BSNE and EC tower site were field had been left unmanaged around instrumentation. Boundary is ~3 m wide in front of a ~3 m wide ditch which within which bulrush grew. The field boundary grew a mixture of agricultural weeds (nettles, chickweed, groundsel) that were regularly removed and sprayed to keep field edge bare, rarely growing above 0.3 m before removal.

At EF-DA, aeolian erosion was quantified using a BSNE situated 5 m NW from the co-located EC tower used to record wind speed and soil data (Figure 6.3). This site is a continuation of the data collected from BSNE 'A' mentioned in Cumming (2018). A description of the field boudry is provided in Table 6.2.

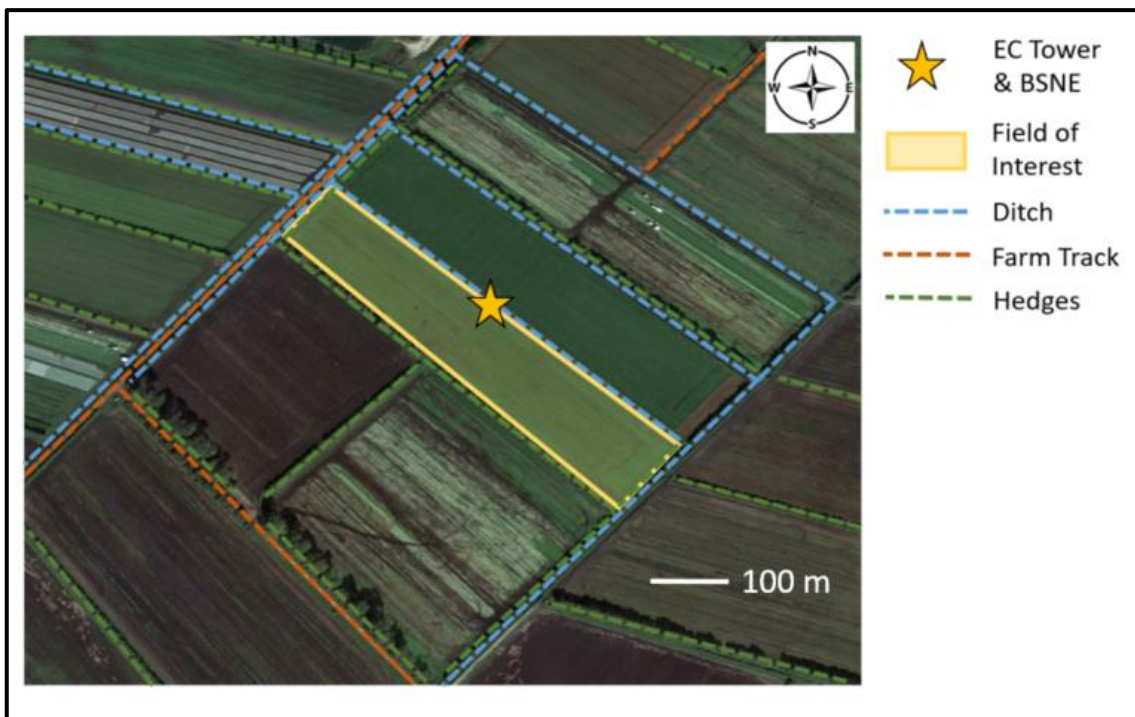


Figure 6.3. Map of field R39 situated within Rosedene farm, EF-DA. BSNE Satellite image provided by Google Maps, 2019.

BSNE passive dust samplers were chosen due to their ease of use. They require minimal maintenance compared to active samplers which require a constant power source. This is coupled with their comparative sampling efficiency compared to more sophisticated active sampling systems (Shao et al., 1993, Goossens et al., 2000).

While BSNEs are known to underestimate the fine sediment fraction (<100 µm), with sampling efficiencies of around 40 % for particles less than 10 µm (Shao et al., 1993, Goossens et al., 2000) and to reduce sampling efficiency at higher wind speeds (Goossens et al., 2000), BSNE samplers have been found to produce representative HMF totals (Goossens and Buck, 2012) with sampling efficiencies of around 90% (Fryrear, 1986, Shao et al., 1993) or better (Goossens et al., 2000). Only one study has quantified BSNE efficiency on peat soils; Warburton (2003) found BSNE's provided sampling efficiencies of between 70 and 120%. Sampling efficiency was not calculated as part of this thesis, so whilst the error is unknown, it likely falls within a similar range to that of Warburton (2003).

Choice of BSNE heights was based on Panebianco et al. (2010), who suggested that a three sampling arrangement of 0.13 m, 0.5 m and 1.5 m above the ground surface could produce acceptable estimates of mass transport. Panebianco et al. (2010) also identified that, while three sampling heights was sufficient, it generally produced lower HMF estimates compared to nine sampling heights which provide a more accurate representation of HMF. The sampling arrays at

EN-SP3 attempted to balance the desire for increased HMF resolution with the practicalities of data collection and processing.

### 6.2.3 Raw Data Collection and Processing

Where possible, dust was collected monthly from the collectors. For each site, all dust collectors were emptied on the same day. Each collector was triple rinsed with distilled water into an individual 250 ml polypropylene bottle for transport to the University of Leicester. A stiff brush was used to agitate the dust to ensure that all dust was removed from the inside of the collector. Occasionally, small insects or vegetation would accumulate within the collectors, which were removed manually before drying.

Bottles were emptied and triple rinsed with distilled water into aluminium foil trays which had been pre-weighed on an analytical balance (OHAUS Adventurer, Parsippany, New Jersey, USA). The trays were dried at 105 °C until at constant weight before being re-weighed. Tray weight was then subtracted leaving the dust weight.

Whilst excess rainwater was able to leave the collectors through the 60 µm mesh side panels, rainwater would often be found in the bottom of the collectors and was collected with the sample. To test for any impact on drying weight, in 2019 rainwater was collected at Engine Farm in a 2 L polypropylene container. After being passed through grade 1 Whatman filter paper, 3 x 300 ml was dried within foil trays and found to add negligible (<0.01 g) weight to the trays.

Data was collected largely without interruption between 22/06/2017 and 03/04/2020 at Rosedene (EF-DA) and from 18/07/2019 to 03/04/2020 at Engine Farm (EN-SP3, Figure 6.4). The aeolian erosion data set reported within this thesis for EF-DA is a continuation of the data set collected by Cumming (2018); only the new dust data are reported here.

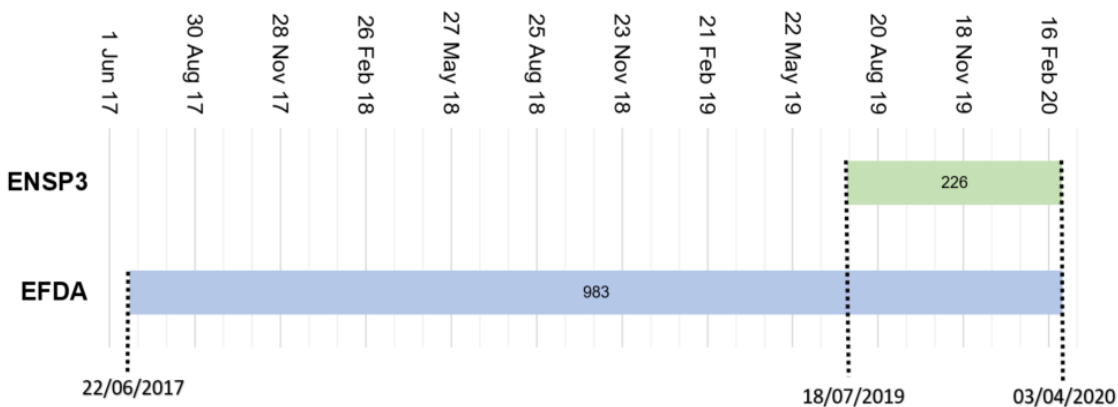


Figure 6.4. Data collection periods for EN-SP3 and EF-DA.

#### 6.2.4 Horizontal Mass Flux (HMF) and Horizontal Mass Transfer (HMT) calculation

Horizontal Mass Flux (HMF) is defined as the mass passing through an area, usually over a period of time (Panebianco et al., 2010). This is expressed by the equation:

$$q \text{ (g m}^{-2}\text{)} = m(g)/a(m^2) \quad \text{Equation 6.1}$$

where 'q' is HMF, 'm' is the mass in grams of sediment measured within the collector and 'a' is the area of the inlet. Initially, HMF is expressed over the time period (number of days) that the sediment was collected over to the nearest day. Sediment was collected at approximately 28 day intervals, however the exact number of days between collections varied. HMF for each array can then be calculated by summing the HMF of each collector within the array.

Typically, values are then expressed per day ( $d^{-1}$ ) dividing HMF over the days it was collected. HMF values can also be added along with the time period they were collected for to create a HMF over a longer time period. This is often done to allow HMF to be expressed as a yearly value ( $yr^{-1}$ ).

Horizontal Mass Transport (HMT) is the integration of the mass passing through a horizontal plane between two defined heights. This is used to more accurately ascertain the approximate mass transport occurring across the entire field boundary between the heights of the lowest and highest collector in the BSNE array. HMT (Q) is calculated, through linearly interpolating HMF between the collection heights and integrating over the vertical profile between the two heights:

$$Q = \int_{zb}^{zt} q \text{ (g m}^{-2}\text{)} \quad \text{Equation 6.2}$$

This is done between each BSNE height in the array before being summed to find the total HMT across the entire array. This provided the HMT across the field boundaries between 0.15 and 2 m at EN-SP3 and 0.15 to 1 m at EF-DA.

This has been shown to be a robust method for estimating HMT (Cumming, 2018, Panebianco et al., 2010) when compared to more complex exponential models. HMT was calculated for all BSNE arrays at all sites. HMT was only calculated between the lowest and highest dust measurement heights due to high inaccuracies when attempting to interpolate to ground level and the difficulty of obtaining measurements below 0.15 m (Panebianco et al., 2010). This means that there will be an underestimation of HMT overall, especially as erosion is seen to increase and is typically considered to be maximal closer to the ground (Dong and Qian, 2007, Panebianco et al., 2010, Mendez et al., 2011). Dust can also be transported at heights above 2 m, but at this

height it is often considered to be negligible in terms of volume due to its small particle size and therefore is not included in flux accounting (Panebianco et al., 2010, Dong and Qian, 2007).

## 6.3 Results

### 6.3.1 Engine Farm, EN-SP3

#### 6.3.1.1 *Environmental Conditions*

Environmental conditions were measured continuously at the Engine Farm flux tower. Additionally, SWC was measured at Sonic Tower 1 (from period 4) and Sonic Tower 3 (from period 7). Environmental data is presented in relation to the dust collection period it represents. Samples were collected regularly with an average period of 26 days (ranging from 35 days for period 5 to 20 days for period 6).

##### 6.3.1.1.1 Wind

The three sonic anemometer arrays showed similar patterns in wind direction, with the wind coming primarily from the SW for most data collection periods. The exception to this was period 4, which indicated a larger spread of wind directions, particularly from the East, and North East (Figure 6.5).

As expected, wind speeds varied with height above the ground surface, with the highest wind speeds measured at 2 m and the lowest at 0.5 m (Figure 6.5). Typically, the highest mean average wind speeds were found at sonic tower 3, which was the most exposed sonic tower on the site. The downwind sonic tower 1 and sonic tower 3 recorded similar wind speeds across all the data periods. Sonic tower 2 was found to give consistently lower wind speed readings, and to have a more erratic wind profile than both towers 1 and 3 (Figure 6.5).

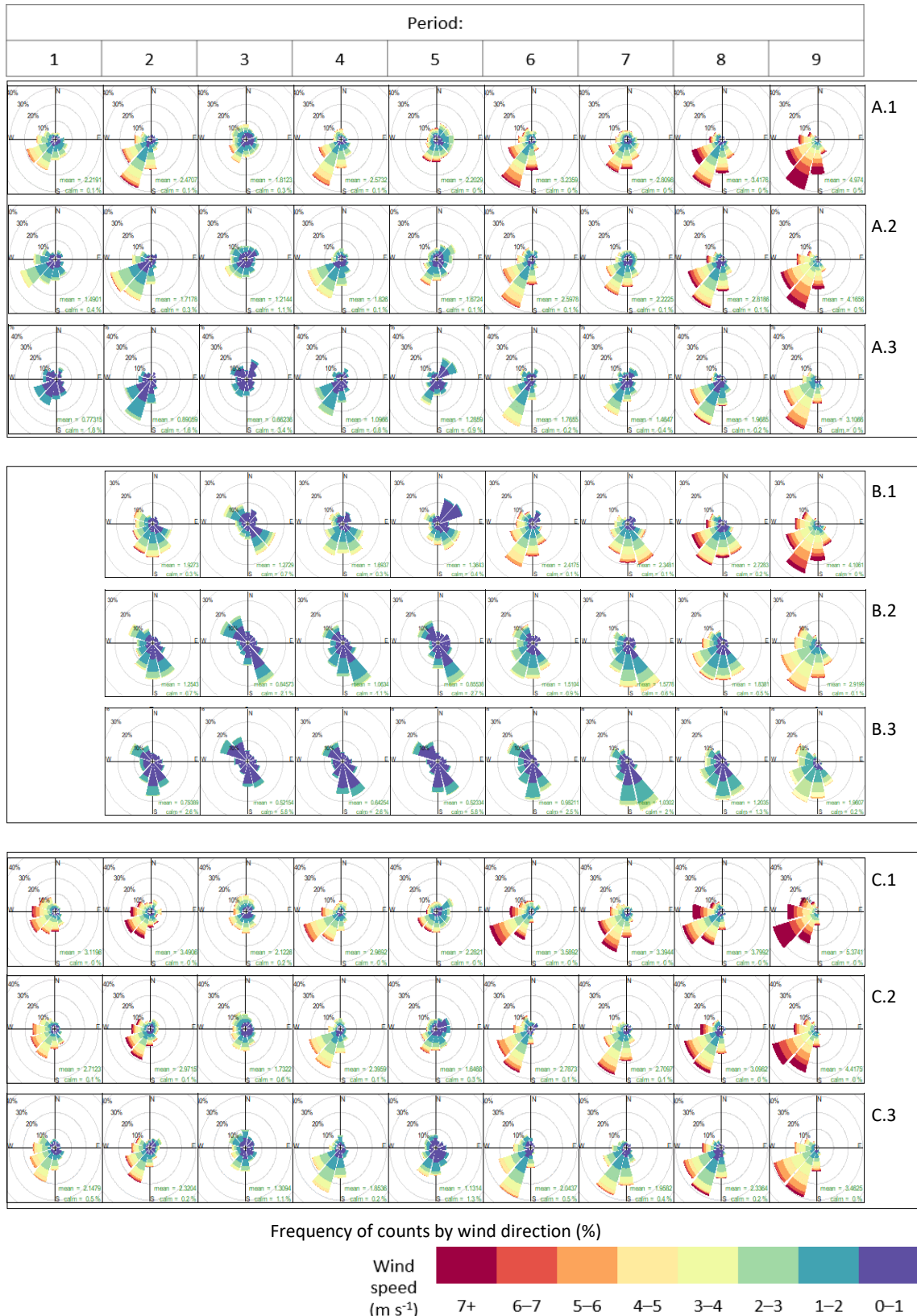


Figure 6.5. Rose plots of wind speed ( $m s^{-1}$ ) and direction recorded by each sonic tower (A: sonic tower 1, B: sonic tower 2, C: sonic tower 3) for each sonic anemometer (1: 2 m, 2: 1 m, 3, 0.5 m) over each data collection periods. Wind speed was measured in 1 minute averaging periods.

#### 6.3.1.1.2 Air and Soil Temperatures

Average soil and air temperatures were similar over the data collection period (18th July 2019 to 4th March 2020). Soil temperature min and max values showed a smaller range and never dropping below 0 (Figure 6.6). Unusually, period 7 coincided with a warmer than average December in 2019, with no frost seen between 17/12/19 and 15/05/20 (Figure 6.6). Overall, winter 2019/2020 was the fifth mildest since 1884 and the fifth wettest since 1862 (UK Met Office, 2020).

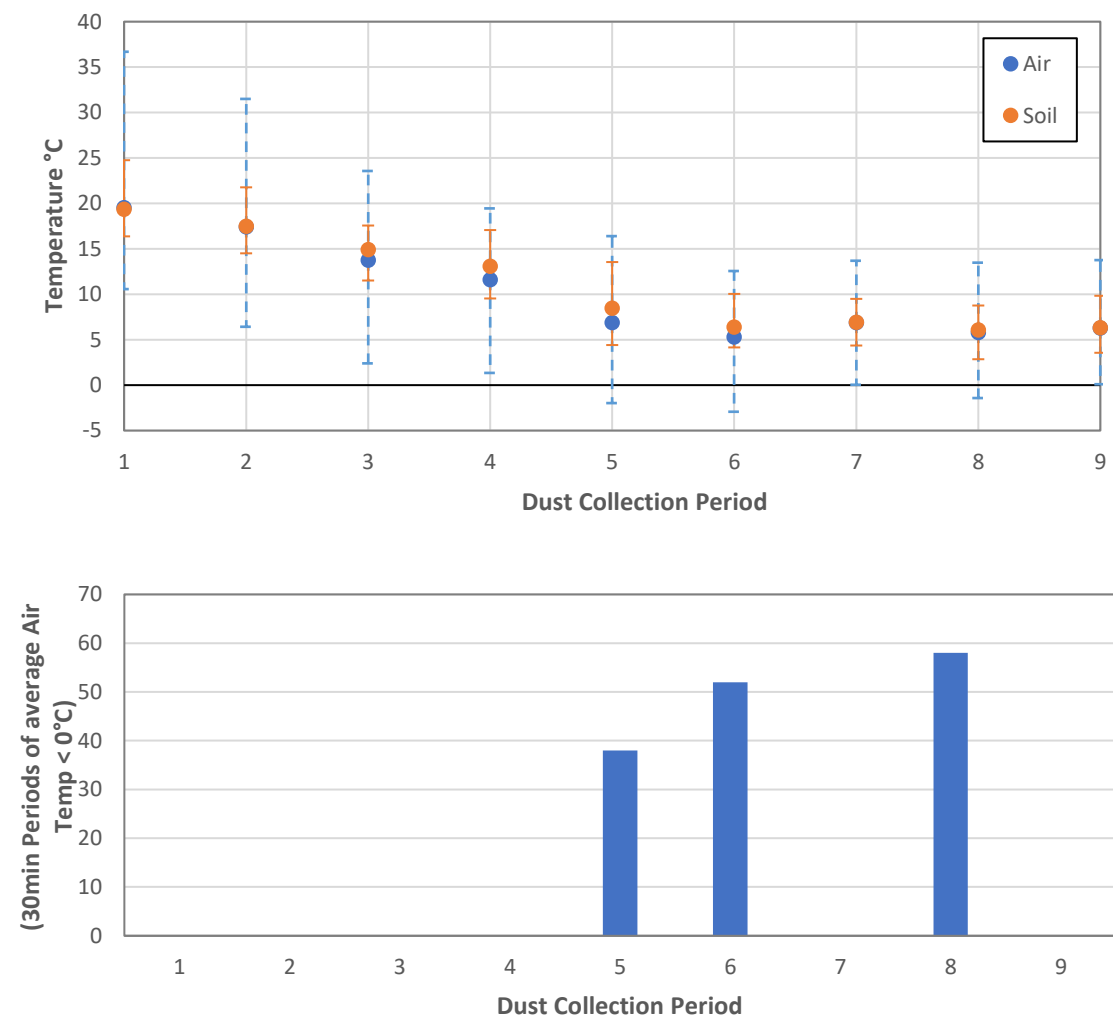


Figure 6.6. Top: Air and Soil temperature over the 9 dust collection periods. Minimum and maximum temperatures recorded over this period are indicated by the error bars. Bottom: Number of 30 min periods which showed an average air temperature of <0 °C indicating a surface frost.

#### 6.3.1.1.3 Rainfall and Soil Water Content

Over the course of the data collection period, Soil Water Content (SWC) was measured at sonic tower 1 and at sonic tower 3 (Figure 6.7). Gaps in data are due to the SWC sensors being installed after the BSNE and sonic towers. SWC steadily increased from mid-September to March before levelling out at 55% and 50% for the upwind and downwind sensors, respectively. Rainfall was

consistent throughout the winter, which included the wettest February on record (UK Met Office, 2020). The upwind side of the field was found to always have a higher SWC than the downwind side.

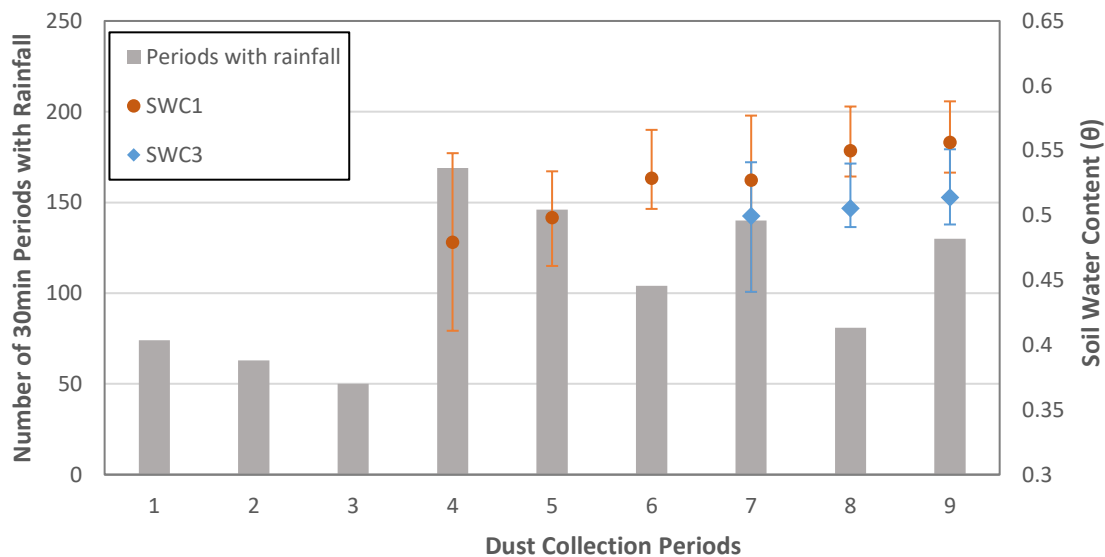


Figure 6.7 Average Soil Water Content ( $\theta$ ) at EN-SP3 over each Dust Collection Period, on the upwind side of the field (measured at sonic tower 1) and downwind side of the field (measured at sonic tower 3). Error bars denote the minimum and maximum SWC measured. Gray bars indicate the number of 30 min periods with recorded rainfall for each dust collection period.

#### 6.3.1.2 Field Conditions

Throughout the data collection period the field was covered by three separate crops (dates for each crop are indicated on Figure 6.8). The primary crop was celery (*Apium graveolens*) that was planted across the field from the upwind side (SE field edge) to the downwind side (NE field edge) over a three week period (Figure 6.8). This produced a lag time in crop height and harvest date across the field. Additional to this, a wildlife strip of Common Millet (*Panicum miliaceum*) was planted on the SW half of the NE field edge in early July (Figure 6.8), while a Phacelia (*Phacelia tanacetifolia*) and Buckwheat (*Fagopyrum esculentum*) cover crop that had previously been planted across the whole field (and was disked into the surface immediately prior to celery planting) was left to grow on the NE half of the NE field edge (Figure 6.8). Due to the top layer of the field being saturated and unworkable by farm machinery until 10<sup>th</sup> March 2020, crop residue was left on the field, leaving sporadic celery growth in the former crop strips where individual plants had been missed during harvesting. Due to the warm winter, the cover strip did not completely die off during December and January, starting to regrow in February. The millet strip was completely dead from December onwards, however, stalks remained on the field and at a significant height. For further detail of field conditions, please see Chapter 3.1.2.1.

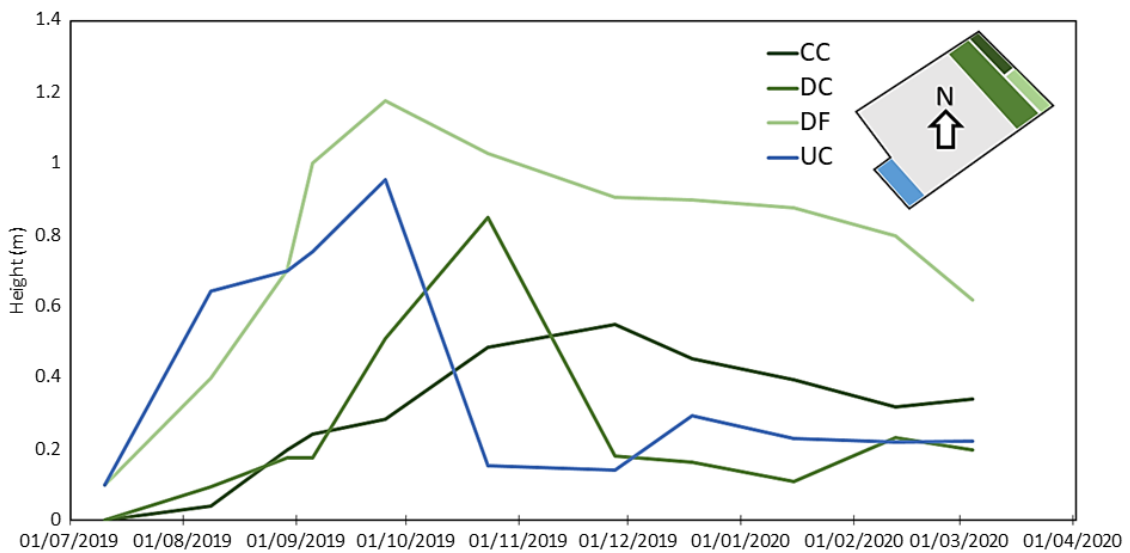


Figure 6.8. Crop growth on the field Engine SP3 whilst BSNEs were present on the field. CC: Cover Crop (dark green), DC: Downwind Celery (green), DF: Downwind Feeder Strip of Common Millet (light green), UC: Upwind Cover crop (Blue). Locations of crop measurements are indicated on the map. Whilst celery was present across the whole field other than the feeder strip and cover strip, it was planted in strips across the field.

#### 6.3.1.3 Horizontal Mass Flux

In general, more dust was collected in the upwind BSNE arrays than the downwind arrays (Table 6.3). The highest amount of total dust (4.723 g) was collected in the upwind array 6 and the lowest amount in the downwind array 1 (3.109 g). The period with greatest dust movement varied depending on the array and which part of the field they were situated on (Table 6.3). Overall HMF average was lowest for arrays 1 and 2 (Figure 6.9). Arrays 3, 4, 5 and 6 saw a similar average throughout the entire data collection period, despite being on opposite sides of the field. Overall, upwind collectors collected an average of  $0.020 \text{ g d}^{-1}$  whilst the downwind collectors collected  $0.017 \text{ g d}^{-1}$  suggesting that more dust was blown onto than off the field.

Table 6.3. Yearly, highest, lowest and overall average HMF ( $\text{g d}^{-1}$ ) from each individual array from EN-SP3. Colours indicate location on the field: blue indicates upwind arrays (BSNE 5 and 6, Sonic 1) while orange denotes downwind arrays, light orange are on the SE field edge (BSNE 1 and 2, Sonic 2) whilst dark orange and on the NE field edge (BSNE 3 and 4, Sonic 3).

BSNE	Total (g)	Highest period ( $\text{g d}^{-1}$ )	Lowest Period ( $\text{g d}^{-1}$ )	Overall average ( $\text{g d}^{-1}$ )
1	3.109	P9 0.019	P7 0.008	0.014
2	3.565	P6 0.020	P7 0.011	0.016
3	4.557	P1 0.032	P5 0.010	0.021
4	3.783	P1 0.025	P8 0.009	0.017
5	4.074	P2 0.029	P8 0.009	0.018
6	4.723	P3 0.034	P8 0.012	0.021

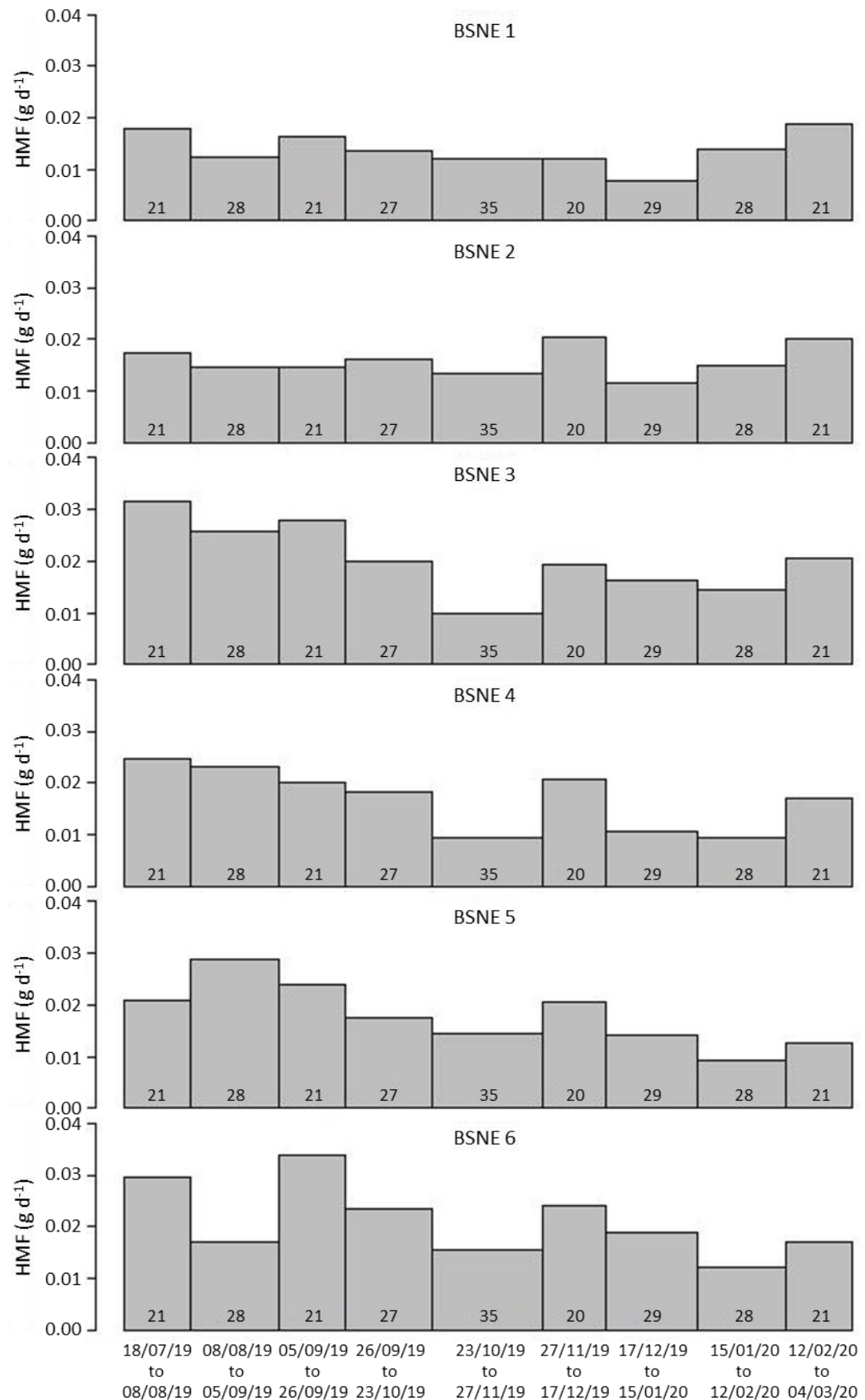


Figure 6.9. Horizontal Mass Flux ( $\text{g d}^{-1}$ ) of dust from EN-SP3. Each bar represents the dust collected across the entire array over the time period. The length (days) of each time period is indicated within the bar. Widths of the bars correspond to the number of days the dust was collected over.

#### 6.3.1.4 Horizontal Mass Transfer

HMT showed very similar trends to HMF, with the upwind collectors showing higher HMT and array 5 showing the highest overall average HMT ( $7.0 \text{ g m}^{-2} \text{ d}^{-1}$ ). The lowest HMT was in downwind arrays 1 and 3 ( $1.3 \text{ g m}^{-2} \text{ d}^{-1}$ ) (Table 6.4). Across the upwind arrays the overall average HMT was  $3.8 \text{ g m}^{-2} \text{ d}^{-1}$ , whilst in the downwind arrays the average HMT was  $2.7 \text{ g m}^{-2} \text{ d}^{-1}$  indicating that over the data collection period, more material was blown onto than off the field (Figure 6.10).

*Table 6.4. Total HMT, highest, lowest and overall average HMT ( $\text{g d}^{-1}$ ) from each individual array from EN-SP3. Colours indicate location on the field: blue indicates upwind arrays (BSNE 5 and 6, Sonic 1) while orange denotes downwind arrays, light orange are on the SE field edge (BSNE 1 and 2, Sonic 2) whilst dark orange and on the NE field edge (BSNE 3 and 4, Sonic 3).*

BSNE	Total HMT ( $\text{g m}^{-2}$ )	Highest period ( $\text{g m}^{-2} \text{ d}^{-1}$ )	Lowest Period ( $\text{g m}^{-2} \text{ d}^{-1}$ )	Overall average ( $\text{g m}^{-2} \text{ d}^{-1}$ )	Yearly Estimate ( $\text{g m}^{-2} \text{ yr}^{-1}$ )
1	531	P9 3.9	P7 1.3	2.3	842
2	561	P9 4.4	P2 1.4	2.4	890
3	777	P1 5.0	P5 1.3	3.4	1233
4	639	P1 4.0	P5 1.7	2.8	1013
5	834	P2 7.0	P8 1.8	3.6	1324
6	931	P6 5.5	P5 3.0	4.0	1477

The daily HMT was extrapolated for the remaining 135 days to provide an estimate for yearly HMT at each collector which followed a similar pattern to the total HMT. It was estimated that 1401 (1324–1477)  $\text{g m}^{-2} \text{ yr}^{-1}$  of soil was blown onto the field through the SW field boundary, whilst 995 (842–1233)  $\text{g m}^{-1} \text{ yr}^{-1}$  was eroded and transported from the field through the NE field boundary (Table 6.4).

Using the HMT and the length of the field boundary, it is possible to calculate the amount of soil that passed through the field boundary between 0.15 and 2 m. Across the SW boundary (321 m length), it is estimated that 0.90 (0.85–0.95)  $\text{t yr}^{-1}$  of sediment is blown onto the field while across the longer NE field boundary (686 m length), it is estimated that 1.4 (1.2–1.7)  $\text{t yr}^{-1}$  of soil is eroded and transported from the field. This equates to a net loss of material from the field of 0.5 (0.35–0.75)  $\text{t yr}^{-1}$ .

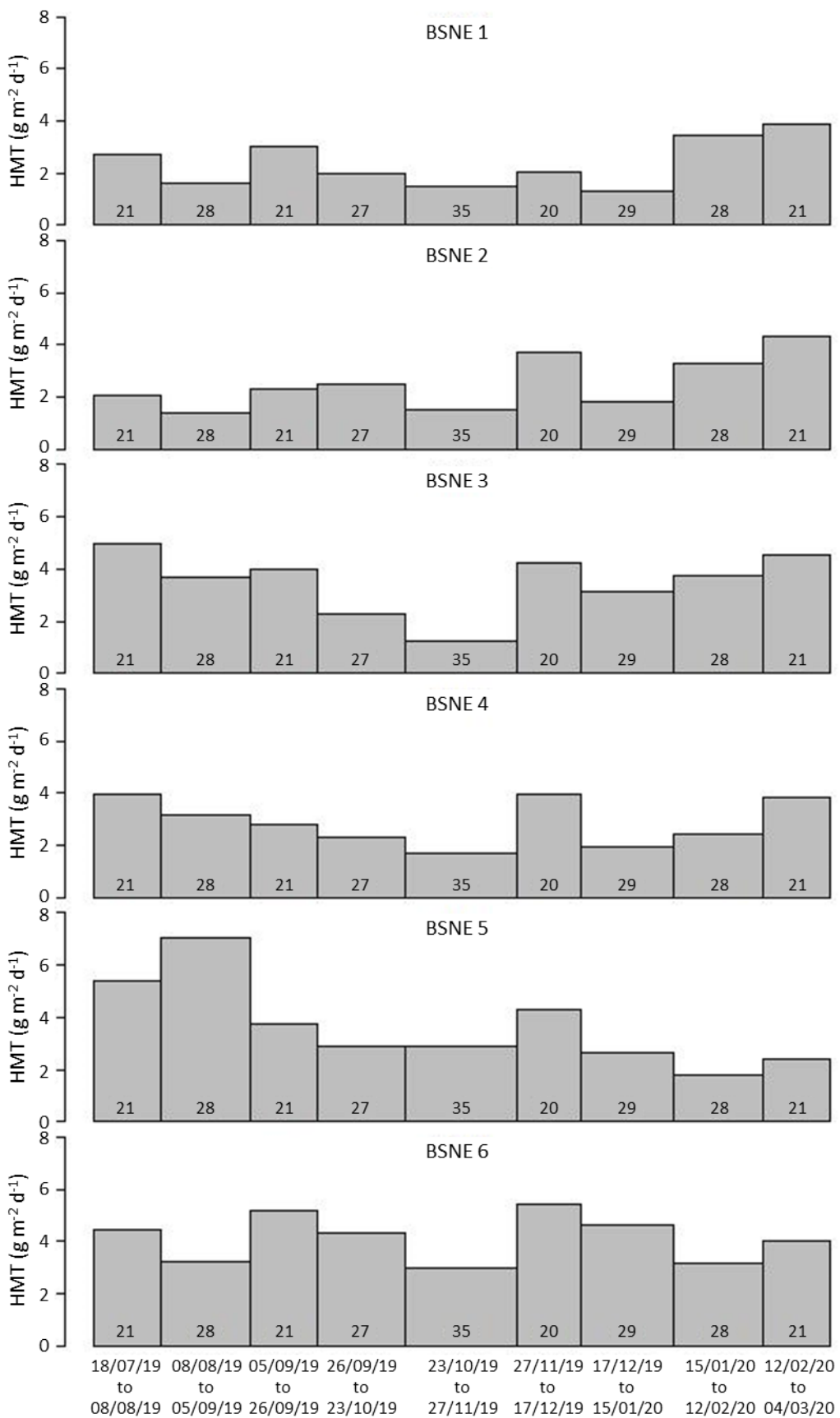


Figure 6.10. Horizontal Mass Transfer ( $\text{g m}^{-2} \text{d}^{-1}$ ) of dust from EN-SP3. Each bar represents the dust collected across the entire array over the time period. The length (days) of each time period is indicated within the bar and corresponds to the bar widths.

### 6.3.2 Rosedene Farm, EF-DA

#### 6.3.2.1 Environmental Conditions

Similar to EN-SP3, environmental conditions were measured continuously throughout the dust data collection period. At Rosedene Farm, environmental data was collected exclusively from the flux tower described in Chapter 3.1.3, situated 10 m SW from the BSNE array. Environmental data is presented in relation to the dust collection period it represents. Regular collection of dust samples from the Rosedene site occurred on average every 28 days. Collection was more irregular prior to the 8<sup>th</sup> collection period with an average length of 44 days for periods 1 to 7 vs. 26 days from period 8 onwards and included the longest period (7) at 99 days long. The shortest periods were 10 and 19, with both 14 days long.

##### 6.3.2.1.1 Wind

Wind direction was predominantly from the S and SW throughout. There were periods of either no dominant wind direction (such as periods 22 and 23) or periods where the predominant wind directions were from the North and East (22, 9 and 18) (Figure 6.11). In 2019 and 2020, higher maximum and average wind speeds occurred in the early spring months (periods 18 to 21 – 07/01/2019 to 10/04/2019 and 30 to 33 – 28/11/2019 to 05/03/2020) and included the highest average wind speed of 4.1 m/s (period 33). Outside of these periods, wind speeds tended to be lower and more consistent.

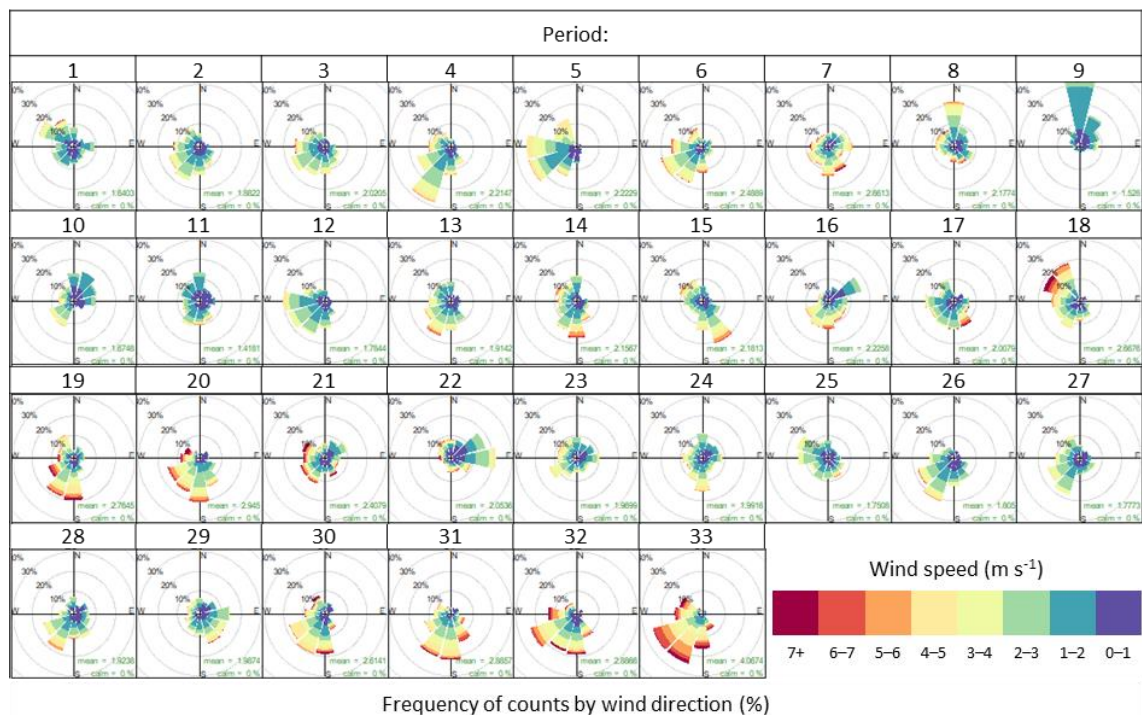


Figure 6.11. Rose plots of wind speed ( $m s^{-1}$ ) and direction recorded for each data collection period recorded from the Csat3 Sonic Anemometer as part of the Rosedene Farm EC tower set up. Wind speed was measured in 30 minute averaging periods.

### 6.3.2.1.2 Air and Soil Temperature

Soil and air temperatures followed a typical seasonal pattern. Period 7 showed the biggest difference between minimum and maximum temperature for soil and air temperatures and the largest number of periods below 0 °C, indicating a potential frost (Figure 6.12). Period 7 was the longest collection period at 99 days long (from 17/01/2018 to 25/04/2018) but also coincided with the ‘beast from the east’ cold wave which occurred in two parts in February and March 2018 (Figure 6.12). Winter 2018/19 was more typical of the long-term average in terms of air temperature; however, numerous late frosts were observed in April (periods 14–22 – 20/09/2019 to 08/05/2020). Comparatively few frost periods occurred in winter 2019/20 (periods 28–33, 03/10/2019 to 05/03/2019), with higher air temperatures indicating a warmer year than the long term average (Figure 6.12).

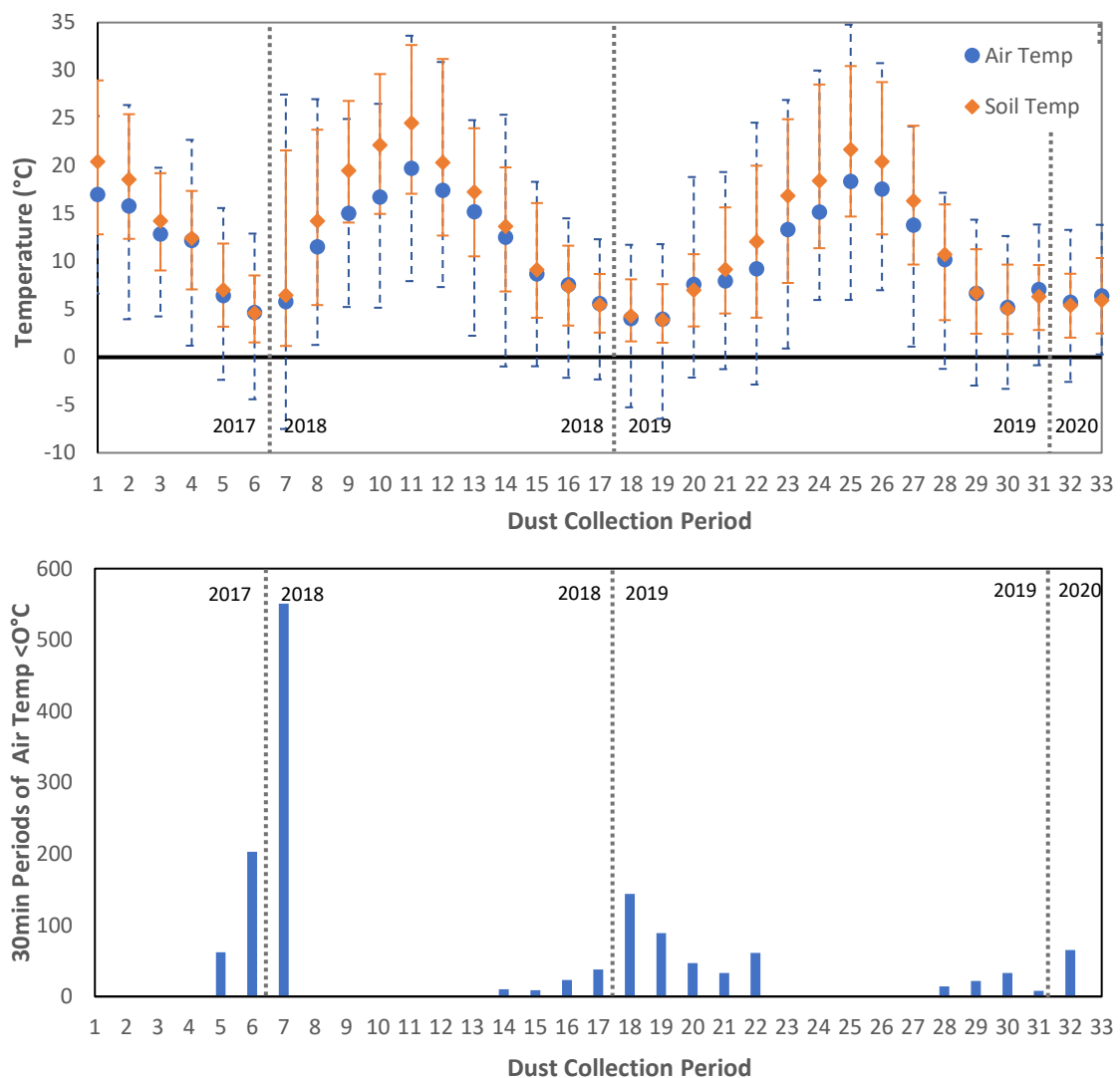


Figure 6.12. **Top:** Air and soil temperature recorded by the Rosedene Flux Tower over the dust data collection period where each point represents the average temperature with error bars indicating the minimum and maximum temperature recorded over the time period. **Bottom:** Number of 30 min averaging periods where air temperature averaged  $< 0^{\circ}\text{C}$ . It should be noted that dust collection periods represent varying lengths of time (see Figure 6.15 for details on period length).

#### 6.3.2.1.3 Rainfall and Soil Water Content

Period 7 had the largest number of rainfall periods, in part due to its increased length. No rainfall was recorded in the 10<sup>th</sup> period of collection, which is also the joint shortest at just 14 days. The large variation in SWC (of up to 33%) within each period was likely due to large individual rainfall events rather than consistent rainfall over the collection period (Figure 6.13). From period 12 onwards, average SWC over the data collection periods remains in the range 45 to 55% with only period 28 showing an increased SWC compared to the periods immediately surrounding it (Figure 6.13).

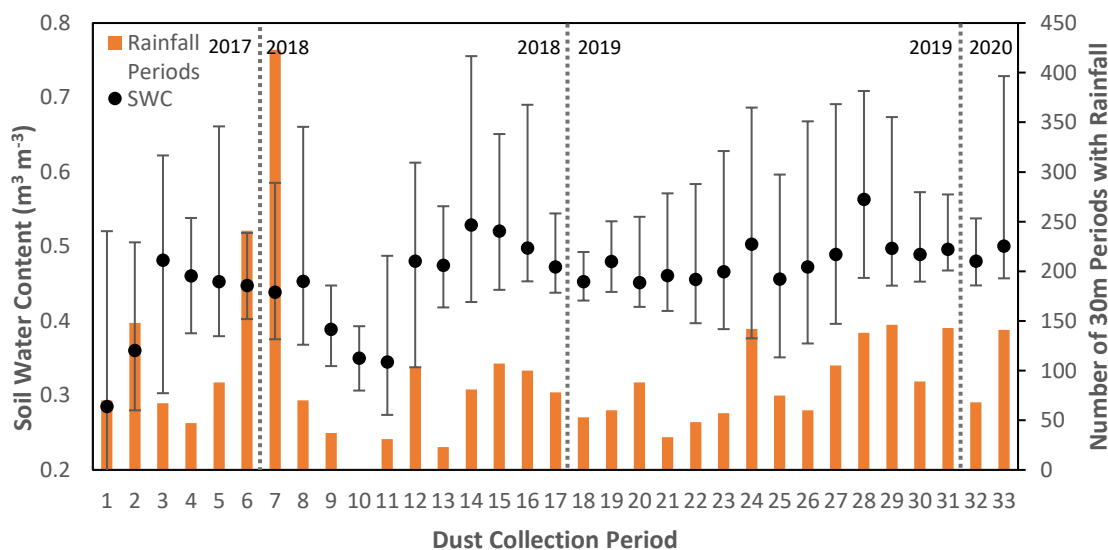


Figure 6.13. Soil Water Content ( $m^3 m^{-3}$ ) average at EF-DA with error bars indicating the minimum and maximum recorded over the period and the number of 30 min averaging periods that recorded rainfall for each of the dust collection periods. It should be noted that dust collection periods represent varying lengths of time (see Figure 6.15 for details on period length).

#### 6.3.2.2 Field Conditions

Between 22/06/2017 to 04/03/2020, three crops were grown on the field: sugar beet was grown in 2017, a lettuce crop in 2018 and a potato crop in 2019. Between crops, the field was ploughed and left fallow allowing weeds to grow when conditions were suitable (for more details see Chapter 3.1.3). Vegetation heights were measured each time dust was collected from the field (Figure 6.14).

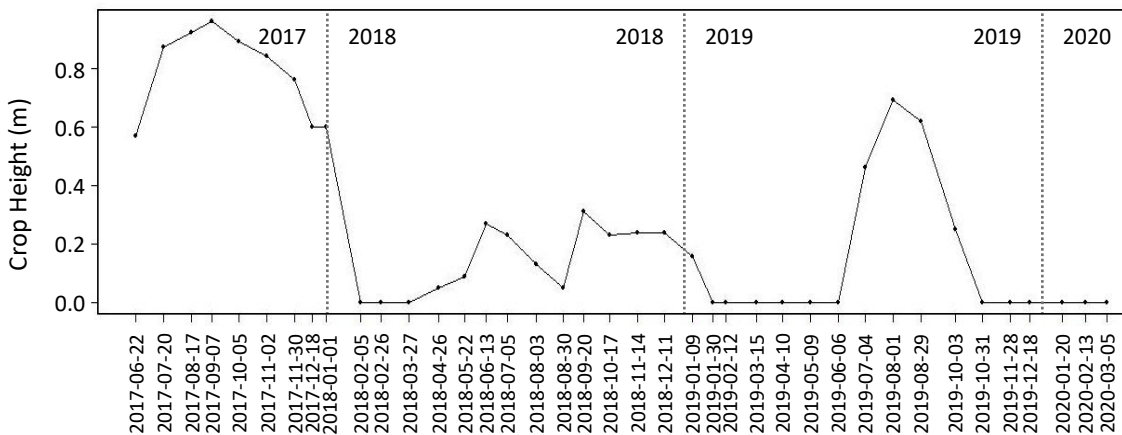


Figure 6.14. Vegetation height from the EF-DA field site from 22/06/17 to 01/03/2020. Each point represents an individual measurement of vegetation height from the field. Lines between points are a linear interpolation.

### 6.3.2.3 Horizontal Mass Flux (HMF) and Horizontal Mass Transfer (HMT)

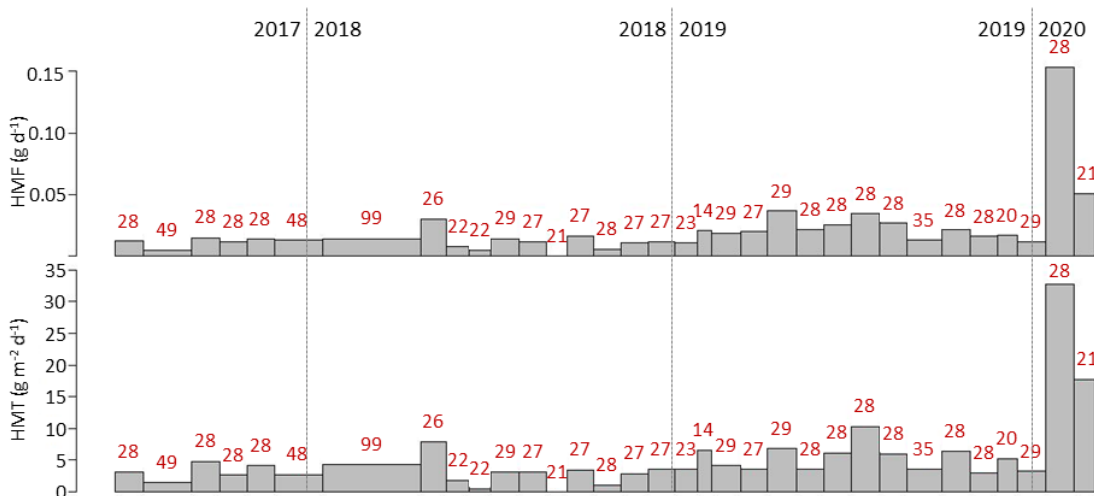
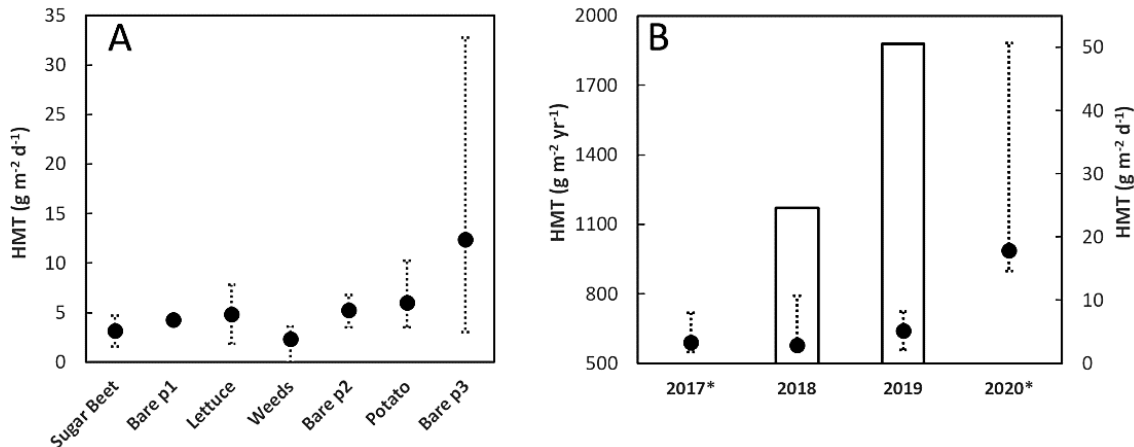


Figure 6.15. Top: Horizontal Mass Flux ( $\text{g d}^{-1}$ ), Bottom: Horizontal Mass Transfer ( $\text{g m}^{-2} \text{d}^{-1}$ ) of dust collected from EF-DA. Each bar represents the dust collected across the entire array over the time period. The width of each bar is proportional to the number of days (indicated above the bar) over which the dust was collected.

Dust was collected from EF-DA between 22/06/2017 and 04/03/2020 over 33 individual periods, including two complete years (2018 and 2019) and three distinct cropping periods (sugar beet, lettuce and potato). The overall average dust erosion was a HMF of  $0.021 \text{ g d}^{-1}$  and an HMT of  $5.3 \text{ g m}^{-2} \text{ d}^{-1}$  (Figure 6.15). Minimum values for HMF and HMT were recorded in period 21, which had no observable erosion. Maximum HMF and HMT values were recorded in period 32 (early 2020) which saw  $0.153 \text{ g d}^{-1}$  HMF and  $32.7 \text{ g m}^{-2} \text{ d}^{-1}$  HMT, closely followed by period 33 which had  $0.051 \text{ g d}^{-1}$  HMF and  $17.7 \text{ g m}^{-2} \text{ d}^{-1}$  HMT.

There were also differences between the years (Figure 6.16). Of the two years with a complete data set, 2018 had an HMT of  $1170 \text{ g m}^{-2} \text{ yr}^{-1}$  ( $2.9 \text{ g m}^{-2} \text{ d}^{-1}$ ), whilst 2019 had an HMT of  $1880 \text{ g m}^{-2} \text{ yr}^{-1}$  ( $5.1 \text{ g m}^{-2} \text{ d}^{-1}$ ). Partial data was collected for 2017 (June–December) and 2020 (January–March). HMT of  $3.3 \text{ g m}^{-2} \text{ d}^{-1}$  was recorded in 2017 and  $17.9 \text{ g m}^{-2} \text{ d}^{-1}$  in 2020 (Figure 6.16). HMT

for 2020 encompassed the two highest periods of HMT (32 and 33) leading to a very high average erosion rate. Overall, when considering complete years of data, there was a loss of  $1.5 \text{ t yr}^{-1}$  in 2018 and  $2.4 \text{ t yr}^{-1}$  in 2019 of material from the field.



*Figure 6.16. A: Average HMT of each different distinct field vegetation (or lack of) period over the data collection period for EF-DA. Error bars indicate the maximum and minimum values of HMT recorded over each cropping period. Due to Bare p1 consisting of a single observation over 90 days, no minimum or maximum is denoted. B: Bars show total HMT ( $\text{g m}^{-2} \text{yr}^{-1}$ ) recorded for years of complete data collection. Points indicate the average HMT ( $\text{g m}^{-2} \text{d}^{-1}$ ) over each individual year over the data collection period. Partial years are denoted by \*.*

## 6.4 Discussion

### 6.4.1 HMF

It has been established previously in the literature that most eroded material is transported within the lowest 0.3 m height above the field surface (Warburton, 2003, Foulds and Warburton, 2007, Panebianco et al., 2010, Cumming, 2018), where saltation of particles is at its highest. This was also observed in this study at both EN-SP3 and EF-DA, with most eroded material collected in the lowest three collectors located between 0 and 0.3 m above the soil surface (Figure 6.17.A).

At EF-DA, an average of 83% of eroded material was collected below 0.3 m. Period 10 was the only outlier, with very little material collected in the 0.15 m collector. This period coincided with the harvesting of lettuce and subsequent weed growth. It is believed that over this period weed growth blocked dust from entering the lowest collectors and that more dust was likely to be blown into the higher collectors due to extensive tractor use throughout the harvesting period which agitated and lofted the dust particles.

A similar distribution was found at Engine Farm (Figure 6.17.B). Across all BSNE arrays, 72% of eroded material was collected in the bottom three collectors at heights of up to 0.3 m above the ground. This is 11% less than the contribution from EF-DA which can mostly be attributed to the additional 2 m collector at EN-SP3 which collected an average of 8.6% of the total HMF. Despite variations in vegetation cover across the field boundaries where the BSNEs were located, the

results do not appear to show an obvious difference in the vertical distribution of eroded material in the collectors.



Figure 6.17. A. Contribution of each collector in the Rosedene Farm BSNE array to the total HMF ( $\text{g m}^{-2}$ ) recorded for each collection period. Period 13 has been left blank due to having no recorded dust collected. B. Contribution of each collector in the Engine Farm BSNE arrays to the total HMF ( $\text{g m}^{-2}$ ) recorded for each collection period.

## 6.4.2 HMT

There have been few studies that have discussed the aeolian erosion of material from peatlands in the UK (Pollard and Millar, 1968, Warburton, 2003, Foulds and Warburton, 2007) and only Cumming (2018) has quantified aeolian erosion from peatlands under agricultural use (EF-DA field site is a continuation of site A used by Cumming (2018)).

### 6.4.2.1 Year Fluxes

The two complete years of data at EF-DA produced erosion rates of 1170 and 1880 g m<sup>-2</sup> yr<sup>-1</sup> in 2018 and 2019 respectively, with 1.5 and 2.4 t yr<sup>-1</sup> of material being transported off of the field in 2018 and 2019. Comparatively, these were higher values than previously recorded by Cumming (2018) between 2013 and 2016 who found erosion rates to be between 230 and 1280 g m<sup>-2</sup> yr<sup>-1</sup>. The higher erosion rate for 2019 was likely due to differences in field cover and cropping during that year compared to previous years.

When the erosion rates are extrapolated over a year (18/07/2019–17/07/2020), EN-SP3 had HMT rates of 1401 (1324–1477) g m<sup>-2</sup> yr<sup>-1</sup> onto the field and 995 (842–1233) g m<sup>-2</sup> yr<sup>-1</sup> off the field. Over a similar length boundary, there would be a net gain of material onto the field of 406 (244–482) g m<sup>-2</sup> yr<sup>-1</sup>. Due to the measured upwind boundary (321 m) being 365 m shorter than the downwind field boundary (868 m), more material was measured being transported off the field 1.4 (1.2–1.7) t yr<sup>-1</sup> than onto the field 0.90 (0.85–0.95) t yr<sup>-1</sup>, despite the higher rate of soil blown onto the field. Whilst it would be possible to calculate the amount of material blown on for the upwind field length, the northern half of the upwind field edge borders a grassed runway strip for light aircraft and a large wildlife strip which is left unmanaged. This is in complete contrast to the measured field edge and thus would not be a representative value.

The overall HMT rates observed at EN-SP3 fall within a similar range to those seen at EF-DA in this and the previous study (Cumming, 2018). Compared to other UK peatland studies, this is higher than the flux of 46–48 g m<sup>-2</sup> yr<sup>-1</sup> measured by Warburton (2003) from an upland blanket bog. Studies on agricultural soils (within the UK and globally) vary with erosion rates, with higher or similar erosion rates found by Wilson and Cooke (1980) of 2000–4400 g m<sup>-2</sup> (single events, UK) and by Fullen (1985) of 600–1000 g m<sup>-2</sup> (single event, UK). Chappell and Warren (2003) used the caesium-137 method to estimate aeolian erosion over a 19 km<sup>2</sup> region of East Anglia. They found fluxes of 3260 g m<sup>-2</sup> yr<sup>-1</sup> into and 3750 g m<sup>-2</sup> yr<sup>-1</sup> out of the study area, higher than the rates seen at either EN-SP3 or EF-DA. Despite this, fluxes roughly balanced at a net loss of soil of 60 g m<sup>-2</sup> yr<sup>-1</sup>, lower than estimated net flux at EN-SP3.

Globally, mineral soil aeolian erosion rates are very variable but are typically less than studies seen in the UK, albeit of the same magnitude: Goossens et al. (2001)  $16 \text{ g m}^{-2} \text{ yr}^{-1}$  (Germany), Chappell and Baldock (2016)  $440 \text{ g m}^{-2} \text{ yr}^{-1}$  (Australia), NRCS (2007)  $470 \text{ g m}^{-2} \text{ yr}^{-1}$  (USA estimation from cropland). It should be noted that these studies are on differing soil types and are conducted primarily on sands or loamy sand, which are thought to be less easily eroded than C rich soils (Chappell et al., 2013b).

#### 6.4.2.2 Time of the year

Time of the year is commonly mentioned both within the literature and as anecdotal evidence from farmers (Pers. Comm. Rob Parker and Martin Hammond) and news reports (BBC News, 2013) as having an effect on peat soil erosion rates, with the Spring months (March, April and May) usually producing the greatest fluxes both in the Fens (Arber, 1946, Cumming, 2018), other peatland (Campbell et al., 2002, Warburton, 2003), and arable sites (Goossens et al., 2001). This time period typically coincides with bare soil in the fields and high winds speeds.

In this study, no correlation was found ( $R_s = -0.24$ ) between HMF data collected over corresponding periods (July 2019–March 2020) at both the EN-SP3 and EF-DA field sites. This suggests that individual field conditions caused by farm and crop management were more important than the time of the year in determining the scale of soil movement.

#### 6.4.2.3 Impacts of Field Management

The lowest recorded erosion rate was  $0 \text{ kg m}^{-2} \text{ d}^{-1}$  HMT at EF-DA over period 13 (30/08/2018–20/09/2028). This coincided with dense weed growth after a partially failed lettuce crop was left on the field (pers. comm. Martin Hammond) and warm, calm summer weather conditions, which are known to cause a reduction in erosion (Campbell et al., 2002, Zobeck et al., 2003, Funk and Engel, 2015).

The differences in erosion between the cropped and bare periods at EF-DA were similar to those seen by Funk and Engel (2015) who found that a 40% cover by sugar beet and maize was enough to protect the field surface from substantial erosion. This is in line with the results for the sugar beet and weed dominated periods in this study (Figure 6.16.A). However, at EF-DA, several periods of cropping showed similar or increased rates of erosion compared to bare periods. For the lettuce crop, the sparse initial field cover provided by this crop is likely to have increased erosion. This result is similar to that obtained by Funk and Engel (2015) who found maize initially exacerbated erosion compared to a bare plot. In 2019, a potato crop grew to provide almost continuous cover, but since potatoes are planted in bare ridges, erosion was high until the potato plants were well established and covered the soil surface. The impacts of these ridges

were studied by Funk and Engel (2015) within a wind tunnel, who showed they increased erosion depending on orientation. These factors contributed to the large range of erosion rates observed during the potato crop (HMT:  $3.5\text{--}10.3 \text{ g m}^{-2} \text{ d}^{-1}$ ), with high rates seen when it was first planted compared to low rates once it was well established.

The highest erosion was recorded from EF-DA in periods 32 ( $32.7 \text{ g m}^{-2} \text{ d}^{-1}$ ) and 33 ( $17.7 \text{ g m}^{-2} \text{ d}^{-1}$ ), i.e., between 16<sup>th</sup> January 2020 and 5<sup>th</sup> March 2020. This corresponded with a period when the field was left bare after tillage, and supports the results of Goossens et al. (2001) who also observed high erosion rates over winter. The period after tillage also left the field more susceptible to erosion, due to the breaking up of soil aggregates (Li et al., 2014) which then also coincided with three winter storms; Ciara (4<sup>th</sup>–12<sup>th</sup> February), Dennis (12<sup>th</sup>–20<sup>th</sup> February) and Jorge (25<sup>th</sup> February–5<sup>th</sup> March), which exacerbated erosion. During this time, the highest average recorded wind speeds for any data collection period were recorded ( $2.8 \text{ m s}^{-1}$  and  $4.0 \text{ m s}^{-1}$ ), coming almost exclusively from the SW (Figure 6.11). Periods of large flux were seen previously on EF-DA by Cumming (2018), who saw peak flux of  $25 \text{ g m}^{-2} \text{ d}^{-1}$  over a 24 day period. It has been shown that large flux events are common, (Radley and Simms, 1967, Wilson and Cooke, 1980, Van Pelt et al., 2004), particularly on arable soils where periods in which the fields are bare coincide with high wind speeds. This can cause a large singular flux event that can characterise the entire collection period.

Despite similar wind speeds found at EN-SP3, individual arrays recorded different peak HMT flux rates at different times (Table 6.4). The overall peak HMT at Engine Farm was  $7.0 \text{ g m}^{-2} \text{ d}^{-1}$  found at upwind array 5 between 8<sup>th</sup> August and 5<sup>th</sup> September 2019. This was during a period of erratic wind direction measure by the nearby sonic tower (Figure 6.10, A.1, and Period 5), where the wind direction alternated from being from the S and SW to the NE and E. This meant that the wind spent equal time coming from off of the field and over the field boundary, allowing sediment from the field to be collected. This likely lead to the increase in HMT over this time period as wind speeds in period 5 ( $1.3, 1.7$  and  $2.2 \text{ m s}^{-1}$  at  $0.5, 1$  and  $2 \text{ m}$  respectively) were almost half those seen at their peak in period 9 ( $3.1, 4.2$  and  $5.0 \text{ m s}^{-1}$  at  $0.5, 1$  and  $2 \text{ m}$  respectively).

#### 6.4.2.4 Impacts of boundary vegetation height on aeolian erosion

To examine the impacts of the height of vegetation within the field boundaries on aeolian erosion, the NE boundary was divided into two sections based on the height of the boundary vegetation. The northern half of the field boundary has low vegetation (LowVeg) heights typically around  $0.2 \text{ m}$  in the winter when the grass is cut, up to  $1.8 \text{ m}$  high sporadic weeds in

summer in front of a ditch, behind which is an open field (BSNE 4) and farmyard (BSNE 3). The southern half of the boundary has high vegetation (HighVeg), characterised by a sedge verge that is cut once a year in the autumn that grows to a height of 1.8 m in summer in front of a ~5 m wide ditch that's bordered by a dense patch of mature poplar trees 20–25 m high (Table 6.2 for more information on field boundaries). It was hypothesised that the impact of having tall downwind field boundary vegetation would cause lifting of the air moving over the field boundary, leading to lower wind speeds and consequently less soil erosion.

Lower wind speeds were recorded on the HighVeg field boundary compared to LowVeg (Table 6.5), particularly below the 0.5 m level where over 72% of eroded material is transported. This translated into a clear difference in the erosion observed at the two field boundaries, with HMT across the HighVeg boundary ( $866 \text{ g m}^{-2} \text{ yr}^{-1}$ ), 257 g  $\text{m}^{-2}$  lower than across the LowVeg ( $1123 \text{ g m}^{-2} \text{ yr}^{-1}$ ). Yearly, this would lead to a difference of  $0.18 \text{ t yr}^{-1}$  more sediment eroded and transported through the LowVeg field boundary ( $0.77 \text{ t yr}^{-1}$ ) compared to the HighVeg ( $0.59 \text{ t yr}^{-1}$ ) (Table 6.5). Overall, these findings indicate that the presence of tall vegetation within the downwind field boundary reduced wind speeds at ground level and consequently the erosion of the field surface.

*Table 6.5. HMT at BSNEs 1, 2, 3 and 4 and average wind speed for sonic towers 2 and 3 over the study period. Table is colour coded by field boundary: Blue, the high vegetation southern part of the eastern field boundary; Green the low vegetation Veg northern part. Estimated amount of sediment eroded across each half of the field boundary is presented.*

Field Boundary	High Vegetation (HighVeg)		Low Vegetation (LowVeg)	
BSNE	BSNE 1	BSNE 2	BSNE 3	BSNE 4
HMT ( $\text{g m}^{-2} \text{ yr}^{-1}$ )	842	890	1233	1013
Average HMT ( $\text{g m}^{-2} \text{ yr}^{-1}$ )	866		1123	
Sediment Eroded ( $\text{t yr}^{-1}$ )	0.59		0.77	
Sonic Tower	Sonic Tower 2		Sonic Tower 3	
Average Wind Speed at 2.0, 1.0 and 0.5 m.	2.2		3.3	
	1.4		2.7	
	0.9		2.1	

#### 6.4.2.5 The Impact of Frosts and Rainfall on Erosion

It had been hypothesised by Arber (1946) that severe winter frosts were a likely factor in contributing to the severe peat blows of spring 1929 through breaking up the soil surface and predisposing it to blows. Warburton (2003), when examining aeolian erosion from an upland blanket peat, found that most dust flux was caused by rain-splash, with precipitation as a key driver of erosion. To examine the impacts of frost and rainfall on erosion, the data from EF-DA was chosen due to its long timescale which included a wide range of weather conditions spanning multiple winters.

The impact of frosts does not appear to be apparent within the EF-DA data set. Whilst there were frosts in each of the preceding years, contrary to what was suggested by Arber (1946), no correlation was observed between the number of 30 min periods with an air temperature of  $< 0^{\circ}$  and the HMT (Figure 6.18 A). Additionally, winter and spring 2020 had the fewest frost periods yet exhibited the highest amount of dust flux. Conversely, 2017 saw the lowest spring fluxes after the winter with the highest number of frost periods. Similarly, no relationship was found between HMT and either rainfall or SWC (Figure 6.18 B and C).

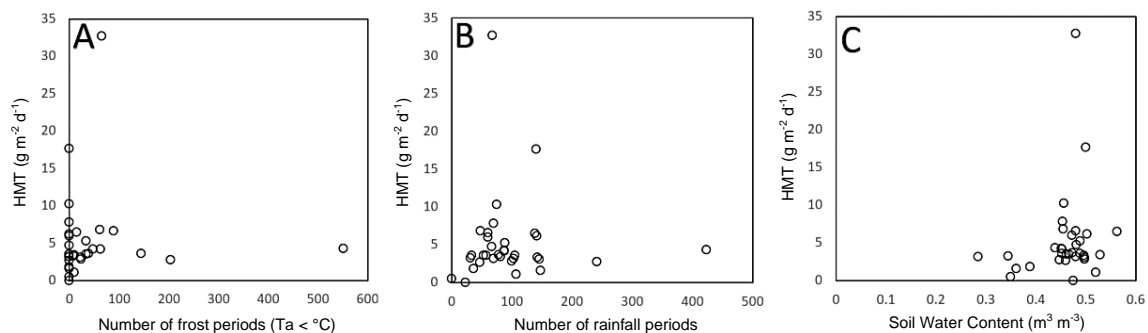


Figure 6.18. The HMT and A: The number of frost periods, B: rainfall periods, C: soil water content each dust collection period.

Overall, this suggests that other factors, such as field and crop management and field boundary vegetation, are more important to HMT. Another likely impact was the length of the sampling periods. Due to long sampling periods (average 28 day length), lack of sampling resolution made it hard to identify relationships between specific environmental variables. This is something which has been suggested previously by Fryrear (1986), with larger sampling resolutions more suited to identifying overall trends, making it hard to identify trends against fast changing environmental variables. For a more accurate examination of the impacts of specific weather events and types, a daily sampling resolution would be best to capture the impacts of daily weather change on erosion.

#### 6.4.2.6 Carbon (C) Flux Approximations

To estimate the C content of the sediment collected within the collectors, topsoil samples were taken from both EN-SP3 and EF-DA from 15 m into the field in front of the BSNE collectors along the length of the field. Loss of Ignition (LOI) was then performed to find the Organic Matter (OM)% within the soil. This was then converted to an approximate C value using the ratio of 0.53 C within OM (Klingenfuß et al., 2014). This method was used due to its ease of use and having too little sediment from the collectors to accurately perform LOI. The C content of the surface soil was estimated at  $15.1 \pm 0.4\%$  at EN-SP3 and  $39.7 \pm 0.5\%$  at EF-DA. While this method of estimating C within eroded sediment is not perfect, with studies on mineral soils finding that C rich fractions of soil are more readily eroded (Leys and McTainsh, 1994, Larney et al., 1998, Li et al., 2007, Chappell et al., 2013b), OM% at EF-DA (75%) were similar to those found by Cumming (2018) within eroded sediments (76%) suggesting that differences between surface soil C and the C within eroded material were minimal.

From EN-SP3, it was estimated that  $150$  ( $130$ – $190$ )  $\text{g C m}^{-1} \text{ yr}^{-1}$  was eroded and transported from the field through the  $686$  m long NE field boundary. This translated to  $0.21$  ( $0.18$ – $0.26$ )  $\text{t C yr}^{-1}$  transported off the field. A similar calculation can be done to find the estimated C blown onto the field through the SW boundary, however, due to being unable to sample soil from the neighbouring field to test C content, there is an increased uncertainty. It was estimated that  $210$  ( $200$ – $220$ )  $\text{g C m}^{-2} \text{ yr}^{-1}$  of C was blown onto the field, equating to  $0.14$  ( $0.13$ – $0.14$ )  $\text{t C yr}^{-1}$  across the  $321$  m long field boundary. Due to the NE field boundary being  $365$  m longer than the SW field boundary, an overall net loss of  $0.07$  ( $0.05$ – $0.12$ )  $\text{t C yr}^{-1}$  was observed from EN-SP3. EF-DA saw a much greater amount of C transported from the field, with  $453 \pm 6 \text{ g C m}^{-2} \text{ yr}^{-1}$  in 2018 and  $728 \pm 9 \text{ g C m}^{-2} \text{ yr}^{-1}$  in 2019. These values translated to  $0.57 \text{ t C yr}^{-1}$  and  $0.92 \text{ t C yr}^{-1}$  transported off of the field across the  $632$  m field boundary in 2018 and 2019, respectively.

EF-DA saw more C transported off of the field than at EN-SP3. This was to be expected, with EF-DA observed to have higher average HMT ( $1525 \text{ g m}^{-2} \text{ yr}^{-1}$ ) than EN-SP3 ( $995 \text{ g m}^{-2} \text{ yr}^{-1}$  across the downwind field boundary), along with the additive effect of the higher C content within EF-DA sediment. A possible reason for this is that soil with a higher organic fraction has been observed to be lighter and therefore more readily eroded (Li et al., 2007). As there is a greater Soil OM % at EF-DA than EN-SP3, topsoil, and therefore C, is more readily transported off the field.

#### 6.4.3 The Fate of Eroded Material

The fate of material eroded from the fields is of primary importance to farmers, who stand to lose the fertile topsoil. Additionally, while the C transported off the fields is a small fraction

compared the amount lost via mineralisation of the peat to CO<sub>2</sub> (Evans et al., 2017b), the amount of material removed remains significant, especially if eroded C becomes more susceptible to mineralisation. Therefore, the fate of the eroded material plays a crucial role in understanding the true impact of aeolian erosion from agricultural fen peatlands.

As it is observed at both sites that erosion occurs primarily at heights of <0.3 m above the ground surface, the vegetation in the field margins likely plays a significant role in the deposition and capture of dust that is being moved close to the ground. Deposition on plant leaves was observed at both the EN-SP3 and EF-DA field sites (Figure 6.19), similar to observations by Cumming (2018). This is also in agreement with other studies (Wilson and Cooke, 1980, Chappell and Warren, 2003, Chappell and Baldock, 2016) who found eroded material primarily accumulated on the field boundaries.

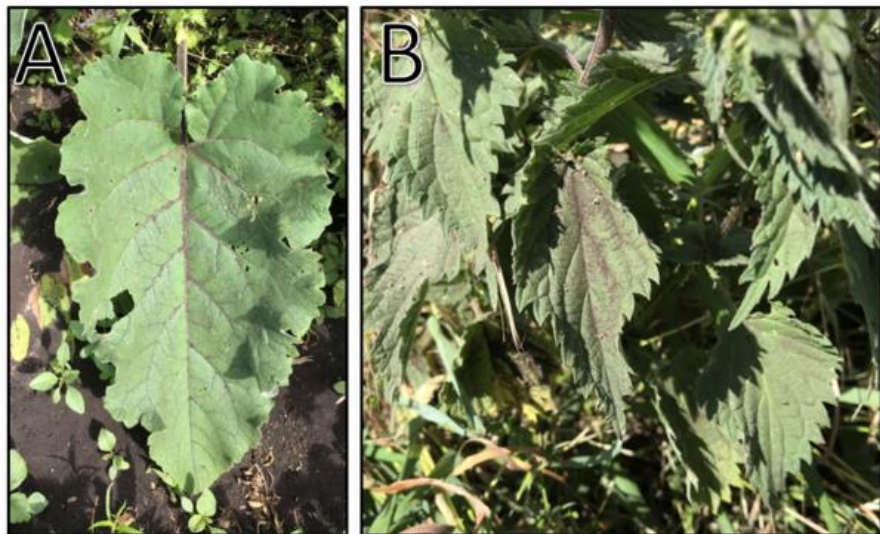


Figure 6.19. Examples of dust that has been deposited on A: a burdock leaf B: nettle leaves, both of which are commonly found within the field boundaries of EN-SP3 and EF-DA.

Deposition of dust into drifts, or as a layer several inches deep on roads (BBC News, 2013) has also been noted for significant erosion events. Both past (Arber, 1946, Radley and Simms, 1967) and present (Pers. Comm. Rob Parker) farmers talk of soil dust being blown into houses and being deposited as a layer on surfaces. This indicates that dust, particularly fine particulates, can be blown to greater heights than measured by the BSNE's and over greater distances. Additionally, Chappell et al. (2013a) suggested that during large dust erosion events, fine sediment (less than 22 µm) transported over large distances may eventually be deposited into the North Sea, leading to a terrestrial C loss.

Lofting and transport has been observed during field management; whilst the field surface is being agitated by machinery, dust can be picked up and lofted up to over 15 m into the air and

blown for greater distances (Goossens et al., 2001). This was observed at Engine Farm, EN-SP3, during the planting of the celery crop in 2019, when machinery was regularly driven over the field. Small dust devils were also observed at Engine Farm and were regular on days during hot and dry weather conditions.

Dust deposition into ditches can be substantial for individual events. Arber (1946) noted that Fenland dykes 1–2 m deep and 2 m across could become choked in a matter of hours during bad blows. It is likely that ditches capture some dust each year, which steadily accrues over time. This will contribute to the Dissolved Organic Caron (DOC) and Particulate Organic Carbon (POC) content of the ditch water where it can be mineralised as CO<sub>2</sub>, representing a significant C emission source (Peacock et al., 2017, Evans et al., 2016).

It is possible that the fate of eroded material is less important than its erosion in the first place, especially in terms of C emission. Once eroded from the field surface, the rate of mineralisation of soil organic matter within the eroded material and the newly exposed soil surface rise as it becomes increasingly exposed to the environment (Lal, 2004, Lal, 2005). This occurs through the degradation of macroaggregates, allowing the organic fraction to be more readily mineralised (Singh and Singh, 1996, Li et al., 2014). Thus, reducing the amount of aeolian erosion from a field can prevent the degradation of the surface soil and help reduce C emissions from the field.

## 6.5 Mitigation of Aeolian Erosion

This research suggests that several farm management practices could be implemented to reduce aeolian soil erosion on organic soils:

- Reduce the length of time when the field is left bare, particularly in the spring months when average wind speeds are highest.
- Maintain or establish well vegetated, tall field boundaries to trap and collect eroded material; taller vegetation will reduce wind speeds whilst also trapping material, thereby reducing the amount entering field ditches.
- Plant small dense strips along field edges that trap dust eroded from the main crop, particularly at times of the year when the main crop has limited surface cover.

## 6.6 Chapter 6 Summary

Within this Chapter, research questions 4 and 5 were addressed with the quantification of aeolian erosion from a wasted (EN-SP3) and deep (EF-DA) agricultural peatland within the East Anglian region over seven months and three years, respectively. Aeolian erosion as assessed

through use of BSNE passive samplers. Differences in erosion rates between the two sites were observed, with more material being transported off from the deep ( $5.3 \text{ g m}^{-2} \text{ d}^{-1}$ ) compared to the wasted peat ( $2.7 \text{ g m}^{-1} \text{ d}^{-1}$ ). In addition to higher HMT, the increased Soil Organic Carbon (SOC) within the deep peat translated to more C loss within eroded sediments compared to the wasted peat.

Erosion between 2018 and 2019 was compared at the deep peatland, with the differences found attributed to field management such as the crop being grown on the field and the length of time the field was left bare. The effects of changing environmental factors were assessed but not found to impact aeolian erosion, although this could be due to coarse data resolution.

The differences between field boundary vegetation types were assessed on the wasted peatland, finding that tall vegetation within the boundary reduced average wind speeds and erosion. Both material transported onto and off of the field was examined, finding that 1401 (1324–1477)  $\text{g m}^{-2} \text{ yr}^{-1}$  of material was being transported onto the field at a higher rate than it was leaving the field (995 (842–1233)  $\text{g m}^{-1} \text{ yr}^{-1}$ ). However, due to the smaller upwind field boundary, an overall net loss of material was measured of 0.5 (0.35–0.75)  $\text{t yr}^{-1}$ . The deep peat site saw higher loss of  $2 \text{ t yr}^{-1}$  across the downwind field boundary. An estimation of the C in sediment was made and found similar results with a higher rate of C transported onto the field and 210 (200–220)  $\text{g C m}^{-2} \text{ yr}^{-1}$  than off 150 (130–190)  $\text{g C m}^{-1} \text{ yr}^{-1}$ , but due to the field boundary size an overall net loss of 0.07 (0.05–0.12)  $\text{t C yr}^{-1}$ . The deep peat site saw higher loss of  $0.75 \text{ t C yr}^{-1}$  across the downwind field boundary.

The fate of the eroded material was discussed, suggesting that once eroded, soil is most likely to be more susceptible to mineralisation than when part of the field. Suggestions are provided to mitigate aeolian erosion from agricultural peatlands.

## 7 Conclusions

This final chapter provides an overview of the research conducted as part of this thesis and a summary of the main findings of the three data chapters. Highlighted are the contributions this thesis has made to further our current knowledge of CO<sub>2</sub> emissions from arable agricultural wasted peatlands and aeolian erosion losses from lowland peatlands in the UK. Specific references are made to the research goals, as set out in the Introduction (Chapter 1.1). Limitations of this work along with suggested avenues for further study are discussed.

### 7.1 Introduction

Lowland peatlands are critical to the UK, both in terms of both C storage and, in the case of fen peatlands, their nutrient stocks which supports widespread intensive agriculture. The overall aim of this thesis was to further our knowledge and understanding of C emissions from arable agricultural of wasted peatlands in eastern England. Prior to this work, there was no representative study of CO<sub>2</sub> emissions from wasted peatlands, even though they make up the majority of the cropland on peatlands within the UK. Peatlands under arable cropland contribute an estimated third of total peatland GHG emissions (Evans et al., 2017b). In addition, and despite widespread local knowledge of the impacts of the ‘fen blow’ phenomenon, very few studies had been conducted on aeolian erosion of peat with none from arable agricultural wasted fen peatland. The five research questions posed in this thesis address these knowledge gaps:

1. What are the key drivers of NEE from a wasted lowland peatland under arable agriculture? (Chapter 4)
2. What are the C emissions from a wasted lowland peatland under arable agriculture with varying crop and field management? (Chapter 5)
3. Do the C emissions from a wasted lowland peatland under arable agriculture vary compared to those from arable agriculture on deeper lowland peat? (Chapter 5)
4. What are the magnitudes of aeolian soil erosion and C flux on deep and wasted lowland peatlands under arable and horticultural agriculture? (Chapter 6)
5. What are the environmental and field management practices that impact aeolian soil erosion? (Chapter 6)

To answer the research questions centred on CO<sub>2</sub> emissions, CO<sub>2</sub> fluxes were measured over a two year period on a wasted, arable agricultural fen peatland (Engine Farm – (EN-SP3)). EN-SP3 represents a typical wasted fen peatland, having undergone drainage and agriculture for decades which has reduced the peat depth from its formerly deep peat status to < 0.4 m. Due

to its homogenous topography and wide expanse, the field was an excellent candidate for the use of the Eddy Covariance technique which was used to obtain CO<sub>2</sub> flux data. In addition, meteorological data and field management events were recorded to allow the examination of the drivers of CO<sub>2</sub> emissions. The magnitude of the CO<sub>2</sub> emissions was then calculated on a daily and yearly timescale. This facilitated a comparison of emissions, firstly between the two years of data collection and secondly with data for similarly cropped peatlands of varying depth and C content. Finally, the two years of CO<sub>2</sub> data were used to provide the first estimate of an Emission Factor (EF) for UK wasted peatland under intensive arable agriculture, paving the way for more accurate national C accounting in the UK peatland emission inventory.

To answer the research questions centred on aeolian erosion, two individual studies were performed. The first on a cropped agricultural deep peat (Rosedene Farm (EF-DA)) was carried out over 3 years and the second on the EN-SP3 over 7 months. The Horizontal Mass Transfer (HMT) was calculated at both sites along with estimations of yearly mass transfer. This allowed for a comparison of how the different cropping and land management practices impact the movement of surface soil, providing an understanding of the differences in erosion rates from a wasted and a deep cropped peatland. In addition, at EN-SP3, wind speed and erosion data were collected across 3 different field boundaries, including both upwind and downwind. This allowed an examination of how boundary vegetation impacted HMT, along with an investigation into how much material was blown onto as well as off the field, providing the basis of a field mass balance.

This chapter summarises the key findings in relation to each of the research questions, along with their contribution to current knowledge, the limitations of this work and suggestion for further research which will help advance our knowledge of GHG emissions and aeolian erosion from agricultural peatlands.

## 7.2 Chapter 4: Drivers of CO<sub>2</sub> from a wasted peatland

### ***Research question 1: What are the key drivers of NEE from a wasted lowland peatland under arable agriculture?***

The drivers of CO<sub>2</sub> fluxes were examined from EN-SP3, a wasted lowland peatland under arable agriculture over two data periods. The first spanned 4<sup>th</sup> May 2018 to 10<sup>th</sup> December 2018, the second 17<sup>th</sup> May 2019 to 17<sup>th</sup> May 2020. CO<sub>2</sub> fluxes from the field during these periods were measured using the EC method and data on environmental conditions and farm management activities were also obtained to allow examination of them as drivers of the CO<sub>2</sub> fluxes.

The drivers of Reco (ecosystem respiration = night time NEE) were examined using an empirical Arrhenius model with air temperature, Ta, the known primary driver of Reco (Lloyd and Taylor, 1994). This was done for each period of data, both over the whole period and for specific field conditions (i.e. bare vs. cropped). For the first data period, Ta related well to Reco during the maize crop ( $R^2 = 0.65$ ) and bare ( $R^2 = 0.79$ ) periods, much better than for the phacelia and buckwheat cover crop ( $R^2 = 0.34$ ), celery crop ( $R^2 = 0.051$ ) and bare ( $R^2 = 0.026$ ) periods in 2019/20. This lack of relation to Ta in 2019/20 was due to the complex situation on the field which resulted in heterogeneous conditions. During the celery crop, a strip of the cover crop was left to grow in front of the flux tower whilst during the bare period, ploughing caused a large spike in emissions due to soil aeration. The residuals of the model were examined in relation to time after ploughing and a strong negative relationship was indicated ( $r_s = -0.72$ ,  $n = 183$ ,  $p < 0.001$ ) confirming that the ploughing event was the likely primary cause of high Reco emissions at the start of the bare period. Similarly, residuals were analysed against Soil Water Content (SWC) to see if it was an additional driving variable. SWC was used due to the water table depth being consistently below the peat soil layer. SWC was not found to be a significant factor in the first data period, although SWC sensors were not installed straight away and only provided intermittent data. During the second period, lower SWC correlated with increased CO<sub>2</sub> emissions as the peat layer dried out within SWC of 0.1–0.15 m<sup>3</sup> m<sup>-3</sup>.

The light use efficiency of the phacelia and buckwheat and celery cropping periods was examined as the primary driver of GPP (Daytime NEE) using PAR through a modified Michaelis-Menten equation (Falge et al., 2001). PAR was only available for the site during the second period. The model explained NEE better for the celery growth period ( $R^2 = 0.38$ ) than for the phacelia and buckwheat growth period ( $R^2 = 0.24$ ). This was particularly the case during the peak growth period (Celery:  $R^2 = 0.79$ , Phacelia and Buckwheat:  $R^2 = 0.24$ ), where the celery crop utilised PAR much better ( $\alpha = 0.11 \pm 0.1 \mu\text{mol } \mu\text{mol}^{-1}$ , GPP<sub>2000</sub> of  $20.54 \pm 0.6$ ) than the phacelia and buckwheat ( $\alpha = 0.03 \pm 0.01 \mu\text{mol } \mu\text{mol}^{-1}$ , GPP<sub>2000</sub>  $11.1 \pm 0.4 \mu\text{mol m}^{-2} \text{s}^{-1}$ ). It is likely that this was due to phacelia and buckwheat crop being grown outside its optimum temperature range for a large portion of the time it was on the field. Trends in the residuals were examined when related to environmental variables to see if any explained additional variation in GPP. SWC was found to be the most important factor in explaining GPP after PAR and was found to be limiting below 0.15 m<sup>3</sup> m<sup>-3</sup> for both cropping periods and increasingly so during both peak cropping periods due to water stress impacting plant growth (Osakabe et al., 2014). For the celery crop, Ta, Ts and VPD all showed moderate positive correlations with the residuals, indicating that they were limiting GPP at high values. This was due to high air temperatures raising the VPD which

would limit GPP since rising VPD reduces C assimilation by 9.4 to 50%, depending on plant species (Grossiord et al., 2020). A stronger positive relationship was found between VPD and the phacelia and buckwheat crop, thought to be due to the higher temperatures that the crop was grown under leading to higher VPD values.

Examination of the drivers of CO<sub>2</sub> was inhibited by several factors. The first was an IRGA malfunction in December 2019 leading to the loss of ~6 months of data during winter 2018/19 and spring 2019 during which the field was bare. Whilst this data could be filled using the relationship derived between Ta and Reco for the preceding bare period, it prevented a more in depth look at the drivers through the winter and spring months. The lack of homogenous crop cover across the field during large periods of 2019 prevented relationships being derived during some periods and made results difficult to interpret. This was not helped by the biometeorological instruments being located within the field margin rather than inside the crop field, which resulted in a disconnect between field conditions and the values measured. Nevertheless, the results here represent an important first step in understanding the CO<sub>2</sub> drivers of an agricultural wasted fen peatland.

### 7.3 Chapter 5: NECB from a wasted peatland

#### ***Research question two: What are the C emissions from a wasted lowland peatland under arable agriculture with varying crop and field management?***

The first measurements of CO<sub>2</sub> flux on a wasted peatland under arable agriculture (EN-SP3) within the UK were quantified over two measurement years (year one: 17<sup>th</sup> May 2018 to 17<sup>th</sup> May 2019 and year two: 17<sup>th</sup> May 2019 to 17<sup>th</sup> May 2020). EC. Fluxes of CO<sub>2</sub> were aggregated into daily and yearly NEE and were partitioned into GPP and Reco to allow examination of the balance of NEE inter-annually and to compare to similar cropped peatlands in the UK and Europe.

Year one saw an NECB (NEE + crop offtake) of  $812 \pm 195.6 \text{ g C m}^{-2} \text{ yr}^{-1}$ , higher than year two at  $540 \pm 181.4 \text{ g C m}^{-2} \text{ yr}^{-1}$ , leading to an overall average emission of  $676 \pm 188.5 \text{ g C m}^{-2} \text{ yr}^{-1}$  over the two years. Differences in the magnitude of the components of NEE were observed. In year one during the period a maize crop was grown, a GPP of  $-17.42 \text{ g CO}_2\text{-C m}^2 \text{ d}^{-1}$  was measured during the peak growth period, higher than peak growth values for both the phacelia and buckwheat cover crop ( $-13.14 \text{ g CO}_2\text{-C m}^2 \text{ d}^{-1}$ ) and the celery crop ( $-8.56 \text{ g CO}_2\text{-C m}^2 \text{ d}^{-1}$ ) grown in the second year. Higher GPP over the peak growth periods was also matched with higher Reco (maize: 9.52, phacelia and buckwheat: 8.22, celery: 5.13 g CO<sub>2</sub>-C m<sup>2</sup> d<sup>-1</sup>), which was due to higher photosynthesis being linked with increased Reco from higher autotrophic respiration (Kuzyakov

and Gavrichkova, 2010). The increase in Reco may also have been due to differences in crop root systems. Maize roots grow deeper and are much more expansive than those of other UK arable crops, likely leading to greater aeration and spatial exploitation of the soil, increasing CO<sub>2</sub> emission. A more detailed examination of differences in the crop root systems and their impact on the soil and subsequently C emissions was outside the scope of this study.

The growth of a cover crop during the second year led to a period of C uptake on the field (average NEE: -0.19 g C m<sup>-2</sup> d<sup>-1</sup>) when the otherwise bare field would have been a net emitter. Despite the high emission following its ploughing in as a green manure (average NEE: 4.73 g C m<sup>-2</sup> d<sup>-1</sup>), the period of uptake contributed to the much lower emissions seen in the second year compared to the first. This high emission was likely primarily driven by the introduction of the more labile C within the cover crop into the surface soil following ploughing, however, examination of this was outside the scope of this study. Due to the complex nature of the cropping in the second year and the impacts of inter-annual weather variations, it was not possible to accurately quantify the impact of cover cropping, which requires further examination in the future using multiple crops over multiple years. The largest single day of emission was seen during ploughing on 10<sup>th</sup> March 2020 due to the aeration of the soil and the ploughing in of crop residues (NEE: 11.36 g CO<sub>2</sub>-C m<sup>2</sup> d<sup>-1</sup>). The period of intense field management during the bare period before the celery crop, which included disking the cover crop into the field, also saw high emissions (NEE: 4.73 g C m<sup>-2</sup> d<sup>-1</sup>) highlighting that working the soil leads to emissions from the field due to increased aeration, confirming the observations of (Morrison et al., 2013). Weather varied between the years, with the hot and dry temperatures in the first year limiting crop growth and also increasing emissions, while warm conditions in winter 2019/20 allowed a 48 m strip of cover crop to continue to have a small C uptake, preventing the otherwise bare field from being a strong C source.

***Research question three: Do the C emissions from a wasted lowland peatland under arable agriculture vary compared to those from arable agriculture on deeper lowland peat?***

To examine the impact of peat wastage on C emissions, the new C emission data from EN-SP3 were compared to similar cropped peatlands across the UK and Europe. This was done to ascertain whether there is a relationship between C emission and either peat depth or SOC%. While no relationship was found between SOC%, a significant relationship was found between peat depth and CO<sub>2</sub> emission ( $564 \times \log(x) + 917$ , p<0.0001, R<sup>2</sup> = 0.70, n = 9) across all the studies. Whilst this relationship was stronger when just the European (excluding UK) studies were examined ( $434 \times \log(x) + 388$ , p<0.0001, R<sup>2</sup> = 0.91, n = 17) the same was not seen when

just the UK studies were examined. This was likely due to only a few studies being performed on arable agriculture on peatland in the UK across a narrow range of peat depths compared to a wider depth range for European studies. Overall, this relationship suggests that as peat depth decreases, there is an increased reduction in CO<sub>2</sub>, particularly below a depth of 1 m. Reasons for this require further investigation, as it seems there is a complex interplay between the water table, soil C and farm management practices influencing the rate of emissions from the peatlands.

EN-SP3 was found to have slightly higher emissions than would be expected based on its shallow peat depth ( $\leq 0.4$  m), with emissions (EN-SP3:  $676 \text{ g C m}^{-2} \text{ yr}^{-1}$ ) similar in magnitude to sites with peat depths of 0.75 m (Redmere:  $678 \text{ g C m}^{-2} \text{ yr}^{-1}$ ) and 1.0 m (Manchester Mosses:  $647 \text{ g C m}^{-2} \text{ yr}^{-1}$ ) (Evans et al., 2021). At EN-SP3, emissions between the two years showed a large variation ( $272 \text{ g C m}^{-2} \text{ yr}^{-1}$ ). The first year had similar emissions to a deep peat site, whilst emissions in the second year were close to what would be expected following the relationship to peat depth. This variation is not uncommon and is within the range of other studies (Poyda et al., 2016), but it does highlight the importance of obtaining emissions values over multiple years, varying cropping regimes and changes in weather to be able to provide an accurate emission value for any particular site.

A first EF of direct CO<sub>2</sub> emissions for cropped wasted peatland was estimated as  $24.8 \text{ tCO}_2\text{e ha}^{-1} \text{ yr}^{-1}$  using the data from EN-SP3. This provided a small reduction in direct CO<sub>2</sub> emissions from the previous estimate of  $26.57 \text{ tCO}_2\text{e ha}^{-1} \text{ yr}^{-1}$ . The new direct CO<sub>2</sub> emission factor was used to calculate an approximate total emission from England's wasted peat of  $3,276 \text{ kt CO}_2 \text{ yr}^{-1}$ , a slight reduction compared to the previous estimate of  $3,510 \text{ kt CO}_2 \text{ yr}^{-1}$  (Evans et al., 2017a). Using the new estimate, all cropped wasted peatlands, given their much larger area, are estimated to emit double the total emissions arising from cropped deep peat. These total annual emissions represent 43% of England's and 21% of the UK's annual CO<sub>2</sub> emissions from peat and serve to highlight the significance of this peatland category as a CO<sub>2</sub> source. Whilst this new knowledge provides an important first step in producing an accurate estimate of emissions from the UK's cropped wasted peatlands, further studies of the scale of emissions from sites across the gradient of peat depths over multiple years is required to provide a complete picture.

Whilst overall the emissions data was considered reliable, as indicated by an EBC of 62% and 81% in 2018 and 2019/20 respectively, accuracy could have been improved through the field cover being homogenous as well as the biometeorlogical instrumentation being located within the cropped portion of the field rather than on the field boundary. The IRGA malfunction which

led to the loss of ~6 months of data resulted in long-term gap filling, making the results of the first year less representative than direct measurements alone. The longest continuous data period possible should be used for the examination of the drivers of emissions and NECB. This led to a small difference (18 days) in the data periods examined between Chapter 4 and 5 for the data from 2018. This had a negligible impact on results.

#### 7.4 Chapter 6: Aeolian erosion from two agricultural fen peatlands within East Anglia

##### ***Research question four: What are the magnitudes of aeolian soil erosion and C flux on deep and wasted lowland peatlands under arable and horticultural agriculture?***

Aeolian erosion was quantified as 1170 and 1880 g m<sup>-2</sup> yr<sup>-1</sup> in 2018 and 2019, respectively, at the deep peat site, EF-DA, with 1.5 and 2.4 t yr<sup>-1</sup> of material being transported off the field across the 632 m field boundary. At the wasted peat site EN-SP3, 1401 (1324–1477) g m<sup>-2</sup> yr<sup>-1</sup> of material was transported onto the field across the 321 m long field boundary and 995 (842–1233) g m<sup>-2</sup> yr<sup>-1</sup> off the field across the 686 m long field boundary. Despite the higher erosion rate measured at the upwind field boundary, more material was measured being transported off the field 1.4 (1.2–1.7) t yr<sup>-1</sup> than onto the field 0.90 (0.85–0.95) t yr<sup>-1</sup>. This was due to it being shorter than the downwind field boundary. However, this highlighted that it is possible for a field to have a net gain of material due to aeolian erosion from surrounding fields depending on field boundary length and orientation.

The magnitude of C being transported within the sediment was estimated for each site. The EF-DA flux was  $453 \pm 6$  g C m<sup>-2</sup> yr<sup>-1</sup> in 2018 and  $728 \pm 9$  g C m<sup>-2</sup> yr<sup>-1</sup> in 2019 which translated to 0.57 t C yr<sup>-1</sup> and 0.92 t C yr<sup>-1</sup> being transported off the field in 2018 and 2019, respectively. This was much higher than EN-SP3, largely due to the higher % of C (39.7%) within the soil at EF-DA, more than double that of EN-SP3 (15.1%). From EN-SP3, it was estimated that 150 (130–190) g C m<sup>-1</sup> yr<sup>-1</sup> was eroded and transported from the field equating to a loss of 0.21 (0.18–0.26) t C yr<sup>-1</sup> transported off the field, whilst 210 (200–220) g C m<sup>-2</sup> yr<sup>-1</sup> of C was blown onto the field, i.e. 0.14 (0.13–0.14) t C yr<sup>-1</sup>. Overall, a net loss of 0.07 (0.05–0.12) t C yr<sup>-1</sup> was measured from EN-SP3. It was not possible to quantify the net balance of erosion or C loss at EF-DA due to only having a collector on the downwind part of the field.

##### ***Research question five: What are the environmental and field management practices that impact aeolian soil erosion?***

No correlation in aeolian losses between the sites was found across the corresponding data collection periods ( $R_s = -0.24$ ) suggesting that individual field conditions are more important. In this regard, patterns of erosion at EF-DA were associated with periods when the field was bare or had just been planted with a crop in a way which exacerbated erosion (such as the planting of potatoes within ridges). The highest erosion rates were measured at EF-DA between 16<sup>th</sup> January 2020 and 5<sup>th</sup> March 2020 of  $25.2 \text{ g m}^{-2} \text{ d}^{-1}$  coinciding with a period just after the field had been tilled in preparation for cropping and the highest average wind speeds ( $3.4 \text{ m s}^{-1}$ ). These results confirm that bare field conditions combined with high wind speeds lead to the biggest erosive losses as observed in other studies (Cumming, 2018). Crop cover was found to be especially important at preventing movement of and capturing sediment, with 83% and 72% of eroded material being transported within 0.3 m of the soil surface at EF-DA and EN-SP3, respectively. Frosts were found to have no impact on erosion within this study. At EN-SP3, the height of the downwind field boundary vegetation was assessed for its impact on erosion. The taller field boundary vegetation was observed to result in lower average wind speeds ( $0.9 \text{ m s}^{-1}$ ) and lower overall erosion ( $0.59 \text{ t yr}^{-1}$ ) than the low vegetation boundary ( $0.77 \text{ t yr}^{-1}$ ,  $2.1 \text{ m s}^{-1}$ ).

The fate of material eroded from the fields was discussed. Due to most material being moved close to the soil surface (up to a height of 0.3 m) at both sites, it is likely that much of the eroded material will be captured within the vegetated field margins, particularly during summer months when they are well vegetated with tall weeds. Much of the material may also be deposited within ditches where it may be mineralised or transported off site. It was beyond the scope of this study to examine the fate of material transported into the ditch network. Fine particles have been observed to be lofted to heights above the range of the BSNE arrays used in this study. These particles have the potential to travel greater distances, i.e. beyond field boundaries. Whilst the measurements undertaken at EN-SP3 did allow some quantification of the balance of dust entering and leaving a field, they still only captured movement over two field boundaries and it is likely that a portion of unmeasured sediment also moved across the other field boundaries.

While being effective at measuring overall trends, the coarse sampling resolution of the aeolian erosion measurements (typically between 20 and 30 days) did not allow for the assessment of individual weather events or field management operations. This may explain why frosts, which break up the soil surface and might be expected to lead to increased erosion, were not found to be a significant factor. It also made it hard to account for wind direction, with dust movement not always coming from across the boundary consistently. A more robust field measurement campaign with BSNEs located along all field boundaries and with monitoring at a higher

frequency would be required to capture these additional flux movements. Employing instruments (such as the DustTrak DRX Aerosol Monitor) that can measure the mass and size fraction of the eroded particles on a more frequent resolution would allow the particle size to be examined, something that cannot be done using BSNEs due to the agitation of the dust particles as they are collected. Finally, further study is required on the fate of the eroded material once it has been deposited within a ditch or field boundary. While it is likely that this transported C becomes more susceptible to mineralisation and quickly becomes CO<sub>2</sub>, there are no current studies that have attempted to quantify this.

## 7.5 Recommendations for future research

The purpose of this work was to provide the first step in understanding the CO<sub>2</sub> emissions from the UK's arable agricultural wasted peatlands and to establish the scale of aeolian erosion from peatlands of differing depth. While these aims have been achieved, further research is required in the following areas.

### 7.5.1 GHG emission from the UK's wasted peatlands

This study provided the first examination and quantification of CO<sub>2</sub> emissions from an arable wasted agricultural fen peatland. This provided a critical first step in understanding and quantifying their contribution to total peatland emissions in the UK. However, the following research should be undertaken to develop our understanding further:

While a cover crop was present at the site in the second year and was associated with lower emissions, the impact of the cover crop was hard to quantify. To better understand the impact of cover cropping on C emissions, further years of data should be collected on a field with a homogeneous crop cover. This will improve EC data quality and allow for a more effective examination of the drivers of emissions. To aid this, locating the flux tower in the centre of the field would be advantageous, allowing more accurate and representative measurements of field conditions. This will also benefit the analysis and interpretation of flux data, with less data removal required and no influence of edge effects on the measured fluxes. Secondly, the highest period of emission from the field occurred after it was disked. It is unknown whether this increased emission was primarily due to the mineralisation of the more labile C within the fresh plant matter disked into the surface, or that, due to a priming effect, the historic C stored within the peatland was also exposed to increased mineralisation. Further study is required to examine if the more labile C introduced into the peatland in effect 'protects' the historic C from being mineralised or if it causes a faster loss of the existing peat.

The Reco observed during the maize crop was much higher than during the phacelia and buckwheat and celery cropping periods. This was thought to be due to the impact of the different rooting profiles, with maize having a larger and more extensive root system. This requires further examination through a study of how root systems impact autotrophic (Ra) and heterotrophic (Rh) respiration. Partitioning of Ra and Rh was not possible in this study but should be attempted in future studies across different crop cycles.

$\text{N}_2\text{O}$  emissions from lowland fen peats under agriculture have been assumed to be low owing to low fertiliser application rates on the nutrient rich peat. During this study, numerous fertiliser applications were made on EN-SP3, likely due to the lower nutrient content of the wasted peat soil. Therefore,  $\text{N}_2\text{O}$  emissions may well be of greater importance to net GHGs on wasted compared to deeper peats. It is recommended that studies using static chambers or automatic  $\text{N}_2\text{O}$  gas analysers which can be run continuously over long periods should be used to quantify the  $\text{N}_2\text{O}$  emissions from wasted peatlands.

Finally, whilst knowledge of the overall  $\text{CO}_2$  emissions from the agricultural wasted peatland in the UK has been advanced, the study of one field, EN-SP3, does not provide a complete picture. Wasted peatlands vary both in peat depth and substrate quality and, as shown in this study, emissions vary with peat depth and also between years. This suggests that further EC studies should be conducted at a number of sites across the range of wasted peat depths (between 0.4 m and 0 m organic layer) to validate the emissions estimate and the relationship with both peat depth and SOC. Additionally, there is currently no defined point at which a wasted peat soil becomes classified as a mineral soil or a ‘former peat’. While this may be hard to quantify due to the mixing of the organic soil layer with the underlying mineral substrate, criteria should be developed to assist with classification. This will help both land managers and those involved in compiling emission inventories to better understand the decline in area of wasted peatlands as they continue to mineralise and, presumably, eventually disappear.

#### 7.5.2 Aeolian erosion from the UK’s peatlands

A quantification of the scale of transport off the study sites was made, along with similar values for onsite transport at EN-SP3; this provided a limited insight into the movement of material. Further studies should investigate movement across all field boundaries to provide a more accurate picture of net gains and losses. Whilst movement across some boundaries not in front of the dominant wind direction will be small, wind direction does vary in all directions throughout a calendar year, and it is likely that a small but still significant movement of material is occurring across these boundaries.

The measurements provided in this thesis provide an improved understanding of the long term magnitude of aeolian erosion at the study sites, but high resolution data should be recorded to provide a more accurate examination of the role of individual field management operations and weather events. Additionally, studies involving high resolution instruments that also measure particle size (such as the DustTrak DRX Aerosol Monitor) are required to gain a fuller understanding of the primary size of the aggregates being eroded. This could help inform future mitigation methods, such as the use of field applications that aggregate the soil surface.

Answering the question ‘where does it all end up?’ will be important for future studies. This study observed that, despite the large amount of material moving across both field boundaries, net movement was much lower. A study on how material moves across a large field or across several adjoining fields, would be useful in understanding the net overall movement of material and its fate. This will become more important for soils with a higher mineral fraction, as it is hypothesised that disaggregated peat soil is more susceptible to mineralisation and quickly becomes CO<sub>2</sub> once eroded. This will be especially important on fields which have lower boundary vegetation and which trap less eroded material.

## 7.6 Chapter 7 Summary

This chapter concludes the thesis by providing an overview of how the thesis advances our knowledge of C emissions from arable agricultural peatlands, primarily cropped wasted peatlands for which no emissions data were previously available. The main results are summarised, followed by a discussion of the limitations of this work and suggestions for further study.

## 8 References

2021. *The Carbon Budget Order*, United Kingdom, HM Government.
- AGRICULTURE AND ARI-FOOD CANADA 1998. *The Canadian System of Soil Classification*, Ottawa, ON, NRC Research Press.
- ARBER, M. A. 1946. Dust-storms in the Fenland round Ely. *Geography*, 23-26.
- AUBINET, M., CHERMANNE, B., VANDENHAUTE, M., LONGDOZ, B., YERNAUX, M. & LAITAT, E. 2001. Long term carbon dioxide exchange above a mixed forest in the Belgian Ardennes. *Agricultural and Forest Meteorology*, 108, 293-315.
- AUBINET, M., GRELLE, A., IBROM, A., RANNIK, Ü., MONCRIEFF, J., FOKEN, T., KOWALSKI, A. S., MARTIN, P. H., BERBIGIER, P. & BERNHOFER, C. 1999. Estimates of the annual net carbon and water exchange of forests: the EUROFLUX methodology. *Advances in ecological research*. Elsevier.
- AUBINET, M., MOUREAUX, C., BODSON, B., DUFRANNE, D., HEINESCH, B., SULEAU, M., VANCUTSEM, F. & VILRET, A. 2009. Carbon sequestration by a crop over a 4-year sugar beet/winter wheat/seed potato/winter wheat rotation cycle. *Agricultural and Forest Meteorology*, 149, 407-418.
- AUBINET, M., VESALA, T. & PAPALE, D. 2012. *Eddy covariance: a practical guide to measurement and data analysis*, Springer Science & Business Media.
- AVERY, B. W. 1980. Soil classification for England and Wales [higher categories]. *Soil classification for England and Wales [higher categories]*.
- BAIN, C., BONN, A., STONEMAN, R., CHAPMAN, S., COUPAR, A., EVANS, M., GEAREY, B., HOWAT, M., JOOSTEN, H. & KEENLEYSIDE, C. 2011. *IUCN UK commission of inquiry on peatlands*, IUCN UK Peatland Programme.
- BAIRD, A. J., BECKWITH, C. W., WALDRON, S. & WADDINGTON, J. 2004. Ebullition of methane-containing gas bubbles from near-surface Sphagnum peat. *Geophysical Research Letters*, 31.
- BALDOCCHI, D. D. 2003. Assessing the eddy covariance technique for evaluating carbon dioxide exchange rates of ecosystems: past, present and future. *Global change biology*, 9, 479-492.
- BARDGETT, R. D., FREEMAN, C. & OSTLE, N. J. 2008. Microbial contributions to climate change through carbon cycle feedbacks. *The ISME journal*, 2, 805.
- BBC NEWS. 2013. *Fen Blow Phenomenon: Farmers count cost of 'perfect storm'* [Online]. Available: <https://www.bbc.com/news/uk-england-22341808> [Accessed 21/07/2020].
- BERGLUND, Ö. & BERGLUND, K. 2010. Distribution and cultivation intensity of agricultural peat and gyttja soils in Sweden and estimation of greenhouse gas emissions from cultivated peat soils. *Geoderma*, 154, 173-180.
- BERGMAN, I., SVENSSON, B. H. & NILSSON, M. 1998. Regulation of methane production in a Swedish acid mire by pH, temperature and substrate. *Soil Biology and Biochemistry*, 30, 729-741.
- BEYER, C., LIEBERSBACH, H. & HÖPER, H. 2015. Multiyear greenhouse gas flux measurements on a temperate fen soil used for cropland or grassland. *Journal of Plant Nutrition and Soil Science*, 178, 99-111.
- BIASI, C., RUSALIMOVA, O., MEYER, H., KAISER, C., WANEK, W., BARSUKOV, P., JUNGER, H. & RICHTER, A. 2005. Temperature-dependent shift from labile to recalcitrant carbon sources of arctic heterotrophs. *Rapid communications in mass spectrometry*, 19, 1401-1408.
- BILLETT, M., CHARMAN, D., CLARK, J., EVANS, C., EVANS, M., OSTLE, N., WORRALL, F., BURDEN, A., DINSMORE, K. & JONES, T. 2010. Carbon balance of UK peatlands: current state of knowledge and future research challenges. *Climate Research*, 45, 13-29.

- BORRELLI, P., BALLABIO, C., PANAGOS, P. & MONTANARELLA, L. 2014. Wind erosion susceptibility of European soils. *Geoderma*, 232, 471-478.
- BORREN, W., BLEUTEN, W. & LAPSHINA, E. D. 2004. Holocene peat and carbon accumulation rates in the southern taiga of western Siberia. *Quaternary Research*, 61, 42-51.
- BRIX, H., SORRELL, B. K. & LORENZEN, B. 2001. Are Phragmites-dominated wetlands a net source or net sink of greenhouse gases? *Aquatic Botany*, 69, 313-324.
- BUBIER, J. L., BHATIA, G., MOORE, T. R., ROULET, N. T. & LAFLEUR, P. M. 2003. Spatial and temporal variability in growing-season net ecosystem carbon dioxide exchange at a large peatland in Ontario, Canada. *Ecosystems*, 6, 353-367.
- BURBA, G. 2013. *Eddy covariance method for scientific, industrial, agricultural and regulatory applications: A field book on measuring ecosystem gas exchange and areal emission rates*, LI-Cor Biosciences.
- BURMAN, P. K. D., SHURPALI, N. J., CHOWDHURI, S., KARIPOV, A., CHAKRABORTY, S., LIND, S. E., MARTIKAINEN, P. J., CHELLAPPAN, S., AROLA, A. & TIWARI, Y. K. 2020. Eddy covariance measurements of CO<sub>2</sub> exchange from agro-ecosystems located in subtropical (India) and boreal (Finland) climatic conditions. *Journal of Earth System Science*, 129, 1-18.
- BURNET FEN DRAINAGE BOARD: CONSERVATION. 2011. *Burnt Fen Conservation Statement* [Online]. Wayback Machine Internet Archive. Available: [https://web.archive.org/web/2011003235358/http://www.elydrainageboards.co.uk/members/burnt\\_fen/conservation.html#](https://web.archive.org/web/2011003235358/http://www.elydrainageboards.co.uk/members/burnt_fen/conservation.html#) [Accessed 26/07/2019].
- BURTON, R. & HODGSON, J. M. 1987. *Lowland peat in England and Wales*, Soil Survey of England and Wales Harpenden.
- BUYANOVSKY, G., WAGNER, G. & GANTZER, C. 1986. Soil respiration in a winter wheat ecosystem. *Soil Science Society of America Journal*, 50, 338-344.
- CAI, T., FLANAGAN, L. B. & SYED, K. H. 2010. Warmer and drier conditions stimulate respiration more than photosynthesis in a boreal peatland ecosystem: analysis of automatic chambers and eddy covariance measurements. *Plant, cell & environment*, 33, 394-407.
- CAMPBELL, D. R., LAVOIE, C. & ROCHEFORT, L. 2002. Wind erosion and surface stability in abandoned milled peatlands. *Canadian journal of soil science*, 82, 85-95.
- CANADA SOIL SURVEY COMMITTEE 1978. *The Canadian system of soil classification*, [Ottawa]; Hull, Que., Research Branch, Canada Dept. of Agriculture ; Available by mail from Print. and Pub. Supply and Services Canada.
- CCC 2021. The CCC's annual assessment of UK progress in reducing emissions and biennial assessment of progress in adapting to climate change. *2021 Progress Report to Parliament*.
- CHAPIN, F. S., WOODWELL, G. M., RANDERSON, J. T., RASTETTER, E. B., LOVETT, G. M., BALDOCCHI, D. D., CLARK, D. A., HARMON, M. E., SCHIMEL, D. S. & VALENTINI, R. 2006. Reconciling carbon-cycle concepts, terminology, and methods. *Ecosystems*, 9, 1041-1050.
- CHAPPELL, A., BALDOCK, J. & ROSSEL, R. V. 2013a. *Sampling soil organic carbon to detect change over time*, Department of Environment.
- CHAPPELL, A. & BALDOCK, J. A. 2016. Wind erosion reduces soil organic carbon sequestration falsely indicating ineffective management practices. *Aeolian Research*, 22, 107-116.
- CHAPPELL, A. & WARREN, A. 2003. Spatial scales of <sup>137</sup>Cs-derived soil flux by wind in a 25 km<sup>2</sup> arable area of eastern England. *CATENA*, 52, 209-234.
- CHAPPELL, A., WEBB, N. P., BUTLER, H. J., STRONG, C. L., MCTAINSH, G. H., LEYS, J. F. & VISCARRA ROSSEL, R. A. 2013b. Soil organic carbon dust emission: an omitted global source of atmospheric CO<sub>2</sub>. *Global Change Biology*, 19, 3238-3244.
- CHARUCHITTIPAN, D., BABEL, W., MAUDER, M., LEPS, J.-P. & FOKEN, T. 2014. Extension of the averaging time in eddy-covariance measurements and its effect on the energy balance closure. *Boundary-Layer Meteorology*, 152, 303-327.

- CHEN, J., WANG, Q., LI, M., LIU, F. & LI, W. 2016. Does the different photosynthetic pathway of plants affect soil respiration in a subtropical wetland? *Ecology and evolution*, 6, 8010-8017.
- CHIMNER, R. A., PYPKER, T. G., HRIBLIJAN, J. A., MOORE, P. A. & WADDINGTON, J. M. 2017. Multi-decadal changes in water table levels alter peatland carbon cycling. *Ecosystems*, 20, 1042-1057.
- CLARK, J. & GODWIN, H. 1962. The Neolithic in the Cambridgeshire fens. *Antiquity*, 36, 10-23.
- CLARK, J., GODWIN, M. & CLIFFORD, M. 1935. Report on recent excavations at Peacock's Farm, Shippea Hill, Cambridgeshire. *The Antiquaries Journal*, 15, 284-319.
- CLYMO, R., TURUNEN, J. & TOLONEN, K. 1998. Carbon accumulation in peatland. *Oikos*, 368-388.
- COUWENBERG, J. 2011. Greenhouse gas emissions from managed peat soils: is the IPCC reporting guidance realistic? *Mires & Peat*, 8.
- CRAINE, J. M., FIERER, N. & MCLAUCHLAN, K. K. 2010. Widespread coupling between the rate and temperature sensitivity of organic matter decay. *Nature Geoscience*, 3, 854.
- CUI, L., KANG, X., LI, W., HAO, Y., ZHANG, Y., WANG, J., YAN, L., ZHANG, X., ZHANG, M. & ZHOU, J. 2017. Rewetting Decreases Carbon Emissions from the Zoige Alpine Peatland on the Tibetan Plateau. *Sustainability*, 9, 948.
- CUI, Q., SONG, C., WANG, X., SHI, F., YU, X. & TAN, W. 2018. Effects of warming on N<sub>2</sub>O fluxes in a boreal peatland of Permafrost region, Northeast China. *Science of The Total Environment*, 616-617, 427-434.
- CUMMING, A. 2018. *Multi-annual carbon flux at an intensively cultivated lowland peatland in East Anglia, UK*. Doctor of Philosophy, University of Leicester.
- DAVIDSON, E. A., BELK, E. & BOONE, R. D. 1998. Soil water content and temperature as independent or confounded factors controlling soil respiration in a temperate mixed hardwood forest. *Global change biology*, 4, 217-227.
- DAVIDSON, E. A. & JANSENS, I. A. 2006. Temperature sensitivity of soil carbon decomposition and feedbacks to climate change. *Nature*, 440, 165.
- DAWSON, J. J. & SMITH, P. 2007. Carbon losses from soil and its consequences for land-use management. *Science of the total environment*, 382, 165-190.
- DAWSON, Q., KECHAVARZI, C., LEEDS-HARRISON, P. & BURTON, R. 2010. Subsidence and degradation of agricultural peatlands in the Fenlands of Norfolk, UK. *Geoderma*, 154, 181-187.
- DE BAETS, S., POESEN, J., MEERSMANS, J. & SERLET, L. 2011. Cover crops and their erosion-reducing effects during concentrated flow erosion. *Catena*, 85, 237-244.
- DE WIT, H. A., AUSTNES, K., HYLEN, G. & DALSGAARD, L. 2015. A carbon balance of Norway: terrestrial and aquatic carbon fluxes. *Biogeochemistry*, 123, 147-173.
- DEPARTMENT OF ENERGY AND CLIMATE CHANGE 2013. Thermal growing season in central England. [Online] <https://www.gov.uk/government/collections/impacts-of-climate-change-in-the-uk>.
- DING, W., CAI, Y., CAI, Z., YAGI, K. & ZHENG, X. 2007. Soil respiration under maize crops: effects of water, temperature, and nitrogen fertilization. *Soil Science Society of America Journal*, 71, 944-951.
- DINSMORE, K. J., BILLETT, M. F. & DYSON, K. E. 2013. Temperature and precipitation drive temporal variability in aquatic carbon and GHG concentrations and fluxes in a peatland catchment. *Global Change Biology*, 19, 2133-2148.
- DINSMORE, K. J., BILLETT, M. F., SKIBA, U. M., REES, R. M., DREWER, J. & HELFTER, C. 2010. Role of the aquatic pathway in the carbon and greenhouse gas budgets of a peatland catchment. *Global Change Biology*, 16, 2750-2762.
- DINSMORE, K. J., SKIBA, U. M., BILLETT, M. F. & REES, R. M. 2009. Effect of water table on greenhouse gas emissions from peatland mesocosms. *Plant and Soil*, 318, 229.
- DONG, Z. & QIAN, G. 2007. Characterizing the height profile of the flux of wind-eroded sediment. *Environmental Geology*, 51, 835-845.

- DONNELLY, C., GREUELL, W., ANDERSSON, J., GERTEN, D., PISACANE, G., ROUDIER, P. & LUDWIG, F. 2017. Impacts of climate change on European hydrology at 1.5, 2 and 3 degrees mean global warming above preindustrial level. *Climatic Change*, 143, 13-26.
- DORREPAAL, E., TOET, S., VAN LOGTESTIJN, R. S., SWART, E., VAN DE WEG, M. J., CALLAGHAN, T. V. & AERTS, R. 2009. Carbon respiration from subsurface peat accelerated by climate warming in the subarctic. *Nature*, 460, 616.
- DYSON, K. E., BILLETT, M. F., DINSMORE, K. J., HARVEY, F., THOMSON, A. M., PIIRAINEN, S. & KORTELAINEN, P. 2011. Release of aquatic carbon from two peatland catchments in E. Finland during the spring snowmelt period. *Biogeochemistry*, 103, 125-142.
- EICKENSCHEIDT, T., HEINICHEN, J. & DRÖSLER, M. 2015. The greenhouse gas balance of a drained fen peatland is mainly controlled by land-use rather than soil organic carbon content. *Biogeosciences*, 12, 5161-5184.
- ELDER, J. W. & LAL, R. 2008. Tillage effects on gaseous emissions from an intensively farmed organic soil in North Central Ohio. *Soil and Tillage Research*, 98, 45-55.
- ELSGAARD, L., GÖRRES, C.-M., HOFFMANN, C. C., BLICHER-MATHIESEN, G., SCHELDE, K. & PETERSEN, S. O. 2012. Net ecosystem exchange of CO<sub>2</sub> and carbon balance for eight temperate organic soils under agricultural management. *Agriculture, ecosystems & environment*, 162, 52-67.
- ELY GROUP OF INTERNAL DRAINAGE BOARDS. 2019. *Burnt Fen District Map* [Online]. Available: <http://www.elydrainageboards.co.uk/internal-drainage-boards/burnt-fen/burnt-fen-internal-drainage-board-map/> [Accessed 26/07/2019].
- EPG, D. C. 2006. UK Emissions by Sources and Removals by Sinks due to Land Use, Land Use Change and Forestry Activities.
- ESRL NOAA. 2021. *Trends in Atmospheric Carbon Dioxide* [Online]. Available: <https://www.esrl.noaa.gov/gmd/ccgg/trends/weekly.html> [Accessed 21/07/2021 2018].
- ESSL, F., DULLINGER, S., MOSER, D., RABITSCH, W. & KLEINBAUER, I. 2012. Vulnerability of mires under climate change: implications for nature conservation and climate change adaptation. *Biodiversity and Conservation*, 21, 655-669.
- EVANS, C., ARTZ, R., MOXLEY, J., SMYTH, M.-A., TAYLOR, E., ARCHER, E., BURDEN, A., WILLIAMSON, J., DONNELLY, D. & THOMSON, A. 2017a. Implementation of an emissions inventory for UK peatlands. Centre for Ecology and Hydrology.
- EVANS, C., MORRISON, R., BURDEN, A., WILLIAMSON, J., BAIRD, A., BROWN, E., CALLAGHAN, N., CHAPMAN, P., CUMMING, A. & DEAN, H. 2017b. Final report on project SP1210: Lowland peatland systems in England and Wales—evaluating greenhouse gas fluxes and carbon balances.
- EVANS, C., PEACOCK, M., BAIRD, A., ARTZ, R., BURDEN, A., CALLAGHAN, N., CHAPMAN, P., COOPER, H., COYLE, M. & CRAIG, E. 2021. Overriding water table control on managed peatland greenhouse gas emissions. *Nature*, 1-7.
- EVANS, C. D., RENOU-WILSON, F. & STRACK, M. 2016. The role of waterborne carbon in the greenhouse gas balance of drained and re-wetted peatlands. *Aquatic Sciences*, 78, 573-590.
- FALGE, E., BALDOCCHI, D., OLSON, R., ANTHONI, P., AUBINET, M., BERNHOFER, C., BURBA, G., CEULEMANS, R., CLEMENT, R. & DOLMAN, H. 2001. Gap filling strategies for defensible annual sums of net ecosystem exchange. *Agricultural and forest meteorology*, 107, 43-69.
- FALGE, E., BALDOCCHI, D., TENHUNEN, J., AUBINET, M., BAKWIN, P., BERBIGIER, P., BERNHOFER, C., BURBA, G., CLEMENT, R. & DAVIS, K. J. 2002. Seasonality of ecosystem respiration and gross primary production as derived from FLUXNET measurements. *Agricultural and Forest Meteorology*, 113, 53-74.
- FAO 1997. *FAO/Unesco Soil Map on the World, Revised Legend, with corrections and updates*, Rome, ISRIC, Wageningen.

- FELDMAN, L. 1994. The Maize Root. In: FREELING, M. & WALBOT, V. (eds.) *The Maize Handbook*. New York, NY: Springer New York.
- FINKELSTEIN, P. L. & SIMS, P. F. 2001. Sampling error in eddy correlation flux measurements. *Journal of Geophysical Research: Atmospheres*, 106, 3503-3509.
- FLANAGAN, L. B. & SYED, K. H. 2011. Stimulation of both photosynthesis and respiration in response to warmer and drier conditions in a boreal peatland ecosystem. *Global Change Biology*, 17, 2271-2287.
- FOKEN, T. 2008. The energy balance closure problem: an overview. *Ecological Applications*, 18, 1351-1367.
- FOKEN, T., GÖOCKEDE, M., MAUDER, M., MAHRT, L., AMIRO, B. & MUNGER, W. 2004. Post-field data quality control. *Handbook of micrometeorology*. Springer.
- FOKEN, T. & WICHURA, B. 1996. Tools for quality assessment of surface-based flux measurements. *Agricultural and forest meteorology*, 78, 83-105.
- FOULDS, S. A. & WARBURTON, J. 2007. Wind erosion of blanket peat during a short period of surface desiccation (North Pennines, Northern England). *Earth Surface Processes and Landforms: The Journal of the British Geomorphological Research Group*, 32, 481-488.
- FOWLER, G. 1932. A skeleton of the early Bronze Age found in the Fens. *Proceedings of the Prehistoric Society of East Anglia*, 6, 362-364.
- FOWLER, G. 1933. Shrinkage of the peat-covered Fenlands. *The Geographical Journal*, 81, 149-150.
- FRANSSEN, H. H., STÖCKLI, R., LEHNER, I., ROTENBERG, E. & SENEVIRATNE, S. I. 2010. Energy balance closure of eddy-covariance data: A multisite analysis for European FLUXNET stations. *Agricultural and Forest Meteorology*, 150, 1553-1567.
- FRANZLUEBBERS, A., HONS, F. & ZUBERER, D. 1995. Tillage and crop effects on seasonal dynamics of soil CO<sub>2</sub> evolution, water content, temperature, and bulk density. *Applied Soil Ecology*, 2, 95-109.
- FRYREAR, D. 1986. A field dust sampler. *Journal of soil and water conservation*, 41, 117-120.
- FULLEN, M. A. 1985. Wind erosion of arable soils in east Shropshire (England) during spring 1983. *Catena*, 12, 111-120.
- FUNK, R. & ENGEL, W. 2015. Investigations with a field wind tunnel to estimate the wind erosion risk of row crops. *Soil and Tillage Research*, 145, 224-232.
- G'S FRESH. 2019. *Grower Profiles* [Online]. Online. Available: <https://www.gs-growers.com/gs-growers/growers-profiles/> [Accessed 26/07/2019].
- GAO, Z., LIU, H., KATUL, G. G. & FOKEN, T. 2017. Non-closure of the surface energy balance explained by phase difference between vertical velocity and scalars of large atmospheric eddies. *Environmental Research Letters*, 12, 034025.
- GLENN, A. J., FLANAGAN, L. B., SYED, K. H. & CARLSON, P. J. 2006. Comparison of net ecosystem CO<sub>2</sub> exchange in two peatlands in western Canada with contrasting dominant vegetation, Sphagnum and Carex. *Agricultural and Forest Meteorology*, 140, 115-135.
- GOOSSENS, D. & BUCK, B. J. 2012. Can BSNE (Big Spring Number Eight) samplers be used to measure PM10, respirable dust, PM2.5 and PM1.0? *Aeolian Research*, 5, 43-49.
- GOOSSENS, D., GROSS, J. & SPAAN, W. 2001. Aeolian dust dynamics in agricultural land areas in Lower Saxony, Germany. *Earth Surface Processes and Landforms: The Journal of the British Geomorphological Research Group*, 26, 701-720.
- GOOSSENS, D., OFFER, Z. & LONDON, G. 2000. Wind tunnel and field calibration of five aeolian sand traps. *Geomorphology*, 35, 233-252.
- GORHAM, E. 1991. Northern Peatlands Role in the Carbon Cycle and Probable Responses to Climatic Warming, Ecological Applications Volume 1, Issue 2. *Ecological Applications* [Online], 1.
- GROSSIORD, C., BUCKLEY, T. N., CERNUSAK, L. A., NOVICK, K. A., POULTER, B., SIEGWOLF, R. T., SPERRY, J. S. & McDOWELL, N. G. 2020. Plant responses to rising vapor pressure deficit. *New Phytologist*, 226, 1550-1566.

- GUARDIA, G., AGUILERA, E., VALLEJO, A., SANZ-COBENA, A., ALONSO-AYUSO, M. & QUEMADA, M. 2019. Effective climate change mitigation through cover cropping and integrated fertilization: A global warming potential assessment from a 10-year field experiment. *Journal of Cleaner Production*, 241, 118307.
- GÜNTHER, A., HUTH, V., JURASINSKI, G. & GLATZEL, S. 2015. The effect of biomass harvesting on greenhouse gas emissions from a rewetted temperate fen. *Gcb Bioenergy*, 7, 1092-1106.
- HADDEN, D. & GRELLE, A. 2017. The impact of cultivation on CO<sub>2</sub> and CH<sub>4</sub> fluxes over organic soils in Sweden. *Agricultural and Forest Meteorology*, 243, 1-8.
- HÁJEK, T. & VICHEROVÁ, E. 2014. Desiccation tolerance of Sphagnum revisited: a puzzle resolved. *Plant biology*, 16, 765-773.
- HALL, D., UPTON, S. & MARSLAND, G. 1994. Designs for a deposition gauge and a flux gauge for monitoring ambient dust. *Atmospheric Environment*, 28, 2963-2979.
- HANNAM J.A., S. R. W., CORSTANJE R., DEEKS L.K., TRUCKELL I., WAINE T. 2014. G's farm scale soil assessment: scoping study. Cranfield University.
- HARDING, R. & LLOYD, C. 2008. Evaporation and energy balance of a wet grassland at Tadham Moor on the Somerset Levels. *Hydrological Processes: An International Journal*, 22, 2346-2357.
- HARPENSLAGER, S. F., VAN DEN ELZEN, E., KOX, M. A., SMOLDERS, A. J., ETTWIG, K. F. & LAMERS, L. P. 2015. Rewetting former agricultural peatlands: Topsoil removal as a prerequisite to avoid strong nutrient and greenhouse gas emissions. *Ecological Engineering*, 84, 159-168.
- HATALA, J. A., DETTO, M., SONNENTAG, O., DEVEREL, S. J., VERFAILLIE, J. & BALDOCCHI, D. D. 2012. Greenhouse gas (CO<sub>2</sub>, CH<sub>4</sub>, H<sub>2</sub>O) fluxes from drained and flooded agricultural peatlands in the Sacramento-San Joaquin Delta. *Agriculture, ecosystems & environment*, 150, 1-18.
- HM GOVERNMENT 2018. A Green Future: Our 25 Year Plan to Improve the Environment. In: DEFRA (ed.). Crown.
- HM GOVERNMENT 2021. England Peat Action Plan. Online.
- HOLDEN, J. 2005. Peatland hydrology and carbon release: why small-scale process matters. *Philosophical Transactions of the Royal Society of London A: Mathematical, Physical and Engineering Sciences*, 363, 2891-2913.
- HOLMAN, I. 2009. An estimate of peat reserves and loss in the East Anglian Fens Commissioned by the RSPB. *Department of Natural Resources Cranfield University, Cranfield, Bedfordshire*.
- HOOIJER, A., PAGE, S., JAUHIAINEN, J., LEE, W., LU, X., IDRIS, A. & ANSHARI, G. 2012. Subsidence and carbon loss in drained tropical peatlands. *Biogeosciences*, 9, 1053.
- HRIBLJAN, J. A., KANE, E. S. & CHIMNER, R. A. 2017. Implications of Altered Hydrology for Substrate Quality and Trace Gas Production in a Poor Fen Peatland. *Soil Science Society of America Journal*, 81, 633-646.
- HSIEH, C.-I., HUANG, C.-W. & KIELY, G. 2009. Long-term estimation of soil heat flux by single layer soil temperature. *International journal of biometeorology*, 53, 113-123.
- HUTCHINSON, J. N. 1980. The Record of Peat Wastage in the East Anglian Fenlands at Holme Post, 1848-1978 A.D. *Journal of Ecology*, 68, 229-249.
- HUTTUNEN, J. T., NYKÄNNEN, H., TURUNEN, J. & MARTIKAINEN, P. J. 2003. Methane emissions from natural peatlands in the northern boreal zone in Finland, Fennoscandia. *Atmospheric Environment*, 37, 147-151.
- IPCC 1996. IPCC guidelines for national greenhouse gas inventories. *Reference manual*, 3.
- IPCC 2006. 2006 IPCC guidelines for national greenhouse gas inventories.
- IPCC 2013. IPCC, 2013: climate change 2013: the physical science basis. Contribution of working group I to the fifth assessment report of the intergovernmental panel on climate change. In: STOCKER, T. F., QIN, D., PLATTNER, G.-K., TIGNOR, M., ALLEN, S. K., BOSCHUNG, J., NAUELS, A., XIA, Y., BEX, B. & MIDGLEY, B. (eds.). Cambridge University Press.

- IPCC 2014. 2013 supplement to the 2006 IPCC guidelines for national greenhouse gas inventories: Wetlands. In: HIRAIshi, T., KRUG, T., TANABE, K., SRIVASTAVA, N., BAASANSUREN, J., FUKUDA, M. & TROXLER, T. (eds.) *IPCC, Switzerland*.
- IUSS WORKING GROUP 2015. World Reference Base for Soil Resources 2014, update 2015 International soil classification system for naming soils and creating legends for soil maps. *World Soil Resources Reports*.
- JEANNEAU, L., BUYSSE, P., DENIS, M., GRUAU, G., PETITJEAN, P., JAFFRÉZIC, A., FLECHARD, C. & VIAUD, V. 2020. Water Table Dynamics Control Carbon Losses from the Destabilization of Soil Organic Matter in a Small, Lowland Agricultural Catchment. *Soil Systems*, 4, 2.
- JIAN, J., DU, X., REITER, M. S. & STEWART, R. D. 2020. A meta-analysis of global cropland soil carbon changes due to cover cropping. *Soil Biology and Biochemistry*, 143, 107735.
- JIANG, C., HAO, Q. & ZHANG, J. Contribution of root respiration to soil respiration in a maize field in Southwest China. Proceedings of the 19th World Congress of Soil Science: Soil solutions for a changing world, Brisbane, Australia, 1-6 August 2010. Congress Symposium 4: Greenhouse gases from soils, 2010. International Union of Soil Sciences (IUSS), c/o Institut für Bodenforschung ..., 32-35.
- JNCC 2011. Towards an assessment of the state of UK Peatlands. *JNCC report*. No. 445.
- JONES, D. L., STYLES, D., CHADWICK, D., EVANS, C., PAGE, S., MORRISON, R., WIGGS, G. & KADUK, J. 2021. *Securing Long-Term Ecosystem Function in Lowland Organic Soils (SEFLOS) Project* [Online]. Available: <https://soilsecurity.org/seflos/> [Accessed].
- JUSZCZAK, R., HUMPHREYS, E., ACOSTA, M., MICHALAK-GALCZEWSKA, M., KAYZER, D. & OLEJNIK, J. 2013. Ecosystem respiration in a heterogeneous temperate peatland and its sensitivity to peat temperature and water table depth. *Plant and Soil*, 366, 505-520.
- KANDEL, T. P., LÆRKE, P. E. & ELSGAARD, L. 2018. Annual emissions of CO<sub>2</sub>, CH<sub>4</sub> and N<sub>2</sub>O from a temperate peat bog: Comparison of an undrained and four drained sites under permanent grass and arable crop rotations with cereals and potato. *Agricultural and Forest Meteorology*, 256, 470-481.
- KARKI, S., ELSGAARD, L. & LÆRKE, P. E. 2015. Effect of reed canary grass cultivation on greenhouse gas emission from peat soil at controlled rewetting. *Biogeosciences*, 12, 595-606.
- KASIMIR-KLEMEDTSSON, Å., KLEMEDTSSON, L., BERGLUND, K., MARTIKAINEN, P., SILVOLA, J. & OENEMA, O. 1997. Greenhouse gas emissions from farmed organic soils: a review. *Soil use and management*, 13, 245-250.
- KIRSCHBAUM, M. U. 1995. The temperature dependence of soil organic matter decomposition, and the effect of global warming on soil organic C storage. *Soil Biology and biochemistry*, 27, 753-760.
- KLINGENFUß, C., ROßKOPF, N., WALTER, J., HELLER, C. & ZEITZ, J. 2014. Soil organic matter to soil organic carbon ratios of peatland soil substrates. *Geoderma*, 235, 410-417.
- KIJUN, N., CALANCA, P., ROTACH, M. W. & SCHMID, H. P. 2015. A simple two-dimensional parameterisation for Flux Footprint Prediction (FFP). *Geosci. Model Dev.*, 8, 3695-3713.
- KÖBKE, S., SENBAYRAM, M., PFEIFFER, B., NACKE, H. & DITTERT, K. 2018. Post-harvest N<sub>2</sub>O and CO<sub>2</sub> emissions related to plant residue incorporation of oilseed rape and barley straw depend on soil NO<sub>3</sub>-content. *Soil and Tillage Research*, 179, 105-113.
- KOHAKE, D., HAGEN, L. & SKIDMORE, E. 2010. Wind erodibility of organic soils. *Soil Science Society of America Journal*, 74, 250-257.
- KORMANN, R. & MEIXNER, F. X. 2001. An analytical footprint model for non-neutral stratification. *Boundary-Layer Meteorology*, 99, 207-224.
- KOTTEK, M., GRIESER, J., BECK, C., RUDOLF, B. & RUBEL, F. 2006. World map of the Köppen-Geiger climate classification updated. *Meteorologische Zeitschrift*, 15, 259-263.
- KUZYAKOV, Y. & GAVRICHKOVA, O. 2010. Time lag between photosynthesis and carbon dioxide efflux from soil: a review of mechanisms and controls. *Global Change Biology*, 16, 3386-3406.

- LAFLEUR, P. M., MOORE, T. R., ROULET, N. T. & FROLKING, S. 2005. Ecosystem Respiration in a Cool Temperate Bog Depends on Peat Temperature But Not Water Table. *Ecosystems*, 8, 619-629.
- LAI, D., ROULET, N., HUMPHREYS, E., MOORE, T. & DALVA, M. 2012. The effect of atmospheric turbulence and chamber deployment period on autochamber CO<sub>2</sub> and CH<sub>4</sub> flux measurements in an ombrotrophic peatland. *Biogeosciences*, 9, 3305.
- LAINE, J. & VASANDER, H. 1996. Ecology and vegetation gradients of peatlands. *Peatlands in Finland*, 10, 20.
- LAL, R. 2004. Soil carbon sequestration impacts on global climate change and food security. *science*, 304, 1623-1627.
- LAL, R. 2005. Soil erosion and carbon dynamics. Elsevier.
- LANGEVELD, C., SEGERS, R., DIRKS, B., VAN DEN POL-VAN DASSELAAR, A., VELTHOF, G. & HENSEN, A. 1997. Emissions of CO<sub>2</sub>, CH<sub>4</sub> and N<sub>2</sub>O from pasture on drained peat soils in the Netherlands. *Developments in Crop Science*, 25, 57-64.
- LARNEY, F. J., BULLOCK, M. S., JANZEN, H. H., ELLERT, B. H. & OLSON, E. C. 1998. Wind erosion effects on nutrient redistribution and soil productivity. *Journal of Soil and Water Conservation*, 53, 133-140.
- LATSHAW, W. & MILLER, E. 1924. Elemental composition of the corn plant. *Journal of Agricultural Research*, 27, 845-861.
- LAUNAY, C., CONSTANTIN, J., CHLEBOWSKI, F., HOUOT, S., GRAUX, A. I., KLUMPP, K., MARTIN, R., MARY, B., PELLERIN, S. & THEROND, O. 2021. Estimating the carbon storage potential and greenhouse gas emissions of French arable cropland using high-resolution modeling. *Global Change Biology*, 27, 1645-1661.
- LAURILA, T., AURELA, M. & TUOVINEN, J.-P. 2012. Eddy covariance measurements over wetlands. *Eddy covariance*. Springer.
- LEIFELD, J. & MENICHETTI, L. 2018. The underappreciated potential of peatlands in global climate change mitigation strategies. *Nature communications*, 9, 1-7.
- LEIFELD, J., MÜLLER, M. & FUHRER, J. 2011. Peatland subsidence and carbon loss from drained temperate fens. *Soil Use and Management*, 27, 170-176.
- LEUNING, R., VAN GORSEL, E., MASSMAN, W. J. & ISAAC, P. R. 2012. Reflections on the surface energy imbalance problem. *Agricultural and Forest Meteorology*, 156, 65-74.
- LEVY, P. E., BURDEN, A., COOPER, M. D., DINSMORE, K. J., DREWER, J., EVANS, C., FOWLER, D., GAIAWYN, J., GRAY, A. & JONES, S. K. 2012. Methane emissions from soils: synthesis and analysis of a large UK data set. *Global Change Biology*, 18, 1657-1669.
- LEYS, J. & MCTAINISH, G. 1994. Soil loss and nutrient decline by wind erosion—cause for concern [Mallee, New South Wales]. *Australian Journal of Soil and Water Conservation (Australia)*.
- LI, J., OKIN, G. S., ALVAREZ, L. & EPSTEIN, H. 2007. Quantitative effects of vegetation cover on wind erosion and soil nutrient loss in a desert grassland of southern New Mexico, USA. *Biogeochemistry*, 85, 317-332.
- LI, Y., YU, H., CHAPPELL, A., ZHOU, N. & FUNK, R. 2014. How much soil organic carbon sequestration is due to conservation agriculture reducing soil erosion? *Soil Research*, 52, 717-726.
- LIMPENS, J., BERENDSE, F., BLODAU, C., CANADELL, J., FREEMAN, C., HOLDEN, J., ROULET, N., RYDIN, H. & SCHAEPMAN-STRUB, G. 2008. Peatlands and the carbon cycle: from local processes to global implications—a synthesis. *Biogeosciences*, 5, 1475-1491.
- LINDSAY, R. 2010. Peatbogs and carbon: A Critical synthesis. *Unpublished report to RSPB Scotland*.
- LINDSAY, R. & IMMIRZI, P. 1996. An inventory of lowland raised bogs in Great Britain.
- LLOYD, C. 2006. Annual carbon balance of a managed wetland meadow in the Somerset Levels, UK. *Agricultural and Forest Meteorology*, 138, 168-179.

- LLOYD, J. & TAYLOR, J. 1994. On the temperature dependence of soil respiration. *Functional ecology*, 315-323.
- LOHILA, A., AURELA, M., TUOVINEN, J. P. & LAURILA, T. 2004. Annual CO<sub>2</sub> exchange of a peat field growing spring barley or perennial forage grass. *Journal of Geophysical Research: Atmospheres*, 109.
- LOISEL, J., YU, Z., BEILMAN, D. W., KAISER, K. & PARNIKOZA, I. 2017. Peatland Ecosystem Processes in the Maritime Antarctic During Warm Climates. *Scientific Reports*, 7, 12344.
- LOZANOVSKA, I., KUZYAKOV, Y., KROHN, J., PARVIN, S. & DORODNIKOV, M. 2016. Effects of nitrate and sulfate on greenhouse gas emission potentials from microform-derived peats of a boreal peatland: A 13 C tracer study. *Soil Biology and Biochemistry*, 100, 182-191.
- MAHRT, L. 1998. Flux sampling errors for aircraft and towers. *Journal of Atmospheric and Oceanic technology*, 15, 416-429.
- MALJANEN, M., HYTÖNEN, J., MÄKIRANTA, P., ALM, J., MINKKINEN, K., LAINE, J. & MARTIKAINEN, P. J. 2007. Greenhouse gas emissions from cultivated and abandoned organic croplands in Finland.
- MALMER, N. & WALLÉN, B. 2004. Input rates, decay losses and accumulation rates of carbon in bogs during the last millennium: internal processes and environmental changes. *The Holocene*, 14, 111-117.
- MANDER, Ü., JÄRVEOJA, J., MADDISON, M., SOOSAAR, K., AAVOLA, R., OSTONEN, I. & SALM, J. O. 2012. Reed canary grass cultivation mitigates greenhouse gas emissions from abandoned peat extraction areas. *Gcb Bioenergy*, 4, 462-474.
- MATYSEK, M., LEAKE, J., BANWART, S., JOHNSON, I., PAGE, S., KADUK, J., SMALLEY, A., CUMMING, A. & ZONA, D. 2019. Impact of fertiliser, water table, and warming on celery yield and CO<sub>2</sub> and CH<sub>4</sub> emissions from fenland agricultural peat. *Science of the Total Environment*, 667, 179-190.
- MAUDER, M., CUNTZ, M., DRÜE, C., GRAF, A., REBMANN, C., SCHMID, H. P., SCHMIDT, M. & STEINBRECHER, R. 2013. A strategy for quality and uncertainty assessment of long-term eddy-covariance measurements. *Agricultural and Forest Meteorology*, 169, 122-135.
- MAUDER, M., DESJARDINS, R. L., PATTEY, E. & WORTH, D. 2010. An attempt to close the daytime surface energy balance using spatially-averaged flux measurements. *Boundary-layer meteorology*, 136, 175-191.
- MCGLOIN, R., ŠIGUT, L., HAVRÁNKOVÁ, K., DUŠEK, J., PAVELKA, M. & SEDLÁK, P. 2018. Energy balance closure at a variety of ecosystems in Central Europe with contrasting topographies. *Agricultural and Forest Meteorology*, 248, 418-431.
- MELILLO, J., STEUDLER, P., ABER, J., NEWKIRK, K., LUX, H., BOWLES, F., CATRICALA, C., MAGILL, A., AHRENS, T. & MORRISSEAU, S. 2002. Soil warming and carbon-cycle feedbacks to the climate system. *Science*, 298, 2173-2176.
- MENDEZ, M. J., FUNK, R. & BUSCHIAZZO, D. E. 2011. Field wind erosion measurements with big spring number eight (BSNE) and modified wilson and cook (MWAC) samplers. *Geomorphology*, 129, 43-48.
- MITSCHE, W. J., BERNAL, B., NAHLIK, A. M., MANDER, Ü., ZHANG, L., ANDERSON, C. J., JØRGENSEN, S. E. & BRIX, H. 2013. Wetlands, carbon, and climate change. *Landscape Ecology*, 28, 583-597.
- MONCRIEFF, J., CLEMENT, R., FINNIGAN, J. & MEYERS, T. 2004. Averaging, detrending, and filtering of eddy covariance time series. *Handbook of micrometeorology*. Springer.
- MONCRIEFF, J. B., MASSHEDER, J., DE BRUIN, H., ELBERS, J., FRIBORG, T., HEUSINKVELD, B., KABAT, P., SCOTT, S., SØGAARD, H. & VERHOEF, A. 1997. A system to measure surface fluxes of momentum, sensible heat, water vapour and carbon dioxide. *Journal of Hydrology*, 188, 589-611.

- MOORE, T. R., ROULET, N. T. & WADDINGTON, J. M. 1998. Uncertainty in Predicting the Effect of Climatic Change on the Carbon Cycling of Canadian Peatlands. *Climatic Change*, 40, 229-245.
- MORRIS, J., GRAVES, A., ANGUS, A., HESS, T., LAWSON, C., CAMINO, M., TRUCKELL, I. & HOLMAN, I. 2010. Restoration of lowland peatland in England and impacts on food production and security. *Report to Natural England. Cranfield University, Bedford*.
- MORRISON, R. 2013. *Land/atmosphere carbon dioxide exchange at semi-natural and regenerating peatlands in East Anglia, UK*. PhD Thesis.
- MORRISON, R., CUMMING, A., TAFT, H., KADUK, J., PAGE, S., JONES, D., HARDING, R. & BALZTER, H. 2013. Carbon dioxide fluxes at an intensively cultivated temperate lowland peatland in the East Anglian Fens, UK. *Biogeosciences Discussions*, 4193-4223.
- MURAKAMI, T., MURAYAMA, S., UCHITSU, M. & YOSHIDA, S. 2002. Root length and distribution of field-grown buckwheat (*Fagopyrum esculentum* Moench). *Soil science and plant nutrition*, 48, 609-613.
- MUSARIKA, S., ATHERTON, C., GOMERSALL, T., WELLS, M., KADUK, J., CUMMING, A., PAGE, S., OECHEL, W. & ZONA, D. 2017. Effect of water table management and elevated CO<sub>2</sub> on radish productivity and on CH<sub>4</sub> and CO<sub>2</sub> fluxes from peatlands converted to agriculture. *Science of the Total Environment*, 584, 665-672.
- MYERS, B., WEBSTER, K. L., MCLAUGHLIN, J. W. & BASILIKO, N. 2012. Microbial activity across a boreal peatland nutrient gradient: the role of fungi and bacteria. *Wetlands ecology and management*, 20, 77-88.
- NATURAL ENGLAND 2010. England's peatlands: carbon storage and greenhouse gases. *Natural England Report NE257*.
- NATURAL ENGLAND. 2011. *Agricultural Land Classification map Eastern Region (ALC008)* [Online]. Available: <http://publications.naturalengland.org.uk/publication/127056?category=5954148537204736> [Accessed 2018/05/10 2018].
- NAZARENKO, L., SCHMIDT, G., MILLER, R., TAUSNEV, N., KELLEY, M., RUEDY, R., RUSSELL, G., ALEINOV, I., BAUER, M. & BAUER, S. 2015. Future climate change under RCP emission scenarios with GISS ModelE2. *Journal of Advances in Modeling Earth Systems*, 7, 244-267.
- NIEVEEN, J. P., JACOBS, C. & JACOBS, A. F. 1998. Diurnal and seasonal variation of carbon dioxide exchange from a former true raised bog. *Global Change Biology*, 4, 823-833.
- NIJP, J. J., METSELAAR, K., LIMPENS, J., TEUTSCHBEIN, C., PEICHL, M., NILSSON, M. B., BERENDSE, F. & VAN DER ZEE, S. E. A. T. M. 2017. Including hydrological self-regulating processes in peatland models: Effects on peatmoss drought projections. *Science of The Total Environment*, 580, 1389-1400.
- NORBERG, L., BERGLUND, Ö. & BERGLUND, K. 2016. Seasonal CO<sub>2</sub> emission under different cropping systems on Histosols in southern Sweden. *Geoderma Regional*, 7, 338-345.
- NRCS, U. 2007. National resources inventory. Washington DC: USDA Natural Resources Conservation Service. 1997 and 2003 Data sets on CD.
- NWAISHI, F., PETRONE, R. M., MACRAE, M. L., PRICE, J. S., STRACK, M. & ANDERSEN, R. 2016. Preliminary assessment of greenhouse gas emissions from a constructed fen on post-mining landscape in the Athabasca oil sands region, Alberta, Canada. *Ecological Engineering*, 95, 119-128.
- OLEFELDT, D., EUSKIRCHEN, E. S., HARDEN, J., KANE, E., MCGUIRE, A. D., WALDROP, M. P. & TURETSKY, M. R. 2017. A decade of boreal rich fen greenhouse gas fluxes in response to natural and experimental water table variability. *Global change biology*, 23, 2428-2440.
- OSAKABE, Y., OSAKABE, K., SHINOZAKI, K. & TRAN, L.-S. P. 2014. Response of plants to water stress. *Frontiers in plant science*, 5, 86.
- OWENS, P., RICKSON, R., CLARKE, M., DRESSER, M., DEEKS, L., JONES, R., WOODS, G., VAN OOST, K. & QUINE, T. 2006. Scoping Study of Soil Loss through Wind Erosion Tillage Erosion and

- Soil Co-Extracted with Root Vegetables. *National Soil Resources Institute Report for DEFRA, Cranfield University*.
- PAGE, S., BAIRD, A., HIGH, K. & KADUK, J. 2020. An assessment of the societal impacts of water level management on lowland peatlands in England and Wales.
- PAGE, S., MORRISON, R., MALINS, C., HOOIJER, A., RIELEY, J. & JAUVAINEN, J. 2011. Review of peat surface greenhouse gas emissions from oil palm plantations in Southeast Asia. *White Paper*.
- PANEBIANCO, J. E., BUSCHIAZZO, D. E. & ZOBECK, T. M. 2010. Comparison of different mass transport calculation methods for wind erosion quantification purposes. *Earth Surface Processes and Landforms*, 35, 1548-1555.
- PANIN, G. Inhomogeneity of the land surface and parameterization of the turbulent fluxes in natural conditions (Session 4: Problems for Flux Measurements studies). 筑波大学陸域環境研究センター報告, GAME-AAN/Radiation 国際ワークショップ予稿集= Bulletin of the Terrestrial Environment Research Center, the University of Tsukuba, Proceedings of the International Workshop on GAME-AAN/Radiation, 2001. 筑波大学陸域環境研究センター, 85-85.
- PAPALE, D., REICHSTEIN, M., AUBINET, M., CANFORA, E., BERNHOFER, C., KUTSCH, W., LONGDOZ, B., RAMBAL, S., VALENTINI, R. & VESALA, T. 2006. Towards a standardized processing of Net Ecosystem Exchange measured with eddy covariance technique: algorithms and uncertainty estimation. *Biogeosciences*, 3, 571-583.
- PARMENTIER, F., VAN DER MOLEN, M., DE JEU, R., HENDRIKS, D. & DOLMAN, A. 2009. CO<sub>2</sub> fluxes and evaporation on a peatland in the Netherlands appear not affected by water table fluctuations. *Agricultural and forest meteorology*, 149, 1201-1208.
- PAWSON, R., ROTHWELL, J., DANIELS, S., LORD, D., EVANS, M. & ALLOTT, T. 2007. Fluvial organic carbon flux from an eroding peatland catchment, southern Pennines, UK. *Hydrology and Earth System Sciences Discussions*, 4, 719-745.
- PEACOCK, M., GAUCI, V., BAIRD, A., BURDEN, A., CHAPMAN, P., CUMMING, A., EVANS, J., GRAYSON, R., HOLDEN, J. & KADUK, J. 2019. The full carbon balance of a rewetted cropland fen and a conservation-managed fen. *Agriculture, Ecosystems & Environment*, 269, 1-12.
- PEACOCK, M., RIDLEY, L. M., EVANS, C. D. & GAUCI, V. 2017. Management effects on greenhouse gas dynamics in fen ditches. *Science of the Total Environment*, 578, 601-612.
- PŁAŻEK, A., SŁOMKA, A., KOPEĆ, P., DZIURKA, M., HORNYÁK, M., SYCHTA, K., PASTUSZAK, J. & DUBERT, F. 2019. Effects of high temperature on embryological development and hormone profile in flowers and leaves of common buckwheat (*Fagopyrum esculentum* Moench). *International journal of molecular sciences*, 20, 1705.
- POLLARD, E. & MILLAR, A. 1968. Wind erosion in the East Anglian Fens. *Weather*, 23, 415-417.
- POYDA, A., REINSCH, T., KLUß, C., LOGES, R. & TAUBE, F. 2016. Greenhouse gas emissions from fen soils used for forage production in northern Germany. *Biogeosciences*, 13, 5221.
- PRESTON, M. D., SMEMO, K. A., MCLAUGHLIN, J. W. & BASILIKO, N. 2012. Peatland microbial communities and decomposition processes in the James Bay Lowlands, Canada. *Frontiers in microbiology*, 3, 70.
- R CORE TEAM 2013. R: A language and environment for statistical computing. R Foundation for Statistical Computing, Vienna, Australia. URL: <http://www.R-project.org/>.
- RADLEY, J. & SIMMS, C. 1967. Wind erosion in east Yorkshire. *Nature*, 216, 20-22.
- REICHSTEIN, M., FALGE, E., BALDOCCHI, D., PAPALE, D., AUBINET, M., BERBIGIER, P., BERNHOFER, C., BUCHMANN, N., GILMANOV, T. & GRANIER, A. 2005. On the separation of net ecosystem exchange into assimilation and ecosystem respiration: review and improved algorithm. *Global Change Biology*, 11, 1424-1439.
- REICHSTEIN, M., REY, A., FREIBAUER, A., TENHUNEN, J., VALENTINI, R., BANZA, J., CASALS, P., CHENG, Y., GRÜNZWEIG, J. M. & IRVINE, J. 2003. Modeling temporal and large-scale

- spatial variability of soil respiration from soil water availability, temperature and vegetation productivity indices. *Global biogeochemical cycles*, 17.
- REITZ, S., KAROWE, D., DIAWARA, M. & TRUMBLE, J. 1997. Effects of elevated atmospheric carbon dioxide on the growth and linear furanocoumarin content of celery. *Journal of Agricultural and Food Chemistry*, 45, 3642-3646.
- REZANEZHAD, F., PRICE, J. S., QUINTON, W. L., LENNARTZ, B., MILOJEVIC, T. & VAN CAPPELLEN, P. 2016. Structure of peat soils and implications for water storage, flow and solute transport: A review update for geochemists. *Chemical Geology*, 429, 75-84.
- RICHARDSON, A. D., BRASWELL, B. H., HOLLINGER, D. Y., BURMAN, P., DAVIDSON, E. A., EVANS, R. S., FLANAGAN, L. B., MUNGER, J. W., SAVAGE, K. & URBANSKI, S. P. 2006. Comparing simple respiration models for eddy flux and dynamic chamber data. *Agricultural and Forest Meteorology*, 141, 219-234.
- RICHARDSON, S. & SMITH, J. 1977. Peat wastage in the East Anglian fens. *European Journal of Soil Science*, 28, 485-489.
- RIUTTA, T., LAINE, J. & TUUTTILA, E.-S. 2007. Sensitivity of CO<sub>2</sub> exchange of fen ecosystem components to water level variation. *Ecosystems*, 10, 718-733.
- ROTHERHAM, I. D. 2013. *Lost Fens: England's Greatest Ecological Disaster*, The History Press.
- ROULET, N. T., LAFLEUR, P. M., RICHARD, P. J., MOORE, T. R., HUMPHREYS, E. R. & BUBIER, J. 2007. Contemporary carbon balance and late Holocene carbon accumulation in a northern peatland. *Global Change Biology*, 13, 397-411.
- RYDIN, H. & JEGLUM, J. K. 2013. *The biology of peatlands*, 2e, Oxford university press.
- SANDSTRÖM, T., KOLMODIN-HEDMAN, B., LEDIN, M.-C., BJERMER, L., HÖRNQVIST-BYLUND, S. & STJERNBERG, N. 1991. Exposure to peat dust: acute effects on lung function and content of bronchoalveolar lavage fluid. *Occupational and Environmental Medicine*, 48, 771-775.
- SCHARLEMANN, J. P., TANNER, E. V., HIEDERER, R. & KAPOS, V. 2014. Global soil carbon: understanding and managing the largest terrestrial carbon pool. *Carbon Management*, 5, 81-91.
- SCHEFFER, R., VAN LOGTESTIJN, R. & VERHOEVEN, J. 2001. Decomposition of Carex and Sphagnum litter in two mesotrophic fens differing in dominant plant species. *Oikos*, 92, 44-54.
- SERDECZNY, O., ADAMS, S., BAARSCH, F., COUMOU, D., ROBINSON, A., HARE, W., SCHAEFFER, M., PERRETTE, M. & REINHARDT, J. 2017. Climate change impacts in Sub-Saharan Africa: from physical changes to their social repercussions. *Regional Environmental Change*, 17, 1585-1600.
- SHAO, Y., MCTAINSH, G., LEYS, J. & RAUPACH, M. 1993. Efficiencies of sediment samplers for wind erosion measurement. *Soil Research*, 31, 519-532.
- SINGH, S. & SINGH, J. 1996. Water-stable aggregates and associated organic matter in forest, savanna, and cropland soils of a seasonally dry tropical region, India. *Biology and Fertility of Soils*, 22, 76-82.
- SMITH, P., LANIGAN, G., KUTSCH, W. L., BUCHMANN, N., EUGSTER, W., AUBINET, M., CESCHIA, E., BÉZIAT, P., YELURIPATI, J. B. & OSBORNE, B. 2010. Measurements necessary for assessing the net ecosystem carbon budget of croplands. *Agriculture, ecosystems & environment*, 139, 302-315.
- SOIL SURVEY STAFF 2014. Keys to Soil Taxonomy. In: USDA-NATIONAL RESOURCES CONSERVATION SERVICE (ed.) 12th ed. Washington, DC.
- STOY, P. C., MAUDER, M., FOKEN, T., MARCOLLA, B., BOEGH, E., IBROM, A., ARAIN, M. A., ARNETH, A., AURELA, M. & BERNHOFER, C. 2013. A data-driven analysis of energy balance closure across FLUXNET research sites: The role of landscape scale heterogeneity. *Agricultural and forest meteorology*, 171, 137-152.
- STRACK, M. 2008. *Peatlands and climate change*, IPS, International Peat Society.

- STRACK, M. & WADDINGTON, J. 2007. Response of peatland carbon dioxide and methane fluxes to a water table drawdown experiment. *Global Biogeochemical Cycles*, 21.
- STULL, R. B. 2012. *An introduction to boundary layer meteorology*, Springer Science & Business Media.
- SUSILAWATI, H. L., SETYANTO, P., ARIANI, M., HERVANI, A. & INUBUSHI, K. 2016. Influence of water depth and soil amelioration on greenhouse gas emissions from peat soil columns. *Soil science and plant nutrition*, 62, 57-68.
- SVENSSON, B. 1980. Carbon dioxide and methane fluxes from the ombrotrophic parts of a subarctic mire. *Ecological Bulletins*, 235-250.
- TAFT, H. E., CROSS, P. A., EDWARDS-JONES, G., MOORHOUSE, E. R. & JONES, D. L. 2017. Greenhouse gas emissions from intensively managed peat soils in an arable production system. *Agriculture, Ecosystems & Environment*, 237, 162-172.
- TAFT, H. E., CROSS, P. A. & JONES, D. L. 2018. Efficacy of mitigation measures for reducing greenhouse gas emissions from intensively cultivated peatlands. *Soil Biology and Biochemistry*, 127, 10-21.
- TEH, Y. A., SILVER, W. L., SONNENTAG, O., DETTO, M., KELLY, M. & BALDOCCHI, D. D. 2011. Large greenhouse gas emissions from a temperate peatland pasture. *Ecosystems*, 14, 311-325.
- TIEMEYER, B., ALBIAC BORRAZ, E., AUGUSTIN, J., BECHTOLD, M., BEETZ, S., BEYER, C., DRÖSLER, M., EBLI, M., EICKENSCHIEDT, T. & FIEDLER, S. 2016. High emissions of greenhouse gases from grasslands on peat and other organic soils. *Global change biology*, 22, 4134-4149.
- TOKIDA, T., MIYAZAKI, T., MIZOGUCHI, M., NAGATA, O., TAKAKAI, F., KAGEMOTO, A. & HATANO, R. 2007. Falling atmospheric pressure as a trigger for methane ebullition from peatland. *Global Biogeochemical Cycles*, 21.
- TRIBOUILLOIS, H., DÜRR, C., DEMILLY, D., WAGNER, M.-H. & JUSTES, E. 2016. Determination of germination response to temperature and water potential for a wide range of cover crop species and related functional groups. *PloS One*, 11, e0161185.
- TUBIELLO, F. N., BIANCALANI, R., SALVATORE, M., ROSSI, S. & CONCHEDDA, G. 2016. A worldwide assessment of greenhouse gas emissions from drained organic soils. *Sustainability*, 8, 371.
- TUBIELLO, F. N., SALVATORE, M., ROSSI, S., FERRARA, A., FITTON, N. & SMITH, P. 2013. The FAOSTAT database of greenhouse gas emissions from agriculture. *Environmental Research Letters*, 8, 015009.
- UK MET OFFICE 2019. Cambridge NIAB. [Online] <https://www.metoffice.gov.uk/pub/data/weather/uk/climate/stationdata/cambridgedata.txt>.
- UK MET OFFICE. 2020. Winter 2019/2020 [Online]. Available: [https://www.metoffice.gov.uk/binaries/content/assets/metofficegovuk/pdf/weather/learn-about/uk-past-events/summaries/uk\\_monthly\\_climate\\_summary\\_winter\\_2020.pdf](https://www.metoffice.gov.uk/binaries/content/assets/metofficegovuk/pdf/weather/learn-about/uk-past-events/summaries/uk_monthly_climate_summary_winter_2020.pdf) [Accessed 22/07/2020].
- UNFCCC 2015. Adoption of the Paris Agreement. United Nations, Geneva.
- VAN GORSEL, E., LEUNING, R., CLEUGH, H., KEITH, H. & SUNI, T. 2007. Nocturnal carbon efflux: reconciliation of eddy covariance and chamber measurements using an alternative to the u \* -threshold filtering technique. *Tellus B*, 59.
- VAN PEEL, R. S., ZOBECK, T. M., POTTER, K. N., STOUT, J. E. & POPHAM, T. 2004. Validation of the wind erosion stochastic simulator (WESS) and the revised wind erosion equation (RWEQ) for single events. *Environmental Modelling & Software*, 19, 191-198.
- VERHOEVEN, J. & TOTH, E. 1995. Decomposition of Carex and Sphagnum litter in fens: effect of litter quality and inhibition by living tissue homogenates. *Soil Biology and Biochemistry*, 27, 271-275.
- VICKERS, D. & MAHRT, L. 1997. Quality control and flux sampling problems for tower and aircraft data. *Journal of Atmospheric and Oceanic Technology*, 14, 512-526.

- WANG, B., JIN, H., LI, Q., CHEN, D., ZHAO, L., TANG, Y., KATO, T. & GU, S. 2017a. Diurnal and Seasonal Variations in the Net Ecosystem CO<sub>2</sub> Exchange of a Pasture in the Three-River Source Region of the Qinghai-Tibetan Plateau. *Plos one*, 12, e0170963.
- WANG, X., SICILIANO, S., HELGASON, B. & BEDARD-HAUGHN, A. 2017b. Responses of a mountain peatland to increasing temperature: A microcosm study of greenhouse gas emissions and microbial community dynamics. *Soil Biology and Biochemistry*, 110, 22-33.
- WARBURTON, J. 2003. Wind-splash erosion of bare peat on UK upland moorlands. *Catena*, 52, 191-207.
- WARD, S. E., OSTLE, N. J., OAKLEY, S., QUIRK, H., HENRYS, P. A. & BARDGETT, R. D. 2013. Warming effects on greenhouse gas fluxes in peatlands are modulated by vegetation composition. *Ecology letters*, 16, 1285-1293.
- WEBB, E. K., PEARMAN, G. I. & LEUNING, R. 1980. Correction of flux measurements for density effects due to heat and water vapour transfer. *Quarterly Journal of the Royal Meteorological Society*, 106, 85-100.
- WEN, Y., ZANG, H., FREEMAN, B., MA, Q., CHADWICK, D. R. & JONES, D. L. 2019. Rye cover crop incorporation and high watertable mitigate greenhouse gas emissions in cultivated peatland. *Land Degradation & Development*, 30, 1928-1938.
- WILCZAK, J. M., ONCLEY, S. P. & STAGE, S. A. 2001. Sonic anemometer tilt correction algorithms. *Boundary-Layer Meteorology*, 99, 127-150.
- WILSON, K. B., BALDOCCHI, D. D., AUBINET, M., BERBIGIER, P., BERNHOFER, C., DOLMAN, H., FALGE, E., FIELD, C., GOLDSTEIN, A. & GRANIER, A. 2002. Energy partitioning between latent and sensible heat flux during the warm season at FLUXNET sites. *Water Resources Research*, 38, 30-1-30-11.
- WILSON, S. & COOKE, R. 1980. Wind erosion. *Soil erosion*, 217251.
- WORRALL, F., CHAPMAN, P., HOLDEN, J., EVANS, C., ARTZ, R., SMITH, P. & GRAYSON, R. 2011. A review of current evidence on carbon fluxes and greenhouse gas emissions from UK peatlands.
- WORRALL, F., REED, M., WARBURTON, J. & BURT, T. 2003. Carbon budget for a British upland peat catchment. *Science of the Total Environment*, 312, 133-146.
- YOUNG, D. M., BAIRD, A. J., CHARMAN, D. J., EVANS, C. D., GALLEGOSALA, A. V., GILL, P. J., HUGHES, P. D., MORRIS, P. J. & SWINDLES, G. T. 2019. Misinterpreting carbon accumulation rates in records from near-surface peat. *Scientific reports*, 9, 1-8.
- YU, G.-R., WEN, X.-F., SUN, X.-M., TANNER, B. D., LEE, X. & CHEN, J.-Y. 2006. Overview of ChinaFLUX and evaluation of its eddy covariance measurement. *Agricultural and Forest Meteorology*, 137, 125-137.
- YU, Z. 2012. Northern peatland carbon stocks and dynamics: a review. *Biogeosciences*, 9, 4071.
- YU, Z., LOISEL, J., BROSSEAU, D. P., BEILMAN, D. W. & HUNT, S. J. 2010. Global peatland dynamics since the Last Glacial Maximum. *Geophysical Research Letters*, 37.
- YULING, F. 2005. Energy balance closure at ChinaFLUX sites. *Sci. China Earth Sci*, 48, 2005.
- ZOBECK, T. M., STERK, G., FUNK, R., RAJOT, J. L., STOUT, J. E. & VAN PEEL, R. S. 2003. Measurement and data analysis methods for field-scale wind erosion studies and model validation. *Earth Surface Processes and Landforms: The Journal of the British Geomorphological Research Group*, 28, 1163-1188.